2017

Techno-Economic Studies of Coal-Biomass to Liquids (CBTL) Plants with CO2 Capture and Storage (CCS)

Yuan Jiang

Techno-Economic Studies of Coal-Biomass to Liquids (CBTL) Plants with CO_2 Capture and Storage (CCS)

Yuan Jiang

Dissertation submitted to the
Benjamin M. Statler College of Engineering and Mineral Resources
at West Virginia University

in partial fulfillment of the requirements for the degree of

Doctor of Philosophy in
Chemical Engineering

Dr. Debangsu Bhattacharyya, Ph.D., Chair
Dr. Richard Turton, Ph.D.
Dr. Brian Anderson, Ph.D.
Dr. Jingxin Wang, Ph.D.
Dr. David DeVallance, Ph.D.

Department of Chemical and Biomedical Engineering

Morgantown, West Virginia
2017

Keywords: coal biomass to liquids, shale gas, carbon capture and storage, modeling, techno-economic analysis, indirect liquefaction, direct liquefaction, hybrid liquefaction

Abstract

Techno-Economic Studies of Coal-Biomass to Liquids (CBTL) Plants with CO_2 Capture and Storage (CCS)

Yuan Jiang

Due to insecurity in the crude oil supply and global warming, various alternative technologies for fuel production are being investigated. In this project, indirect, direct, and hybrid liquefaction routes are investigated for production of transportation fuels from coal and biomass. Indirect coal liquefaction (ICL) and direct coal liquefaction (DCL) technologies are commercially available, but both processes are plagued with high carbon footprint. Furthermore, significant amount of hydrogen is required in the DCL process leading not only to higher cost but resulting in considerable amount of CO_2 production. Addition of biomass and application of carbon capture and storage (CCS) technologies are studied for reducing the carbon footprint. However, these two options can lead to higher capital and operating costs. Due to easy availability and low cost of the shale gas in the U.S., utilization of shale gas in the direct and hybrid routes was investigated for producing hydrogen at a lower cost with reduced CO_2 emission in comparison to the traditional coal gasification route. Because the quality of the syncrude produced from ICL and DCL technologies vary widely, the hybrid coal liquefaction technology, a synergistic combination of ICL and DCL technologies, is investigated for reducing the penalty of downstream syncrude upgrading unit through optimal blending.

In the indirect CBTL plant, coal and biomass are first gasified to syngas. Then the syngas is converted to syncrude via Fischer-Tropsch (FT) synthesis. CO_2 is captured from both raw syngas and FT vapor product. In the direct CBTL plant, coal and biomass are directly converted into syncrude in the catalytic two-stage liquefaction (CTSL) unit by adding hydrogen produced from gasification of coal/biomass/liquefaction residue or reforming of shale gas. Significant amount of CO_2 that is generated in the hydrogen production unit(s) is captured to satisfy the target extent of CO_2 capture. In the hybrid CBTL plant, pre-processed coal and biomass are sent to either syngas

production unit or the CTSL unit. Produced syngas is sent either to FT unit or hydrogen production unit. Naphtha and diesel products from the FT unit and the CTSL unit are blended to reduce the syncrude upgrading penalty. Different CCS technologies are considered and optimized for the indirect, direct and hybrid CBTL plant depending on the sources of CO_2 containing stream and corresponding CO_2 partial pressure.

While several studies have been conducted for indirect CBTL processes, studies on direct and hybrid CBTL processes at the systems level and investigation of CCS technologies for these processes are scarce. With this motivation, high fidelity process models are developed for indirect, direct, and hybrid CBTL plants with CCS. These models are leveraged to perform comprehensive techno-economic studies. Contributions of this project are as follows: (1) development of the systems-level and equipment-level process models and rigorous economic models in Aspen Plus, Aspen Custom Modeler, Aspen Exchanger Design and Rating, and Aspen Process Economic Analyzer platforms, (2) sensitivity studies to analyze the impact of key design parameters (i.e. biomass/coal ratio, operating conditions of key equipment, extent of CCS, CCS technologies, blending ratio of the syncrude and products in the hybrid route) and investment parameters (i.e. price of coal and biomass, project life, plant contingency and plant capacity) on key efficiency measures, such as thermal and carbon efficiency, as well as economic measures, such as the net present value, internal rate of return and break-even oil price, (3) comparisons and analyses of trade-offs of indirect, direct, and hybrid CBTL technologies.

Dedicated to

My family and friends

Acknowledgement

I would like to express my deepest gratitude to Dr. Debangsu Bhattacharyya, who served as my research advisor, for his guidance, patience and support. His knowledge and expertise helped significantly with process conceptual design, modeling, optimization and solving engineering problems in Aspen simulation packages. I am also very grateful to my committee members, Dr. Jingxin Wang and Dr. David DeVallence, who I collaborated with in this research work, for their solid knowledge of biomass utilization and pretreating, risk assessment, and life cycle analysis. I would like to thank my committee members, Dr. Richard Turton and Dr. Brian Anderson, for their keen insight, support, advice and guidance in this research work. I would like to thank Mr. Greg Henthorn, Mr. Travis Buggey, and Dr. Shawn Grushecky, who I collaborated with in this research work, for their industrial experience and solid knowledge in financial and marketing studies.

I would like to thank Weiguo Liu for being great partners in this project. Thanks to all my fellow lab members, Dustin, Job, Jacob, Prokash, Qiang, Qiao, Anderson, Josh, Ben, Samson, Smita, Sarah, Danny, Yifan, Anca, Chirag, John, Paul, Ryan, Goutham, Pushpitha, Christian for their great company and for keeping things fun and interesting in the lab. I would like to thank my dear friends Qian, Xiao, Qiao, Shi, Kai, Xin, Shuyun, Taiwo, Xiaoyan, Lei, Yan, Xiaonin, Juan Carlos, Manish, Prathyusha, Yueting, Ting and many others for making my stay at Morgantown exciting and memorable.

I would like to thank Ms. Linda Rogers for helping me with all necessary paper works, Dr. Charter Stinespring for his academic advises, and WVU librarians for helping me to find literatures and books relevant to this work.

I would like to acknowledge financial support from U.S. Department of Energy through grant no. DE-FE0009997 titled “Feasibilities of a Coal-Biomass to Liquids Plant in Southern West Virginia”.

Table of Contents

List of Figures

List of Tables

Nomenclature

Abbreviations

A	Ash
ACM	Aspen Custom Modeler
ADF	axial dispersed flow
AGR	acid gas removal
APEA	Aspen Process Economic Analyzer
ASF	Anderson-Schulz-Flory
ASU	air separation unit
ATR	autothermal reformer
AUM	Analyzer Utility Modules
BEOP	break-even oil price
BFD	block flow diagram
BFW	boiler feed water
BOP	balance of plant
BTL	biomass to liquids
C	carbon
CAPEX	capital expenditure
CBTL	coal biomass to liquids
CCR	continuous catalyst regeneration
CCS	carbon capture and storage
CEPCI	Chemical Engineering Plant Cost Index
CG	co-gasification
CI	cetane index
COP	crude oil price
COS	carbonyl sulfide
CTL	coal to liquids
CTSL	catalytic two-stage liquefaction
DAF	dry ash-free
DAO	deashed oil

D-CBGTL	direct coal biomass gas to liquids
D-CBTL	direct coal-biomass to liquids
DCL	direct coal liquefaction
DEPG	dimethylether of polyethylene glycol
DIP	direct permanent investment
EBR	ebullated bed reactors
EDR	Exchanger Design and Rating
EDS	Exxon Donor Solvent
EIA	Energy Information Administration
EOP	equivalent oil price
EOS	equation of state
FBP	final boiling point
FC	fixed carbon
FG	fuel gas
FT	Fischer-Tropsch
FTL	Fischer-Tropsch liquids
GHG	greenhouse gases
GO	gas oil
GT	gas turbine
GTL	gas to liquids
H	hydrogen
HC	hydrocarbon
H/C	hydrogen to carbon molar ratio
HCL	hybrid coal liquefaction
HCR	hydrocarbon recovery
HCU	hydrocarbon upgrading
HDT	hydrotreating
HHV	higher heating value
HP	high pressure
HPF	high pressure flash
HRSG	heat recovery and steam generation

HTI	Hydrocarbon Technologies Inc.
HTS	high temperature shift
HVGO	heavy vacuum gas oil
IBP	initial boiling point
ICL	indirect coal liquefaction
I-CBTL	indirect coal-biomass to liquids
IGCC	integrated gasification combined cycle
IP	intermediate pressure
ISBL	inside battery limit
LCA	life cycle assessment
LG	light gases
LHHW	Langmuir-Hinshelwood Hougen-Watson
LHV	lower heating value
LP	low pressure
LPF	low pressure flash
IRR	internal rate of return
LTFT	low temperature Fischer-Tropsch
LTS	low temperature shift
LV	liquid volumn
LVGO	light vacuum gas oil
M	moisure
MDEA	methyldiethanolamine
MEA	monoethanolamine
MGAS	METC Gasifier Advanced Simulation
MOC	material of construction
MON	motor octane number
MW	molecular weight
N	nitrogen
NBP	normal boiling point
NETL	National Energy Technology Laboratory
NPV	net present value

NREL	National Renewable Energy Laboratory
O	oxygen
O&M	operating and maintenance
OPEX	operating expenditure
OSBL	outside battery limit
PAA	pre-asphaltene and asphalten
PERC	Pittsburgh Energy Research Center
PFR	plug flow reactor
POC	proof of concept
POX	partial oxidation
PSA	pressure swing adsorption
PZ	piperazine
RM	refinery margin
RON	research octane number
ROSE-SR	Residual Oil Supercritical Extraction-Solids Rejection
RSC	radiant syngas cooler
RVP	Reid vapor pressure
S	sulfur
SBCR	slurry bed column reactor
SCFB	standard cubic feet per barrel
SHR	syngas heat recovery
SMR	steam methane reforming
SRC	Solvent Refined Coal
STM	steam
SWS	sour water stripper
TEG	triethylene glycol
TPC	total project cost
VLE	vapor-liquid equilibrium
VM	volatile material
VT	vent
WGS	water gas shift

Roman symbols

C	Molar concentration; unit cost; Molar concentration in $kmol/m^3$
C_0	Base cost
C_p	Heat capacity in $kJ/(kg\ K)$
D_a	Axial dispersion coefficient in m^2/s
D_T	Reactor diameter in m
E	Activation energy
F	Mass or energy flowrate; molar flowrate in $kmol/s$; mass flowrate in kg/s
F_{FG}	Fuel gas flowrate
F_{GO}	Gas oil flowrate
F_{H_2}	H_2 reacted per barrel of wax
g	Acceleration of gravity in m^2/s
Δh	Steam turbine stage enthalpy drop
ΔH_r	Reaction heat in $kJ/kmol\ H_2$
h	Specific enthalpy in $kJ/kmol$ or kJ/kg
H_{mix}	Heat capacity of gas-slurry mixture in $J/(m^3 slurry\ K)$
k	Reaction rate constant; kinetic constant in s^{-1}
K_{eq}	Equilibrium constant
k_{is}	Steam turbine stage head coefficient
M	Methane factor; mass fraction
n	total number of trains
$(N+2A)_F$	Catalytic reforming unit feed composition
N_s	Steam turbine stage specific speed
P	Pressure or partial pressure; Pressure in Pa
r	Reaction rate
R	Gas constant
S	Selectivity; actual capacity
S_0	Base capacity
S_{max}	Maximum capacity
Sf	Scaling factor

S.V.	Superficial velocity
t	Reaction time
T	Temperature; Temperature in K
U	Mean diameter peripheral velocity of steam turbine; superficial velocity in m/s
V	Volumetric flow rate
W_i	Steam turbine stage power output
W_n	Weight fraction of hydrocarbon with n carbon atoms
W_{net}	Net power output of the steam turbine
x	EBR slurry recycle fraction
Greek symbols	
α	Chain growth probabilities
ε	Holdup
η	Efficiency
η_{st}	Steam turbine stage isentropic efficiency
ρ	Density in kg/m^3
v_{ex}	Exhaust velocity of the last stage of steam turbine
Subscripts	
ex	Steam turbine last stage
g	Gas phase
i	Steam turbine stage index, component index
is	Isentropic condition
l	Liquid phase
s	Solid phase
sl	Slurry phase
Superscripts	
F	EBR fresh feed
in	EBR inlet
N	EBR net product
out	EBR outlet
R	EBR recycle oil

Chapter 1 Introduction

1.0 Overview

Due to the, the insecurity of crude oil supply and price, global warming and climate change, various alternative technologies for fuel production are being investigated. Among the potential technologies, indirect coal liquefaction (ICL) and direct coal liquefaction (DCL) technologies are commercially available for producing alternative transportation fuels. However, both processes are plagued with high capital investment and high CO_2 emission. (Vasireddy et al., 2011) Because the syncrude produced in the ICL and DCL reactors cannot satisfy the current specification of transportation fuels, additional upgrading technologies are required. For example, syncrude from the ICL process has low octane number for naphtha cut but high cetane number for diesel cut, while syncrude from the DCL process has high octane number for naphtha cut but low cetane number for diesel. Therefore the hybrid coal liquefaction (HCL), a combination of ICL and DCL technologies, can reduce the penalty of downstream syncrude upgrading unit by optimal blending. Addition of biomass and application of carbon capture and storage (CCS) technologies are two possible solutions to reduce the carbon footprint, but would lead to higher operating cost and capital investment. Additional upgrading technologies are required to satisfy the current specification of transportation fuels for both ICL and DCL processes. Because of the difference in the properties of DCL and ICL syncrude, the HCL process, can reduce the penalty of syncrude upgrading unit by optimal blending. While there are some studies that have been conducted for indirect coal-biomass to liquids (CBTL) plants with CCS, few studies have been conducted for direct and hybrid CBTL processes at the systems level. With this motivation, techno-economic studies are conducted in Aspen Process Economic Analyzer (APEA) environment for indirect, direct, and hybrid CBTL plants with CCS using high fidelity system-level and equipment-level models developed in Aspen Plus, Aspen Custom Modeler (ACM), Aspen Exchanger Design and Rating (EDR), Matlab, and Excel.

1.1 Coal Liquefaction

In the ICL process, coal is first gasified to syngas, mainly H_2 and CO. Then the syngas is converted to syncrude via Fischer-Tropsch (FT) synthesis. The FT process, first introduced in 1920s and commercialized later on, is one of the most popular and mature technologies. The FT process can produce fuels using the syngas derived from coal, biomass, natural gas, or a combination of those feedstocks, which is also called the indirect liquefaction. Several commercial coal-based (CTL) and natural gas-based (GTL) FT plants were built in the last century. (Steynberg and Dry, 2004) Many of these plants are still producing significant amount of transportation fuel. (Dry, 2002; Steynberg and Dry, 2004; Kreutz et al., 2008) In the DCL process, coal is directly converted into syncrude in the direct liquefaction reactor by adding hydrogen produced from coal gasification or steam methane reforming (SMR). Various DCL technologies have been developed in the last hundred years such as Solvent Refined Coal (SRC)-I and SRC-II, Exxon Donor Solvent (EDS), H-Coal and catalytic two-stage liquefaction (CTSL) by Hydrocarbon Technologies Inc. (HTI), Japan's NEDOL and so on. (Vasireddy et al., 2011; Shui et al., 2010; Mochida et al., 2014) The Shenhua DCL plant in Inner Mongolia, China, which is the only operating commercial scale DCL plant after World War II, has been developed based on the NEDOL process and the HTI's CTSL process. (Mochida et al., 2014) It is widely accepted that the direct liquefaction route has relatively higher product yield (Bellman et al. 2007) and higher thermal efficiency (Winslow and Schmetz, 2009) than the indirect route.

Because the syncrude produced in either ICL or DCL plant cannot satisfy the current specification of transportation fuels, additional upgrading technologies are required. For example, syncrude from the ICL process has low octane number for naphtha cut but high cetane number for diesel cut, while syncrude from the DCL process has high octane number for naphtha cut but low cetane number for diesel. Therefore the HCL plant, a combination of ICL and DCL technologies, can reduce the penalty of downstream syncrude upgrading unit by optimal blending. In the HCL plant, pre-processed coal is sent to either gasification unit or the direct liquefaction unit. Syngas from the gasification unit is sent either to the FT unit or the hydrogen production unit. Naphtha and diesel products from the FT unit and the CTSL unit are blended to reduce the syncrude upgrading penalty.

1.2 Biomass, Shale Gas and Carbon Capture and Storage

The life cycle greenhouse gases (GHG) emission for producing either DCL or ICL liquids is about double of that for producing them from the petroleum source (Vasireddy et al., 2011; Bartis et al., 2008; Edwards, 2011). In order to convert coal (H/C ≈ 0.8) to transportation fuels (H/C ≥ 1.8), we need to either reject carbon in form of CO_2 (i.e. ICL) or add hydrogen from external sources (i.e. DCL). (Jiang and Bhattacharyya, 2014; 2015; 2016; Vasireddy et al., 2011) In the ICL plant, a significant amount of CO_2 is produced in the gasification unit and the FT unit and captured from both raw syngas and FT vapor product. In the DCL process, significant amount of H_2 is required, and therefore high amount of CO_2 is generated in the hydrogen production unit.

Coal gasification technology has been applied in the commercialized Shenhua DCL plant for producing make-up hydrogen because of the relatively low cost and sufficient supply of coal in China. A recent study shows that about 0.48 tonne of CO_2 is released per barrel of transportation fuels produced in the Shenhua DCL plant, where about 80% of CO_2 is produced in the gasification-based hydrogen production unit. (Vasireddy et al., 2011) If natural gas is available locally with reasonable price, hydrogen can also be produced by SMR with less GHG emission in comparison to coal gasificaiton. (Williams and Larson, 2003) Even though the conventional feedstock for the SMR unit is natural gas, due to abundant and cheap shale gas that is now available in the United States, shale gas is a potential feedstock in the SMR unit. However, because of the higher ethane and propane content in the shale gas in comparison to the natural gas, an adiabatic pre-reformer is preferred to convert ethane and propane before the main steam reforming reactor to prevent coke formation on reformer walls and catalyst surfaces. (Nagaoka et al., 2007; Yang et al., 2011; Christensen, 1996) It has been reported that the current commercial hydrogen production technologies, either gasification or SMR, are usually associated with a large amount of CO_2 emission.

Recently, wide interests in coal-biomass co-liquefaction processes are being catalyzed by the relatively low prices of coal and the environmental sustainability of biomass in order to reduce the life cycle GHG emission of coal liquefaction processes. (Larson and Jin, 1999; Wang et al., 2009) Biomass is a carbon-neutral feedstock, because the CO_2 released to the atmosphere is

reutilized by biomass. Adding moderate amounts of biomass to coal for liquids production can substantially reduce the carbon footprint of CBTL processes. (Liu et al., 2011; NETL, 2009)

In additional, several pre- or post-combustion CO_2 capture technology can also be implemented in the CBTL processes to further reduce the GHG emissions and satisfy the targeted extent of CCS. Deployment of suitable CCS technologies can reduce the carbon footprint of CTL/CBTL processes significantly with reasonable plant investment. (Edwards, 2011) Different CCS technologies are considered and optimized for the indirect, direct and hybrid CBTL plant depending on the sources of CO_2 containing stream and corresponding CO_2 partial pressure.

In the open literature, some studies have been conducted for either equipment-level or system-level modeling of the ICL route but without developing detailed models for the carbon capture facilities. (Liu et al, 2011; Bechtel, 1998; Baliban et al, 2010) Very few studies have been conducted for the plant-wide model of the DCL plant (Bechtel and Amoco, 1991; Winslow and Schmetz, 2000). Studies are rare on the HCL route and application of CCS, utilization of biomass and shale gas on both DCL and HCL processes. Hence, in this project, we consider an indirect liquefaction route, a direct liquefaction route, and a hybrid liquefaction route for the production of liquid fuels from coal and biomass. The focus is on process technologies and configurations that can maximize the liquid fuel production.

1.3 Objective

In this study, a techno-economic study was conducted in APEA environment for indirect, direct, and hybrid CBTL plants with CCS using high fidelity system-level and equipment-level models developed in Aspen Plus, ACM, EDR, Matlab and Excel, as shown in Figure 1.1. The objective is to utilize the computational modeling tools to analyze the effects of biomass, shale gas utilization and CCS application on the overall thermal efficiency and economic performance of different liquefaction technologies.

To summarize, impacts of various technologies, design parameters, operating conditions and investment parameters (economic assumptions) on various economic performance measures are investigated.

For all the CBTL technologies, following tasks have been performed:

- High-fidelity plant-wide models have been developed for indirect, direct, and hybrid CBTL plant. The process models have been developed using Aspen Plus and ACM while the techno-economic studies are conducted using APEA. For all cases, carbon capture facilities are designed to capture 90% of CO_2 produced in the plant.
- The base case uses 92% coal and 8% biomass (dry weight % basis) with a plant size of 10,000 barrels per day located in West Virginia using indirect technology. For all cases, coal type is selected to be Illinois No. 6, while different biomass types are evaluated. Table 1.1 shows that the sensitivity studies have been conducted by considering different feedstock and configurations

For the indirect CBTL plant, following specific tasks have been performed:

- A comparison of the post-FT CO_2 capture technologies has been done to select the most economical technology for removing CO_2 from the FT vapor that includes light hydrocarbons and unconverted syngas.
- The impact of changes in the H_2/CO ratio on the utilities consumption, carbon efficiency, and product selectivity has been evaluated, which was not well addressed in the open literature for CBTL plant with CCS.
- A novel integrated hydrotreating approach has been considered for product upgrading, which has been considered in the open literature for petroleum refinery but not for FT syncrude.

For the direct CBTL plant, following specific tasks have been performed:

- A high-fidelity mathematical model has been developed for the three-phase ebullated bed direct liquefaction reactor in ACM.
- A comparison of capture technologies has been done to select the most economical technology for removing CO_2 from the stream at the medium pressure level containing light hydrocarbons and unconverted syngas. The extent of CO_2 capture from each CO_2 containing streams are optimally designed.
- Different hydrogen sources have been considered.

For the hybrid CBTL plant, following specific tasks have been performed:

- The product recovery and upgrading section has been optimally designed to upgrade syncrude from both direct and indirect liquefaction route to on-spec gasoline and diesel.
- Hydrogen network has been designed to satisfy the hydrogen requirement for both direct liquefaction reactor and hydrocarbon upgrading section.

In addition, techno-economic analysis focused on the following areas:

- A comprehensive estimate of the capital and operating costs have been made for the indirect, direct and hybrid CBTL plants.
- Various economic matrices such as the net present value (NPV), internal rate of return (IRR), and break-even oil price (BEOP) have been generated for all cases listed in Table 1.1.
- A number of sensitivity studies have been performed for all cases considering the process design criteria, market factors and governmental policies that would potentially affect the commercial success of a CBTL plant in West Virginia. Sensitivity studies include, but are not limited to, process operating conditions, environmental performance criteria, plant location and capacity, and investment parameters.

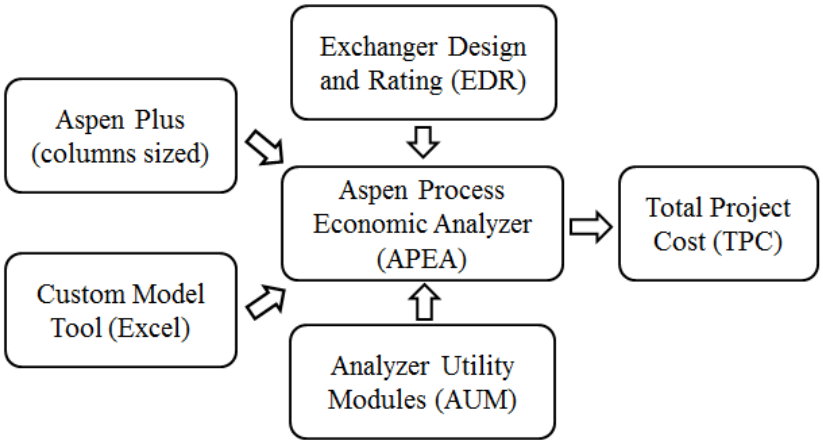

Figure 1.1 Procedural of techno-economic analysis in multi-software environment

Table 1.1 Summary of case studies

Case No.	Liquefaction	Biomass type	Hydrogen source	Carbon capture
1	indirect	wood chip	N/A	Yes
2	indirect	wood chip	N/A	No

3	indirect	torrefied wood	N/A	Yes
4	indirect	bagasse	N/A	Yes
5	direct	wood chip	gasification	Yes
6	direct	wood chip	gasification	No
7	direct	wood chip	SMR	Yes
8	direct	wood chip	SMR	No
9	hybrid	wood chip	gasification	Yes
10	hybrid	wood chip	SMR	No

Chapter 2 Literature Review

2.1 Indirect Coal Liquefaction

In the ICL plant, the key technology is the FT synthesis. The FT technology, first introduced in 1920s and commercialized later on, is one of the most popular and mature technologies. The FT process can produce fuels using the syngas derived from coal, biomass, natural gas, or a combination of those feedstocks. Several commercial CTL and GTL FT plants were built in the last century. Many of these plants are still producing significant amount of transportation fuel. (Dry, 2002; Kreutz et al., 2008) In the ICL plant, coal is first converted into syngas in the gasification unit and then converted into syncrude by FT synthesis, which can be upgraded into on-spec transportation fuels.

Most of the existing works in the open literature consider that the syngas produced in the gasifier is sent to the FT reactor without adjusting the H_2/CO ratio mainly because the typical Fe-based FT catalyst catalyzes the water gas shift (WGS) reaction. (Bechtel, 1992) This strategy needs to be revisited if CO_2 compression is considered for storage. If the H_2/CO ratio is optimally adjusted by using WGS reactor(s) before the FT reactor, then a significant portion of CO_2 can be captured by using a physical solvent such as Selexol before the FT unit in the acid gas removal (AGR) unit due to higher partial pressure of CO_2. This can not only reduce the penalty for CO_2 capture, but can also reduce the duty for CO_2 compression as CO_2 can be flashed off by pressure swing at relatively higher pressure than the chemical processes. In the work of Liu et al. (Liu et al., 2011), a WGS reactor is used to increase the H_2/CO ratio from 0.67, which is the typical composition of coal-derived syngas, to about 1. According to Dry (Dry, 2002), the composition of syngas should match the overall usage ratio of H_2/CO in the FT reactors for increasing the plant efficiency. It can be noted that the typical inlet H_2/CO ratio of Sasol's low-temperature FT (LTFT) process is about 1.7. (Dry, 2002) Other studies show that syngas with H_2/CO ratio greater than 2 can greatly reduce the WGS (James et al., 2013) reaction on the Fe-based FT catalyst. However, a higher H_2/CO ratio at the inlet of the FT reactor can result in more methane

formation in the FT reactor decreasing the overall fuel yield. (Dry, 2002) Thus, the WGS reactor and the AGR unit before the FT unit should be optimally designed by considering the tradeoffs between fuel yield and penalty due to CO_2 capture and compression. (Reed, 2007; Larson et al., 2010)

In the ICL plant, as H_2/CO ratio in the FT inlet stream is increased, more light hydrocarbons are produced in the FT reactor. A portion of these light hydrocarbons can be used to produce gasoline through the C_3-C_5 Alkylation unit and C_4 Isomerization unit. However, consideration of these technologies may not be desired for small scale FT plants, because these technologies add to the complexity and are expected to have low temperature distillation systems with large penalty. (Bechtel, 1998; 1993) On the other hand, the light hydrocarbons can be either used as fuel gas in the process furnace, or sent to the combined cycle for power production, or recycled back to the FT reactor through an autothermal reformer (ATR) to produce syngas, which, in turn, increase the fuel yield. (Baliban et al., 2010; Jiang and Bhattacharyya, 2014) The ATR uses a combination of exothermic partial oxidation and endothermic steam reforming reactions usually on Ni/Al_2O_3 catalysts while operating at thermally neutral condition. (Rafiq et al., 2012) Many studies of ATR available in the open literature focus on the hydrogen production from natural gas or light hydrocarbons, which usually has a high steam/carbon ratio in the feed in order to obtain high H_2/CO ratio in the product. For the ICL application, with moderate H_2/CO ratio requirement in syngas, a low steam/carbon ratio can be used in the ATR unit to reduce the utility cost. (Steynberg and Dry, 2004) In some studies conducted for the FT application, ATR unit is modeled as equilibrium reactor in Aspen Plus. (Liu et al., 2011; Larson et al., 2010) Due to the key role that the ATR plays, a kinetic model is more appropriate for this unit especially when its feed composition vary widely.

The liquid product from the FT reactor is sent to the product upgrading section. In the conventional product upgrading section, syncrude is first separated into naphtha, diesel and wax and then sent to two different hydrotreating units and hydrocracking unit. Instead, integrated hydrotreating of the syncrude can increase the thermodynamic efficiency and reduce the footprint of the upgrading section. In the integrated hydrotreating unit, the entire syncrude is first hydrotreated and then separated into different products for further upgrading. There is hardly any

work in the existing literature on the use of an integrated hydrotreater for upgrading syncrude from the indirect process. It should be noted that integrated hydrotreating has been considered for upgrading of hydrocracked residuum petroleum crude oil (Cavallo et al., 2008), whole crude oil (Jarullah et al., 2012) and syncrude from coal direct liquefaction (Comolli et al., 1995). It is, therefore, reasonable to consider that integrated hydrotreating can also be applied to upgrading of the FT syncrude because the type of components, such as paraffin, olefin and oxygenate, carbon number and boiling point range of FT syncrude and the main desired reactions, such as hydrodeoxygenation, hydrodemetallization and hydrogenation of alkenes are similar to those in the applications cited before. (Comolli et al., 1995; Cavallo et al., 2008; Jarullah et al., 2012) In the open literature, some rigorous models have been developed for optimization and scaling up of the integrated hydrotreater based on the hydrodynamics, kinetics, heat and mass balance. (Jarullah et al., 2012) Other studies have considered simple correlations for estimating the performance of the conventional separated hydrotreating unit. (Fahim et al., 2010) For a plant-wide modeling aspect, a simplified yield model is required for the integrated hydrotreating unit, which can be simply integrated with other unit operation in Aspen Plus.

In the FT plant, the hydrotreated diesel can automatically satisfy most of the property specifications for commercial diesel. However, the straight run FT naphtha mainly contains n-paraffin, resulting in very low octane number, and needs to be further upgraded. The FT naphtha upgrading technology has been well described in the Bechtel reports (Bechtel, 1998; 1993) and has been considered in most of the recent studies on the FT plant. (Liu et al., 2011; Guo et al., 2011) In these designs, the isomerization unit increases the research octane number (RON) of the light naphtha to about 82-85 while the catalytic reforming unit increases the RON of the heavy naphtha to about 95-100. (Bechtel, 1993) Typical selection of technologies in commercial plants can also be found in the open literature. (Klerk, 2011; Klerk and Furimsky, 2010) However, as the gasoline and diesel specifications continue to change especially with respect to their environmental impacts, suitable technologies should be selected. For example, the designs considered in the Bechtel reports (Bechtel, 1998; 1993) can lead to violation of aromatics content in the gasoline pool (Guo et al., 2011) mainly due to large quantity of high aromatics-containing gasoline from the catalytic reforming unit. One of the alternative approaches is to apply the heavy naphtha isomerization technology that can increase the octane number of the straight run

heavy naphtha without producing aromatics. However, as the heavy naphtha is not only active for the isomerization reactions but also for the cracking reactions, the heavy naphtha isomerization technology will produce high amounts of fuel gas and reduce the overall gasoline yield. Previous studies indicate that with tolerable fuel gas production, the isomerization technologies can only increase the octane number to about 80-90. (Liu et al., 2011; Guo et al., 2011; Watanabe et al., 2008; Ramos et al., 2007) Therefore, as the key design parameters such as the H_2/CO ratio in the FT plant are changed, the product upgrading section needs to be appropriately designed in order to satisfy all specifications.

The H_2 required in the product upgrading section is considerable because the technologies, such as hydrotreating, hydrocracking, consume large amount of H_2 and operates under a H_2-rich environment. Moreover, hydrogen production is now under pressure as a result of recent rules of cutting down the GHG emission. (Jia, 2010) In the ICL plant, H_2 can be recovered from unreacted syngas and purged gas from the upgrading section, while the remaining gases can be sent to the combined cycle plant. The H_2 production and recovery units are expected to have a strong impact on the thermodynamic efficiency of the ICL plant. Hence, a good estimation of H_2 consumption is required for the efficiency analysis of the ICL plant.

In the ICL plant, the process fuel is supplied by the purged light gas and the unreacted syngas. The excess light gas and unreacted syngas can be sent to the combined cycle plant for electricity generation. An optimized heat recovery and steam generation (HRSG) unit can considerably increase the efficiency of the power plant. In recent years, a number of researchers have optimal designed the triple-pressure HRSG unit with reheat and evaluated the performance and efficiency of the integrated gasification combined cycle (IGCC) plant using steady-state simulation and analysis tools. (Chiesa and Lozza, 1999; Chiesa and Consonni, 1999; Kunze and Spliethoff, 2010, Bhattacharyya et al., 2011) In typical combined cycle power plants, the high pressure (HP) section pressure is higher than 140 bar and the exhaust steam from the HP section is reheated for power plant application. For the once-through CTL process, the HRSG unit can be designed similar to the IGCC plant described in the open literature. (Bhattacharyya et al., 2011) However, if a high amount of the FT gas is recycled, very little high temperature heat would be available for superheating the intermediate pressure steam produced due to the large FT exotherm

(Martelli et al., 2012) Unlike the IGCC plants, the fuel to the gas turbine in the ICL plant is mainly the off-gas produced from the refinery and FT synthesis, which is usually not a large quantity. Typical differences in the design of HRSG unit between the IGCC and ICL plants have been reported in the literature. (Steynberg and Nel, 2004; Martelli et al., 2012) In this study, the HRSG unit was designed especially for cases when a large amount of FT gas is recycled for higher fuel yield resulting in deficiency of high temperature heat, while the customized steam turbine was modeled using a rigorous stage by stage method. (Lozza, 1990)

2.2 Direct Coal Liquefaction

Even though the DCL technology is claimed to have higher thermal efficiency than the ICL technology (Williams and Larson, 2003), most published studies on systematic analysis of synthetic fuel processes focused on the ICL technology instead of the DCL technology. (Baliban et al., 2011; Liu et al., 2015; NETL, 2007) For improving the performance and economics of the DCL process, there has been strong focus on design and optimization of liquefaction reactor, separation system, and hydrogen production. Instead of the earlier single-stage liquefaction reactors, two-stage liquefaction technology has been developed. (Vasireddy et al., 2011) Compared to the single-stage technology, the two-stage technology results in higher solid conversions and liquid fuel yield as well as lower heteroatom content and hydrogen consumption. (Shui et al., 2010) In the two-stage technology, the operating conditions of the two reactors in series are optimized for coal dissolution in the first-stage and hydrotreating/hydrocracking in the second stage. (Shui et al., 2010) The Shenhua DCL plant in Inner Mongolia, China, which is the only operating commercial scale DCL plant after World War II, has been developed based on the NEDOL process and the HTI's catalytic two-stage liquefaction (CTSL) process. (Mochida et al., 2014) Other than that, the Residual Oil Supercritical Extraction-Solids Rejection (ROSE-SR) process can be combined with the traditional vacuum distillation technology to increase the oil recovery in the separation system with lower utility consumption leading to higher process efficiency. (Comolli et al., 1995; Gearhart and Nelson, 1983) Separation of ash and unreacted coal from heavy liquids is difficult because of the small size of solid particles, the small difference in densities between solids and liquids, and the high viscosity and melting point of the liquids. In the ROSE-SR unit, a mixture of benzene, toluene, and/or xylene can be used as solvent near their critical temperature and pressure because of their high solubility of direct

liquefaction liquids. (Debyshire et al., 1984) The ROSE-SR process can recover 85-93% of the solvent as a supercritical fluid in the second stage settler saving about 40-50% of utility in comparison to evaporation. (Gearhart and Nelson, 1983) Furthermore, partial oxidation (POX) of residues from the vacuum distillation and ash containing carbonaceous solid can be used for producing hydrogen from liquefaction residues reducing need for external hydrogen requirement. (Vaezi et al, 2011; Najjar and Gates, 1990; Koseoglu, 2014) Since 1970's, Texaco Inc. has conducted a series of studies on the suitability of using coal liquefaction residues as feedstocks to entrained flow gasifiers where the liquefaction residues were fed into the gasifier as a molten fluid or water slurry. (Texaco, 1984; Robin, 1977)

Despite several efforts to increase the process efficiency of the DCL processes, the life cycle GHG emission for producing the DCL liquids is about double of that for producing them from the petroleum source (Vasireddy et al., 2011). In order to convert coal (H/C $\approx$ 0.8) to transportation fuels (H/C $\geq$ 1.8), we need to either reject carbon in form of CO_2 (i.e. ICL) or add hydrogen from external sources (i.e. DCL). (Jiang and Bhattacharyya, 2014; 2015; 2016; Vasireddy et al., 2011) In DCL plants, the H/C ratio is increased by adding gaseous hydrogen to a slurry mixture of coal and recycled coal-derived liquids, so-called H-donor solvent, at high temperature and pressure in presence of catalysts. Coal gasification technology has been applied in the commercialized Shenhua DCL plant for producing make-up hydrogen because of the relatively low cost and sufficient supply of coal in China. Mixtures of coal, biomass, and liquefaction residues can also be converted to syngas by co-gasification (CG). (Jiang and Bhattacharyya, 2014; Bechtel and Amoco, 1992) If natural gas is available locally with reasonable price, hydrogen can also be produced by steam methane reforming (SMR) with less GHG emission in comparison to coal gasificaiton. (Williams and Larson, 2003) Even though the conventional feedstock for the SMR unit is natural gas, due to abundant and cheap shale gas that is now available in the United States, shale gas is a potential feedstock in the SMR unit. However, because of the higher ethane and propane content in the shale gas in comparison to the natural gas, an adiabatic pre-reformer is preferred to convert ethane and propane before the main steam reforming reactor to prevent coke formation on reformer walls and catalyst surfaces. (Nagaoka et al., 2007; Yang et al., 2011; Christensen, 1996) It has been reported that the current commercial hydrogen production technologies, either gasification or SMR, are usually associated

with a large amount of CO_2 emission. A recent study shows that about 0.48 tonne of CO_2 is released per barrel of transportation fuels produced in the Shenhua DCL plant, where about 80% of CO_2 is produced in the gasification-based hydrogen production unit. (Vasireddy et al., 2011) The CTSL unit is the key section of the DCL process. In the CTSL unit, coal and biomass are mixed with hot recycle solvents in the slurry tank, preheated and then sent to two ebullated bed reactors in a close-coupled mode with recycled and make-up H_2 stream. (Valente and Cronauer, 2005) Because of the heavy oil produced from the second stage is recycled to form feed slurry and fed back to the first stage, the two stages are interrelated and treated as a single unit in this study. (Valent and Cronauer, 2005) The yield of liquids and their hydrocarbon distribution from the coal liquefaction reactors are estimated based on the operating data from the DCL proof-of-concept (POC) facility reported by HTI in 1995. (Comolli et al., 1995) The operating conditions in POC-01 Period 26 were recommended by HTI's study because of its higher efficiency and better operability, and therefore, are considered in our baseline study. (Comolli et al., 1995; Bechtel and Amoco, 1990)

In the Shenhua DCL plant, ebullated bed reactors (EBRs) are used in the CTSL unit. (Wu et al., 2015) The EBR is novel gas-liquid-solid three-phase reactors, which have been widely considered for the petroleum residue hydrocracking and hydrodesulphurization processes. (Martinez et al., 2010) The Shenhua DCL plant, the only commercial DCL plant under operating after World War II, also used EBRs for coal hydrogenation. EBRs are preferred in DCL process because of their small axial temperature distribution (backmixing), large reactor volume utilization (small gas holdup) and negligible solid precipitation (large superficial liquid velocity). (Wu et al., 2015; Robinson, 2009) The EBR is basically a slurry bubble column reactor (SBCR) in which the solid particles are held in suspension mostly by the upward movement of the liquid-phase rather than only the gas-phase as in a SBCR. In the EBR, part of the liquid from the reactor top section is collected in the recycle cup and then sent back to the reactor bottom by the ebullating pumps to achieve high liquid-phase velocity. Shan et al. and Jiang et al. reported an eight-lump kinetic models, which can be applied for both coal slurry pre-heater and CTSL reactors. (Shan et al., 2015; Jiang et al., 2015)

One advantage of DCL process is that the products can be processed as traditional petroleum product without extensive renewal of current infrastructures. (Vasireddy et al., 2011) Compared with typical petroleum oils, the DCL syncrude obtained from the two-stage liquefaction of bituminous coals is usually low in boiling range, low in hydrogen and high in oxygen, low in heteroatom contents and high in contents of cyclic compounds, and mainly composed of paraffins, naphthenes, and aromatics. (Shinn, 1984; Vasireddy et al., 2011; Mochida et al., 2014) On the other hand, the bio-liquids usually contain high amount of oxygenates, such as cyclic ketones, alkyl-phenols, methoxy-phenols, napthols, which can be converted to cyclohexane, alkyl-cyclohexane by hydrotreating. (Stevens, 1987; Elliott, 1980; Behrendt et al., 2008) Despite these differences, the syncrude produced in the direct liquefaction plant with only coal or low biomass/coal ratio is very similar to petroleum and can be processed through petroleum refining technologies, where hydroprocessing is a major technology. (Zhou and Rao, 1992)

2.3 Coal Biomass Co-Processing

It is reported that the life cycle CO_2 emission of fuels from a conventional CTL plant is roughly twice of that of fuels from petroleum. (Bartis et al., 2008; Edwards, 2011) Recently, wide interests in CBTL fuel process are being catalyzed by the relatively low prices of coal and carbon-neutrality of biomass. (Larson and Jin, 1999; Wang et al., 2009) Biomass is a carbon-neutral feedstock, because the CO_2 released to the atmosphere is reutilized by biomass. Adding moderate amounts of biomass to coal for liquids production can substantially reduce the carbon footprint of CBTL processes. (Liu et al., 2011; NETL, 2009)

In the indirect CBTL (I-CBTL) processes, both coal and biomass are fed to the gasification unit to be converted into syngas. Typically two separated gasifiers are considered for the I-CBTL plant- one for coal, and the other for biomass. (Liu et al., 2011; Baliban et al., 2011) However, both large-scale slurry-fed (GEE-Texaco type) and dry-fed (Shell-type) entrained-flow gasifiers as well as some fluidized bed gasifiers (IGT-type) have successfully handled coal mixed with moderate amount of biomass. Because biomass gasification technology is limited to smaller scale application (Long and Wang, 2011), applying a co-gasification technology can utilize biomass in large scale gasification plants with less number of trains, making the I-CBTL process more compact and economical. In this paper, we have developed and validated a yield model for

coal-biomass co-gasification process. A study is also conducted to demonstrate the effect of biomass/coal ratio on the syngas composition and downstream processes.

Instead considering two separate gasifiers, one for coal and the other for biomass, applying co-gasification technology can reduce the footprint and capital cost of the syngas production unit. However, because of the significant difference in physical and chemical properties between coal and biomass, it is critical to study the properties of coal and biomass and apply thermal pretreatments, especially torrefaction, to convert biomass to a more homogeneous and energy-dense solid, which has properties similar to coal. (Batidzirai et al., 2013) Torrefaction is a pretreatment method where biomass is subjected to moderate heating (200-300 ^{o}C) in a low oxygen environment. Other than reducing feedstock variability and improving energy density, biomass torrefaction can also reduce the penalty of biomass storage, transportation and grinding, an reduce the O/C ratio in biomass and therefore increase the H_2 and CO yield in the gasifier. (Prins et al., 2006; Couhert et al., 2009) Even though torrefaction technology can improve the properties and thermal behavior of biomass, the process itself is energy and capital intensive. Batidzirai et al. indicated that the production costs for torrefied woody biomass are ranging from 2.3 to 4.8 US$/GJ$_{HHV}$ for short term production and from 2.1 to 5.1 US$/GJ$_{HHV}$ for long term production. (Batidzirai et al., 2013) Associated technical and economic challenges proved the technology from fully commercialized. Hence, it is important to systematically analyze the economic and thermal performance of torrefied biomass in the I-CBTL plant with CCS. Because the capital investment, thermal and mass efficiency, and product performance of the torrefaction process strongly depend on the raw biomass properties and the operating conditions. In this study, hardwood torrefied at 270 ^{o}C is selected as the alternative feedstock. (Ibrahim et al., 2013) As reported, the mass efficiency of the torrefaction process with the specified operating condition of this study is 71.6 % (dry basis). (Ibrahim et al., 2013) Considering the capital cost, the price of torrefied biomass is set to be $140/dry tonne for the techno-economic analysis. (Batidzirai et al., 2013)

In the direct CBTL (D-CBTL) processes, a small amount of biomass can be co-fed with coal to the direct liquefaction reactors in order to reduce the GHG emission. (Stiller et al., 1996; Rafiqul et al, 2000; Comolli et al., 1994) Several experimental studies have been conducted on coal-

biomass co-liquefaction. (Rafiqul et al., 2000; Tchapda and Pisupati, 2014; Shui et al., 2011) Some researchers have reported that co-liquefaction of biomass and coal under mild condition (about 350^{o}C) has higher conversion and oil yield than those that would be predicted based on a simple linear combination of the conversion and oil yield of liquefaction of biomass and coal independently. (Tchapda and Pisupati, 2014; Coughlin and Davoudazdeh, 1986) This could be a result of the difference in the thermal rupture temperature between coal and biomass. Biomass has a higher conversion and lower thermal rupture temperature than coal, and can produce free radicals at lower temperature to promote the reaction of coal. (Shui et al., 2011) However, the synergistic effect reduces with the increasing temperature and pressure, as -the reactivity of coal increases. (Shui et al., 2011; Anderson and Tuntawiroon, 1993) Ai performed a series of preliminary studies on co-processing of Shenhua coal and Sawdust at 450^{o}C, which is similar to the operating conditions in the commercial DCL reactors, and observed that presence of sawdust resulted in apparent improvement of coal conversion. (Ai, 2007) Their study also shows that because of the higher H/C ratio of biomass compared to that of coal, the hydrogen consumption in the direct liquefaction plant and CO_2 emission associated with hydrogen production can be reduced by increasing the biomass content in the system. (Ai, 2007) However, the D-CBTL process has been barely modeled in details at either equipment-level or system-level especially with a focus on reduction of GHG emission from this process. Most of the modeling works available in the open literature focus on the indirect approach to coal-biomass co-liquefaction. (Jiang and Bhattacharyya, 2014; 2015; 2016; Baliban et al., 2011; Liu et al., 2015) Numerical modeling of both liquefaction and hydrogen production sections as part of the D-CBTL technology can be helpful in reducing GHG emission and improving thermal efficiency of this technology.

2.4 Carbon Capture and Storage

Most of the CTL pilot and commercialized plants built in last century do not consider CCS. Deployment of suitable CCS technologies can reduce the carbon footprint of CTL/CBTL processes significantly. (Edwards, 2011) In the ICL and I-CBTL processes, CO_2 is generated not only in the gasification unit but also in the FT unit. CO_2 produced by the Fe-based FT catalyst is quite high because of the higher water WGS reaction activity of the Fe-based catalysts in comparison to the Co-based catalysts. Even for H_2/CO ratio as high as 2.1, the CO_2 selectivity is

still around 10-15 mol% of total carbon on Fe-based catalysts. (Warzel, 2006) To reduce the recover the valuable products, CO_2 must be removed from both the gasification unit and the FT unit. In the AGR unit after the gasifier, H_2S is also captured in addition to CO_2 to protect the downstream catalysts. The CO_2 capture unit after the FT unit removes CO_2 from the FT reactor effluent.

For the AGR unit in the ICL and I-CBTL processes, physical absorption can be feasible because of the high partial pressure of CO_2 is high. Physical absorption is preferred because of lower penalty for CO_2 capture in comparison to the chemical solvents. For example, the heating requirement in the stripper when the physical solvent Selexol is used for CO_2 capture is only 25% of that when the chemical solvent MEA (30 wt%) is used. (Bechtel, 1992) If a physical solvent is used, CO_2 can be released simply by pressure swing at different pressure levels. Therefore, the CO_2 compression penalty can be greatly reduced. (Bhattacharyya et al., 2011) Selexol and Rectisol (chilled methanol) are two widely-used physical solvents. Rectisol has been considered in the work of Liu et al. (Liu et al., 2011), while a dual-stage Selexol unit has been considered in a study published by the National Energy Technology Laboratory (NETL, 2007).

For CO_2 capture after the FT process, typically a chemical solvent is used. The chemical solvents such as the amines offer higher selectivity and therefore result in negligible loss of hydrocarbons. (Bechtel, 1992) The secondary and tertiary amines are more suitable where the partial pressure of CO_2 is high. In addition, the secondary and tertiary amines have lower solvent loss, lower heating requirement, and lesser corrosivity than the primary amines. (Kohl and Nielsen, 1997) On the other hand, the physical solvents have significantly higher solubility of hydrocarbons that can lead to loss of valuable products. However, the utility requirement is much less in comparison to the chemical solvents. Even though the amine-based technologies are usually used for post-FT CO_2 capture (Bechtel, 1992), the appropriate technology, physical or chemical, should be selected by comparing the combined energy penalty due to loss of hydrocarbons and utility of each candidate technology for the same extent of CO_2 capture. For a fair comparison, each capture technology should be appropriately designed to minimize the loss of energy. For example, intercooling of the solvent in the absorber can be considered to reduce the energy penalty. (Kohl and Nielsen, 1997; Xu et al., 1998)

Appling CCS technology to the FT plant can significantly reduce the carbon footprint at the cost of considerable increase in capital and operating costs, which can significantly affect the economic feasibility of the technology. In the existing literature, most studies on modeling and optimization of different CCS technologies have been done from the perspective of power plant application (Bhattacharyya et al., 2011; NETL, 2010). Even though some outstanding studies have been conducted for the FT plant with CCS (Liu et al., 2011; Reed, 2007; Larson et al., 2010), the impact of key global design parameters such as the H_2/CO ratio in the FT inlet stream is not evaluated. Hence, further studies are required for a better understanding of the impact of those global design parameters when the product upgrading section and the combined cycle power plant is considered for an I-CBTL plant producing on-spec transportation fuel.

In the DCL and D-CBTL processes, significant amount of CO_2 is generated for producing H_2 irrespective of whether gasification or SMR technology is used. The CO_2 present in the product stream from these processes (or from the downstream of the WGS reactors, if used) has to be removed to produce high-purity hydrogen even if CCS is not considered. Additional CO_2 might need to be captured if considering high extent of CCS. In most commercial plants, CO_2 is typically captured by physical or chemical absorption. (Kohl and Nielsen, 1997) In the chemical absorption processes, the main utility consumption is in the reboiler of the solvent stripper. In the physical absorption process, the solvent can be simply recovered by pressure swing, but solvent chilling may be necessary leading to signification utility consumption. The selection of the appropriate technology mainly depends on the CO_2 partial pressure (P_{CO_2}), extent of CO_2 capture, other components present in the stream. If P_{CO_2} in the stream to be treated is high enough to provide sufficient driving force and concentration of hydrocarbon is low, physical absorption is preferred because it is energy-efficient and the captured CO_2 is released at relatively high pressure (HP) resulting in lower power consumption in the downstream CO_2 compressor. Otherwise, chemical absorption process is preferred for CO_2 removal, where CO_2 is typically released at low pressure (LP), because the stripper pressure is limited by the solvent decomposition temperature. (Kohl and Nielsen, 1997) For example, the physical absorption technologies (i.e. Selexol, Rectisol) are preferred for pre-combustion CO_2 capture from the syngas generated by the coal gasification mainly because of high P_{CO_2} and lack of hydrocarbons

while chemical absorption technologies (i.e. MEA, MDEA) are preferred for the post-combustion CO_2 capture from the low pressure flue gas. (NETL, 2010; Liu et al., 2011; Bhattacharyya et al., 2011) Even though, large number of studies have been conducted on selection of CCS technologies for different CO_2-producing technologies, such as the FT technology (NETL, 2007), IGCC (Bhattacharyya et al., 2011), pulverized coal combustion and natural gas combined cycle (NGCC) (NETL, 2010), not much studies have been conducted on selection of technologies for CCS in the direct liquefaction technology.

2.5 Techno-Economic Analysis

Both the ICL processes using FT synthesis as well as the DCL processes using CTSL technology have been commercialized in the last century. (Steynberg and Dry, 2004; Vasireddy et al., 2011) The synthetic fuels produced via the both ICL and DCL route can be upgraded to have similar properties as fuels produced from petroleum crude and therefore can be directly used in the current gasoline and diesel engines with no modification. However, uncertainty in the economic feasibility and high CO_2 emission are the two major reasons preventing the deployment of either ICL or DCL plants in the United States. (Liu et al., 2011; Baliban et al., 2010; Bartis et al., 2008) Addition of moderate amount of biomass to the feed and inclusion of CCS processes can reduce the environmental footprint of CTL plants, but at the cost of higher capital investment and larger operational penalty. (Liu et al., 2011; Williams and Larson, 2003; Tchapda and Pisupati, 2014; Wu et al., 2012; NETL, 2007c)

For improving the overall economics of the CBTL plant with CCS, techno-economic studies can be very helpful. Bechtel Corporation conducted baseline design and economic analysis for ICL plants and in direct biomass to liquids (BTL) plants with different types of coal and different product upgrading strategies (Bechtel, 1998) However, carbon capture technologies have not been considered in these studies. Several studies have been conducted by the U.S. DOE's National Energy Technology Laboratory (NETL) such as feasibility studies for a large scale ICL plant with CCS (NETL, 2007a), a small scale ICL plant without CCS (NETL, 2007b) and a small scale I-CBTL plant with CCS (NETL, 2009). The National Renewable Energy Laboratory (NREL) conducted a techno-economic analysis for an indirect BTL plant without CCS. (NREL, 2010) Liu et al. conducted a performance and cost analysis by considering different plant

configurations for the CTL, BTL and CBTL plants such as with or without CCS and light gas recycle stream. (Liu et al., 2011) Baliban et al. conducted a comprehensive economic analysis for different process alternatives for production of FT liquids from coal, biomass, and natural gas. (Baliban et al., 2010)

It needs to be pointed out that the straight run syncrude from the FT reactor usually contains a significant amount of heavy wax, and the naphtha cut has relatively low octane number which cannot satisfy the current specification of gasoline. Hence, the product upgrading unit is necessary for a FT plant producing on-spec transportation fuels. Hydrocracking, hydrotreating, isomerization and catalytic reforming are the most commonly considered technology for upgrading FT liquids. (Bechtel, 1998b; Bechtel, 1993a) For maximizing one of the products (mainly gasoline, diesel, and jet fuel), technologies such as oligomerisation, aromatic alkylation, M/ZSM-5 aromatisation can be considered. (Klerk, 2011; Klerk and Furimsky, 2010) For a small scale FT plant, the desired refinery configuration should be simple to keep the capital investment reasonable. (Bechtel, 1998b)

As mentioned before, the CO_2 emission of the CBTL plants can be significantly reduced by applying CCS technologies. Liu et al. selected the Rectisol process for both pre- and post-FT CO_2 removal for the ICL or I-CBTL processes (Liu et al., 2011). Dual-stage Selexol and MDEA units have also been considered for pre- and post-FT CO_2 removal (NETL, 2007). H_2 from carbonous and non-carbonous sources has been added into the CTL, BTL and CBTL processes to avoid CO_2 generation in the FT plant. (Baliban et al., 2010) In the studies discussed above, selection of the CCS technologies has been done without systematically considering the capital expenditure (CAPEX) and operating expenditure (OPEX) of the candidate technologies. Studies conducted by Bechtel Corporation have compared several technologies for post-FT CO_2 removal, such as Rectisol, Ryan-Holmes cryogenic distillation, MEA, and inhibited MDEA (Bechtel, 1992), where the captured CO_2 is directly vented into atmosphere as CO_2 storage or utilization is not considered in that study. In the previous studies conducted by our group for CBTL plants, high fidelity models of various CCS technologies were developed for technology selection and optimization (Jiang and Bhattacharyya, 2014; Jiang and Bhattacharyya, 2015) for minimization

of utility consumption. However, the capital investment is not considered in those studies and needs to be addressed for fair comparison.

Techno-economic analyses conducted for FT processes have been mainly done by changing the plant configuration (Baliban et al., 2010; Liu et al., 2011), or some investment parameters (Baliban et al., 2010; NETL, 2007a; NETL, 2007b). There is hardly any techno-economic analysis of CBTL plants in the existing literature where the effect of the key design parameters has been studied while keeping the plant configuration the same. In the existing studies on FT plants with CCS (Liu et al., 2011; NETL 2007a; Niziolek et al, 2014), values of the key design variables are kept unchanged in comparison to the FT plants without CCS. However, the plant performance strongly depends on those key design parameters, such as biomass/coal ratio, H_2/CO ratio in the FT inlet stream, extent of CCS. (Jiang and Bhattacharyya, 2015) As an example, the typical H_2/CO ratio at the inlet of the FT reactor for iron-based catalysts is 2:1 (mol/mol) for the conventional CTL plants without CCS, while previous study of our group indicates that the overall utility consumption can be reduced by increasing the H_2/CO ratio in the FT inlet stream for the CTL plants without CCS. (Jiang and Bhattacharyya, 2015) However, final design decisions can only be taken by performing techno-economic analysis.

Even though several studies are conducted for the ICL processes, the same ideas should also work for the DCL processes in general. Unlike the ICL process, very less CO_2 is generated in the liquefaction reactor. However, significant amount of hydrogen is required in the process, which is associated with CO_2 releasing. (Jiang and Bhattacharyya, 2016a) It is reported that the capital investment in and CO_2 emission from the Shenhua DCL plant with coal-derived hydrogen and a capacity of 16,300 bbl/day are about $1.46 billion (reported in 2008) and 0.48 tonne CO_2 per barrel liquids. (Vasireddy et al, 2011; Williams and Larson, 2003; Robinson, 2009; Wu et al, 2015) Claimed by multiple researchers, DCL processes may have better economic performance than ICL processes due to their higher thermal efficiency. (Jiang and Bhattacharyya, 2016a; Williams and Larson, 2003) Robinson et al. claims that the economic performance of DCL and ICL process are similar. (Robinson, 2009) However, there is hardly any techno-economic study of the DCL technology conducted by using rigorous process and economic models especially when considering CO_2 capture, biomass co-processing and different H_2 sources. Most of the techno-economic studies in the open literature were conducted for the ICL processes, IGCC

plants and coal-firing power plants rather than DCL processes. (Jiang and Bhattacharyya, 2014; 2015; 2016; NETL, 2007; Baliban et al., 2011; Liu et al., 2015) Due to the difference in the conversion mechanisms, CO_2 emission sources, and process configurations, the effect and penalty of adding biomass and CCS are expected to be different between those two liquefaction approaches. Those effects and penalty can only be disclosed based on a rigorous techno-economic analysis of relevant processes, which has not been done in the open literatures.

As mentioned in Section 2.3, several experimental studies have been conducted for co-processing coal and biomass using direct liquefaction processes (Rafiqul et al., 2000; Tchapda and Pisupati, 2014; Shui et al., 2011), but those processes have been barely modeled at either equipment-level or system-level. CCS technologies have been widely studied and embedded in the ICL process (NETL, 2007), IGCC process (Bhattacharyya et al., 2010), pulverized coal combustion and NGCC process (NETL, 2010), but not yet in DCL processes. Even though some preliminary economic feasibility studies have been conducted for DCL processes, but none of those studies were embedded with CCS technologies. (Bechtel and Amoco, 1992) From those studies, physical absorption and chemical absorption are two most commonly considered technologies. The selection of technologies mainly depends on the CO_2 partial pressure and relative selectivity of CO_2 compared with other components in the streams to be treated. (Kohl ad Nielsen, 1997; Bechtel, 1993)

As mentioned before, the carbon footprint of the energy conversion processes can always be reduced by adding biomass and applying CCS technologies at the cost of higher operating and capital investment. In order to promote the development and commercialization of those more sustainable processes, government subsidies, such as tax benefits, carbon tax and other environmental credits, are being offered in a number of countries or areas. (Jiang and Bhattacharyya, 2016c) For example, US government provides residential renewable energy tax credit to household using solar, wind, geothermal and some other renewable energy sources. (DSIRE, 2016) What's more, the product price of a power plant with one of the Renewable Energy Certificates can be about $2/MWh to $15/MWh higher than the average marketing values. (EERE, 2016) Another widely mentioned credits in this area is carbon credit or carbon tax, a generic term defined for GHG emission trading approach. A carbon tax is a specific price

the government charges for carbon content in fuels ranging from $15 to $30 per ton in most proposals. With this idea, the captured CO_2 can be traded as product in the carbon-constrained market subject to carbon tax. Even though the idea of carbon tax has not been applied yet, and the regulations of renewable energy and other potential credits have not been set up for the facilities like CBTL by now, it is possible that the CBTL plants with CCS can take some of the environmental credits just like other renewable or alternative energy system.

Chapter 3 Modeling of an Indirect Coal-Biomass to Liquids Plant

3.0 Overview

The net GHG emissions of conversional FT synthetic fuels derived from coal are about double of those from petroleum fuels. Adding moderate amounts of biomass to coal can substantially reduce the carbon footprint of the indirect fuel production plant. The indirect CBTL technology with CCS is more environmental friendly than the conventional ICL processes. This chapter focuses on the selection of CCS technologies and obtaining their optimal operating conditions for a CBTL plant. A detailed process model is developed in Aspen Plus V7.3.2 for this purpose. In this plant, syngas is produced in the biomass/coal-fed co-gasifier. Then, a sour WGS reactor converts a portion of the CO in the syngas to CO_2 to obtain the desired H_2/CO ratio in the syngas feed to the FT unit. Substantial amount of CO_2 is captured before the FT reactor by using a dual-stage, selective physical solvent-based process. In the FT unit, the Fe-based catalyst is used in the LTFT slurry reactor to convert syngas to hydrocarbons. For selection of the post-FT CO_2 capture technology, three candidate technologies- Selexol, MEA and MDEA/PZ, are evaluated. The results show that the MDEA/PZ technology with intercooling has the lowest overall penalty. A simple configuration is considered for product upgrading to satisfy the product specification in a small scale liquefaction plant, where a novel integrated hydrotreating approach is proposed and modeled. This technology is compared with the conventional separate hydrotreating approach. In addition, the impact of H2/CO ratio, biomass/coal ratio, CCS technology selection and the extent of CCS on key performance measures are investigated in this paper.

In summary, following works are presented in this chapter. (1) A detailed process model of an indirect CBTL plant with CCS has been developed. The focus is on technologies, configurations, and process operation that can produce higher amount of syncrude with less utility consumptions and low GHG emission. (2) Studies are conducted on the impact of the biomass/coal feed ratio on the overall process thermal efficiency. (3) The Selexol based CO_2 capture process is optimally designed for CO_2 capture before the FT process to obtain about 90% carbon capture in the CBTL plant producing raw syncrude. (4) A comparison of the CO_2 removal technologies applied after

the FT synthesis block is done to select the most economical technology for removing CO_2 from the FT product. The three solvents considered are Selexol, MEA, and MDEA/PZ. Intercooling is considered for the amine-based processes. (5) A sensitivity study is conducted to determine the optimal pressure level of flash vessels in the Selexol unit. (6) A sensitivity study is conducted to evaluate the effect of the lean solvent loading on the performance of the MDEA/PZ based CO_2 removal process with intercooling. (7) The impact of changes in the H_2/CO ratio on the utilities consumption, carbon efficiency, and product selectivity is evaluated. (8) A simplified product upgrading section is considered for small scale application to produce on-spec fuel with reasonable yield. (9) A novel integrated hydrotreating approach is considered for FT product upgrading, which has been considered for petroleum refinery but not for FT syncrude in the open literature. The model is developed based on the atom balance and the plant performance data available in the open literature, and can be easily integrated with other unit operation of indirect CBTL plant in Aspen Plus.

3.1 Conceptual Design and Modeling

The block flow diagram (BFD) of the indirect CBTL plant with CCS (I-CBTL-CCS) is shown in Figure 3.1. In the I-CBTL plant, syngas is produced in a gasifier co-fed with coal and biomass slurry and oxygen produced in an air separation unit (ASU). (Jones et al., 2011) After scrubbing, the syngas is split between a single stage sour WGS reactor unit such that a desired H_2/CO ratio of the clean syngas is achieved at the inlet of the FT reactor. (Jiang and Bhattacharyya, 2014) Due to presence of the gasifier and availability of the syngas at high pressure, the authors considered it appropriate to set the environmental targets at par with the integrated gasification combined cycle (IGCC) plants. (NETL, 2010) Therefore, the SO_2 emissions target was set at 0.0055 kg/ GJ. The WGS catalyst also causes almost complete hydrolysis of carbonyl sulfide (COS) to form H_2S that is then captured in the AGR unit. A separate COS hydrolysis unit is considered for the stream that bypasses the WGS reactor for satisfying the overall SO_2 emissions target. The dual-stage Selexol technology is selected for the AGR unit to remove H_2S and CO_2 selectively. (Bhattacharyya, et al., 2011; Jones et al., 2012) H_2S is separated in the first stage of the Selexol unit and sent to the Claus unit for converting it to elemental sulfur. (Bhattacharyya, et al., 2011; Jones et al., 2012) In the second stage, CO_2 is separated and sent to the compression unit before sending it for sequestration. (Bhattacharyya, et al., 2011) In the LTFT reactor, the

clean syngas from the Selexol unit and the recycled gas from the ATR unit are converted to syncrude. The vapor phase product is sent to the post-FT CO_2 removal unit where MDEA/PZ is used as the solvent. (Jiang and Bhattacharyya, 2014) Removed CO_2 is sent to the CO_2 compression unit for sending it through the pipeline for sequestration. A significant portion of the vapor product from the FT reactors is sent back to the FT reactor through the ATR, while the remaining portion is sent to a pressure swing adsorption (PSA) unit to satisfy the H_2 requirement for the product upgrading section. The liquid products are sent to the product upgrading section, shown in Figure 3.2, to produce on-spec gasoline and diesel. The sour water and black water produced in the process are treated and recycled back to the coal-slurry preparation section and to the scrubber for quench (NETL, 2010). The sour water stripper (SWS) is a major consumer of the stripping steam. Part of the off-gas from the entire process is used as utilities, while the remaining portion is used in a combined cycle plant. The combined cycle plant uses a gas turbine integrated with the HRSG unit that operates under three different pressure levels.

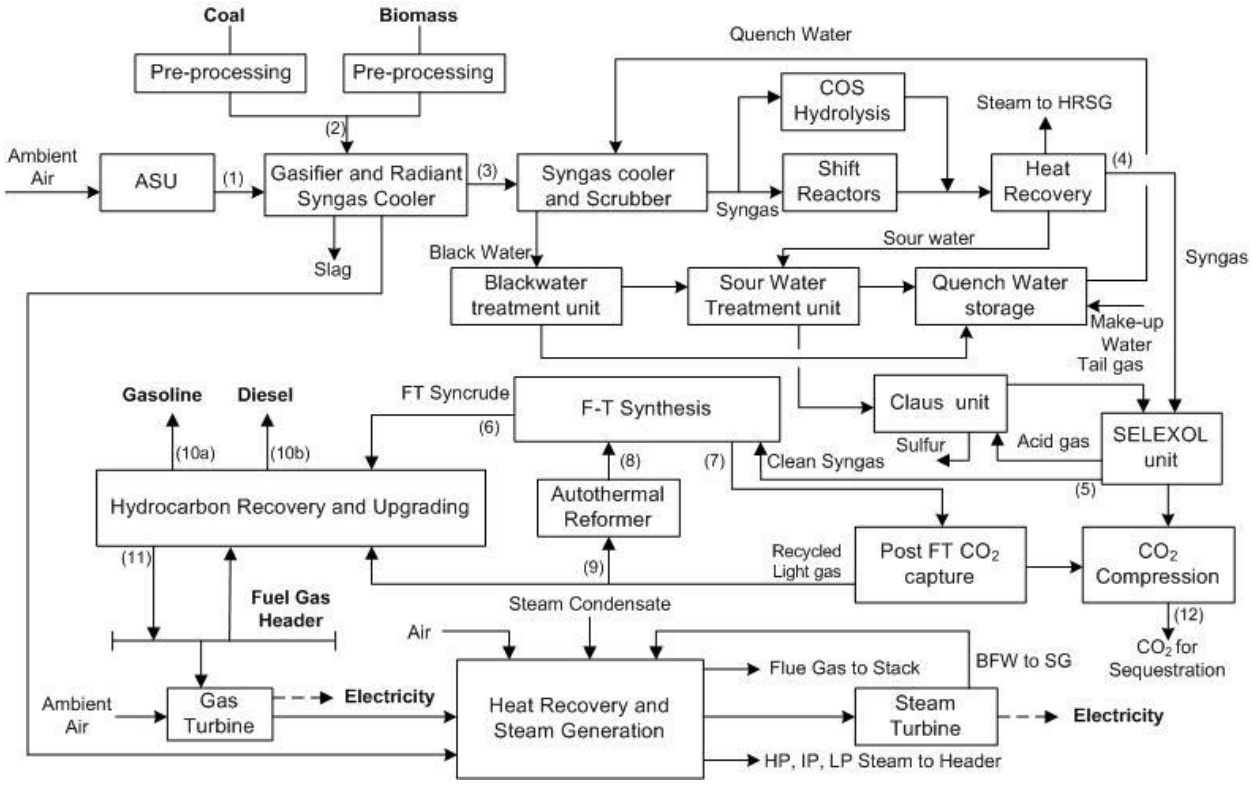

Figure 3.1 BFD of the I-CBTL-CCS plant (base case)

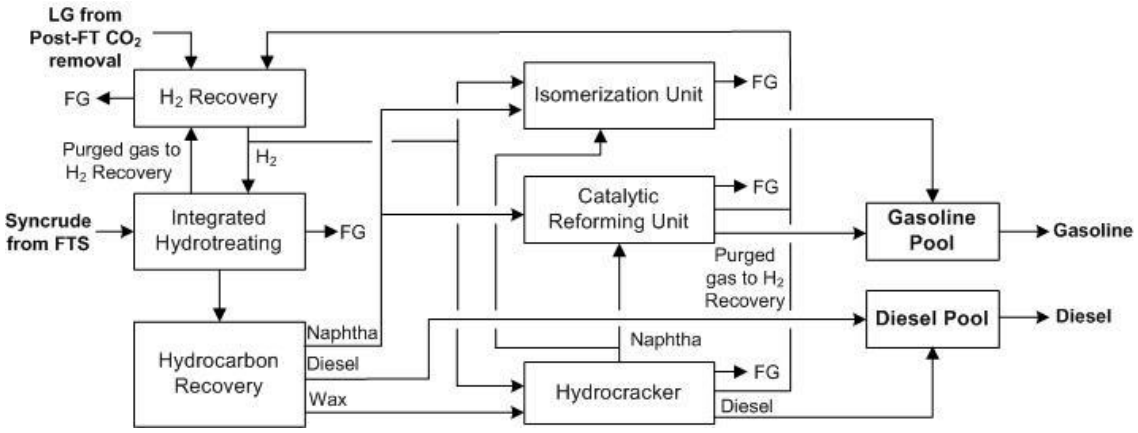

Figure 3.2 BFD of the novel product upgrading section in the I-CBTL plant

In the product upgrading section, a novel integrated hydrotreater is proposed. This integrated hydrotreater is expected to have a higher process thermodynamic efficiency and more compact design than the traditional approach. The light gases and H_2-rich stream from the product upgrading section are sent to the PSA unit to produce pure H_2 for hydroprocessing. A hydrocracking unit is used to produce naphtha and diesel from wax. A combination of the isomerization unit and catalytic reforming unit is considered for satisfying the current specifications for gasoline. (Klerk, 2011)

The plant-wide model is built in Aspen Plus V7.3.2. Models of individual sections are developed based on the experimental or operational data, whenever available, in the open literature. If yield models are developed for a unit/section in Excel, then Aspen User2 Blocks are used to integrate that with the Aspen Plus models of other unit operations. A stage-by-stage calculation of steam turbine expansion line is coded in Matlab to obtain a more accurate estimation of the power output from the steam turbine at different operating conditions. The proximate and ultimate analysis of Illinois No.6 coal and different types of biomass used in this study can be found in Table 3.1. (Jiang and Bhattacharyya, 2014; 2015; 2016; Bhattacharyya et al., 2011; Bain, 1992; Ibrahim et al., 2013)

Table 3.1 Proximate and ultimate analysis of coal and biomass feedstock

	Proximate analysis (dry basis)				Ultimate analysis (dry basis)					
	M	FC	VM	A	A	C	H	N	S	O

Coal	3.08	50.65	37.85	11.50	11.50	71.00	4.80	1.40	3.20	8.00
Wood chip	9.58	16.55	82.51	0.94	0.94	48.51	6.17	0.12	0.04	44.22
Bagasse	10.60	14.80	82.10	3.10	3.10	47.90	6.20	0.60	0.01	42.19
Torrefied wood	3.80	70.85	27.55	1.60	1.60	58.40	5.70	0.08	0.02	35.80

3.2 Syngas Production

In the syngas production section, coal and biomass is co-gasified to form raw syngas, which is sent to the heat recovery section followed by the WGS unit and the AGR unit to produce clean syngas with the H_2/CO ratio desired in the downstream FT unit.

3.2.1 Co-Gasification

The technology for co-gasifying coal and moderate amount of biomass is nearing commercialization. (Liu et al., 2011) In the base case, the feed to the gasifier contains 92 wt% of Illinois No. 6 coal and 8 wt% of wood chip (dry basis). The coal-biomass co-gasifier is simulated by combining a reactor model for coal gasification based on minimization of the Gibbs free energy with a yield model for biomass gasification, with the assumption that the interaction between coal and biomass is negligible due to the low biomass to coal ratio and the yield of the co-gasifier is a linear combination of these two model. This assumption is consistent with experiment done by Andre (Andre et al., 2005), which shows an approximate linear correlation between syngas composition and biomass to coal ratio. The reactor model for coal gasification has been developed by considering restricted equilibrium and has been reported by our group previously (Bhattacharyya, et al., 2011) since the WGS reaction catalyzed by the ash as well as the uncatalyzed WGS reaction continue till the reaction is quenched. (Kasule et al., 2012) The yield of each species for biomass gasification is generated by the following correlation, $y = A + BT + CT^2$, that has been developed for the fluidized bed IGT gasifier. (Bain, 1992) In the work of Bain, the values of the parameters *A*, *B*, and *C* have been determined from the regression analysis of the experimental data available for a biomass gasifier operating between 754-982 ^oC at 2300 kPa. In this work, for satisfying the elemental balance the MGAS model of Syamlal and Bisset (Kasule et al., 2012; Syamlal and Bisset, 1992) is used to obtain the final yield of major gas components from the proximate and ultimate assays, tar and char compositions, and

preliminary prediction of product distribution from temperature correlation shown above. Table 3.2 compares the results from our model for biomass gasification with the experimental data (Bain, 1992) obtained at 830 ^{o}C. As seen in Table 3.2, the model is satisfactory.

Table 3.2 Validation of the yield model developed for biomass gasification

Gas (mol%)	Experimental	Our Model	error%
CO	8.73	9.26	-6.14
CO_2	21.31	20.35	4.50
CH_4	8.41	7.69	8.56
H_2	17.07	15.91	6.77
H_2O	43.20	45.72	-5.82
NH_3	0.48	0.48	0

3.2.2 Heat Recovery and Water Gas Shift

The syngas from the gasifier goes to the radiant syngas cooler (RSC) to generate HP steam, which can be sent to the HRSG section for superheating for power generation. As shown in Figure 3.3, syngas is then sent to the scrubber where quench water is used to decrease the temperature of the syngas to the desired value. (Bhattacharyya et al., 2011) After scrubbing, a portion of the syngas enters an adiabatic sour WGS reactor, while the remaining portion enters a COS hydrolysis unit. The reversible WGS reaction is shown in Reaction (3.1) with the kinetics given by Eq. (3.2) for a cobalt molybdenum-based catalyst, which is a sour WGS catalyst. (Bhattacharyya et al., 2011; Overstreet, 1974; Berispek, 1975) The equilibrium constant is given by Eq. (3.3) (Bhattacharyya et al., 2011). The WGS reactor is modeled as an adiabatic plug flow reactor (PFR) in Aspen Plus.

$$CO + H_2O \leftrightarrow CO_2 + H_2 \tag{3.1}$$

$$-r_f = 2.6 \times 10^4 \exp\left(-\frac{E_f}{RT}\right)[CO]\frac{kmol}{m^3 s} \tag{3.2}$$

$$K_{eq} = \exp(-4.33 + \frac{8240}{T}) \quad for\ 1060 \le T \le 1360 \tag{3.3}$$

where $E_f = 53127$ kJ/kmol, CO in kmol/m^3 , and T in ^{o}R.

The Langmuir-Hinshelwood Hougen-Watson (LHHW) kinetics, Eq (3.5), is used to simulate the COS hydrolysis reaction shown in Reaction (3.4). The kinetics captures the inhibiting effect of water and the adsorption or the surface reaction of COS being the rate-determining step, which gives good agreement between the experimental and simulation results. (Williams et al., 1999) The kinetic parameters are obtained from the open literature. (Svorones and Bruno, 2002; Williams et al., 1999) A design spec is used in Aspen Plus to manipulate the split fraction of the syngas sent to the WGS reactor to obtain the desired H_2/CO ratio.

$$COS + H_2O \rightarrow CO_2 + H_2S \tag{3.4}$$

$$r = \frac{kP_{COS}}{1 + KP_{H_2O}} \tag{3.5}$$

where $k = 6.4322\exp\left[\frac{11{,}144}{R}\left(\frac{1}{T} - \frac{1}{373.73}\right)\right]$, $K = 1.3 \times 10^{-7}\exp\left(\frac{10010}{T}\right)$, T in K, P in kPa, r in kmol/kg-hr.

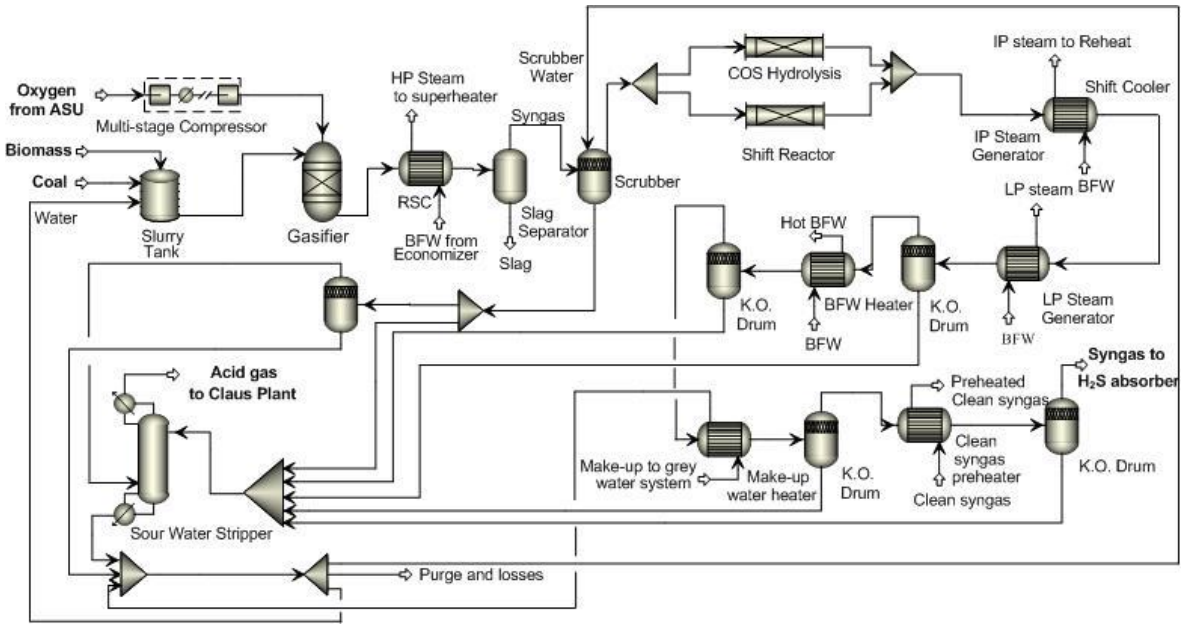

Figure 3.3 Configuration of the syngas production section and water treatment units

The syngas from the WGS and the COS hydrolysis reactors is combined and then sent to the heat recovery section where a series of heat exchangers is used to cool down the syngas by generating intermediate pressure (IP) steam, LP steam and heating boiler feed water (BFW). The hot side outlet temperatures of the IP steam generator, the LP steam generator and the BFW heater are set to 191 ^{o}C, 138 ^{o}C, and 121 ^{o}C, respectively. The condensate from the heat recovery section

contains very high amount of NH_3 and is sent to a SWS. The NH_3-rich gas from the SWS is sent to the Claus furnace while the clean water from the bottom of the SWS is recycled to the gasification section. The SWS column is simulated in Aspen Plus by using 'RadFrac' block. For the thermodynamic model, 'ELECNRTL' is used for liquid phase and 'SRK' is used for the vapor phase.

3.2.3 Acid Gas Removal and CO_2 Compression

In this work, the dual-stage Selexol unit, as shown in Figure 3.4, is used for selectively removing H_2S in the first stage followed by removal of bulk CO_2 in the second stage from the sour syngas by using dimethylether of polyethylene glycol (DEPG) as the solvent. (Bhattacharyya et al., 2011) This configuration is similar to the work of Bhattacharyya et al. The tail gas from the Claus unit is recycled to the first stage of the H_2S absorber. The off-gas from the top of the H_2S absorber is sent to the CO_2 absorber. A portion of the loaded solvent from the CO_2 absorber is sent to the H_2S absorber. The remaining portion of the loaded solvent is heated and sent to a series of flash vessels to recover H_2 and flash off CO_2. The CO_2 is flashed off in a series of three separators operating at decreasing pressure levels. The semi-lean solvent from the last separator is cooled by exchanging heat with the loaded solvent and then chilled to 2^oC using NH_3 as the refrigerant before returning it to the CO_2 absorber. The flow rate of the refrigerant in the vapor-compression cycle is determined by a design specification considering a minimum temperature approach of 5.5 ^oC. Equilibrium stage models are developed for all the columns by using the RadFrac block in Aspen Plus. The PC-SAFT EOS is used for calculating the thermodynamic properties. (Bhattacharyya et al., 2011; Gross and Sadowski, 2001) Detailed information on the modeling approach of the AGR unit for the IGCC power plant can be found in Bhattacharyya et al. (Bhattacharyya et al., 2011) Due to the considerable difference in the operating pressure of the gasifier between the IGCC power plant and I-CBTL plant, the operating pressure of the AGR unit in this work is different than the previous work. (Bhattacharyya et al., 2011) The solvent circulation rate in the AGR unit as part of the I-CBTL plant is expected to be higher, because of the lower CO_2 partial pressure in the I-CBTL plant than that in the IGCC plant. The solvent circulation rate is manipulated by a 'design spec' in Aspen Plus to achieve 90% CO_2 capture.

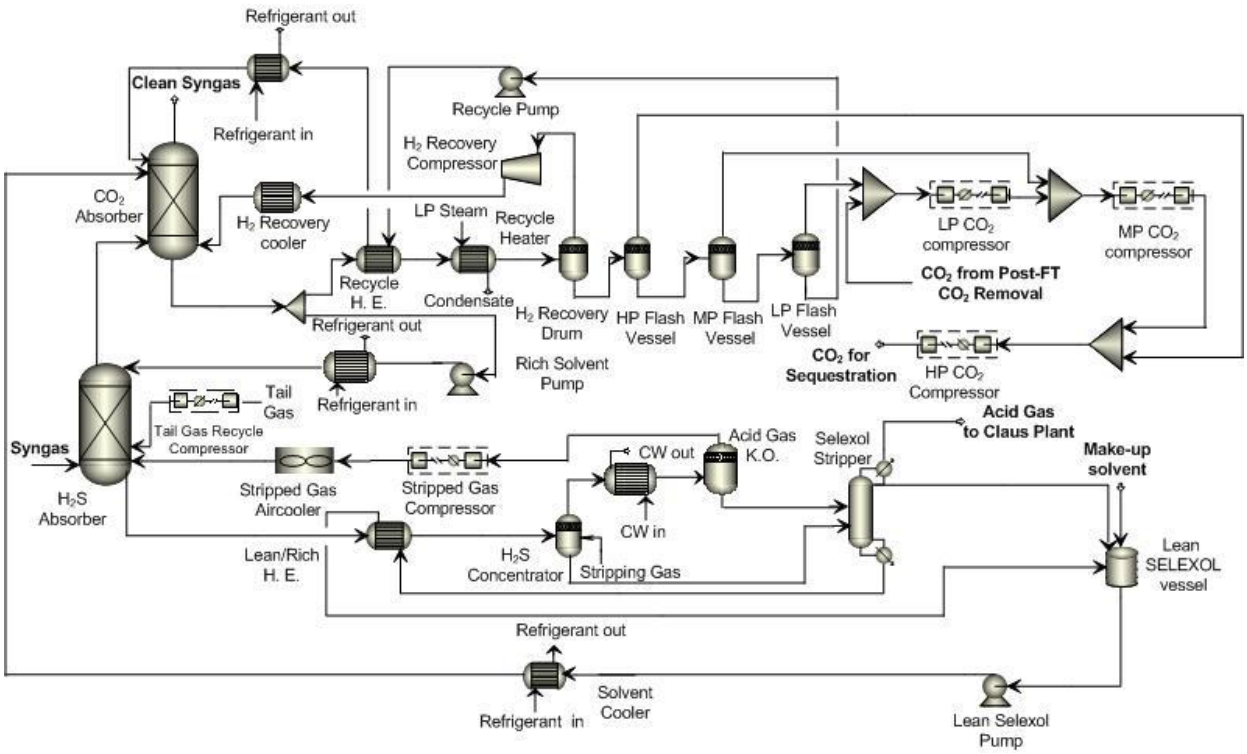

Figure 3.4 Configuration of the Selexol unit and the CO_2 compression

The CO_2 captured from the pre-FT (Selexol unit) and post-FT CO_2 removal units is compressed by a split-shaft multistage compressor. A separate CO_2 compression unit is considered for post-FT CO_2 capture only while selecting the post-FT CO_2 removal technology. Once the most suitable technology is selected, only one integrated CO_2 compression section is considered for the entire plant. It should be noted that the CO_2 stream from the post-FT CO_2 removal unit can be mixed with the CO_2 stream from the LP flash drum in the pre-FT unit as both these streams have similar pressure, if amine-based CO_2 capture technology is selected for post-FT CO_2 removal. If the single-stage Selexol technology is selected for post-FT CO_2 removal, then the CO_2 streams from the post-FT CO_2 removal unit are available at three pressure levels and can be mixed with the CO_2 streams from the pre-FT unit depending on the pressure level. The final pressure of the sequestration-ready CO_2 is 15.16 MPa. Impurity limits in the CO_2 to be sequestered (Bhattacharyya et al., 2011) should be satisfied. The limits on H_2S, CH_4, and SO_2 are automatically satisfied, but the H_2O content in the stream out of the LP flash vessel is higher than the limit, i.e. 0.015 vol %. 90% of the incoming water in the CO_2 stream is removed by cooling and flashing. The remaining amount of water that needs to be removed to satisfy the limits is

removed in an absorber using triethylene glycol (TEG) as the solvent. The modeling approach for this section can be found in the work of Bhattacharyya et al. (Bhattacharyya et al., 2011)

3.2.4 Claus Unit

The Claus unit is a gas desulfurizing process recovering elemental sulfur from the acid gas stream generated from the gasifier and the SWS column. It includes one thermal stage and two catalytic stages. More details about this unit can be found in the work of Bhattacharyya et al. and the plant configuration is shown in Figure 3.5. (Bhattacharyya et al., 2011)

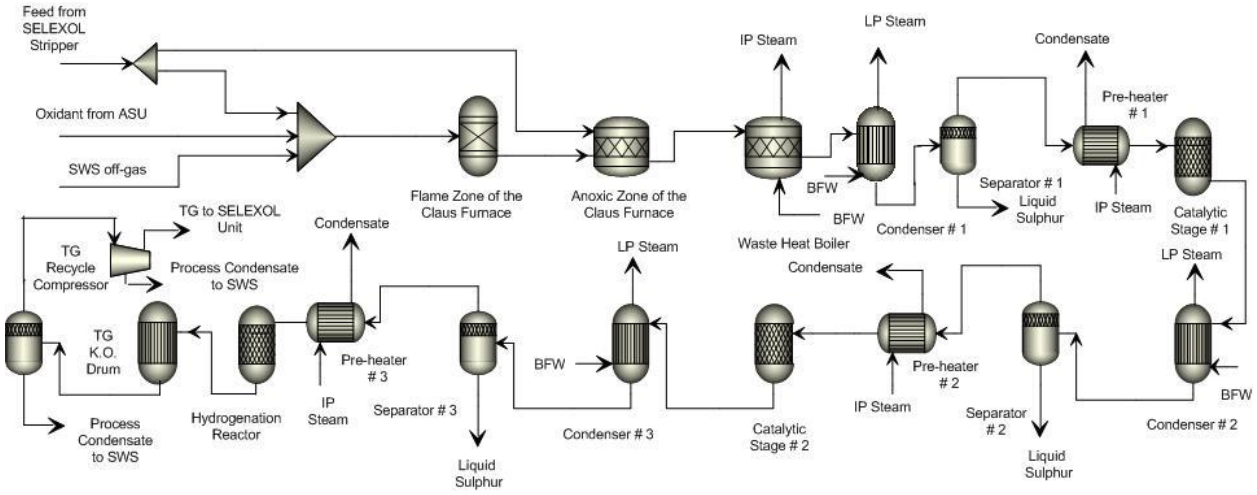

Figure 3.5 Configuration of the Claus unit (Bhattacharyya et al., 2011)

3.3 Syncrude Production

In the syncrude production section, the clean syngas from the Selexol unit and the recycled gas from the ATR unit are sent to the LTFT reactor to be converted into syncrude. The vapor phase product is sent to the post-FT CO_2 removal unit. (Jiang and Bhattacharyya, 2014)

3.3.1 Fischer-Tropsch Synthesis

The model of the FT Synthesis section has been developed in Excel and connected to Aspen Plus via a User2 block, where total mass and atom conservations are satisfied by using a VBA solver code. As mentioned before, a Fe-catalyzed slurry phase LTFT technology is considered in this study because of its high efficiency and flexibility. It has been reported that the capital cost of a slurry reactor is only 25% of a multi-tubular system. The slurry reactor has also lesser temperature gradient resulting in higher conversion. The on-line removal and addition of catalyst

also allows longer reactor runs for slurry reactor. (Dry, 2002; Espinoza, et al., 1999) In the Fe-catalyzed slurry phase FT reactors, following main reactions take place.

$$CO + 2H_2 \rightarrow -(CH_2) - + H_2O \quad (3.6a)$$

$$H_2O + CO \rightarrow CO_2 + H_2 \quad (3.6b)$$

A yield model is developed for obtaining the product distributions of a LTFT reactor based on the information available in the open literature. (Bechtel, 1992; Kuo, 1983; 1985; Fox and Tam, 1995; Bechtel, 1990) Anderson-Schulz-Flory (ASF) theory is often used to estimate the FT product distribution. As increasing wax yield is the key objective of LTFT process, the wax selectivity (S_{wax}, wt%) is often used as the indicator to calculate the ASF parameters. (Dry, 2002; Bechtel, 1992) The correlations for wax yield vs. operating conditions were reported in the open literature. (Bechtel, 1992; Kuo, 1985; Bechtel, 1998) It is modified in this study to generate more accurate estimations of the FT product distribution from operating temperature (*T*), pressure (*P*) and superficial velocity (*S.V.*) in the low operating temperature range shown in Eq. (3.7) and Eq. (3.8). The coefficients determined via linear regression of 12 sets of experimental data obtained from the Mobil's pilot plant data (Kuo, 1985) are as follows: *a=-0.1306, b=121.0773, c=271.6, d=-112.21,* where all the terms are in SI unit. The selectivity of CO_2 is calculated by WGS ratio (K_{WGS}) defined in Eq. (3.9), with a value of 2.69 for LTFT reactors when a low CO_2 -selective Fe-based catalyst is used. (James et al., 2013; Fox and Tam, 1995; Bai et al., 2002)

$$S_{wax} = aT + \frac{bP}{S.V.} \quad (3.7)$$

$$\text{Syngas Conversion (\%)} = c\left(\frac{k \cdot P}{S.V.}\right) + d \qquad \text{where } k = \exp\left(-\frac{100}{RT}\right) \quad (3.8)$$

$$K_{WGS} = \frac{(H_2)(CO_2)}{(H_2O)(CO)} \quad (3.9)$$

Because the H_2/CO ratio in the syngas has a strong effect on the product distribution from the FT process, another correlation is developed to estimate the wax selectivity at different inlet H_2/CO ratios at a constant temperature, shown in Eq. (3.10). It has been reported that the slurry reactors tend to produce more wax than the fixed bed reactors with Fe-based catalysts at similar operating conditions, the product selectivity of the fixed bed reactors is more sensitive to H_2/CO ratio in comparison to the slurry bed reactors, and the wax selectivity could be correlated to the inlet

H_2/CO ratio. (Jager and Espinoza, 1995; Dry, 1981; Espinoza and Steynberg, 1999; Steynberg and Dry, 2004) For regressing the parameters a and b in Eq. (3.10), experimental data for wax selectivity in slurry bed reactors due to changes in the H_2/CO ratio are needed. However, there are very few experimental data in the open literature for wax selectivity in the Fe-catalyst based LTFT reactors for low H_2/CO ratio. (Kuo, 1983; 1985) Therefore, it was decided to regress the parameters with the data for low H_2/CO ratio, extrapolate the correlation for high H_2/CO ratio, and compare with the data available for the fixed bed reactors at high H_2/CO ratio to see if the trends are similar. Figure 3.6 shows that the trend of wax selectivity estimated by the correlation for the slurry bed reactors is similar to that for the fixed bed reactors. It should be noted that the wax selectivity for the fixed bed reactor has been reported by Dry. (Dry, 2002; Steynberg and Dry, 2004)

$$S_{wax} = 33.6 + \frac{13.1}{H_2/CO} \tag{3.10}$$

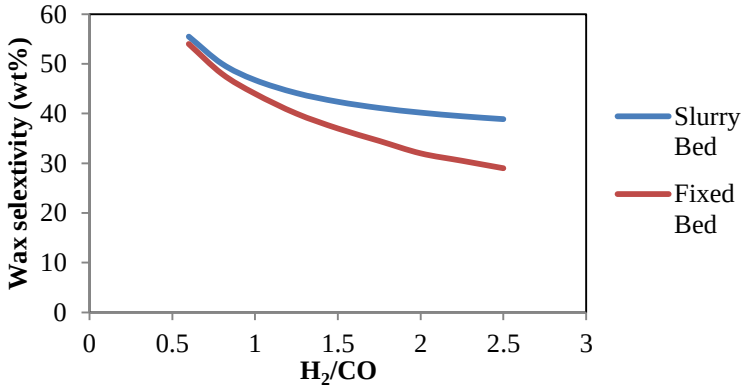

Figure 3.6 Effect of syngas composition on wax selectivity

By using the calculated wax yield, the chain growth probabilities (α) in the ASF theory can be calculated by the polynomial $\alpha - S_{wax}$ correlations shown in Eq. (3.11a) – (3.11c). (Bechtel, 1992) Then Eqs. (3.11d) – (3.11f) are used for predicting the carbon number distribution in the hydrocarbon products. In these equations, W_n denotes the weight fraction of hydrocarbon with n carbon atoms and M is the methane factor, which is applied for methane selectivity estimation and defined as the actual methane yield divided by what would be predicted from the observed value of α_2. (Fox and Tam, 1995) This model has been proven to match the LTFT experimental data. (Bechtel, 1992) Triple values of α are used to explain the high methane yield and change in the chain growth probability at certain point due to the vapor-liquid equilibrium in the reactor,

which cannot be accounted for by the conversional single α value method. The two break point is set to be n_1=1, and n_2=21. It should be noted that n_2 is also set to be the starting carbon number for wax.

$$S_{wax} = 1401-4427(\alpha_2) + 3375(\alpha_2)^2 \quad (3.11a)$$

$$S_{wax} = -36687 + 125834(\alpha_3) + 1439067(\alpha_3)^2 \ + 54888(\alpha_3)^3 \quad (3.11b)$$

$$M = \frac{(1-\alpha_1)^2}{(1-\alpha_2)^2} = 6.413 - 0.0580(S_{wax}) + 0.00165(S_{wax})^2 + 7.986 \times 10^{-6}(S_{wax})^3 \quad (3.11c)$$

$$W_1 = (1-\alpha_1)^2 x \quad (3.11d)$$

$$W_n = n(1-\alpha_2)^2 \alpha_2^{n-1} y \qquad n = 2,3,4,\ldots,20 \quad (3.11e)$$

$$W_n = n(1-\alpha_3)^2 \alpha_3^{n-1} z \qquad n = 21,22,\ldots \quad (3.11f)$$

where x, y, z are given by:

$$x/y = \alpha_2/(M\alpha_1)$$

$$z/y = [(1-\alpha_2)^2\alpha_2^{20}]/[(1-\alpha_3)^2\alpha_3^{20}]$$

$$y = 1\Big/\left(\sum_{n=2}^{20} W_n + \sum_{n=21}^{\infty} W_n\, z/y + W_1\, x/y\right)$$

For the same carbon number, components in the FT liquid are not only normal paraffin, but also olefin, and oxygenates. (Kuo, 1985) The olefin components have to be hydrotreated before sending them to the upgrading blocks. Since the olefin content in the FT crude can be high, the olefins fraction γ is an important variable that should be satisfactorily estimated. The olefins fraction will decrease with an increase in the carbon number, and the value finally settles down to 0.7 when the carbon number is larger than 6. (Fox and Tam, 1995) Table 3.3 lists the typical value of γ obtained experimentally. (Kuo, 1985)

Table 3.3 Olefins fraction versus carbon number in FT hydrocarbons

C_n	2	3	4	5	6	7+
olefins%	0.72	0.82	0.72	0.72	0.72	0.7

The wax obtained from the FT reactor can be treated as a single lumped C_{20+} wax pseudo component. From the modified ASF theory, the average carbon number of the C_{20+} wax can be calculated using the following equation (Fox and Tam, 1995):

$$C_{avg} = n + \alpha_3/(1-\alpha_3) \quad (3.12)$$

Besides alkenes, oxygenates produced at the FT reaction also need to be hydrogenated for stability of final products. Hence, it is also important to predict the oxygenate yield correctly. The total oxygenate yield in our model is obtained by using a polynomial correlation, given by Eq. (3.13), published in the open literature (Bechtel, 1992; Fox and Tam, 1995). The species distributions for oxygenates are the average value of the reported pilot data. (Kuo, 1983; 1985) It can be noted that the species distributions for oxygenates are not strong function of operating condition. (Bechtel, 1992a; Kuo, 1983; 1985)

$$S_{OxyV} = 0.39 \quad (3.13a)$$

$$S_{OxyW} = 1.128(S_{wax}) + 0.05558(S_{wax})^2 \quad (3.13b)$$

$$S_{OxyHC} = 1.351(S_{wax}) + 0.1331(S_{wax})^2 + 0.1105(S_{wax})^3 \quad (3.13c)$$

where S_{OxyV}, S_{OxyW}, S_{OxyHC} denote oxygenate weight percent in vapor, water, and oil phase.

16 sets of experimental data from Run 256-7 conducted by Mobil in 1985 (Kuo, 1985) are used for validating the model at several different operating conditions. Figure 3.7 shows a comparison, between the results of the modified model and the experimental data to check the model accuracy, where HC and Oxy denote hydrocarbons (no including wax), and oxygenates, respectively.

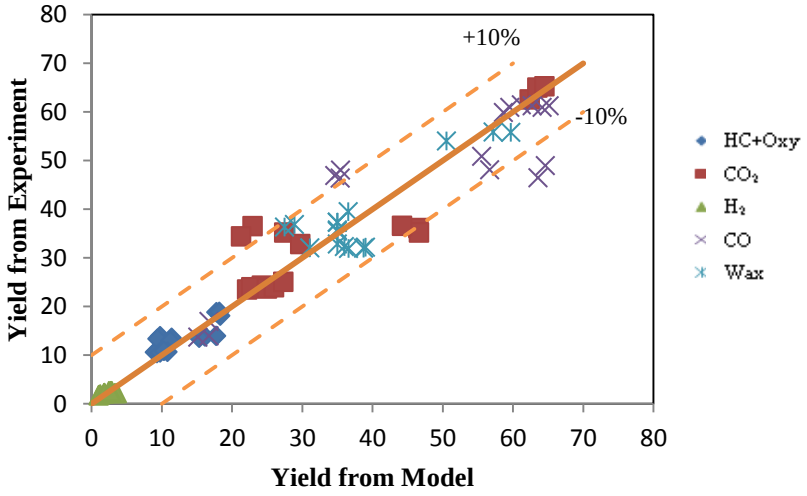

Figure 3.7 Comparison between the model results and experimental data

3.3.2 Post-FT CO_2 Capture Unit

The products from the FT reactor, especially when Fe-based FT catalyst is used, can contain high amount of CO_2 that must be removed. In this study, we have considered CCS where the captured CO_2 is sent to the CO_2 compression unit for sequestration. Solvent-based and other technologies, such as high concentration MEA, inhibited MDEA, Benfield hot K_2CO_3, Rectisol, Ryan-Holmes cryogenic distillation, membrane, and PSA, have been compared by Bechtel for post-FT CO_2 removal. (Bechtel, 1992) It was observed that the chemical absorption and the Ryan-Holmes process were the most likely candidates for FT application because of very little loss of valuable components, such as H_2, CO and light hydrocarbons. The chemical absorption process was selected for the baseline design instead of the Ryan-Homes process because of its lower capital cost. (Bechtel, 1992) The inhibited MDEA is preferred over the MEA process because of its less corrosiveness and about 13.8% lesser steam consumption. (Bechtel, 1992)

Three solvents are evaluated in this study, one physical solvent, Selexol, and two chemical solvents, methyl diethanolamine (MDEA)/ piperazine (PZ) and monoethanolamine (MEA). The advantages of chemical solvents over physical solvents are that the hydrocarbon loss is very low due to lower selectivity towards hydrocarbons, and the process could be operated at low pressure. In addition, a high level of CO_2 removal can be achieved in order to avoid CO_2 accumulation in downstream equipment. However, the chemical solvents suffer a higher parasitic loss, mainly due to the considerable amount of steam required for solvent regeneration (Bechtel, 1992), in comparison to the physical solvents. Another disadvantage of most chemical solvents is the relatively lower operating pressure for solvent regeneration than that of the most physical solvents in order to avoid solvent degradation. This results in more power consumption for CO_2 compression section. It should be noted that 98% of CO_2 removal is specified for baseline design of the chemical absorption processes in this work.

3.3.2.1 MDEA/PZ

The PZ activated MDEA is a chemical solvent with high potential for CO_2 capture at reduced energy consumption in comparison to MEA. The stripper reboiler duty of MDEA/PZ system is expected to be lower than the MEA system (Kohl and Nielsen, 1997; Neveux, et al., 2013) PZ, a

cyclic amine, is added to MDEA to improve solvent performance. (Xu et al., 1998; Puxty and Rowland, 2011; Plaza, 2012)

The process flow diagram is shown in Figure 3.8. Three packed columns are considered in the CO_2 removal unit, one for absorption, two for solvent regeneration. The FT vapor stream enters at the bottom of the absorption column while the recycled lean solvent enters at the top of absorption column. The rich solvent leaving the bottom of the absorber is heated by the lean solvent out of the stripper bottoms and sent to the strippers to remove CO_2. In the I-CBTL process, the operating pressure of the absorber is much higher than those of the strippers. For satisfactory vapor velocity in the stripper, two strippers are used for one absorber. This is also consistent with the open literature. (Bechtel, 1992)

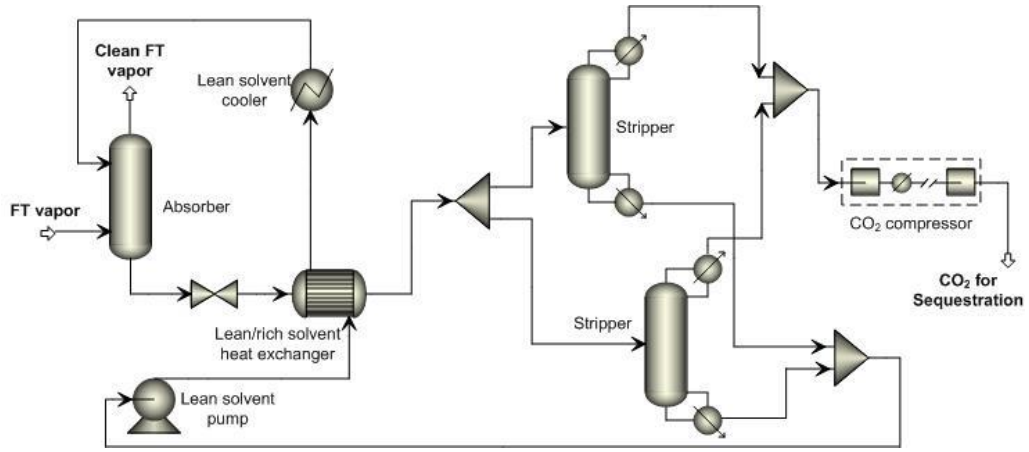

Figure 3.8 Amine-based CO_2 removal unit

The lean solvent at the base case condition constitutes of 21 wt% MDEA and 5 wt% PZ aqueous solution with loading of 0.06 mol of CO_2/mol of amine group. Reactions considered in the rate-based model of the column are shown below, where Reactions 3.14 a-e are assumed to be at equilibrium. Reactions 3.14 f-m are modeled using power law kinetics as shown in Eq. (3.15). The reactions listed, kinetic model, thermodynamic model and related constants are obtained from recent works. (Austgen et al., 1991; Hilliard, 2008; Bishnoi and Rochelle, 2000)

$$2H_2O \leftrightarrow H_3O^+ + OH^- \quad (3.14a)$$

$$HCO_3^- + H_2O \leftrightarrow CO_3^{2-} + H_3O^+ \quad (3.14b)$$

$$PZH^+ + H_2O \leftrightarrow PZ + H_3O^+ \quad (3.14c)$$

$$HPZCOO + H_2O \leftrightarrow PZCOO^+ + H_3O^+ \quad (3.14d)$$

$$MDEAH^+ + H_2O \leftrightarrow MDEA + H_3O^+ \quad (3.14e)$$

$$CO_2 + OH^- \rightarrow HCO_3^- \quad (3.14f)$$

$$HCO_3^- \rightarrow CO_2 + OH^- \quad (3.14g)$$

$$PZ + CO_2 + H_2O \rightarrow PZCOO^- + H_3O^+ \quad (3.14h)$$

$$PZCOO^- + H_3O^+ \rightarrow PZ + CO_2 + H_2O \quad (3.14i)$$

$$PZCOO^- + CO_2 + H_2O \rightarrow PZ(COO^-)_2 + H_3O^+ \quad (3.14j)$$

$$PZ(COO^-)_2 + H_3O^+ \rightarrow PZCOO^- + CO_2 + H_2O \quad (3.14k)$$

$$MDEA + CO_2 + H_2O \rightarrow MDEAH^+ + HCO_3^- \quad (3.14l)$$

$$MDEAH^+ + HCO_3^- \rightarrow MDEA + CO_2 + H_2O \quad (3.14m)$$

$$r = k\left(\frac{T}{T_0}\right)^n \exp\left[-\frac{E}{R}\left(\frac{1}{T} - \frac{1}{T_0}\right)\right]\prod_{i=1}^{N} C_i^{a_i} \quad (3.15)$$

Intercooling of the solvent in the absorber is considered in the baseline design for decreasing the utility consumptions. In the Aspen Plus environment, the intercooling is modeled by the pumparound option in the RadFrac block. The pumparound flow rate is set to be the lean solvent flow rate. The cooling temperature is set to be 40^{o}C. Norton IMTP 1.5in, metal packing is used. The electrolyte NRTL properties package in Aspen Plus V7.3 is used. Column design carried out with the following objectives:

(1) The CO_2 stream concentration should meet the recommended design basis for the CO_2-sequestration gas for a remote, deep, geological storage site;

(2) The stripper column temperature should be chosen in a way that prevents solvent degradation;

(3) The CO_2-lean FT product must be free of solvent.

A design spec is used for capturing 98% CO_2 by manipulating the solvent recycle rate.

3.3.2.2 MEA

MEA is another popular chemical solvent for CO_2 capture. The plant configuration and modeling approach are similar to Section 3.3.2.1. Reactions considered are shown below. Reactions 3.16 a-c are considered to be equilibrium-limited. Reactions 3.16 d-g are simulated by using power law kinetics as shown in Eq. (3.15). (Zhang et al., 2009) The kinetic model and the pilot plant data for model validation are available in the open literature. (Dugas, 2006; Hikita et al., 2006) In

agreement with the existing studies (Bechtel, 1992; Dugas, 2006), the lean solvent is 30 wt% aqueous solution of MEA with CO_2 loading of 0.27 mol of CO_2/mol of amine group. The system design is subjected to the same constraints and operating conditions mentioned in Section 3.3.2.1.

$$H_2O + MEAH^+ \leftrightarrow MEA + H_3O^+ \quad (3.16a)$$

$$2H_2O \leftrightarrow H_3O^+ + OH^- \quad (3.16b)$$

$$HCO_3^- + H_2O \leftrightarrow CO_3^{2-} + H_3O^+ \quad (3.16c)$$

$$CO_2 + OH^- \rightarrow HCO_3^- \quad (3.16d)$$

$$HCO_3^- \rightarrow CO_2 + OH^- \quad (3.16e)$$

$$MEA + CO_2 + H_2O \rightarrow MEACOO^- + H_3O^+ \quad (3.16f)$$

$$MEACOO^- + H_3O^+ \rightarrow MEA + CO_2 + H_2O \quad (3.16g)$$

3.3.2.3 Single-Stage Selexol Unit

The single-stage Selexol technology is considered here as another potential technology to remove CO_2 from the FT product due to its low utility consumption of the capture process itself and the downstream CO_2 compression. The drawback of the Selexol technology is hydrocarbon loss. Hydrocarbon loss and utility saving for Selexol are compared with the previous two chemical solvents. The modeling approach is similar to that mentioned in Section 3.2.3. The rich solvent from the bottom of the absorber is sent to a H_2 recovery vessel to recover 70% of H_2 and then to a series of flash vessels to remove CO_2 from the solvent. Lean solvent out of the flash vessel again is chilled and sent back to the absorber. The configuration is shown in Figure 3.9. The temperature of the chilled lean solvent is 2 ^oC, and the operating pressure of the absorber is 1965 kPa. The operating pressures of HP, MP and LP flash drums are determined by an optimization study discussed in Section 3.6. The percentage of CO_2 captured is set to be 93% in this case. It can be noted that the extent of CO_2 capture is lower than the chemical solvents due to the relatively low operating pressure of the post-FT CO_2 capture unit that limits the extent capture for the physical solvent.

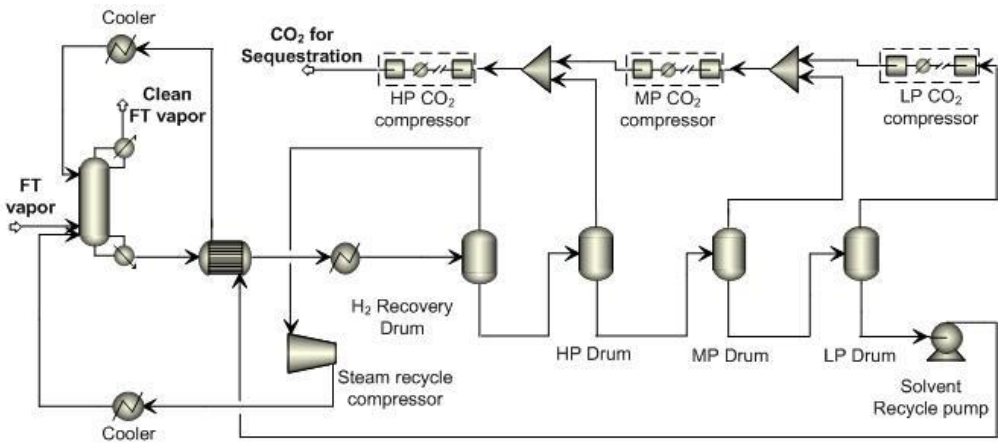

Figure 3.9 Configuration of the single-stage Selexol unit

3.3.3 Autothermal Reformer

The ATR unit uses a combination of exothermic partial oxidation and endothermic steam reforming reactions while operating under thermally neutral conditions to achieve optimum efficiency with less complicated facilities and less or no external energy in comparison to the steam reforming units. The process can practically approach adiabatic conditions if appropriately designed. Figure 3.10 gives the configuration of the ATR unit, where light gases from the post-FT CO_2 captured unit is first preheated by the hot ATR product, before sending to the ATR. For modeling purpose, the ATR reactor is simulated as a combination of an RGibbs reactor and a PFR. The ATR reactor feed is separated in a dummy component separator, where C_1 and C_{2+} hydrocarbons are separated, and the steam/carbon and oxygen/carbon ratios of the two streams are maintained to be the same as in the feed. Availability of information on reforming kinetics of C_{2+} hydrocarbons is scarce in the open literature. However, several studies indicate that reforming of C_{2+} hydrocarbons are faster than methane reforming and results in methane formation. (Ayabe et al., 2003; Schadel et al., 2009; 2005) Hence, it is assumed that chemical equilibrium is reached for C_{2+} hydrocarbon and therefore, these reactions are modeled by using the RGibbs block. The product of the RGibbs block is mixed with the C_1 stream and sent to a PFR, where the methane reforming reaction is considered. The key reactions of methane autothermal reforming on Ni/Al_2O_3 catalysts are shown in Table 3.4 with the kinetic parameters obtained from the open literature. (Rafiq et al., 2012) A high steam/carbon ratio is usually used to increase the H_2 yield. If moderate H_2/CO ratio is required in the syngas, a low steam/carbon ratio can be used in the ATR unit to reduce the utility cost. (Steynberg and Dry, 2004) The

steam/carbon ratio from 0.5 to 3.0 is studied in this study. The oxygen flowrate is manipulated to achieve a reactor outlet temperature of 982ºC. The SRK equation-of-state (EOS) is used to calculate the thermodynamic properties.

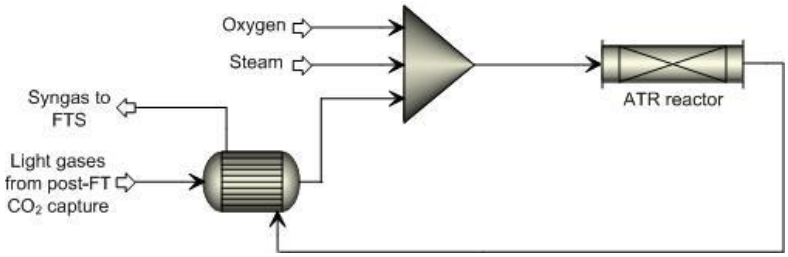

Figure 3.10 Configuration of the ATR unit

Table 3.4 Reactions considered in the kinetic model (Rafiq et al., 2012)

Name	Reaction	Reaction Heat	Kinetic Equation
Combustion	$CH_4 + 2O_2 \rightarrow CO_2 + 2H_2O$	exothermic	$r_1 = k_1 \cdot P_{CH4} \cdot P_{O2}$
Steam Reforming	$CH_4 + H_2O \leftrightarrow CO + 3H_2$	endothermic	$r_2 = k_2 \cdot P_{CH4} \cdot P_{H2O}\left(1 - \frac{P_{CO} \cdot P_{H2}^3}{K_1 \cdot P_{CH4} \cdot P_{H2O}}\right)$
Dry Reforming	$CH_4 + CO_2 \leftrightarrow 2CO + 2H_2$	endothermic	$r_3 = k_3 \cdot P_{CH4} \cdot P_{CO2}\left(1 - \frac{P_{co}^2 \cdot P_{H2}^2}{K_2 \cdot P_{CH4} \cdot P_{CO2}}\right)$
Water-Gas Shift	$CO + H_2O \leftrightarrow CO_2 + H_2$	slight exothermic	$r_4 = k_4 \cdot P_{CO} \cdot P_{H2O}\left(1 - \frac{P_{CO2} \cdot P_{H2}}{K_3 \cdot P_{CO} \cdot P_{H2O}}\right)$

Figure 3.11 shows that the simulation results agree well with the data available in the open literature for the ATR unit as part of a CTL plant for different feed compositions and operating conditions. (NETL, 2007; Bechtel, 1993) It should be noted that, in the CTL plant, the recycle gas to the ATR unit contains not only light hydrocarbons, but also some unconverted syngas, that strongly impacts the product distribution because of the WGS reaction. The data considered for model validation cover the range of feed compositions and operating conditions listed in Table 3.5. Appendix A provides detailed stream information for various cases that have been considered for model validation.

Table 3.5 Range of feed composition and operating conditions for ATR model validation

	Steam/Carbon (mol/mol)	Oxygen/Carbon (mol/mol)	Syngas/Hydrocarbons (mol/mol)	Outlet Temperature (°C)
Minimum	3.76	0.509	3.125	971
Maximum	1.23	0.157	13.15	982

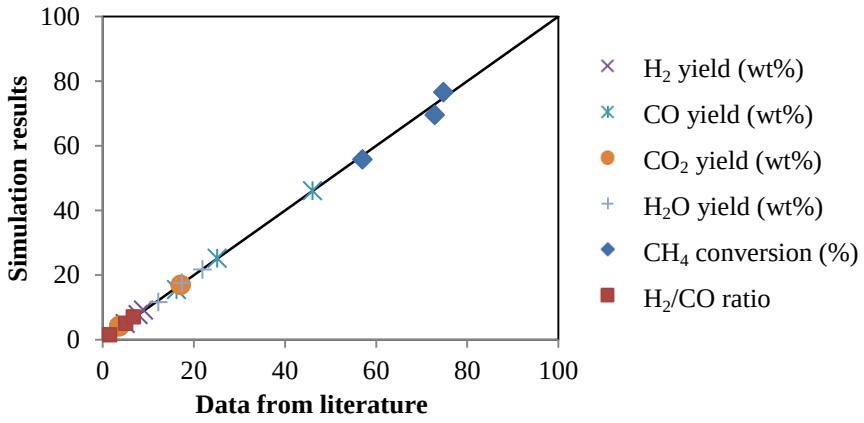

Figure 3.11 ATR model validation

3.4 Hydrocarbon Recovery and Upgrading

In the hydrocarbon recovery and upgrading section, syncrude produced in the FT unit is separated into light gases, light naphtha, heavy naphtha, diesel and wax and then sent to a series of upgrading units to be converted into on-spec gasoline and diesel.

3.4.1 Hydrotreating and Hydrocarbon Recovery

In the hydrocarbon recovery and upgrading section, an integrated hydrotreating approach is proposed, as shown in Figure 3.12, for increasing the thermodynamic efficiency and for making the plant footprint smaller, in comparison to the conventional separated hydrotreating approach shown in Figure 3.13. In the conventional separated hydrotreating approach, the crude is first separated into different streams in flash drums and distillation columns. Then naphtha and diesel are sent to two different hydrotreating units, while wax is sent to a hydrocracking unit. In contrast, in the integrated hydrotreating unit, the raw syncrude is first preheated by the hot treated syncrude and then heated by a furnace to reach the required temperature before being sent to the reactor. After being cooled, the treated syncrude is sent to a high-pressure flash (HPF) drum followed by a low-pressure flash (LPF) drum to recover the H_2 and light gases (LG). Then it is sent to the main distillation column through a series of heat exchangers.

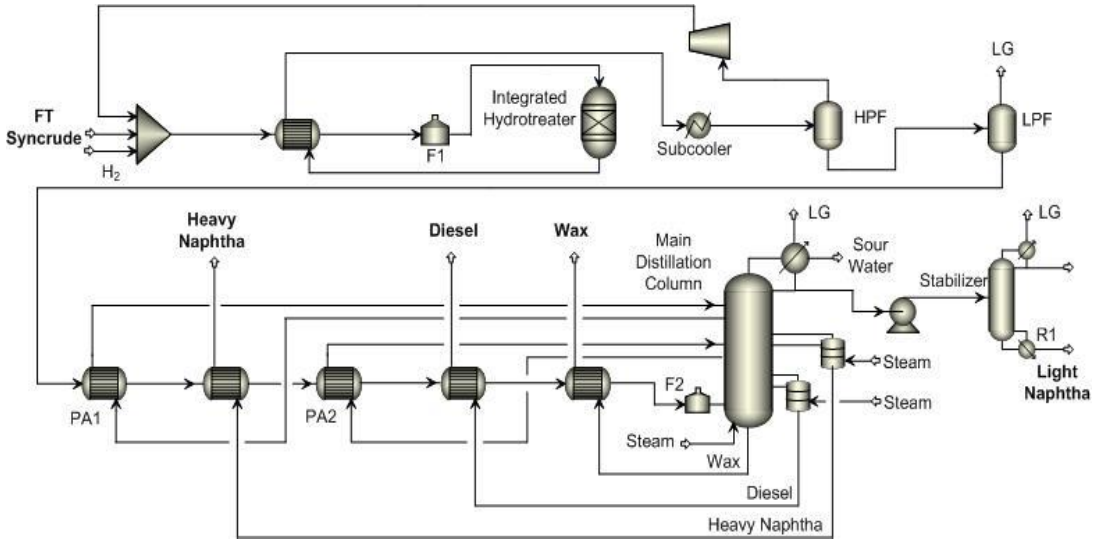

Figure 3.12 Configuration of the novel integrated hydrotreating approach

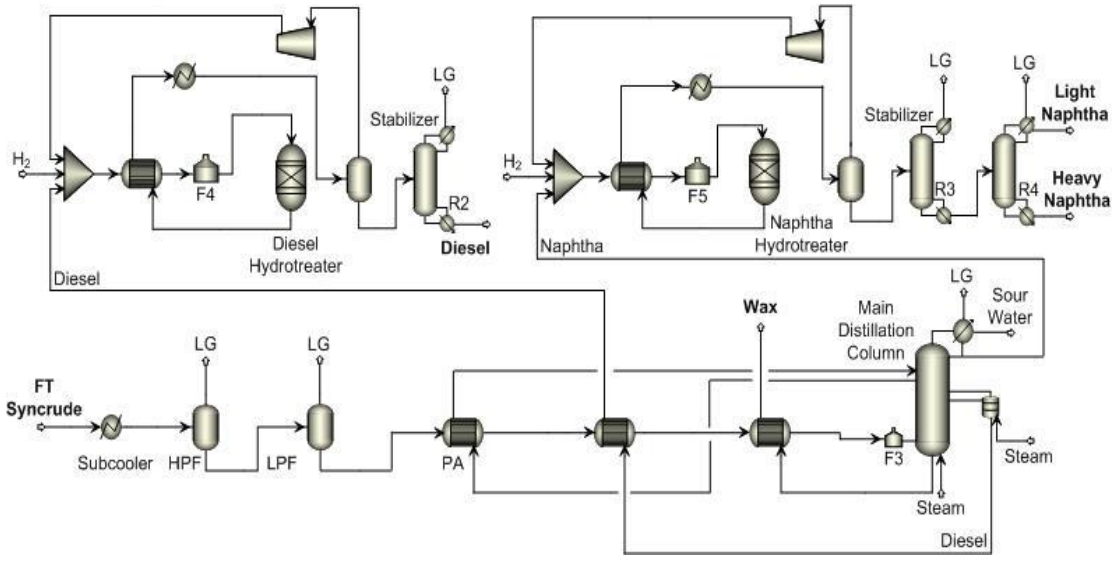

Figure 3.13 Configuration of the conventional separated hydrotreating approach

In this study, the correlations given by Bechtel (Bechtel, 1993; 1998) are applied for the material and energy balance estimation of the conventional hydrotreating units for naphtha and diesel, while a simple yield model is developed in Excel for the integrated hydrotreater unit for obtaining reasonable estimates of H_2 and utility consumption.

To simplify the calculation of H_2 requirement in the novel integrated hydrotreating unit, a number of assumptions have been made. The operating condition is considered to be similar to

that in the conversional diesel hydrotreater (58 bar, 297 ^{o}C), which is much severe than the operating conditions in the naphtha hydrotreaters. Hence, it is assumed that the naphtha cut gets completely hydrotreated, and the amount of diesel cut that gets hydrotreated depends on the catalyst type and experimental Bromine Number of hydrotreated diesel. Typically, the Bromine Number of the hydrotreated FT diesel is lesser than 6.0 g Br/100g when catalyzed by NiMo/Al_2O_3. (Lamprecht, 2007) Hence, in the yield model developed, we have considered 5 wt% of unsaturated diesel that corresponds to 6.0 g Br/100g. Because Fe-catalyst FT syncrude contains only small amount of oxygenates and no sulfur and nitrogen, the main reactions considered is hydrogenation of alkenes and hydrodeoxygenation. With the detailed component distribution in the reactor inlet (Jiang and Bhattacharyya, 2014), the H_2 consumption can be estimated by atom balance with the following assumptions: (1) Reacted olefins are converted to the corresponding saturated paraffin compound; (2) Wax remains mainly unreacted in this integrated hydrotreater as wax hydrotreating needs much severe reaction conditions; (3) Yields of light gases produced by the side hydrocracking reaction are assumed to be similar to the conventional hydrotreating units; (4) All oxygenates are hydrotreated and converted to water and corresponding paraffin compound.

Most of the heat required for preheating the hydrotreater feed can be recovered by exchanging heat between the feed stream and hydrotreater outlet stream, while the remaining heat is supplied by the feed furnace. Because of the wide variation in the thermodynamic properties of isomers of C_5 to C_8, a statistical model of the isomer distribution of paraffin in the LTFT product developed by Weller and Friedel is considered for more accurate energy calculation. (Weller and Friedel, 1949) The detailed isomer distribution is reported in Table 3.6.

Table 3.6 Isomer distribution of hydrocarbons in LTFT product

Isomer	Molar fraction	Isomer	Molar fraction
1-Pentene	1	n-Heptane	0.877
n-Pentane	0.95	2-methyl hexane	0.046
i-Pentane	0.05	3-methyl hexane	0.077
1-Hexene	1	1-Octene	1
n-Hexane	0.896	n-Octane	0.845
2-methyl pentane	0.057	2-methyl heptane	0.039

3-methyl pentane	0.047	3-methyl heptane	0.072
1-Heptene	1	4-methyl heptane	0.044

Due to the limited information available on hydrotreating of the FT liquids, the yield model is validated by comparing the calculated product distribution and hydrogen consumed with those reported by Bechtel (Bechtel, 1998) with the same feed composition. The composition of oxygenates in the feed was not specified in the Bechtel report. Hence, for generating the final product distribution we have assumed that oxygenates in naphtha and diesel are represented by $C_{4.78}H_{11.14}O_{1.1}$ and $C_{9.08}H_{18.94}O_{1.1}$, respectively. (Fox and Tam, 1995; Otgonbaatar, 2011) Table 3.7 lists the results and shows that the errors in yields of major products are within 5 %. It should be noted that the syncrude composition reported by Bechtel (Bechtel, 1993; 1998) is similar to the base case of this study. It is assumed that the hydrocarbon distribution does not change significantly in the range of operating conditions considered in the sensitivity studies conducted in this work.

Table 3.7 Validation of the model of the integrated hydrotreater

wt%	Bechtel	Model	Error%
H_2 consumption	1.10	1.07	-2.8
Major products			
Light gases	2.97	2.96	0.34
Naphtha	39.3	39.1	0.33
Diesel	57.8	57.9	0.29

In both hydrotreating approaches, the raw or hydrotreated syncrude is cooled to about 40 ^{o}C and sent to the HPF drum (38 bar) to recover the H_2-rich gas. The bottom stream of HPF drum is sent to the LPF drum (8 bar) from where the light gases are recovered and sent to the fuel gas header. Then a complex distillation column is used to separate the syncrude into products with different boiling point range, as shown in Table 3.8. Stabilizer is used to separate light gases from the light naphtha stream. The ASTM D86 cut points of the hydrocarbons are specified to ensure that the final product pools satisfy the desired gasoline and diesel specs. The cut points of light naphtha are specified for satisfying the gasoline specs. The cut points of heavy naphtha and diesel are specified to satisfy the specs of the gasoline and diesel pools, respectively.

PetroFrac model is used to design and simulate the main distillation column, where BK10 EOS is used as the thermodynamic model because the distillation system contains species of wide boiling point range. (Tarighaleslami et al., 2012; Doust et al., 2012) Stabilizer is simulated via RadFrac model using SRK EOS as the thermodynamic model because the system mainly contains lighter hydrocarbons.

Table 3.8 Product specification of the hydrocarbon recovery system

Integrated approach		Separated approach	
Product	ASTM D86 cut point	Product	ASTM D86 cut point
Light naphtha	52°C - 94 °C	Naphtha	50°C – 174°C
Heavy naphtha	104 °C - 174°C	Diesel	190°C - 316 °C
Diesel	190 °C - 316 °C	Wax	327 °C - FBP
Wax	327 °C - FBP		

The specifications of the hydrocarbon recovery system is listed in Table 3.9 and Table 3.10, which are obtained based on the traditional crude oil distillation technology (Ji and Bagajewicz, 2002; Bagajewicz and Ji, 2011) and the multicomponent distillation column used in the Bechtel's FT process design (Bechtel, 1993) with limited information. In the hydrocarbon recovery system, the syncrude passes through a preheating train with several heat exchangers using the pump-around streams and the product streams that need to be cooled before entering the main distillation column. A feed furnace is used for the crude oil distillation tower instead of reboiler, evaporating only a small portion of the wax. The feed furnace is specified by applying a fractional overflash of 3.2 % LV. Stripping stream is used for decreasing the partial pressure of the hydrocarbons in order to prevent decomposition, which occurs at high temperature (about 371 °C). A commonly-used value for stripping stream to product ratio is about 2.27-4.54 kg/bbl. (Ji and Bagajewicz, 2002; Bagajewicz and Ji, 2011) Pump-arounds are used as main means to obtaining intermediate heat recovery. Liquid is withdrawn from the tray on or above the lower product draw tray, cooled, and returned to a tray, 2-3 trays above, but below the upper product draw. (Ji and Bagajewicz, 2002; Bagajewicz and Ji, 2011) As a result, the size and heat duty of the feed furnace and the overhead condenser could be reduced significantly. Meanwhile, the top reflux and the column diameter could also be reduced. In this study, the outlet temperatures of the two pump-around exchangers are selected to increase the heat recovery as much as possible within operating constraints.

Table 3.9 Column specification of the hydrocarbon recovery section

	Integrated approach	Separated approach
Number of trays		
Main column	30*	23*
Heavy naphtha side stripper	5	NA
Diesel side stripper	5	5
Stabilizer	20	20
Locations		
Feed to main column	26*	19*
Stripping steam to main column	30*	23*
Heavy naphtha product draw and return	15,14	NA
Diesel product draw and return	24,23	17*,16
Pump-around 1 draw and return	15,12	NA
Pump-around 2 draw and return	24,21	17,14
Feed to stabilizer	10	10

Stabilizers are designed using short cut model in Aspen Plus®; numbers with * are obtained from the open literature

Table 3.10 Specification of the column operating condition

	Integrated approach	Separated approach
Main column		
Condenser temperature (ºC) *	37.8	37.8
Overhead pressure (kPa) *	600	600
Pressure drop per tray (kPa) *	1.38	1.38
Feed furnace fractional overflash (%LV)	3.2	3.2
Bottom product to feed ratio (kg/kg)	0.48	0.48
Stripping steam to bottom product ratio (kg/bbl)	4.54	4.54
Side strippers		
Stripping steam to heavy naphtha ratio (kg/bbl)	2.27	NA
Stripping steam to diesel ratio (kg/bbl)	2.27	2.27
Pump-around and preheating train		
Pump-around 1 return temperature (ºC)	82.2	NA
Pump-around 2 return temperature (ºC)	282.2	83.3
Heavy naphtha heat exchanger hot stream temperature drop (ºC)	66.7	NA
Diesel heat exchanger hot stream temperature drop (ºC)	85.6	51.7
Wax heat exchanger hot stream temperature drop (ºC)	193.3	194.4

Numbers with * are obtained from the open literature

3.4.2 Isomerization, Catalytic Reforming, and Wax Hydrogracking

The wax stream from the main distillation column is sent to the wax hydrocracking unit to produce shorter-chain hydrocarbons that are then separated into light naphtha, heavy naphtha, and diesel. A simple yield model is developed by multivariable regression using the experimental data reported by UOP for their single-stage HC Unibon process. (Shah, 1988) The HC Unibon technology is a fixed-bed catalytic process that uses high activity bifunctional catalyst and has been developed to maximize diesel production for full conversion application. (Shah, 1988) The H_2 reacted per barrel of wax (F_{H_2}) depends on the gasoline to diesel ratio if the conversion is the same. Eq. (3.17) gives an estimation of F_{H_2} of wax hydrocracking unit correlated to the weight percentage of C_{7+} product ($W_{C_{7+}}$), where F_{H_2} is in standard cubic feet per barrel (SCFB) of wax. (Shah, 1988) Information on utility consumption is available in the open literature (Shah, 1988) and assumed to be proportional to the feed flow rate. It is noted that the wax hydrocracking model does not provide the isomer distribution of the naphtha cut required for modeling the naphtha upgrading units. Hence, a typical composition of naphtha cut from open literature is used in this study. (Gamba et al., 2010; Teles an Femandes, 2007) The yield model developed based on UOP's data is consistent with the experimental data reported by Sasol shown in Table 3.11. (Leckel, 2005; 2007)

$$F_{H_2} = 2215 - 15.427 W_{C_{7+}} \quad (3.17)$$

Table 3.11 Model validation of the FT wax hydrocracking unit

wt%	Model	Leckel	Error%
C_1-C_4	7.55	7.6	-0.65
C_5-C_9	33.8	34	-0.46
C_{10}-C_{22}	58.6	58	1.05

For naphtha upgrading, the UOP Penex^{TM} process is considered for light naphtha isomerization due to its low cost. A simplified yield model has been reported by Bechtel for this process. (Bechtel, 1993) The selectivity of isomer is about 98.3 wt% and the make-up hydrogen rate is about 0.14 wt% of light naphtha feed rate. Utility consumption is assumed to be proportional to the feed flow rate. (Bechtel, 1993; 1998) The UOP continuous catalyst regeneration (CCR) Platforming technology is selected to increase the octane number of FT heavy naphtha by

converting them into aromatics. According to the experimental data provided by UOP, this technology for catalytic reforming is able to increase the RON of FT heavy naphtha to about 100. (Bechtel, 1993; Shah, 1990) The Aspen Tech Reformer model under the Aspen One package is used for estimating the process yield and product properties. First, the target RON, the flowrate, and composition of the feed are specified in the Aspen Tech Reformer model. Then the simulation is run and the results are compared with the data provided in Bechtel's report (Bechtel, 1993), as shown in Table 3.12. It shows that the results obtained from the Aspen Tech Reformer are satisfactory.

Table 3.12 Model validation of the catalytic reforming unit

	Aspen	Bechtel	error %
H_2 wt%	4.14	3.44	
C_1-C_5 wt%	8.68	10.67	
Reformate wt%	87.00	85.89	1.39
Specific gravity	0.80	0.77	3.49
RON	95	95	0
Benzene wt%	0.66	0.70	-5.71
Aromatic wt%	66.14	65.90	0.36

3.4.3 Hydrogen Network

In the product upgrading section, H_2 produced in the catalytic reforming unit and the purged gases from the hydroprocessing units, shown in Figure 3.14, are sent to the H_2 recovery unit, a polybed PSA process, to produce a portion of the pure H_2 for hydroprocessing. The remaining H_2 requirement can be satisfied by sending a portion of the FT vapor (Stream 7 in Figure 3.1) to the PSA unit to recover H_2 from the unconverted syngas. In this study, component separator block is used for simulating the PSA unit with the H_2 purity and recovery efficiency of the PSA unit assumed to 99.9% and 50.7%, similar to the Bechtel design that uses a standard ten-bed system. (Bechtel, 1993) In should be noted that the PSA unit is an unsteady state process, where a number of adsorber vessels is cycled in a desired sequence changing their pressure typically between 2620 kPa and 690 kPa for adsorption and desorption, respectively. (Bechtel, 1993) In this study, it is assumed that the number of beds in the PSA unit and the sequence have been appropriately designed so that the H_2 is available continuously at the desired rate. A model of the

H_2 network is developed to estimate the flowrate of the make-up H_2 stream and the amount of FT vapor that can be recycled back to the FT reactor.

The high H_2 partial pressure in the hydroprocessing reactors is usually maintained by recycling unreacted H_2. The product from the hydroprocessing reactor is cooled and sent to a H_2 recovery flash drum. The majority of the vapor stream is sent back to the reactor and the rest is purged and sent to the PSA H_2 recovery unit to avoid light gas accumulation in the reactor. The model of product yield and H_2 reacted in the hydrotreating and hydrocracking units are developed in Excel as reported in Sections 3.4.1 and 3.4.2. The purge rate is manipulated to maintain the H_2 partial pressure required by corresponding hydroprocessing unit, while flowrate of the make-up H_2 is manipulated to achieve the required H_2/Oil ratio in the reactor. BK10 EOS is used to estimate the vapor-liquid equilibrium in the flash drum.

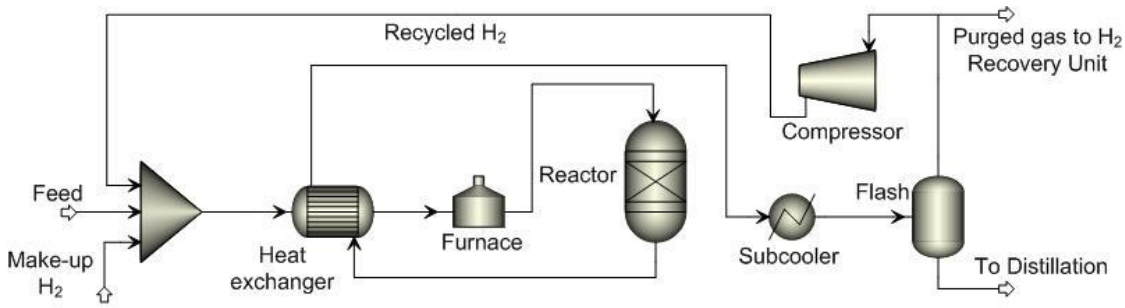

Figure 3.14 General configuration of the hydroprocessing unit

3.4.4 Blending Rules for Fuel Property Estimation

The final gasoline product is a blend of the isomers produced from the isomerization unit and the reformates produced from the catalytic reforming unit. The nonlinear blending rules used to estimate the Reid vapor pressure (RVP), RON, motor octane number (MON) of the gasoline blend are shown in Eq. (3.18) to Eq. (3.20), provided by the Ethyl Corporation (Maples, 2000), which is one of the widely used rules for petroleum product. Other properties of the blends are estimated by linear blending model or Aspen Plus Petroleum Characterization.

$$(RVP)_{mix} = \left[\sum v_i (RVP)_i^{1.25}\right]^{1/1.25} \tag{3.18}$$

$$R = \bar{R} + 0.03324[\overline{RJ} - \bar{R} \cdot \bar{J}] + 0.00085\left[\left(\overline{O^2}\right) - (\bar{O})^2\right] \tag{3.19}$$

$$M = \bar{M} + 0.04285[\overline{MJ} - \bar{M} \cdot \bar{J}] + 0.00066\left[\left(\overline{O^2}\right) - (\bar{O})^2\right] - 0.00632\left[\frac{\left(\overline{A^2}\right) - (A)^2}{100}\right]^2 \quad (3.20)$$

where the terms represent volumetric average values of properties as following:
R=RON, M=MON, J=RON-MON, RJ=R×J, MJ=M×J, O=Olefins vol%, A=Aromatics vol%

It has been reported that the FT diesel has high Cetane number and can satisfy the specification of diesel without any further upgrading except hydrotreating. The diesel pool in our design is a blend of diesel cuts from hydrocarbon recovery section and hydrocracking section. The properties of the diesel mixture are estimated by volumetric average, and the properties of individual diesel blend are available in the Aspen Plus report and open literature. (Bechtel, 1993; Shah, 1988) The Cetane index (CI) is the substitute measure of the Cetane number and can be estimated by ASTM D976 method shown in Eq. (3.21).

$$CI = 454.74 - 1641.416D + 774.74D^2 - 0.554B + 97.803(logB)^2 \quad (3.21)$$

where D = density at 15 ^{o}C in g/ml and B = mid-boiling temperature (D86) in ^{o}C.

3.5 Integrated Combined Cycle Power Plant

In the integrated combined cycle power plant, part of fuel gas and waste heat recovered from other unit operations are converted into multiple pressure level steams and electricity, which can be consumed as utilities in the process or considered as by-product for making profit.

3.5.1 Energy Balance and Gas Turbine

The fuel gas from the PSA unit and the hydrocarbon upgrading section provides fuel required in the FT synthesis and the entire hydrocarbon upgrading units. The remaining portion is sent to the gas turbine (GT) for electricity production as shown in Figure 3.15. The appropriate GT frame for this CBTL plant is selected to be GEE MS7001EA, which has a designed power rating of 85 MW, a simple cycle efficiency of 32.7% (for natural gas firing). This frame can be used for H_2-rich (H_2% >50%) gas. Chiesa et al. have evaluated the possibility of burning H_2-rich gas in large heavy-duty gas turbine designed for natural gas. (Chiesa et al., 2005) If H_2-rich gas is fed into GT, steam or nitrogen dilution is required to control NO_x emission, and several strategies can be considered for proper operation. (Chiesa et al., 2005) In this study, nitrogen dilution is selected for NO_x emission control, taking advantage of the existing ASU. It is assumed that the GT has

been appropriately modified so that it can be operated by firing H_2 rich gas with the pressure ratio and first rotor inlet temperature similar to the case for firing natural gas (Chiesa et al., 2005), while the turbine outlet temperature is about 10-15ºC lower. (Chiesa et al., 2005) The modeling approach reported by Bhattacharyya et al. (Bhattacharyya et al., 2011) is used to estimate the GT performance. The operating conditions of MS7001EA firing natural gas are obtained from the open literature. (GEE) For firing H_2-rich (about 60% H_2 concentration) gas in the GT for I-CBTL application, the N_2 to fuel ratio is manipulated to reduce the stoichiometric flame temperature to 2027ºC in order to control the NO_x emission. (Chiesa et al., 2005) The combustion air is compressed to 12.7 atm in an axial flow compressor. The GT combustor temperature is maintained at 1150ºC with a specified heat loss of 1.5% of the fuel gas LHV by manipulating the combustion air flow. The GT firing temperature is maintained at 1125ºC by manipulating the air flow rate to the combustor outlet gas before the first expansion stage. The exhaust temperature is maintained at 528ºC by manipulating the isentropic efficiency. (Bhattacharyya et al., 2011; Chiesa et al., 2005; GEE)

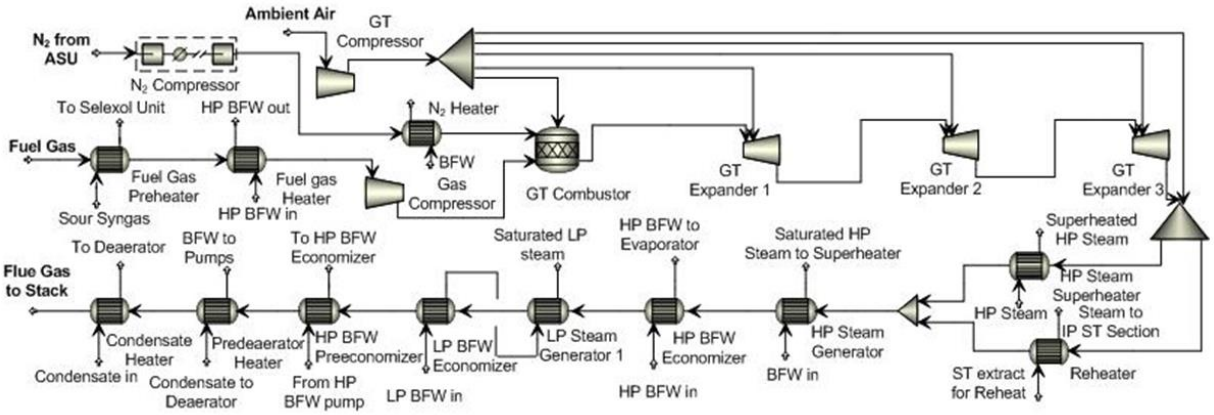

Figure 3.15 Configuration of the combined cycle power plant (fuel side)

3.5.2 Heat Recovery and Steam Generation, and Steam Turbine

A model of the triple-pressure HRSG with reheat is developed for the indirect CBTL process, with the configuration shown in Figure 3.16 and Table 3.13. The steam for power generation is mainly produced by recovering heat from the gas turbine exhaust flue gas, syngas cooler, heat recovery exchangers and the FT reactor cooling system. Part of the steam produced is sent to other units for operating. The pressure levels and steam turbine inlet conditions are specified based on the studies conducted recently for FT application (Bechtel, 1998; Martelli et al., 2012;

Steynberg and Nel, 2004), while 6% pressure drop is considered for the reheat section. (Spencer et al., 1963) The minimum temperature of flue gas to the stack is set at 120ºC. (Bhattacharyya et al., 2011)

Table 3.13 Configuration and operating conditions of the HRSG section and steam header

Steams	Pressure (kPa)	Temperature (ºC)	From	To
HP steam to ST	7419	373.9	SHR, HRSG	ST HP section
IP steam to ST	2172	346.1	SHR, Claus, FT (through reheater)	ST IP section
LP steam to ST	365	141.7	SHR, HRSG	ST LP section
HP steam to header	4137		ST	Upgrading unit, ATR
IP steam to header	931		ST	SWS, Selexol unit
LP steam to header	365		SHR, HRSG	MDEA/PZ unit, upgrading unit

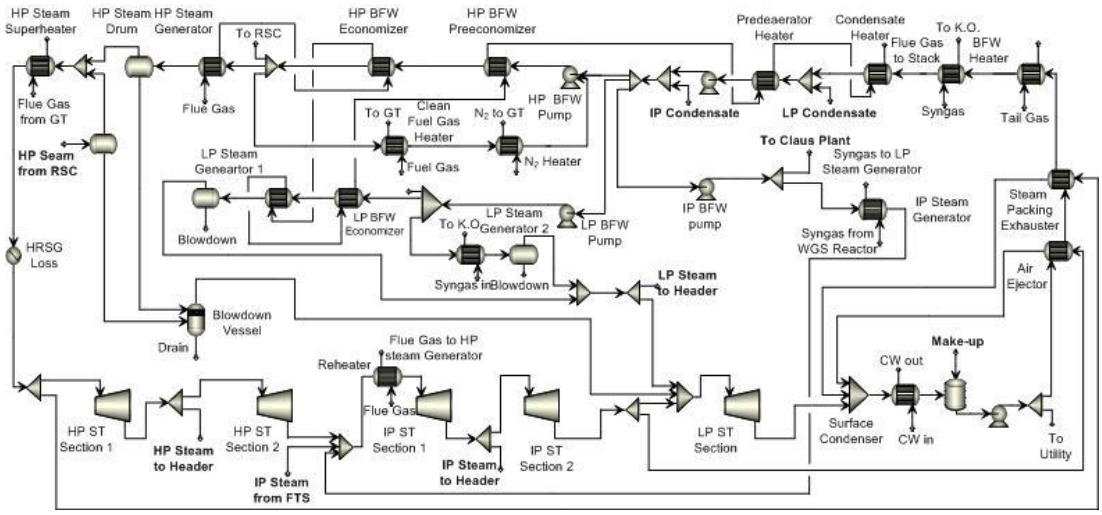

Figure 3.16 Configuration of the combined cycle power plant (steam side)

For the performance of a three-pressure-level steam turbine with multiple steam addition and extraction points, a simple stage-by-stage calculation is done in Matlab based on the algorithm presented by Lozza. (Lozza, 1990) In the model, the steam properties are evaluated by the IAPWS IF97 correlations and coded in Matlab. (IAPWA, 1997) Given the flowrate, pressure and temperature of the stage inlet, specific speed (N_s), stage isentropic enthalpy drop (Δh_{is}) and the outlet steam condition can be solved by Eq. (3.22), Eq. (3.23) and IAPWS IF97 correlations. The stage power output (W_i) is calculated by Eq. (3.24), where isentropic efficiency (η_{st}) is a known function of N_s and the average moisture content across the stage given by Lozza. (Lozza, 1990)

The net power output of the steam turbine is shown in Eq. (3.25). If no information is available, the exhaust velocity of last stage (u_{ex}) is assumed to be 250 m/s. (Baily et al., 1967)

$$N_s = (RPM/60) \cdot \sqrt{V_{ex}}/(\Delta h_{is})^{0.75} \quad (3.22)$$

$$\Delta h_{is} = k_{is} \cdot u^2/2 \quad (3.23)$$

where V_{ex} is the volumetric flow rate at stage outlet under isentropic condition in m^3/s;

Δh_{is} is the stage isentropic enthalpy drop in J/kg;

u is the mean diameter peripheral velocity of steam turbine in m/s, which is given by a function of stage number (Lozza, 1990);

k_{is} is the stage head coefficient, and correlated with N_s.

$$W_i = \Delta h_i = m_i \cdot \Delta h_{is,i} \cdot \eta_{st,i} \quad (3.24)$$

$$W_{net} = \eta_g \cdot \eta_m \cdot \eta_l \cdot \left(\sum_i W_i - m_{last\ stage} \cdot \Delta h_{ek}\right) \quad (3.25)$$

where, η_g, η_m, η_l are the generator loss, mechanical loss and sealing loss, which is a function of steam turbine power rating (Lozza, 1990); $\Delta h_{ek} = u_{ex}^2/2$ is the energy loss due to axial exhaust velocity.

3.6 Results and Discussion

Preliminary Studies were conducted for a simplified once-through I-CBTL plant with CCS for selection of technologies and operating conditions, as discussed in Section 3.6.1, while comprehensive sensitivity studies were conducted for the more efficient I-CBTL configuration as discussed in Section 3.1.

3.6.1 Preliminary Studies of the Once-Through I-CBTL-CCS Plant

A once-through I-CBTL configuration as shown in Figure 3.17 is considered for preliminary selection of technologies and operating conditions, as discussed in Section 3.6.1. To obtain the base case design, the optimal technology for post-FT CO_2 capture is selected in Section 3.6.1.3. Since the candidate technologies should first be optimally designed for a fair comparison, the optimal lean solvent loadings for the MEA and MDEA/PZ systems with intercooling and the optimal pressure levels for the Selexol unit are first obtained in Section 3.6.1.1 and Section 3.6.1.2. For brevity, the effect of the lean solvent loading for only the MDEA/PZ system is presented. This is followed by a study that helps selecting the optimal post-FT CO_2 capture

technology for the base case. The material and energy balance and the effect of FT inlet H_2/CO ratio were discussed in Section 3.6.1.4 and Section 3.6.1.5.

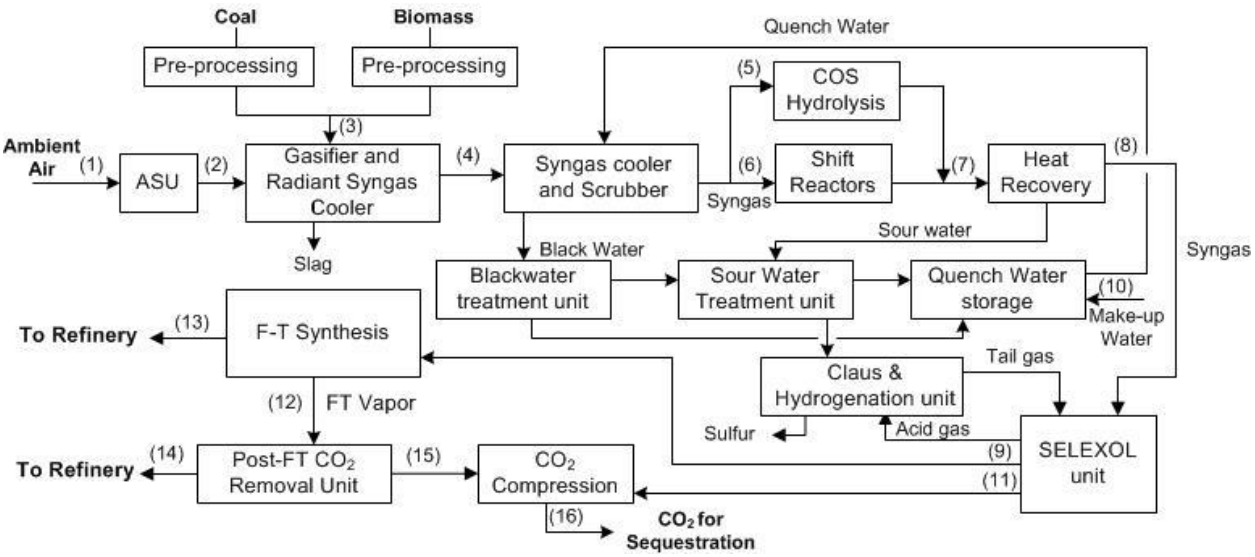

Figure 3.17 BFD of the once-through I-CBTL-CCS plant

3.6.1.1 Effect of Lean Solvent Loading on MDEA/PZ CO_2 Removal Unit

Lean solvent loading is one of the key operating conditions for amine-based CO_2 removal systems. A decrease in the lean solvent loading can reduce the solvent circulation rate required for the same extent of CO_2 removal. However, it can result in an increase in the heat requirement for solvent regeneration. Six values of lean solvent loading are investigated. Table 3.14 shows the variations in the key performance variables as the lean solvent loading is changed. It should be noted that the solvent circulation rate is manipulated to achieve 98% of CO_2 removal for these studies. The inlet FT stream composition can be found in Table 3.18 Stream 12. In these studies, the lean solvent loading is calculated in terms of moles of CO_2 per moles of amine groups. The costs of cooling water, LP steam, and power are taken as \$0.354/GJ, \$13.28/GJ, and \$16.8/GJ, respectively. (Turton et al., 2012) Table 3.14 shows that the utility cost first decreases as the lean solvent loading is increased. But with further increase in the lean solvent loading, the utility cost increases. The optimum lean solvent loading is found to be about 0.06 mol CO_2/ mol amine group for the FT product. It can be noted that the optimum value of lean loading can change if the gas composition, operating pressure and/or extent of CO_2 removal change. In this study, the utility consumption does not change significantly with the lean solvent loading, which is consistent with the experimental data (Seagraves and Weiland, 2009) and simulation results

(Salkuyeh and Mofarahi, 2013) available in the open literature for MDEA-based system and relatively low range of lean solvent loading and high operating pressure. One reason of this insensitivity is that with the decreasing of lean solvent loading, the temperature increasing from the exothermic reaction in the column increases and the CO_2 loading of the rich solvent decreases, which will limit the extent of the increase in the CO_2 capacity of the solvent, a function of the difference in CO_2 loading of the rich and the lean solution. Hence, the solvent circulation rate will not decrease as much as we expected with the decreasing lean solvent loading. Another reason is that the absorber is operated at higher pressure level than the normal post-combustion CO_2 removal system, which increases the effect of physical absorption step. From Salkuyeh and Mofarahi's work (Salkuyeh and Mofarahi, 2013), the effect of lean solvent loading on the utility consumption decreases with the increasing absorption pressure.

Table 3.14 Effect of lean solvent loading in the MDEA/PZ based CO_2 capture unit

Lean loading (mol CO_2/mol amines)	Solvent/CO_2 (mol/mol)	Cooling Water (GJ/hr)	Reboiler Duty (GJ/hr)	Pumping Power (kW)	Utility Cost ($/hr)
0.03	19.00	118.93	120.33	876.94	1694
0.05	19.47	118.64	120.18	888.87	1692
0.06	19.71	118.56	120.05	895.55	1690
0.08	20.22	118.82	120.27	909.78	1694
0.09	20.49	119.25	120.68	918.17	1700
0.10	20.77	119.30	120.88	924.25	1703

3.6.1.2 Effect of the Flash Operating Pressure on the Single-Stage Selexol Unit

In the single-stage Selexol unit for post-FT CO_2 capture, 93% CO_2 capture is achieved in the absorber and released in a series of flash drums at decreasing pressure levels. The reduction of the power consumption of this unit with the CO_2 compression can be achieved by operating the HP, MP and LP flash drums at optimum pressures. With different operating pressures of the LP flash drum, the CO_2 loading in the lean solvent recycled back to the absorber becomes different, which will significantly affect the solvent circulation rate of the system with the same extent of CO_2 removal. If the operating pressure of the LP flash drum is fixed, the solvent circulation rate does not change much with change in the pressures of MP and HP flash drums, but the relative

distribution of CO_2 obtained from the three flash drums will change, which will affect the power consumption of the CO_2 compression system. In this study, first the MP and HP drum pressures are fixed at 414 kPa and 690 kPa, respectively to study the effect of the operating pressure of the LP flash drum. Once the optimum LP drum pressure is obtained, the effect of the MP and HP flash drum pressures are obtained.

Figure 3.18 shows, as expected, that the solvent circulation rate increases with the increasing pressure of the LP flash vessel. With the increasing solvent circulation rate, the total power consumption increases mainly due to the increase in the refrigeration load and power consumption by the solvent circulation pump. An increase in the solvent circulation rate also results in higher loss of hydrocarbons. The optimal pressure of the LP drum is found to be 138 kPa. Once this pressure is fixed, Figure 3.19 shows the effect of the change in the pressure of the MP and HP flash drums. From Figure 3.19, the optimal pressures of the MP and HP flash drums are 310 kPa and 621 kPa, respectively. Figure 3.19 shows that the total power consumption does not change significantly in the pressure range studied. It should be noted that the pressures of the HP and MP drums were not changed widely as these pressures are constrained by the operating pressure of the H_2 flash drum (1.1 MPa). Furthermore, the CO_2 compressor consumes about 33% power in the Selexol unit, while the remaining power is consumed for solvent chilling and circulation.

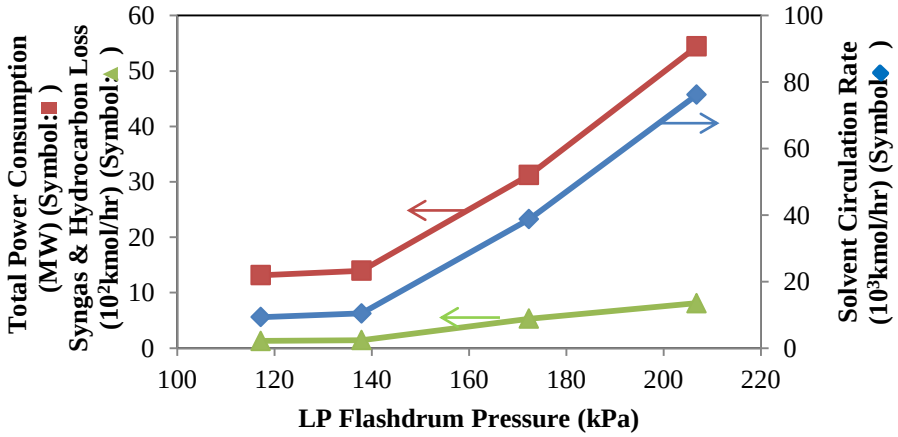

Figure 3.18 Effect of LP Flashdrum Pressure

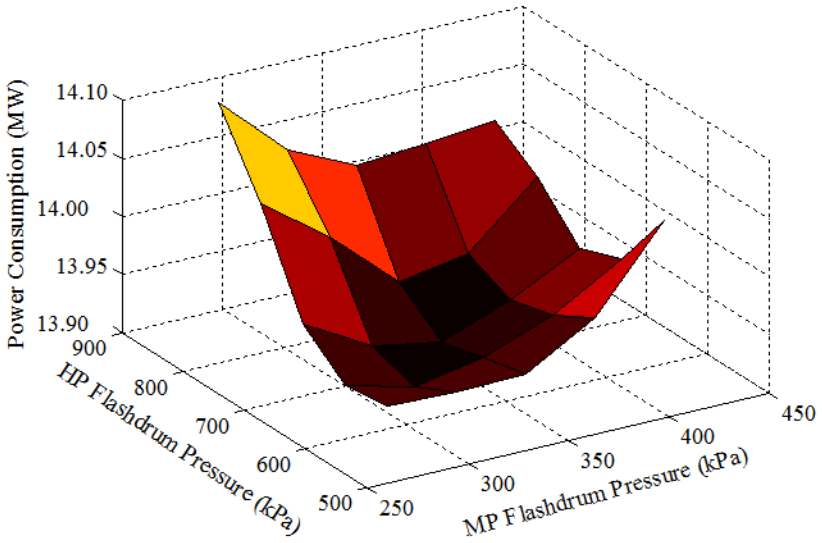

Figure 3.19 Effect of Pressures of MP and HP Flashdrums

3.6.1.3 Selection of the Post-FT CO_2 Capture Technology

In this section, three solvents, MEA, MDEA/PZ, and Selexol, are evaluated for removing CO_2 from the FT hydrocarbons. As mentioned before, the selectivity of Selexol, a physical solvent, is poor, and as a result significant amount of hydrocarbons can be lost. The lower heating value (LHV) of total hydrocarbon lost in the Selexol unit is calculated and converted to equivalent utility consumption for a fair comparison with the amine-based CO_2 removal technologies. The hydrocarbon loss and corresponding LHV loss in the Selexol unit are shown in Table 3.15. The loss is found to be about 15 wt% of total hydrocarbon produced. Table 3.16 indicates that the Selexol technology is not suitable for removing CO_2 from the FT product because of the considerable hydrocarbon loss. It also shows that the intercooling can significantly reduce the total utility cost of MEA and MDEA/PZ based CO_2 removal units. The MDEA/PZ CO_2 removal unit with intercooling gives the lowest utility cost and is therefore considered to be the desired technology for all following base case studies. It is also noted that the steam consumption of MDEA/PZ system is 14.4% less than that the MEA system, which might be more economic than the inhibited MDEA system (13.8% less than the MEA system) selected by Bechtel (Bechtel, 1992) as their base case. Additionally, it can be noted that the MDEA/PZ as a solvent is also advantageous due to its lower corrosion and lower vapor pressure in comparison to MEA.

Table 3.15 Hydrocarbon loss in the single-stage Selexol unit

	HC Loss (kg/hr)	Heat Loss (GJ/hr)
C_1	267	13.3
$C_{2=}$	1393	66.5
C_2	533	25.1
$C_{3=}$	1825	83.4
C_3	396	18.2
$C_{4=}$	1544	69.7
C_4	581	27.0
$C_{5=}$	1156	52.3
C_5	414	18.6
$C_{6=}$	630	28.1
C_6	217	9.6
Total		411.8

Table 3.16 Comparison of the three CO_2 removal technologies (including CO_2 compressing)

	Selexol	MEA w/o*	MEA w/*	MDEA/PZ w/o	MDEA/PZ w/**
Power (MW)	13.92	6.20	6.13	6.03	5.88
Cooling Water (GJ/hr)	30.84	175.65	167.32	164.81	147.33
Reboiler Duty (GJ/hr)		146.23	137.94	136.81	120.05
Heat Lost (GJ/hr)	411.8				
Utility Cost ($/hr)	6322	2379	2262	2240	2001

* w/o denotes without intercooling, and w/ denotes with intercooling; the lean solvent loading of MEA units is 0.27 mol CO_2/ mol amine (Dugas, 2006).
** the technology selected for all following base case studies

3.6.1.4 Material and Energy Balance of the Once-through I-CBTL-CCS Plant

The operating conditions of the key units for the base case are summarized in Table 3.17. In the base case, the H_2/CO ratio and the biomass/coal weight ratio are set to 2 and 8/92 (dry); the total feed flowrate of coal and biomass is 246.6 ton/hr and the MDEA/PZ with intercooling process is used for post-FT CO_2 removal. Considering the valid range for the available correlations and the economic analysis available in the open literature (Bechtel, 1992; Kou, 1985; Fox and Tam, 1995), the operating condition of the FT reactor for the base case is decided to be 257^{o}C and 2 MPa. In our base case design, the inlet H_2/CO ratio is set to 2 to decrease the selectivity of main byproduct CO_2 and the utilities consumption in the CCS facilities. After the operating pressure of the FT unit is decided, the operating pressure of other units is calculated by considering pressure

drop in all equipment. The operating temperature of each unit is decided based on the optimization studies available in the open literature (Bhattacharyya et al., 2011; Bechtel, 1992; Bain, 1992).

Table 3.17 Summary of the operating condition of key units

	Pressure (kPa)	Temperature (^{o}C)
Syngas Production		
ASU Air Compressor	1310	
Oxygen Compressor	2400	
Gasifier	2380	850
Fischer-Tropsch		
FT Reactor	2000	257
Selexol		
H_2S Absorber	2048	2
CO_2 Absorber	2013	2
H_2S Concentrator	1930	117
Selexol Stripper*	600	41/153
H_2 Recovery Drum	1620	
LP Flash Vessel	241	
Post-FT CO_2 Removal		
Absorber	1965	38
Stripper*	172	38/116

*For strippers, the temperatures of condensers and reboilers are listed.

Table 3.18 lists the flow rate of the key species in the main streams numbered in Figure 3.17 for the base case conditions. In the base case, 6% of carbon in the coal and biomass is vented to the atmosphere in form of CO_2, 53% of carbon is stored in the captured CO_2, while the remaining carbon is converted to the FT syncrude and fuel gas. To simplify the results and discussion of the plant utility consumptions, the plant shown in Figure 3.17 is divided into four sections for showing the results and discussion. They are syngas production section, CCS section, FT synthesis section and others. Table 3.19 lists the main utility consumptions for the base case. The syngas production and the CCS sections are the two main consumers of the electric power, consuming about 54% and 36%, respectively, of total power demand. The production of purified syngas has been reported to cost 60-70% of the total capital and running cost in conventional CTL plants without CCS facilities. (Dry, 2002) The HP, IP and LP steam are generated from the

syngas production and cleanup section, Claus unit, and the FT synthesis section. The strippers and heaters in the once-through I-CBTL plant consume IP and LP steam. It can be noted that the HP steam generated in the radiant syngas cooler can be used to produce electricity. The power consumptions in the remaining units are calculated based on the utility summary available in the open literature (Reed et al., 2007; NETL, 2010; Bechtel, 1998) by scaling up with respect to the coal and biomass flowrate (dry).

Table 3.18 Stream summary of the once-through I-CBTL-CCS plant

Stream	1	2	3	4	5	6	7	8
Name	Air	O_2	Coal & Biomass	Raw syngas	Raw syngas	Raw syngas	Shifted syngas	Cooled syngas
Temperature (^oC)	15	32	16	850	208	208	301	21
Pressure (kPa)	103	2,380	2,380	2,380	2,324	2,324	2,289	2,082
Flowrate (kg/hr)								
H_2O	5,792			74,468	105,675	132,678	186,570	467
CO_2	386			162,520	72,014	90,412	288,921	288,830
O_2	197,602	184,434						
N_2	643,327	2,794		5,988				
CH_4				2,436	1,080	1,356	2,436	2,431
CO				239,229	106,056	133,159	158,774	158,769
COS				272	118	150	14	14
H_2				16,402	7,271	9,131	22,190	22,190
H_2S				5,897	2,604	3,266	5,947	5,919
Coal			226,972					
Biomass			19,623					
Slag				24,916				
C_2-C_4				231	104	127	231	231
C_5-C_{10}								
C_{11}-C_{20}								
Wax								
Oxygenates								

Stream	9	10	11	12	13	14	15	16
	Clean syngas	Make-up water	CO_2	FT vapor	FT liquid	Light gases	CO_2	CO_2
Temperature (^oC)	3	16	37	38	38	39	38	89
Pressure (kPa)	2,013	1,014	203	1,979	1,979	1,965	172	15,272
Flow Rate (kg/hr)								
H_2O	535	173,089	5	272	109	272	73	78
CO_2	28,550		260,280	58,846	1,538	1,175	57,671	317,951
O_2								
N_2								
CH_4	2,350		73	3,211	27	3,211		73

CO	153,834	4,940	12,211	41	12,193	18	4,958
COS							
H_2	22,136	64	5,135	5	5,126	9	73
H_2S							
Coal							
Biomass							
Slag							
C_2-C_4	27	204	6,446	1,021	6,446		204
C_5-C_{10}			3,012	13,531	3,012		
C_{11}-C_{20}			9	12,760	9		
Wax				27,189			
Oxygenates			689		689		

Table 3.19 Summary of the utilities in the once-though I-CBTL-CCS plant

Power Consumptions (MW)		%	Steam Generation (GJ/hr)	
Syngas Production	88.2	53.58	Syngas Production	
Syngas Generation	77.1	46.84	Radiant Syngas Cooler (HP steam)	-240.6
Steam Generation	0.5	0.3	Heat Recovery (IP steam)	-113.2
Black and Sour Water Treatment	10.6	6.44	Heat Recovery (LP steam)	-348.1
CO_2 Capture and Storage	59.5	36.15	SWS Reboiler (IP steam)	79.6
Selexol	33.1	20.11	Fischer-Tropsch Synthesis	
MDEA/PZ	0.9	0.55	IP Steam Generator (IP steam)	-369.1
CO_2 Compression	25.5	15.49	CO_2 Capture and Storage	
Fischer-Tropsch Synthesis	0.9	0.55	Selexol Striper Reboiler (IP steam)	197.9
Others	16	9.72	MDEA/PZ Striper Reboiler (LP steam)	120.1
Total	164.6	100	Others (IP steam)	4.5

3.6.1.5 Effect of the FT Inlet H_2/CO Ratio on the FT Unit

As shown before, the high H_2/CO ratio results in a decrease in the utilities consumption in the CCS units. However, an increase in the H_2/CO ratio raises the light gas selectivity and reduces the fuel yield of the CBTL plant. Figure 3.20 shows the carbon number distribution in light hydrocarbons from C_1 to C_{20} (weight basis) for different H_2/CO ratios. The summary of product selectivity and carbon efficiency of the entire once-through I-CBTL plant can be found in Table 3.20.The figure shows a high yield of CH_4 in comparison to other hydrocarbons, which is consistent with the experimental results available in the open literature. (Bechtel, 1992a; Kuo, 1985; 1983; Steynberg and Dry, 2004) The higher the H_2/CO ratio is, the higher the selectivity of light hydrocarbons is. However, the H_2/CO ratio is not expected to affect the overall syngas

conversion significantly. According to Figure 3.23, the CO_2 selectivity increases with a decrease in the inlet H_2/CO ratio. However, when H_2/CO ratio increases, more CO in the raw syngas is converted to CO_2 in the WGS unit and captured in the Selexol unit. As a result, lower amount of syngas enters the FTS unit. In summary, the overall carbon efficiency, defined as fraction of carbon in feed converted to hydrocarbon, of the CBTL plant does not change much with the change in the H_2/CO ratio, but the utilities consumption in the CCS unit and CH_4 production does. This study suggests that an optimal H_2/CO ratio exists. The optimum can be determined by conducting a techno-economic analysis. To evaluate the impact of the H_2/CO ratio on the plant economics, the product upgrading section needs to be considered.

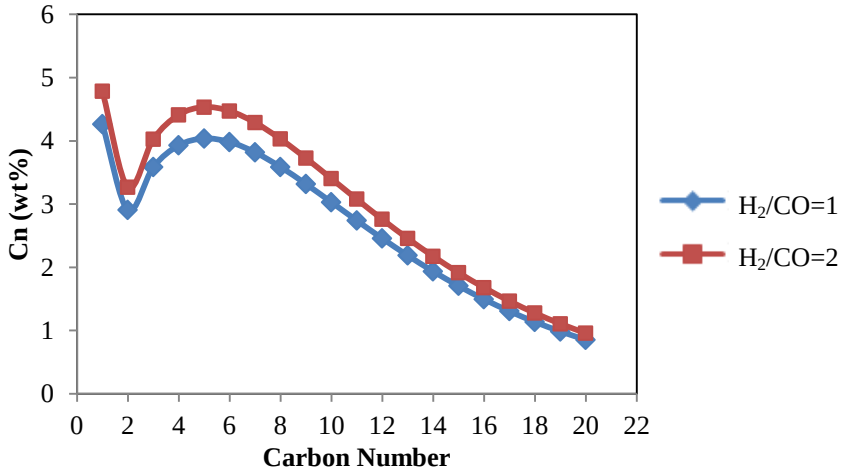

Figure 3.20 Carbon number distribution

Table 3.20 Effect of the H_2/CO ratio on the FT unit

H_2/CO	2	1.7	1.5	1.3	1
Carbon Efficiency (%)	34.7	35.1	35.4	35.5	35.6
C_1-C_4 (wt%)	16.48	16.16	15.88	15.51	14.68
C_5-C_{10} (wt%)	27.53	27.00	26.52	25.91	24.51
C_{11}-C_{20} (wt%)	15.80	15.49	15.22	14.86	14.07
Wax (wt%)	40.19	41.35	42.38	43.72	46.74

3.6.2 Sensitivity Studies of the Base Case I-CBTL Plant

With the preliminary decisions made in Section 3.6.1, Section 3.6.2.1 showed the material and energy balance of the base case I-CBTL-CCS plant with the configuration discussed in Section

3.1. A number of studies have been conducted for analyzing the effects of key design parameters that are listed in Table 3.21. First, the effect of steam to carbon ratio on the ATR unit is discussed in Section 3.6.2.2. Then the advantage of the novel integrated hydrotreating approach is discussed in Section 3.6.2.3 where it is compared with the conventional separated hydrotreating approach. Sections 3.6.9 to 3.6.10 show evaluation of the impact of the H_2/CO ratio in the FT inlet stream, biomass/coal ratio and extent of CCS on the thermal efficiency and fuel yield of the novel I-CBTL plant. Section 3.6.11 discusses the effect of different biomass types on the plant performance. The properties of the upgraded FT fuels are discussed in Section 3.6.12. Finally, the results of the base case are compared with other related studies available in the open literature.

Table 3.21 Key design parameters of the I-CBTL-CCS plant (base case)

Design parameter	Value
Biomass type	Bagasse
Plant capacity (bbl/day)	10,000
Biomass/coal (wt/wt, dry)	8/92
Hydrotreating approach	Integrated
Steam/carbon ratio in the ATR inlet	0.63
H_2/CO in FT inlet stream (mol/mol)	2
CO_2 captured in Selexol unit (%)	90
CO_2 captured in MDEA/PZ unit (%)	98
CO_2 stream to compression section (%)	100

3.6.2.1 Material and Energy Balance of the I-CBTL-CCS Plant

The material and utility summaries of the base case can be found in Table 3.22 and Table 3.23. The costs of raw materials, products and utilities are listed in Table 3.24. (Turton et al., 2012) Table 3.23 indicates that syngas production and CCS are the two major utility consumers in the I-CBTL plant, with is consistent with open literature. (Jiang and Bhattacharyya, 2014; Dry, 2002; Kreutz et al., 2008) It should be noted that the process fuel required in the I-CBTL plant is supplied by the fuel gas header while the steams and electricity are supplied by the combined cycle plant.

Table 3.22 Summary of material balance of the I-CBTL-CCS plant (base case)

Steam	1	2	3	4	5	6	7	8	9	10	11	12
Temperature (^oC)	32	16	850	284	258	49	49	261	38	25	38	81
Pressure (kPa)	2380	2380	2380	2289	1999	1965	1965	1999	1965	101	138	15,270
Flowrate (kg/hr)												
Coal		173747										
Biomass		15021										
H_2O			57005	149827	409	109	267	5281	195			30
CO_2			124409	204043	20451	1398	54057	2202	397			229545
O_2	141,184											
N_2	2139		4584	4583								
CH_4			1865	1863	1676	30	3743	721	2751		1130	309
CO			183130	132431	130823	39	11897	22168	8732		3187	4745
COS			208	109								
H_2			12570	16203	16154	7	5509	5594	4043		1474	64
H_2S			45142	4547								
C_2-C_4			177	177		910	6512	14	3479		6853	141
C_5-C_{10}						13933	3251	1531	1531		1725	
C_{11}-C_{20}						12036	7	1	1			
Wax						25632						
Oxygenates						3279	774	553	553			
Gasoline										18391		
Diesel										30579		

Table 3.23 Summary of utility consumption of the I-CBTL-CCS plant (base case)*

Sections	Power	74 bar steam	42 bar steam	21 bar steam	9.3 bar steam	3.7 bar steam	Fuel
	MW	kg/hr	kg/hr	kg/hr	kg/hr	kg/hr	GJ/hr
Syngas Production	59.48	(119895)		(25667)	58340	(119680)	8.31
Syncrude Production	0.88		6784	(186727)			19.97
CO_2 Capture & Storage	42.24				79538	50841	
Product Upgrading	1.16		213			1190	87.31
Fuel Gas Header							(699.51)
Others	12.94			(4266)			
Gas Turbine	(56.52)						583.92
HRSG	(72.44)	119895	(6997)	216660	(137878)	67649	

* ( ) means utility generation

Table 3.24 Cost of raw materials, products and utilities

	Cost		Cost
Coal ($/dry ton)	46	LP steam ($/GJ)	13.28

Biomass ($/dry ton)	80	MP steam ($/GJ)	14.19
Gasoline ($/gallon)	3.024	Electricity ($/GJ)	16.8
Diesel ($/gallon)	2.902	Cooling water ($/GJ)	0.354

3.6.2.2 Effect of the Steam to Carbon Ratio at the ATR Inlet

The effect of steam/carbon ratio in the ATR unit is evaluated by fixing the H_2/CO ratio in the FT inlet to 2, the same as the base case condition. As seen in Table 3.25, the results indicate that the H_2/CO ratio in the ATR outlet and the utility consumptions increase with the increase in the steam/carbon ratio. As the H_2 demand should be satisfied, a higher H_2/CO ratio in the ATR outlet would require a lower extent of reactions in the WGS reactor and therefore the percent of CO_2 captured by physical solvent in the Selexol unit decreases with the increasing steam/carbon ratio. As a results, the penalty of CCS increases as the steam/carbon ratio is increased. Furthermore, the FT reactor is usually operated with an inlet H_2/CO ratio less than 2.1. Therefore, a low steam/carbon ratio is recommended at the ATR inlet for FT application. (Steynberg and Dry, 2004) In order to prevent coking, the steam/carbon ratio is set to be 0.63 for the base case. (Steynberg and Dry, 2004)

Table 3.25 Effect of steam to carbon ratio on the performance of ATR unit

Steam/Carbon (mol/mol)	0.5	1.0	2.0	3.0
Performance				
H_2 produced (kmol/hr)	759	791	822	857
CO produced (kmol/hr)	486	454	394	359
H_2 produced/CO produced (mol/mol)	1.6	1.7	2.1	2.4
H_2/CO in ATR outlet (mol/mol)	3.4	3.6	4.1	4.8
Utilities				
O_2 consumed (kg/hr)	7335	7947	9075	10598
Steam consumed (kg/hr)	5460	10729	21368	33440
CO_2 captured by Selexol unit (%)	79.3	78.8	77.5	75.1

3.6.2.3 Advantages of the Integrated Hydrotreating Unit

By comparing configuration of the integrated hydrotreating approach (Figure 3.12) with the conventional separated hydrotreating approach (Figure 3.13), it clearly shows that the integrated hydrotreating approach can reduce the plant footprint and make the plant more compact. In the

integrated hydrotreating approach, the entire hydrotreated syncrude is sent to the main distillation column to separate the product to light naphtha, heavy naphtha, diesel and wax, which is similar to the main distillation column in the separated hydrotreating approach design. The only difference in the main distillation columns is that the heavy naphtha side-stripper is not considered in the separated approach, because the entire naphtha cut is sent to the naphtha hydrotreating unit together and then separated in another distillation column. One advantage of the integrated hydrotreating approach is to eliminate some distillation columns from the conventional approach, which are required to remove light gases from the products and separate light naphtha from heavy naphtha, thus consuming considerable amount of plant fuel because of the large reboiler duty (R_2, R_3, and R_4 in Figure 3.13). The disadvantage of the integrated hydrotreating approach is that the wax, which does not necessarily need to be hydrotreated, is also sent to the hydrotreating unit, resulting in the increase in the preheat furnace duty and the hydrotreater reactor size. However, the temperature increase in the furnace is very low, just about 20ºC and the wax remains in liquid phase. Therefore the increase in the heat duty and the volumetric flowrate to the reactor is not very large. For the separated hydrotreating approach, the utility consumptions in and capital investment for naphtha and diesel hydrotreating units are given by Bechtel (Bechtel, 1993; 1998), and then the capital investment is escalated with the Chemical Engineering Plant Cost Index (CEPCI). (Turton et al., 2012) For the remaining units, the utility consumptions and capital investment are estimated using Aspen Plus and APEA, respectively. All of the columns are sized in Aspen Plus; all of the heat exchangers are sized in EDR; and the remaining equipment items are sized in APEA. The materials of construction (MOC) for all the equipment are selected based on the operating temperature, service stream and industry application experience. In the hydrotreating unit, the reactor and the H_2 compressor are constructed by stainless steel and the hydrotreater feed furnace is constructed by Cr-Mo low alloy steel, while the other components are constructed by carbon steel. Detailed specifications of the APEA model for capital investment estimation can be found in Appendix B. Table 3.26 and 3.27 show the comparison of heat consumption and capital investment between the two hydrotreating approaches. It is observed that the integrated hydrotreating approach can reduce the heat consumption by about 30% and the capital investment by about 25%.

Table 3.26 Major utility consumptions of the two hydrotreating approaches

Integrated hydrotreating			Separated hydrotreating		
Unit	Description	GJ/hr	Unit	Description	GJ/hr
F_1	Hydrotreating preheater	4.26	F_3	Furnace of main column	24.75
F_2	Furnace of main column	23.70	F_5+R_3+R_4	Naphtha hydrotreating	19.83
R_1	Reboiler of stabilizer	3.67	F_4+R_2	Diesel hydrotreating	3.44
STM	Stripping steam	2.51	STM	Stripping steam	2.18
COM	Hydrogen compressor	3.87	COM	Hydrogen compressor	3.87
Total		38.01	Total		54.07

Table 3.27 Capital investment of the two hydrotreating approaches

Integrated hydrotreating		Separated hydrotreating	
Section	MM$	Section	MM$
Integrated hydrotreating loop	8.17	Hydrocarbon recovery	2.56
Hydrocarbon recovery	3.43	Naphtha hydrotreating	4.70
		Diesel hydrotreating	9.45
Total	11.60	Total	16.71

3.6.2.4 Effect of H_2/CO Ratio in the FT Inlet Stream

In the I-CBTL plant, the H_2/CO ratio in the syngas can be adjusted in the WGS reactor before sending to the Selexol unit, as shown in Figure 3.1. Studies indicate that the H_2/CO ratio in the FT inlet stream not only affects the penalty of CCS but also the fuel product yield and distribution. (Jiang and Bhattacharyya, 2014; Steynberg and Dry, 2004) Hence, in this study, a sensitivy study is conducted by changing the H_2/CO ratio from 1 to 2.25 and keeping the raw materaial flowrate and other design parameters the same as the base case.

Figure 3.21 indicates that with an increase in the H_2/CO ratio in the FT inlet stream, the penalty of CCS keeps reducing in a once-through I-CBTL plant without product upgrading. For the Selexol unit, the solvent circulation rate reduces with increasing H_2/CO ratio because of the higher partial pressure of CO_2, which can provide more driving force for the physical absorption process. For the MDEA/PZ unit, the solvent circulation rate decreases because the CO_2 selectivity in the FT reactor decreases with the increasing H_2/CO ratio, as shown in Figure 3.22. (Jiang and Bhattacharyya, 2014) The CO_2 can be recovered from the Selexol unit at different

pressure levels, usually higher than the pressure of the CO_2 released in the chemical absorption unit, which indicates that the penalty of CO_2 compression section can be reduced as larger potion of CO_2 is captured in the Selexol unit. In Figure 3.21, the total utility cost of CCS is calculated by Eq. (3.26), where F_u is the utility consumption of u^{th} type of utility in GJ/hr; C_u is its unit cost in \$/GJ listed in Table 3.24.

$$C_{CCS}^{u} = \sum C_u F_u \tag{3.26}$$

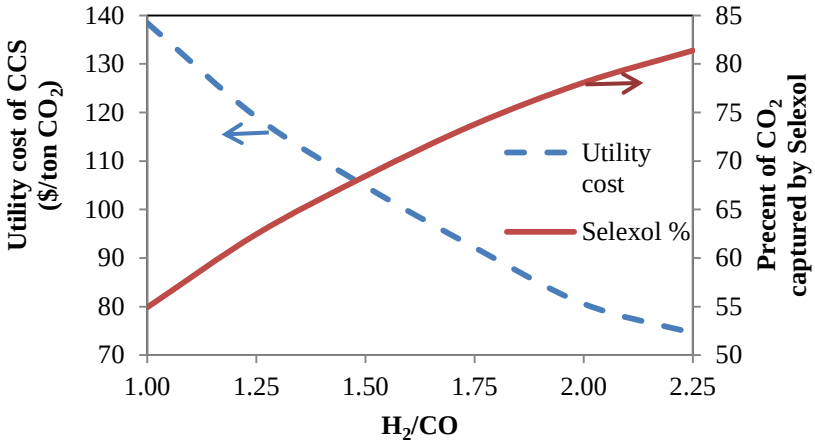

Figure 3.21 Effect of H_2/CO ratio on the penalty of CCS

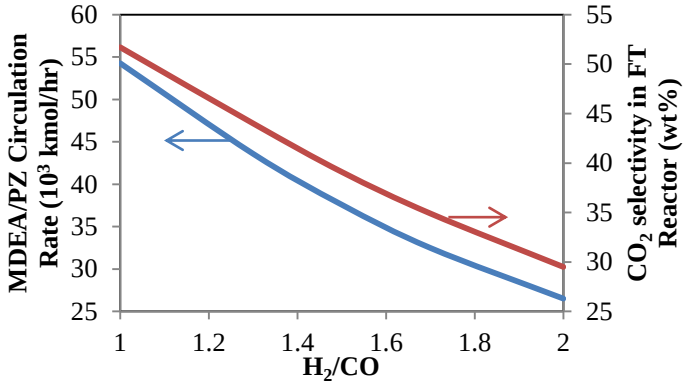

Figure 3.22 Effect of the H_2/CO ratio in the post-FT CO_2 capture unit

Because the H_2/CO ratio in the FT inlet has a strong impact on the hydrocarbon selectivity in the FT reactor (Jiang and Bhattacharyya, 2014; Steynberg and Dry, 2004; Dry, 1981), the product distribution and the fuel yield of the I-CBTL plant highly depend on the H_2/CO ratio in the FT inlet. Figure 3.23 indicates that the gasoline to diesel ratio keeps increasing with increasing

H_2/CO ratio, because the FT reaction produces lighter hydrocarbon with higher H_2/CO ratio in the inlet. (Jiang and Bhattacharyya, 2014; Steynberg and Dry, 2004; Dry, 1981) Figure 3.24 to Figure 3.26 also show that the fuel yield, overall plant efficiency and plant profit increase with the increasing H_2/CO ratio but with decreasing slope. That is because with a higher H_2/CO ratio, the H_2 conversion decreases in the FT reactor. As a result, the recycled light gases from the post-FT CO_2 capture unit has a higher H_2 percentage, and a smaller portion is needed to be sent to the H_2 plant to produce the H_2 required for the product upgrading section. A larger portion can be sent back to the FT unit through the ATR to produce more syncrude. In the meanwhile, less amount of light gas is purged from the H_2 unit, which is then sent to the combined cycle plant for power production, where no CO_2 capture facilities are considered for the flue gas. Hence, with the same extent of CO_2 removal in the Selexol unit and the MDEA/PZ unit, the electricity production and overall CO_2 emission in plant also decrease with the increase in the H_2/CO ratio. However, it is expected that with a very high H_2/CO ratio, the fuel yield will decrease as more amount of carbon in the feedstock gets converted to CO_2 and removed by the Selexol unit before being sent to the FT unit for fuel production. In this study, H_2/CO ratio larger than 2.25 is not considered because of the absence of the experimental data of FT reactor operated at very high H_2/CO ratio. It should be noted that in Figure 3.25, the thermal efficiency is defined as energy output (fuels and electricity) to input (coal and biomass) ratio in HHV basis, while the carbon efficiency is defined as percent of carbon in the feedstock converted into fuels. The profit function in Figure 3.26 is defined as Eq. (3.27), where C_i is the unit cost of i^{th} item listed in Table 3.24; F_i is the material or energy flow rate of the i^{th} item.

$$PF = \sum_{prod} C_p F_p - \sum_{feed} C_f F_f - \sum_{utility} C_u F_u \tag{3.27}$$

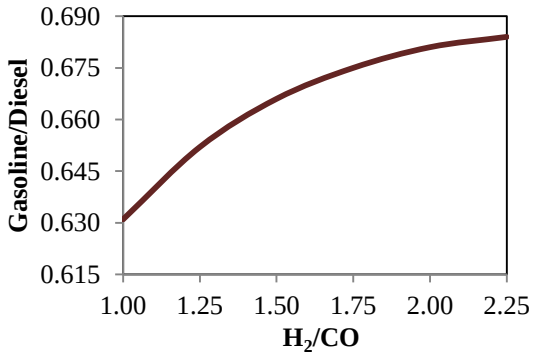

Figure 3.23 Effect of H_2/CO ratio on the product distribution

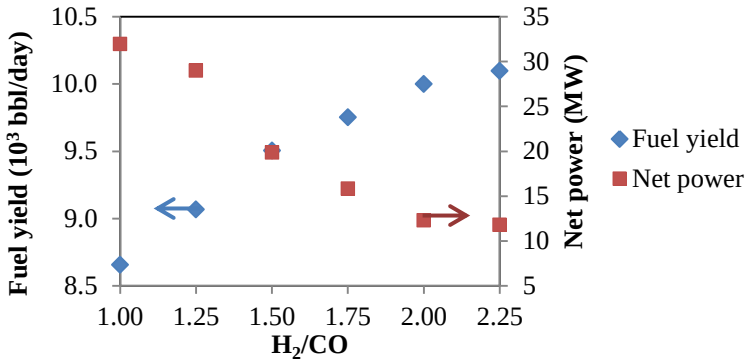

Figure 3.24 Effect of H_2/CO ratio on the fuel yield

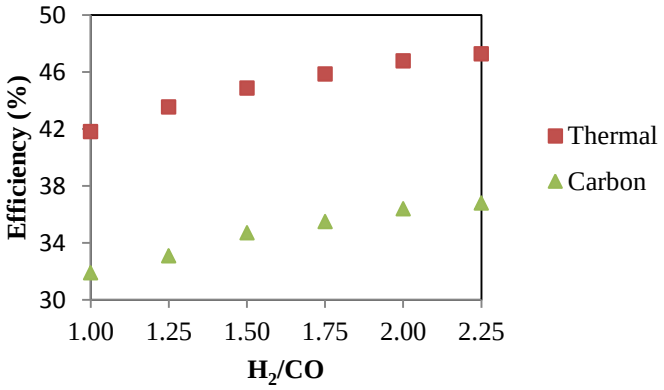

Figure 3.25 Effect of H_2/CO ratio on the plant efficiency

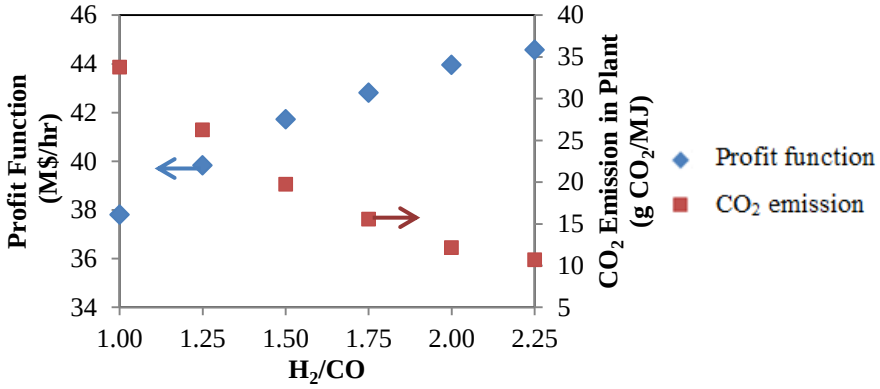

Figure 3.26 Effect of H_2/CO ratio on the plant profit and CO_2 emission

3.6.2.5 Effect of Biomass to Coal Ratio

As mentioned before, the carbon footprint of the I-CBTL plant can be decreased by increasing the biomass content in the feedstock. In this study, a sensitivity analysis is conducted for

biomass/coal weight ratios of 8/92, 15/85, 20/80 (dry) to estimate the effect of feedstock composition on the plant performance, especially product yield and the plant efficiency. Relatively low biomass content is considered in this study mainly considering sustainability of the plant. (Wang and McNeel, 2009) For the alternative cases, the total amount of dry feed, and other design parameters are fixed to be the same as the base case. The simulation results are presented in Table 3.28. It shows that as the biomass content keeps increasing, the overall fuel production and the plant thermal efficiency decreases, mainly because of the relatively high oxygen content in the biomass. Our previous study has shown that an increase in the biomass/coal ratio results in an increase in the H_2/CO ratio in the raw syngas (Stream 3 in Figure 3.1). (Jiang and Bhattacharyya, 2014) As a consequence, the extent of the WGS reaction and the heat recovery decreases if the H_2/CO ratio keeps increasing in the raw syngas while the H_2/CO ratio at the WGS outlet (Stream 4 in Figure 3.1) remains constant. (Jiang and Bhattacharyya, 2014)

Table 3.28 Effect of biomass/coal ratio on the I-CBTL-CCS plant

Biomass/coal	dry weight	8/92	15/85	20/80
Feedstock				
Coal (dry)	ton/hr	153.44	141.80	133.49
Biomass (dry)	ton/hr	13.29	24.93	33.24
Product				
Gasoline	bbl/hr	4,050	3,848	3,721
Diesel	bbl/hr	5,950	5,656	5,465
Total FT liquid	bbl/hr	10,000	9,504	9,186
Net Electricity	MW	12.28	9.81	7.62
Thermal Efficiency	HHV			
FT liquid	%	45.9	44.7	44.0
Net Electricity	%	0.9	0.7	0.6
Total	%	46.8	45.4	44.6

3.6.2.6 Effect of Biomass Types

Impact of biomass type on the performance of the I-CBTL process is shown in Table 3.29. The results indicate that the thermal efficiency of wood chips is lower than bagasse and torrefied wood due to the higher oxygen content and lower hydrogen/carbon ratio in wood chips as shown

in Table 3.1. The carbon efficiency remains similar because all the other key design parameters remain the same and the biomass/coal ratio is small in the feedstock.

Table 3.29 Alternative biomass as feed stock

Biomass type		Wood chips	Bagasse	Torrefied wood
Feedstock				
Coal (dry)	ton/hr	153.8	153.4	153.3
Biomass (dry)	ton/hr	13.5	13.3	13.8
Product				
Gasoline	bbl/day	4050	4050	4050
Diesel	bbl/day	5950	5950	5950
Electric Power	MW	5.09	12.28	30.00
Analysis				
C Captured by FTL	%	36.3	36.4	38.2
Thermal Efficiency	% (HHV)	46.1	46.8	47.9

3.6.3 Properties of the Gasoline and Diesel Product

As discussed in Section 3.4, with the simplified refinery design shown in Figure 3.2, the required specifications of gasoline and diesel can be achieved by adjusting the D86 95 vol% cut point of the light and heavy naphtha stream of the main distillation column. In the base case, the D86 95 vol% cut point of the light and heavy naphtha stream is set to be 94℃ and 174℃, respectively. Table 3.30 shows the values of the final gasoline blends properties and the selected USA standard of gasoline. Table 3.31 shows that the conceptual design developed in this study can produce on-specification diesel; and the estimated properties from our model are consistent with the industrial data. (Leckel, 2010)

Table 3.30 Estimated properties of the gasoline pool and specifications of US gasoline

		USA Specification		
Fuel property	Product	min	max	Source
Restrictions on boiling range				
D86 50 vol% (ºC)	92.8	76.7	121	ASTM D4814
D86 90 vol% (ºC)	139.4		190	ASTM D4814
RVP (kPa)	47.9		54	ASTM D4814
Restrictions on composition				

Aromatics (vol%)	34.1		35	CA RFG*
Benzene (vol%)	0.4		1	40 CFR 80
Sulfur (ppm, wt)	0		20	40 CFR 80
Road Octane Number ([R+M]/2)	87.2	87		

* flat limit of small refinery from California RFG, Phase 3

Table 3.31 Estimated properties of the diesel pool and specifications of No.2 Diesel

		Sasol	USA Specification		
Fuel property	Product	LTFT	Min	Max	Source
Restrictions on boiling range					
Density at 15 ºC (kg/m^3)	769	772		876	ASTM D975
Flash Point (ºC)	60	60	52		ASTM D975
Restrictions on composition					
Aromatic (vol%)	0	0.7		35	ASTM D975
Sulfur (ppm, wt)	0	<5		15	ASTM D975
Cetane Number	>70	>70	40		ASTM D975
Cetane Index	>70		40		

3.6.4 Model Validation and Comparison of the Novel I-CBTL Plants

Table 3.32 shows a comparison of the material and energy balances of the indirect CBTL plant with CCS (base case) with the data available in the open literature for the indirect CTL plant. (NETL, 2007; Bechtel, 1998; Liu et al., 2011) As shown in Table 3.32, the overall thermal efficiency and the carbon efficiency of the base case analyzed in this project is similar to those of the previous studies. The efficiency obtained in this study is slightly higher than the data reported by other studies with the similar extent of CO_2 capture mainly due to the difference in feedstock, CO_2 capture technology, extent of CO_2 capture, product upgrading technologies and their operating conditions as discussed in the previous sections.

Table 3.32 Material and energy balance of the I-CBTL plant

		Bechtel	NETL[a,]	Liu et al.	Liu et al.	Base case[b]
Report Year		1993	2007	2011	2011	2014
Feedstock						
Coal (dry)	ton/hr	702.13	908.54	892.02	94.88	153.44
Biomass (dry)	ton/hr	0	0	0	126.83	13.29
Product						

Propane	ton/hr	6.45	0	0	0	0
Butanes[c]	ton/hr	(11.98)	0	0	0	0
Gasoline	bbl/day	23,943	22,173	N/A	N/A	4,050
Diesel	bbl/day	24,686	27,819	N/A	N/A	5,950
Total FT Liquid	bbl/day	48,629	49,992	50,000	9,845	10,000
Electric Power	MW	-54.32	124.25	295	53	12.28
Analysis						
CO_2 Removal Technology		Rectisol MDEA	Selexol, MDEA	Rectisol	Rectisol	Selexol, MDEA/PZ
CCS		No	Yes	Yes	Yes	Yes
C Captured by FTL	%	N/A	35.5	34.1	33.7	36.4
C Captured by CCS	%	0	56.6	51.6	53.7	56.9
Thermal Efficiency[d]	% (HHV)	51.8	42.4	46.0	47.5	46.8

a) Additional refinery is required for producing on-specification gasoline; efficiency is expected to be higher.
b) Data generated in this study
c) In Bechtel's refinery design, purchased n-butane are required for the upgrading section, such as C_4 isomerization and alkylation unit. (Bechtel, 1993; 1998)
d) The HHV of FT derived gasoline and diesel is assumed to be 45,471 kJ/kg and 47,655 kJ/kg.

3.7 Conclusions

A plant-wide model of an I-CBTL plant with CCS has been developed in Aspen Plus 7.3.2. This model can reasonably estimate the plant performance with different design parameters and be used for techno-economic analysis. The comparison between the three post-FT CO_2 removal technologies shows that the MDEA/PZ CO_2 removal technology has lesser overall penalty than the Selexol and MEA CO_2 removal technologies. Intercooling of the solvent in the absorber is found to decrease the solvent circulation rate and utility consumption for both MDEA/PZ and MEA cases. The optimum lean solvent loading for CO_2 removal from the FT product stream is found to be 0.06 mol CO_2/ mol amine when MDEA/PZ is used as the solvent.

Sensitivity studies have been conducted to analyze the impact of key design parameters on the performance of the novel I-CBTL plant. The results indicate that low steam/carbon ratio in the ATR inlet is prefered in FT application as a high H_2/CO ratio in the ATR outlet would result in higher penalty for CCS. The integrated hydrotreating approach can reduce the utility and capital investment in the product upgrading section. The fuel yield is found to increase with the decrease in the biomass/coal ratio and the increase in the H_2/CO ratio in the FT inlet stream. The thermal efficiency is found to increase with the decrease in the biomass/coal ratio, the increase in the H_2/CO ratio in the FT inlet stream and the decrease in the extent of CCS. The thermal and carbon

efficiency of the base case are about 46.7% and 36.4%, respectively, which is higher than the data reported in open literature for similar product yield and extent of CO_2 capture. 56.9% of carbon in the feed is stored in the captured CO_2, while 6.7% of carbon is vented to the atmosphere. It should be noted that for optimizing the key design parameters, the thermal and carbon efficiencies should not be the only criteria. A techno-economic study that captures the impact of the key design parameters on the capital and operating costs needs to be considered.

Chapter 4 Techno-economic Analysis of an Indirect Coal-Biomass to Liquids Plant

4.0 Overview

The ICL process using the FT synthesis technology has been commercialized in the last century. The synthetic fuels produced via the FT route can be upgraded to have similar properties as fuels produced from petroleum crude and therefore can be directly used in the current gasoline and diesel engines with no modification. However, uncertainty in the economic feasibility and high CO_2 emission are the two major reasons preventing the deployment of ICL plants in the United States. Addition of moderate amount of biomass to the feed and inclusion of CCS units can reduce the environmental footprint of CTL plants, but at the cost of higher capital investment and larger operational penalty. For improving the overall economics of the indirect CBTL plant with CCS, techno-economic studies can be very helpful.

With this motivation, a techno-economic study is conducted using APEA based on the process model presented in Chapter 3. This chapter focuses on the economic analysis of the I-CBTL process, while Chapter 3 focused on the process modeling approach. (Jiang and Bhattacharyya, 2014; 2015) Multiple technologies are considered for CCS and hydrocarbon upgrading without changing the plant configuration considerably. The equipment items located inside battery limit (ISBL) are designed using multiple software, such as Aspen Plus, EDR and APEA, while the outside battery limit (OSBL) equipment items are designed based on the utility requirement using Analyzer Utility Modules (AUM) in APEA. Impacts of CCS and product upgrading technologies as well as investment parameters, and key process design parameters on various economic performance measures such as NPV, payout period, IRR and BEOP are studied.

4.1 Steady-State Modeling and Simulation

The process models have been developed using Aspen Plus 7.3.2, Excel, Matlab as explained in Chapter 3. Most of the models are developed using Aspen Plus blocks and validated by comparing with the experimental data available in the open literature. Yield models based on the

experimental data are developed for the biomass gasification, FT reactor and some of the hydrocarbon upgrading reactors in Excel. Aspen User2 blocks are used to integrate the Excel models with other blocks in Aspen Plus. A stage-by-stage model is developed in Matlab to estimate the performance of the steam turbine. Table 4.1 summarizes the general simulation approach, operating conditions and corresponding references for the key equipment items/sections in the I-CBTL plant. Illinois No.6 coal, bagasse, torrefied wood and wood chips are used as feedstock in this study. The proximate and ultimate analysis of coal and biomass, detailed simulation approach, operating conditions, and design specifications can be found in Chapter 3.

Table 4.1 Summary of simulation approach and operating conditions

Blocks	Highlight of simulation approach	Operating conditions
Gasification	Equilibrium model for coal gasification and yield model for biomass gasification	Fluidized bed reactor at 2380 kPa, 850 ^{o}C
WGS	PFR model in Aspen Plus with LHHW kinetics	Adiabatic single stage with inlet temperature of 250 ^{o}C
Selexol unit	Dual-stage Selexol unit modeled in Aspen Plus using RadFrac blocks for absorbers	2048 kPa, 2 ^{o}C (solvent chilling temperature)
Fischer-Tropsch	Yield model using modified correlation from open literatures and ASF theory for conversion and product distribution	Fe-catalyzed slurry bed reactor at 2000 kPa, 257 ^{o}C
Post-FT CO_2 removal	RadFrac with equilibrium stage for physical absorption and rate-based stage for chemical absorption	Absorber at 1965 kPa, 38 ^{o}C (MEA or MDEA/PZ) or 2 ^{o}C (Selexol)
CO_2 compression	Multistage compressor in Aspen Plus	15.3 MPa for CO_2 pipeline
Autothermal reformer	PFR model in Aspen Plus with power law kinetics	1965 kPa, adiabatic with outlet temperature of 982 ^{o}C
Hydrocarbon recovery	PetroFrac for distillation columns	
Hydrogen recovery	A polybed PSA process modeled in Aspen Plus using component separator block	Adsorption at 2620 kPa and desorption at 690 kPa
Hydroprocessing	Yield model developed for reactors; heat exchanger, compressor, distillation column modeled using Aspen Plus library blocks	
Isomerization	Same as above	UOP Penex process
Catalytic reforming	Aspen Tech Reformer under the Aspen One package	UOP CCR Platforming technology
Combined cycle power plant	Stage-by-stage estimation of steam turbine performance in Matlab; Aspen Plus standard models for others	Three pressure level HRSG with reheat, 7419/2172/365 kPa

4.2 Economic Analysis

The economic analysis is performed using APEA V8.4 with default pricing basis of 2013 dollars for estimating capital cost of equipment. The steady state model in Aspen Plus is directly 'exported' to APEA with information of streams and equipment items as well as the energy and material balance. Every equipment item is mapped to the appropriate project component in APEA. Additional specifications as shown in Table 4.2 and 4.3 are provided in APEA for profitability analysis. Table 4.2 lists the price of raw materials and products, labor and product for base case scenario. The prices of coal and crude oil are obtained from the US Energy Information Administration (EIA) website. The type of coal used in this study is Illinois No.6 coal, while the crude oil price (COP) used for comparison is the refiner acquisition cost of crude oil of PADD1 area (the east coast of US). It should be noted that with the current volatile price of crude oil, it is difficult to reach definitive conclusions. Therefore the authors decided to use the 2014 prices of products and raw materials as basis for this study, then conduct some sensitivity study. The delivered biomass price is assumed to be $80/dry ton. (Wu et al., 2012) Table 4.3 lists the specified values of investment parameters in APEA for the estimation of key economic performance measures, such as NPV, payout period, IRR and BEOP. In Sections 4.3.2 to 4.3.9, the sale price of FT gasoline and diesel is defined as COP plus refinery margin (RM), where the BEOP is defined as the COP for which the NPV of the plant is zero. The RM used in this study is $0.333/gallon for gasoline and $0.371/gallon for diesel. (Baliban et al., 2011) The estimation of capital cost, specification of operating and maintenance (O&M) cost and the approach to economic analysis and sensitivity studies are discussed in Sections 4.2.1 to 4.2.3.

Table 4.2 Prices of raw material, labor and product (base case)

	Cost ($/unit)		Cost ($/unit)
Coal[(1)] ($/ton)	44.7	Supervisor ($/hr)	80
Wood chip ($/dry ton)	80.0	Crude oil price[(1)] ($/bbl)	107
Operator ($/hr)	50	Electricity ($/MWh)	50

(1) Last accessed on EIA website on Aug. 20, 2014

Table 4.3 Investment parameters (base case)

Parameter	Value	Parameter	Value
Start date of engineering	2014	Utility escalation (%/year)	1

Contingency percent	18%	Working capital percentage (%/FCI)	12
Number of years for analysis	30	Operating charges (% of labor costs)	25
Tax rate	40%	Plant overhead	50%
Interest rate/desired rate of return	10%	General & administrative expenses	8%
Project capital escalation (%/year)	1	Length of start-up period (weeks)	40
Products escalation (%/year)	1	Operating hours per period	8000
Raw material escalation (%/year)	1	Construction time	2.5 yr

4.2.1 Estimation of the Total Project Cost

In this study, the key equipment items are designed and their capital costs are estimated in multiple-software environment. Figure 4.1 shows the methodology for estimating the total project cost (TPC). For process units, of which detailed models are developed for all standard process components, such as heat exchangers, columns, compressors, pumps and vessels, in Aspen Plus, rigorous cost estimations are conducted in APEA using Icarus database. For other units, the equipment items, especially the reactors and process auxiliaries, of which the costs cannot be estimated by simplified process models and Icarus database, are mapped as quoted equipment in APEA using Excel-based Custom Model Tool for cost estimation.

Table 4.4 shows the methodology of sizing and estimating cost of standard process components. Spares are considered for all pumps. All the compressors are mapped as centrifugal compressor without spare except the tail gas compressor, which is mapped as reciprocating compressor with a spare, due to the relatively smaller flow rate. The MOC for all the equipment items are selected based on the operating temperature, service stream composition, and common industry practice. (NETL, 2009; Kohl and Nielsen, 1997; NREL, 2006; Tsai, 2010) The MOC for most of the equipment items, excluding the quoted equipment, is carbon steel, while the MOC for H_2 compressor, NH_3 compressor, hydrotreating reactor and part of the amine plant is stainless steel (SS316 or SS304) to avoid the corrosion problem. Feed furnace of the hydrotreater is constructed by Cr-Mo alloy (A213F or A213C) for applicability in hydrogen service at high temperature. Table 4.5 gives the specification of an amine based CO_2 removal unit (one process alternative for the post-FT CO_2 capture unit) in APEA for demonstrating the mapping step and the design step in APEA. Stainless steel are used as main construction material or cladding material to avoid corrosion for all columns and some of heat exchangers and pumps in this process section, as

suggested by Kohl and Nielsen. (Kohl and Nielsen, 1997) The complete equipment list and detailed specifications for all units in the I-CBTL plant with CCS are provided in Appendix B.

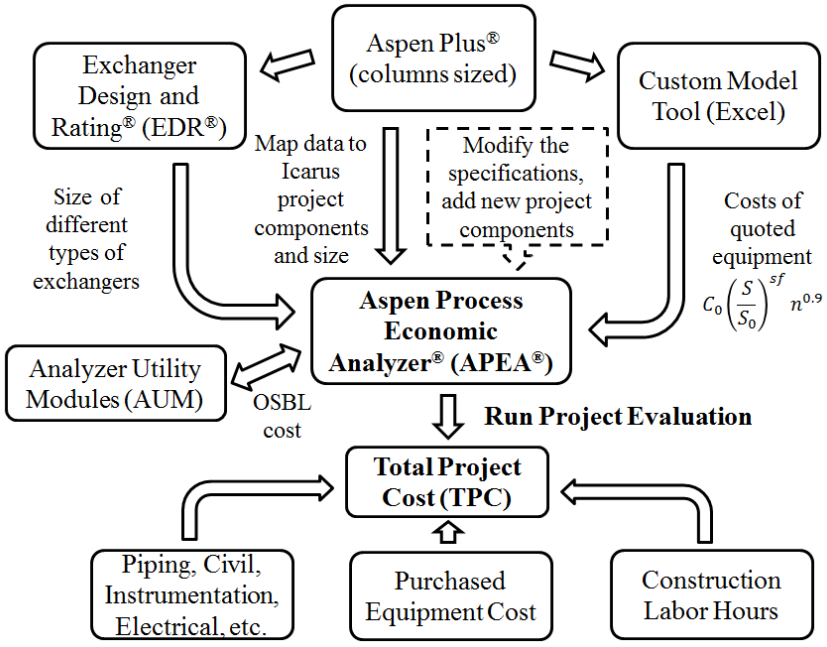

Figure 4.1 Methodology for TPC estimation

Table 4.4 Sizing and cost estimation of project component

Equipment	Model	Sizing	Cost
Heat exchanger	HeatX in Aspen Plus	Aspen EDR	APEA with Icarus database
Columns	RadFrac or PetroFrac in Aspen Plus	Aspen Plus tray/packing sizing	APEA with Icarus database
Vessels, pumps, compressors, etc.	Standard model in Aspen Plus	APEA sizing expert using respective ASTM standards	APEA with Icarus database
Others	Simplified models or correlations	N/A	Cost correlation from open literature

Table 4.5 Detailed component specification for MDEA/PZ post-FT CO_2 capture unit

Description	# Req	# Spares	Model in APEA	Sizing	Cost	MOC
Absorber	1	0	TW PACKED	Aspen Plus	Icarus	A516[(1)], M107YC
Absorber intercooling	1	0	HE FLOAT HEAD	EDR	Icarus	A285C, A214
Lean/rich heat exchanger	1	0	HE PLAT FRAM	EDR	Icarus	SS316
Solvent stripper - condenser	2	0	HE FIXED T S	EDR	Icarus	T150A, SS316
Solvent stripper - drum	2	0	HT HORIZ DRUM	APEA	Icarus	A516
Solvent stripper - reboiler	2	0	RB U TUBE	EDR	Icarus	316LW, SS316
Solvent stripper - reflux pump	2	2	CP CENTRIF	APEA	Icarus	SS316

Solvent stripper - tower	2	0	TW PACKED	Aspen Plus	Icarus	304L, M107YC
Solvent cooling	1	0	HE FLOAT HEAD	EDR	Icarus	A285C, A214
Solvent recycle pump	1	1	CP CENTRIF	APEA	Icarus	SS316

(1) With 1/8 inch SS304 cladding

For the reactors, product upgrading units and auxiliaries, the parameters for the cost correlations, Eq. (4.1) and Eq. (4.2), are shown in Table 4.6, which are directly obtained from the open literature or derived using the data available in the open literature. (Baliban et al., 2011; Bechtel, 1998; NETL, 2007; Shah, 1988) In Eq. (4.1) and (4.2), *DIP* is the direct permanent investment (includes ISBL cost and OSBL cost), *BOP* is the balance of plant percentage (site preparation, utility plants, etc.), C_0 is the base cost, S_0 is the base capacity, S is the actual capacity, *sf* is the scaling factor, and n is the total number of trains. Multiply trains are considered, if the throughput of a certain unit exceeds the maximum capacity (S_{max}).

$$DIP = (1 + BOP)C_0\left(\frac{S}{S_0}\right)^{sf} n^{0.9} \tag{4.1}$$

$$ISBL\ cost = C_0\left(\frac{S}{S_0}\right)^{sf} n^{0.9} \tag{4.2}$$

It should be noted that two methods are applied to estimate the OSBL cost in this study. For the units with missing design and operating information, Eq. (4.1) is applied, where BOP includes the cost associated with the utility plants. For the unit with all information available, especially utility consumption, AUM in APEA can be applied to estimate the OSBL cost of the plant. In the I-CBTL plant (shown in Figure 3.1), fuels, steam, and electricity required are supplied by the fuel gas header and the combined cycle plant, which is included in ISBL. (Jiang and Bhattacharyya, 2015) Cooling water system is the major OSBL plant considered in this study, with the design approach in AUM shown in Figure 4.2.

Table 4.6 Capital cost correlation for quoted equipment items

Unit name	C_0 (MM$)[1]	S_0	Smax	S_0 Basis	units	*sf*	Eq	Reference
Biomass handling and drying	27.82	2000		dry feed	TPD	0.67	1	Baliban et al.
Coal handling and drying	81.67	2464	2616	dry feed	TPD	0.67	1	Baliban et al.
Gasifier	136.30	2464	2616	dry feed	TPD	0.6	1	Baliban et al.
Sour WGS	3.14	2556	2600	output	TPD	0.65	2	Baliban et al.
COS hydrolysis	3.05	4975	7500	output	TPD	0.67	2	Baliban et al.

Claus	24.09	125		sulfur	TPD	0.67	2	Baliban et al.
CO_2 compressor	31.63	11256		CO_2	TPD	0.75	2	NETL
Fischer-Tropsch synthesis	40.71	226669	228029	feed	Nm^3/h	0.75	2	Bechtel Corp.
Autothermal reformer	3.27	430639	9438667	output	Nm^3/h	0.67	1	Baliban et al.
Wax hydrocracking	9.60	97.92	2656	feed	TPD	0.55	2	Shah et al.
Isomerization	0.99	13.06	2720	feed	TPD	0.62	2	Bechtel Corp.
Catalytic reformer	5.36	36.99	8160	feed	TPD	0.6	2	Bechtel Corp.
Hydrogen recovery (PSA)	0.84	944		H_2	Nm^3/h	0.55	2	Bechtel Corp.
Air separation unit (ASU)	57.57	1839	2500	TPD	O_2	0.50	2	Baliban et al.

(1) The costs of quoted equipment are escalated with CEPCI.

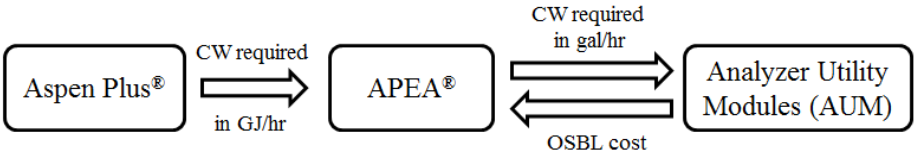

Figure 4.2 Methodology for cooling water system cost estimation using AUM

4.2.2 Estimation of Operating and Maintenance Cost

Cost of the raw materials is the major contributor to the O&M cost. This is estimated from the material balance obtained from the process model developed in Aspen Plus and the unit prices listed in Table 4.2. The utility cost usually makes a large contribution to the O&M cost. However, in the I-CBTL plant with the plant construction shown in Figure 3.1, fuels, steam, electricity are generated internally. (Jiang and Bhattacharyya, 2015) As the circulating water system is designed using AUM, process water is the only external utility considered in the economic model. The costs of catalyst and chemicals are estimated based on the data available in the open literature. The initial costs of the catalysts in all reactors, excluding hydrotreater, are included in the ISBL cost. For the hydrotreating catalyst and chemicals like Selexol and amine solvents for CO_2 capture, the cost for initial loading is accounted for by inserting quoted equipment in APEA with specified cost. The cost of catalyst in the catalytic reforming unit is not explicitly considered in this project, because the correlation for the UOP CCR Platforming technology is considered, where the initial catalyst cost and capital cost of catalyst regeneration facilities are already included in the ISBL cost and the annual cost for catalyst replacement is relatively low and therefore ignored. (Bechtel, 1993; Meyer, 2003) The catalyst replacement rate in the FT process is specified to be 0.5% per day of total catalyst inventory, while a 5-year catalyst life is assumed for other catalysts. (Bechtel, 1993; 1998) The replacement rates of chemicals (Selexol and amine solvent) are assumed to be the same as reported in a NETL study.

(NETL, 2007) With the availability of unit costs for replacing catalyst and chemicals included, the replacement cost is annualized, and included in APEA. Table 4.7 lists the initial and replacement costs of major catalysts and chemicals considered in the I-CBTL plant.

Table 4.7 Costs of catalysts and chemicals in the I-CBTL plant (base case, 10k bbl/day)

	Unit Cost[(1)] ($/unit)	Unit	Initial[(2)] (M$)	Replacement[(2)] ($/day)	Cost source
Catalyst					
Fischer Trospch	4.80	kg	with equipment	7404	Bechtel, 1998
Sour WGS	16774	m^3	with equipment	710	NETL, 2007
COS hydrolysis	2.01	kg	with equipment	65	NETL, 2007
Claus unit	4414	m^3	with equipment	395	NETL, 2007
Autothermal reformer	37080	m^3	with equipment	510	NETL, 2007
Hydrotreating	34.17	kg	1090	582	SRI, 2007
Hydrocracking	34.17	kg	with equipment	414	SRI, 2007
Isomerization[(3)]	0.180	bbl FF	with equipment	540	Meyer, 2003
Chemicals					
Selexol solvent	3804	m^3	1010	456	NETL, 2007
Amine solvent	2.16	kg	218	60	NETL, 2007
Total			2318	11136	

(1) Costs listed are the original value published in different years.
(2) The costs of catalyst and chemicals are escalated with the average Producer Price Index.
(3) $0.18/bbl fresh feed is the total replacement cost of catalyst and adsorbent.

4.2.3 Methods for Profitability Analysis and Sensitivity Studies

Once all the information required by APEA is specified, profitability analysis and sensitivity studies are conducted by the Decision Analyzer tool available in APEA, which is a user friendly Excel interface that reports the important economic measures. For sensitivity studies, if the key design parameters, listed in Table 4.8 excluding plant capacity, are changed, the process model in Aspen Plus is updated and a new APEA file is created by importing the updated steady-state simulation results and following the procedure discussed in Sections 4.2.1 and 4.2.2. If the key design parameters remain the same, sensitivity studies can be conducted in APEA only using the scenario created by the original Aspen Plus model. The sensitivity studies related to investment parameters listed in Table 4.3 as well as the raw material, labor, utility and product prices listed in Table 4.2 can be conducted in the Excel file generated by Decision Analyzer. The sensitivity study related to plant capacity is also conducted in Decision Analyzer. The entire plant is

rescaled by Decision Analyzer, while most of the standard equipment is resized and evaluated with the new plant capacity. For quoted equipment, the capital cost is estimated by Excel-based Custom Model Tool for the new plant capacity and multiple train may be considered if the throughput existing the up limit. Figure 4.3 summarizes the general approach for economic analysis and sensitivity studies.

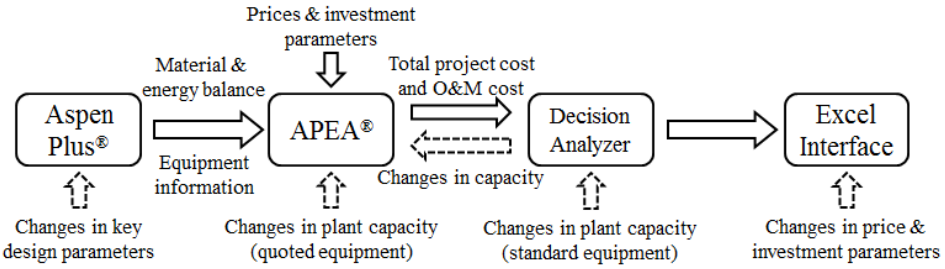

Figure 4.3 Economic analysis and sensitivity studies in multi-software environment

4.3 Results and Discussion

An early study of NETL claimed that increasing the percentage of biomass in the feedstock would increase capital and operating costs due to the higher raw material cost and reduced economies of scale and recommended that modest biomass percentages in I-CBTL plant would provide affordable fuels from domestic biomass feedstock and enable considerable reduction in GHG emission. (NETL, 2009) Due to the high transportation cost, low energy density and limited long-term availability of biomass, the capacity of BTL or CBTL are constrained. (Wang and McNeel, 2009) As the concern about economic and environmental sustainability, the biomass to coal mix ratio and plant size are set to be 8/92 and 10k bbl/day for the base case, while sensitivity studies are conducted by increasing the mix ratio and plant size up to a reasonable value, 20/80 and 50k bbl/day, to demonstrate the impacts of mix ratio and plant capacity on the economic performance. (NETL, 2009; Liu et al., 2015; Wang and McNeel, 2009) Given the steady-state model developed in Aspen Plus, the key design parameters and process performance measures are shown in Table 4.8 for the base case scenario of the I-CBTL plant with CCS.

Table 4.8 Key design parameters and plant performance measures (base case)

Key design parameters	Value	Plant performance	Value
Plant capacity (bbl/day)	10000	Coal/biomass (ton/hr, dry)	153.8/13.5

Biomass type	Wood chip	FT gasoline (bbl/day)	4050
Biomass/coal (wt/wt, dry)	8/92	FT diesel (bbl/day)	5950
Hydrotreating approach	Integrated	Net power output (MW)	2.50
Post-FT CO_2 capture technology	MDEA/PZ	Carbon captured by FTL (%)	36.3
H_2/CO in FT inlet stream (mol/mol)	2	Carbon captured by CCS (%)	56.9
Extent of CCS (%)	High(1)	Thermal efficiency (%, HHV)	45.9

(1) All CO_2 streams removed from pre- and post-FT CO_2 removal units are sent to compression section

The steady-state process models have been validated in Chapter 3. (Jiang and Bhattacharyya, 2014; 2015) Validation of the economic model is discussed in Section 4.3.1. With the validated process and economic models, profitability of the plant is analyzed in Section 4.3.2 for base case scenario using the investment parameters listed in Section 4.2. Sensitivity studies were also performed by changing raw materials, product prices, and key investment parameters. Then the key design parameters of the process, which have significant impact on the economic performance of the I-CBTL plant, are identified. Since the ICL process without CCS has already been commercialized since 1950s (Dry, 2002), the focus of this study is on evaluation of the effects of the key design parameters that affect the performance and profitability of an I-CBTL plant with CCS as reported in Sections 4.3.3 to 4.3.8. In Section 4.3.9, August, 2015 prices of raw material and product is considered in order to capture the impact of the current low price of crude oil.

4.3.1 Economic Model Validation

There is scarcity of techno-economic studies on I-CBTL-CCS plants in the open literature. As the feed contains only 8 wt% biomass, the effect of biomass on the capital investment is not expected to be significant. Therefore, the capital cost estimates is compared with the previous studies conducted for ICL plants with most similar plant configurations. However those studies have different plant capacities in comparison to this study. Therefore, the base case plant is rescaled using APEA Decision Analyzer and the procedure discussed in Section 4.2.3. For each case study, the investment parameters, such as plant contingency and working capitals, tax rate, escalation rate and plant contingency, which affect the TPC, are specified to be the same as those in the references for the case studies. (Bechtel, 1998; NETL, 2007) Table 4.9 summarizes the results of the comparison of the economic model developed in APEA with three different case studies - two large scale plants, and one small scale plant. (Bechtel, 1998; NETL, 2007) As seen

in Table 4.9, the relative difference in TPC between our estimate and reported data is within 6%. The main difference is due to plant configuration such as the application of CCS technology, the approach of hydrocarbon upgrading, and the key design parameters such as the H_2/CO ratio in the FT inlet stream. Detailed comparison of each breakdown plant section for all three cases is provided in the Appendix C. It should be noted that the capital investment given in the original reports (Bechtel, 1998; NETL, 2007) is escalated using CEPCI values for fair comparison.

Table 4.9 Summary of the capital investment comparison

	Case 1	Case 2(1)	Case 3(1)	Base Case
Capacity (bbl/day)	48629	49992	9609	
Difference in plant construction				
CO_2 capture & storage	No	Yes	No	Yes
Naphtha upgrading	Yes	No	No	Yes
Light gases to gasoline	Yes	No	No	No
Total project cost (TPC, 2014 MM$)				
TPC calculated	4905.6	5137.6	1185.2	
TPC reported	4748.5	5214.3	1124.1	
Difference in TPC (%)	-3.31	1.47	-5.44	

(1) Additional 25% process contingency is considered for FT process and added to the calculated TPC for Case 2 and Case 3 for fair comparison.

Plant profitability measures are compared with the NETL studies for both a large scale plant with CCS and a small scale plant without CCS. (NETL, 2007) For this study, the economic assumptions are the same as the NETL studies, where the prices of coal, operator, naphtha, diesel and electricity were set to be $36.63/ton, $34.78/hr, $1.5/gallon, $1.96/gallon and $52/MWh for the large scale design and $54.77/ton, $32.5/hr, $1.3/gallon, $1.96/gallon and $35/MWh for the small scale design. For both cases, 26%, 30 years, 40%, 3% and 2% were considered for project contingency, number of years for analysis, tax rate, plant outputs escalation and coal price escalation, respectively. (NETL, 2007) Table 4.10 shows that the profitability measures obtained from our study are similar to the large scale NETL studies, rather some improvement in these measures is observed for our study mainly due to changes in plant configuration and differences in the key design parameters. The net present value of the small scale case is lower than the NETL case due to the additional capital and operating cost of CCS, which is not considered in the small scale NETL design. Further discussions can be found in Section 4.3.3-4.3.8.

Table 4.10 Comparison of the profitability with the NETL's indirect ICL case studies

	Large Scale		Small Scale	
	Estimated	Difference	Estimated	Difference
Plant capacity (bbl/day)	49992	0	9609	0
Total project cost* (MM$, 2006)	4463	-1.4%	980	0.4%
Net present value (MM$, 2006)	1667	8.0%	133	56%
Payback period (year)	5	0	7	0

*The capital cost are escalated with the CEPCI

4.3.2 Profitability Analysis and Identification of Key Design Parameters

For the base case scenario (Table 4.8, 10k bbl/day) with economic parameters specified in Table 4.2 and Table 4.3, the NPV, IRR, payback period, and BEOP are $179 MM, 11.5%, 7 year and $95.5/bbl, respectively. Table 4.11 lists the economic measures of the I-CBTL plant with different capacities. It shows that for the current plant design and specified economic parameters, the BEOP of FT liquids can be reduced to about $77.8/bbl and the IRR can be increased to about 14.0%, if the plant capacity is increased to 50k bbl/day. Figure 4.4 and Figure 4.5 show the sensitivities for $\pm$25% changes in the major plant economic inputs for both small scale and large scale plants. The results show that the BEOP is between $88/bbl and $106/bbl for a small scale operation and between $72/bbl to $86/bbl for a large scale operation. 7% increase in BEOP is observed, if high project contingency (26%) is considered due to the novelty of the indirect CBTL plant with CCS.

Table 4.12 shows the contribution of each unit to the BEOP of the I-CBTL plant. The results indicate that feedstock cost contributes about half of the BEOP, while the other half of the BEOP is due to the capital cost. The syngas production section contributes about 60% of the total capital investment, which is similar to the data reported in the open literature. (Dry, 2002) The CCS units, including pre- and post- FT CO_2 removal process and CO_2 compression process, also consume a significant amount of utilities and capital investment. As noted before, the utilities such as fuel gas, steam and electricity are generated inside the plant and therefore utilized in the process. The change in utility consumption is reflected by the change in net power output of the CBTL plant. As seen in Table 4.12, the main consumers of utilities are the syngas production

unit and the CCS unit. Therefore selections of the CCS technologies and related design parameters are critical for reducing the BEOP of the I-CBTL plant with CCS.

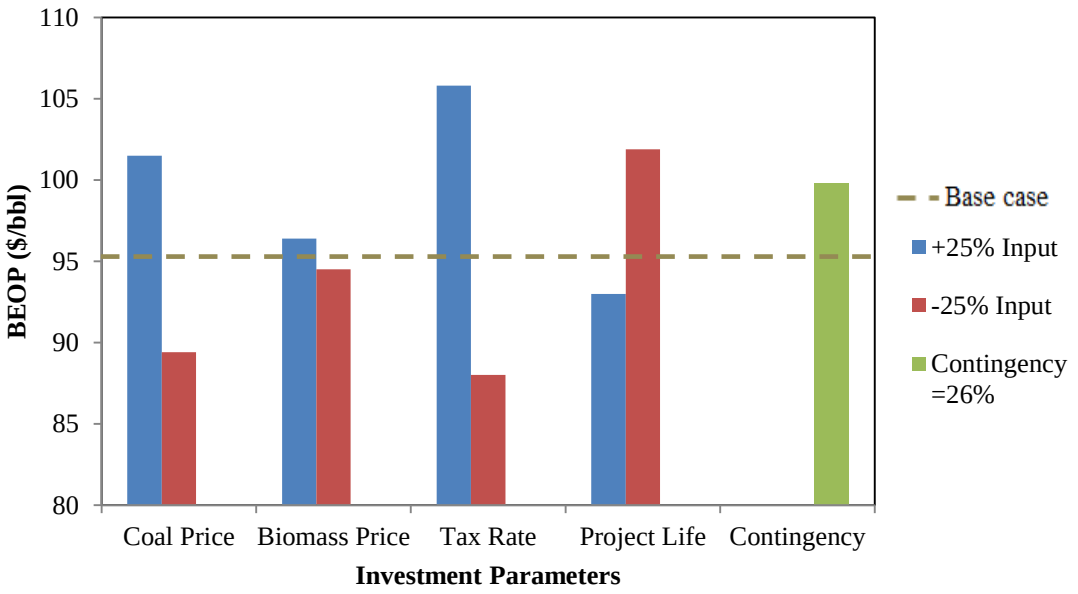

Figure 4.4 Sensitivity studies of the small scale I-CBTL-CCS plant (10k bbl/day)

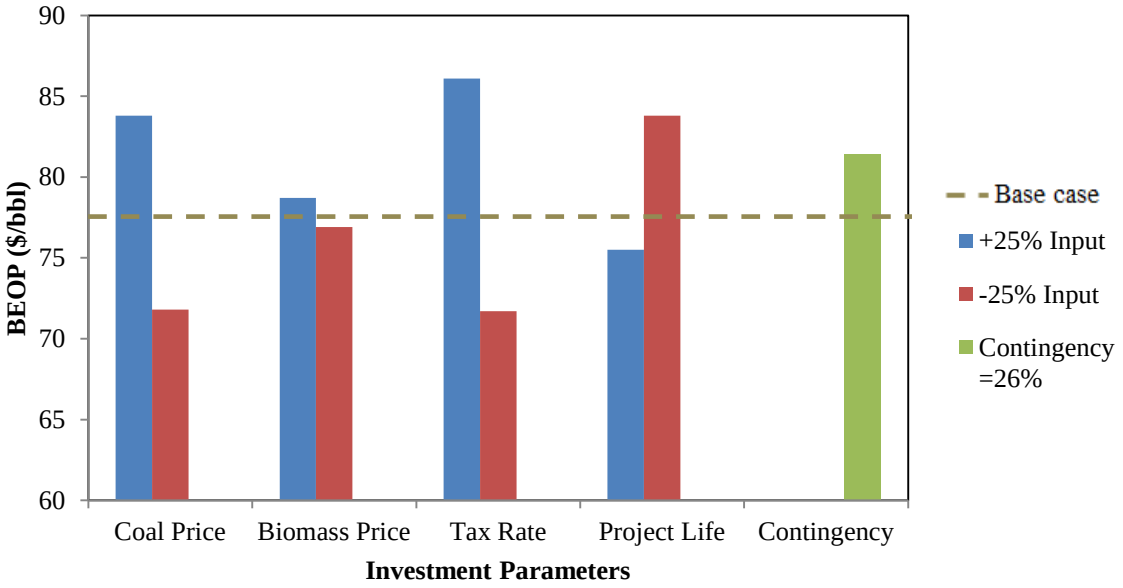

Figure 4.5 Sensitivity studies of the large scale I-CBTL-CCS plant (50k bbl/day)

Table 4.11 Effect of plant capacity on the economic performance (I-CBTL-CCS)

Cases	Small scale	Medium scale	Large scale
Plant capacity (bbl/day)	10000	30000	50000
Net present value (MM$)	179	771	2057
Internal rate of return (%)	11.5	12.2	14.0
Payback period (year)	7	6	5
Break-even oil price ($/bbl)	95.5	89.8	77.8

Table 4.12 Contribution to the BEOP of the I-CBTL-CCS plant (10k bbl/day) [(1)]

Percentage	Feedstock	Capital[(2)]	Electricity	Steam	Fuel
Total	55.18	45.63	(0.81)	0.00	0.00
Process units					
Syngas production[(3)]		57.5	51.0	(52.9)	1.2
Syncrude production		10.7	0.8	(46.0)	2.9
CO_2 capture & storage[(4)]		11.5	36.2	35.6	0.0
Product upgrading		10.6	1.0	0.4	12.5
Fuel gas header		0.0	0.0	0.0	(100)
Others		3.0	11.1	(1.1)	0.0
Gas turbine		2.8	(46.7)	0.0	83.5
HRSG & steam turbine		3.9	(55.4)	64.1	0.0

(1) ( ) indicates utility generation
(2) Annualized by assuming 10-year economic life of equipment
(3) ASU is included in the syngas production section
(4) Including pre- and post- CO_2 capture units and CO_2 compression unit

4.3.3 Different Carbon Capture Technologies

As mentioned earlier, a dual-stage Selexol process is selected for selectively removing CO_2 and H_2S produced in the gasifier. The Selexol technology is widely considered for acid gas capture because of its relatively low capital and operating costs when the partial pressure of CO_2 is relatively high. (Jiang and Bhattacharyya, 2014; 2015; Doctor et al., 1994; Mohammed et al., 2014) Three different carbon capture technologies are considered in our earlier study for post-FT CO_2 capture-single-stage Selexol unit, MEA absorption unit and MDEA/PZ absorption unit. (Jiang and Bhattacharyya, 2014) That study indicated that the MDEA/PZ unit has the lowest utility consumption among these three technologies. Table 4.13 gives the economic analysis for all three technologies considering both utility consumption and capital investment. The result shows that the BEOP for the MDEA/PZ unit is slightly lower than the BEOP for the MEA unit

because of the lower utility consumption in the MDEA/PZ unit while the capital investment are similar and overall thermal efficiency of the I-CBTL process remains relatively unchanged for both of these technologies. A considerable increase in BEOP is observed for the single-stage Selexol unit due to the loss of light hydrocarbons in the physical absorption process, which results in higher feed flowrate and larger throughput of each section for achieving the same fuel production rate. Hence, the MDEA/PZ technology is selected for the base case and other sensitivity studies.

Table 4.13 Effect of different CCS technologies for post-FT CO_2 capture (10k bbl/day)

	Single-stage Selexol	MEA	MDEA/PZ
Thermal efficiency (%, HHV basis)	40.8	45.7	45.9
Total project cost (MM$)	1332	1280	1281
Net present value (MM$)	54	175	179
Internal rate of return (%)	10.4	11.4	11.5
Payback period (year)	9	7	7
Break-even oil price ($/bbl)	103.6	95.7	95.5

4.3.4 Integrated Hydrotreating versus Separated Hydrotreating

In this study, two hydrotreating routes, namely novel integrated hydrotreating (Figure 3.12) and conventional separated hydrotreating (Figure 3.13), are considered for upgrading FT liquids. (Jiang and Bhattacharyya, 2015) In the novel integrated hydrotreating approach, the syncrude is hydrotreated before sent to a separation unit for further upgrading, while the syncrude is first separated and then sent to several separated hydrotreating units in the conventional process. The integrated hydrotreating approach has the potential to reduce the utility consumption and capital investment of the hydrotreating units by about 30%, because of higher thermal efficiency and smaller plant footprint. (Jiang and Bhattacharyya, 2015) For detailed technical discussion on these units, interested readers are referred to Sections 3.4.1 and 3.6.2.3. The techno-economic analysis, reported in Table 4.14, shows that the integrated hydrotreating approach can reduce the BEOP of FT liquids by about 0.5%. It should be noted that the changes in the overall thermal efficiency and economic performance due to the change in the hydrotreating approach are not significant because the total utility and capital cost of the entire product upgrading section contribute only about 10% of the entire I-CBTL plant, as shown in Table 4.12.

Table 4.14 Effect of different hydrotreating approaches (10k bbl/day)

	Integrated	Separated
Thermal efficiency (%,HHV)	45.9	45.9
Net present value (MM$)	179	171
Internal rate of return (%)	11.5	11.4
Payback period (year)	7	7
Break-even oil price ($/bbl)	95.5	96.0

4.3.5 H_2/CO Ratio in the FT Inlet Stream

Section 3.6.2.4 indicated that with an increase in the H_2/CO ratio in the FT inlet stream, the utility consumption in the CCS units keep reducing and the overall thermal efficiency of the I-CBTL plant keeps increasing. (Jiang ang Bhattacharyya, 2015) With an increasing H_2/CO ratio, the partial pressure of CO_2 in the Selexol unit inlet increases as more CO_2 generated in the WGS reactor, which accelerates physical absorption and reduces the solvent circulation rate. At the meanwhile, CO_2 selectivity decreases with the increasing H_2/CO ratio in the FT unit using Fe-based catalyst. (Jiang and Bhattacharyya, 2015; James et al., 2013) As a consequence, the amount of CO_2 needs to be removed in the post-FT CO_2 removal unit decreases. Table 4.15 shows the effect of the H_2/CO ratio on the profitability of the I-CBTL plant. It is observed that the BEOP of the I-CBTL plant with CCS can be reduced by about 10% if the H_2/CO ratio in the FT inlet stream is increased to 2.0, which is the stoichiometric ratio of the FT reaction. The process becomes more profitable with higher H_2/CO ratio not only because of the increasing thermal efficiency, which leads to smaller equipment size, but also because of the reduction in the solvent circulation rate in the CCS units, which leads to lesser capital investment. (Jiang and Bhattacharyya, 2015) Table 4.15 shows that the rate of decrease in the BEOP is lesser when H_2/CO ratio is increased from 1.5 to 2 in comparison to when it is increased from 1.0 to 1.5. Under current conceptual design, as the H_2/CO ratio keeps increasing, larger portion of carbon in the feedstock is converted to CO_2 in the WGS reactor and removed from the system in the pre-FT CO_2 removal unit before being sent to the FT unit. (Jiang and Bhattacharyya, 2015) Thus, amount of clean syngas sent to the downstream FT reactors decreases with the increasing H_2/CO ratio. Therefore the relative improvement in the capital and operating costs becomes smaller with

the increase in the H_2/CO ratio. Higher H_2/CO ratio beyond H_2/CO ratio of 2 is not considered in this study due to lack of operational or experimental data for FT reactor beyond H_2/CO ratio of 2.

Table 4.15 Effect of the H_2/CO ratio in the FT inlet stream (10k bbl/day)

H_2/CO ratio (mol/mol)	1.0	1.5	2.0
Thermal efficiency (%,HHV)	40.8	43.9	45.9
Total project cost (MM$)	1439	1312	1281
Net present value (MM$)	9	139	179
Internal rate of return (%)	10.1	11.1	11.5
Payback period (year)	9	8	7
Break-even oil price ($/bbl)	106.5	98.1	95.5

4.3.6 Extent of Carbon Capture and Storage

Applying CCS technologies to the I-CBTL will obeviously increase both operating and capital costs and considerably affect the profitability of the plant. The CCS section contributes about 11.5% of total capital investment and 35% of utility consumption, as shown in Table 4.12. It is noted that CO_2 removal units are still required in a FT plant, even though CCS is not considered. (Liu et al., 2011; Bechtel, 1998; Kreutz et al., 2008) The difference between the cases with and without CCS is whether removed CO_2 being sent to a CO_2 compression section for pipeline transportation and sequestraion or direct vent to the atmosphere. Hence, the penalty of CCS in an indirect liquefaction plant is not expected to be as significant as coal-fired power plant. For a FT plant with recycle stream, Liu et al. reported a CCS penalty of \$12.4/ton CO_2, including CO_2 compression, pipeline and sequestration. (Liu et al., 2011) If only considering the capital and operating cost of the CO_2 comprssion section reported by Liu et al. (Liu et al., 2011), the penalty is about \$6.2/ton CO_2, corresponding to a utility consumption of 91kWh/ton CO_2 and a capital investment of 67 million 2007 US dollar for capturing 29039 ton CO_2 per day. (Liu et al., 2011) With the proposed plant configuration and modeling approach in this paper, the penaly of CCS is about \$6.1/ton CO_2 for the base case, considering the captial and operating cost of CO_2 compression section and assuming 10-year economic life of equipment and a electricity cost of \$0.06/kWh from grid, which is closed to the data reported by Liu et al. (Liu et al., 2011; Turton et al., 2012) Our previous study showed that the thermal efficiency of the I-CBTL plant will be 1.4% less than that of an I-CBTL plant without CCS, if 90% and 98% CO_2 in the inlet streams

are removed in the pre- and post-FT CO_2 capture units for both cases, corresponding to 56.9% of carbon in the feedstock. (Jiang and Bhattacharyya, 2015) The techno-economic studies shown in Table 4.16 indicate that the BEOP of the FT liquids will increase by about 5% due to CCS. This value is lower than what reported by Liu et al. (10%) (Liu et al., 2011), because downstream CO_2 pipeline and sequestration facility is not included in our analysis.

Table 4.16 Effect of the extent of CCS (10k bbl/day)

Extent of CCS	High	Intermediate	Low	No CCS
CO_2 stream to compression unit (%)	100	75	50	0
Thermal efficiency (%,HHV)	45.9	46.3	46.6	47.3
Net present value (MM$)	179	192	208	245
Internal rate of return (%)	11.5	11.6	11.7	12.0
Payback period (year)	7	7	7	7
Break-even oil price ($/bbl)	95.5	94.6	93.6	91.3

4.3.7 Biomass to Coal Ratio in the Feedstock

Chapter 3 showed that as the biomass content is increased (keeping the biomass content as high as 20%), overall fuel production and the plant thermal efficiency slightly decrease, mainly because of the relatively high oxygen content in the biomass. (Jiang and Bhattacharyya, 2015) From Table 4.12, it is noted that the raw material cost contributes more than half of the BEOP of the indirect CBTL plant. Table 4.17 indicates that when the biomass content increases from 8% to 20% with the same extent of CCS (not considering the carbon credit of biomass), the BEOP increases by about 4% due to lower plant efficiency, larger equipment size, higher feedstock price of biomass, less net electricity produced as by product and reletively more expensive biomass preprocessing unit. If carbon credit for biomass is considered, less CO_2 needs to be captured and stored. The results show that the BEOP increases by about 3% even when carbon credit of biomass is taken into account.

Table 4.17 Effect of the coal biomass mix ratio (10k bbl/day)

Biomass/Coal (wt/wt)	8/92	15/85		20/80	
Carbon credit	Base case	No	Yes	No	Yes
Thermal efficiency (%, HHV)	45.9	44.5	44.7	43.7	43.9

Net present value (MM$)	179	135	140	119	129
Internal rate of return (%)	11.5	11.1	11.1	11.0	11.0
Payback period (year)	7	8	8	8	8
Break-even oil price ($/bbl)	95.5	98.6	98.3	99.5	98.9

4.3.8 Biomass Type

Bagasse and torrefied wood are selected as an alternative biomass input to the indirect CBTL plant, which have a higher thermal efficiency but higher price than wood chips, as shown in Chapter 3. The thermal efficiency of the I-CBTL plant using bagasse is slightly higher than that using wood chips with the same biomass to coal ratio and all other key design parameters because of lower oxygen content and higher hydrogen/carbon ratio in the bagasse. (Jiang and Bhattacharyya, 2015) For economic analysis, the bagasse price is set to be $108/ dry ton, 35% higher than that of wood chips in dry basis (IRENA, 2012; Gonzales et al., 2011) The torrefied wood price is set to be $140/dry ton. (Batidzirai et al., 2013) Table 4.18 shows that torrefied biomass is a more economic option for the indirect liquefaction process.

Table 4.18 Effect of the biomass type (10k bbl/day)

	Wood chip	Bagasse	Torrefied wood
Thermal efficiency (%,HHV)	45.9	46.6	47.5
Net present value (MM$)	179	172	255
Internal rate of return (%)	11.5	11.4	12.1
Payback period (year)	7	7	7
Break-even oil price ($/bbl)	95.5	95.9	89.8

4.3.9 Economic Feasibility of the I-CBTL Plant at Low Crude Oil Price

Since the end of 2014, the crude oil price has dropped considerably. In this section, August, 2015 prices of gasoline, diesel and coal is considered in order to evaluate the impact of the current low price of crude oil. The results are shown in Table 4.19. As expected, both small scale and large scale CBTL plants are not competitive with the traditional petroleum refineries when the crude oil price is so low. In particular, the small scale I-CBTL plant does not seem to be economically viable even with significant decrease in coal and biomass prices. For the large scale I-CBTL

plant, the price of coal and biomass would have to decrease to about 57% of the current price for making the I-CBTL plant at par with the typical petroleum refinery.

Table 4.19 Economic feasibility with 2015 pricing basis

Plant capacity (bbl/day)	10000		50000	
Coal ($/ton)	34.0	0	34.0	19.3
Biomass ($/dry ton)	61.5	0	61.5	35.0
Crude oil ($/bbl)	62	62	62	62
Net present value (MM$)	-427	-84	-650	0
Internal rate of return (%)	6.1	9.3	8.5	9.7
Payback period (year)	N/A	N/A	N/A	N/A
Break-even oil price ($/bbl)	88.7	88.7	71.1	71.1

4.4 Conclusions

In this chapter, a techno-economic study is conducted for an I-CBTL plant with CCS in APEA based on the process model developed in Aspen Plus. (Jiang and Bhattacharyya, 2014; 2015) Impacts of the key economic inputs, technology selection, and key process design parameters on the main economic measures, such as NPV, IRR, payback period and BEOP have been evaluated. The economic model is first compared with the data reported in the open literature. The feedstock cost contributes about half of the BEOP, while the syngas production unit and the CCS units are the two major contributors to the plant operating and capital costs. For the small scale plant (10k bbl/day), the BEOP is found to be between $88/bbl to $106/bbl for $\pm$25% changes in the major project economic inputs. For the large scale application (50k bbl/day), the BEOP reduces to about $72/bbl to $86/bbl for same changes in the economic inputs. It is observed that among the three CCS technologies considered in this study for post-FT CO_2 capture unit, the MDEA/PZ technology is the best option. The integrated hydrotreating technology can slightly reduce the BEOP of the indirect CBTL plant. The BEOP of the I-CBTL plant increases, if the H_2/CO ratio in the FT inlet stream is decreased, extent of CCS is increased or the biomass content in the feedstock is increased even when carbon credit of biomass is taken into account. It is also observed that with the 2015 low COP, the I-CBTL plant is not economically viable. If the COP stays so low, considerable decrease in the coal and biomass

costs and large throughput would be required to make the I-CBTL plant competitive with the petroleum refineries.

Chapter 5 Modeling of Direct Coal Liquefaction Reactors

5.0 Overview

The catalytic two stage liquefaction (CTSL) unit is the core of any direct coal liquefaction (DCL) processes. In the Shenhua DCL plant, two ebullated bed reactors (EBRs) in sequence are used in the CTSL unit to directly convert coal to syncrude. (Wu et al., 2015) The EBR is basically a slurry bubble column reactor (SBCR) in which the solid particles are held in suspension mostly by the upward movement of the liquid-phase rather than only the gas-phase as in traditional SBCRs. Compared with other types of three-phase reactors, EBRs have small axial temperature distribution because of strong backmixing (Gruyl and Parmentier, 2008), high utilization of the reactor volume because of small gas holdup, and negligible solid precipitation because of large superficial liquid velocity. (Wu et al., 2015; Robinson, 2009) Therefor, EBRs are preferred by the DCL reactions, which have relatively low reaction rates. In this section, a mathematical model is developed in Aspen Custom Modeler (ACM) for ebullated-bed DCL reactors based on rigorous reaction kinetics, hydrodynamics and mass and heat balances.

5.1 Configuration of the Catalytic Two Stage Liquefaction Unit

In the CTSL unit as shown in Figure 5.1, pulverized coal is first mixed with the liquefaction solvent from the separation unit and Fe-based liquefaction catalyst to form the coal slurry, where Fe loading on the catalyst is 1 wt% of dry coal. (Shan et al., 2015; Jiang et al., 2015; Wu et al., 2015) The coal slurry is then mixed with hydrogen and sent to the coal slurry pre-heater. Then the heated coal slurry mixed with hydrogen is sent to two EBRs in sequence, where coal is converted to syncrude. As shown in Figure 5.1, a portion of the slurry from the reactor top section is collected in the recycle cup and then sent back to the reactor bottom by the ebullating pumps to achieve high liquid or slurry-phase velocity.

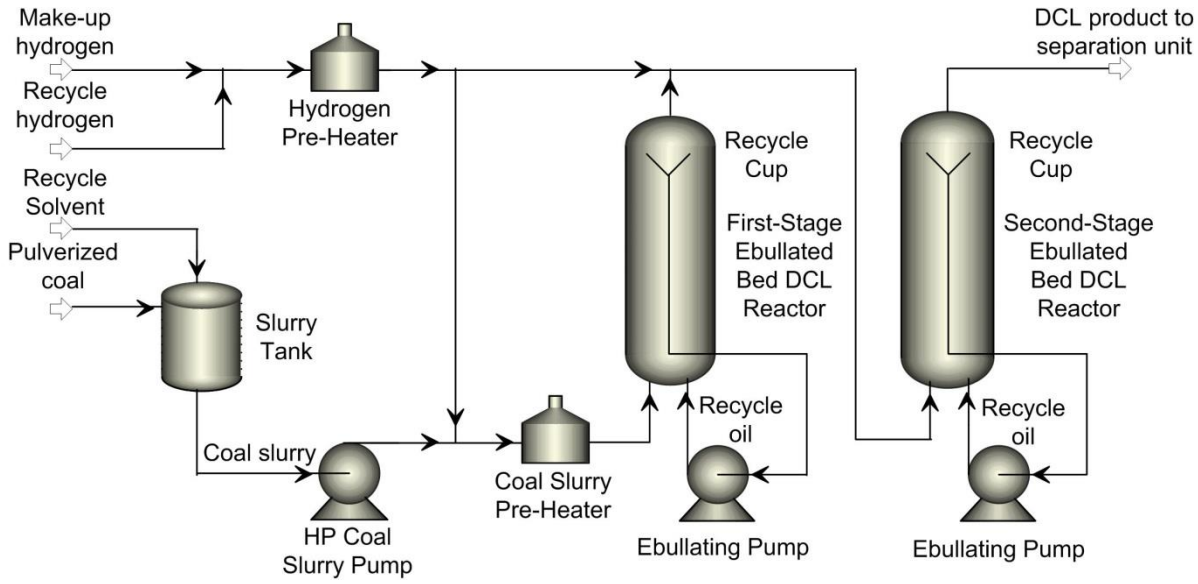

Figure 5.1 Plant configuration of the CSTL unit in the DCL process

5.2 Steady-State Modeling Approach

In this study, the CTSL unit is modeled in ACM, as shown in Figure 5.2. Enthalpy balances are considered for the mixers (M1, M2, M3, MR1, MR2), splitter (SPL) and heaters (H2HT). Pumps (PF, P1, P2) are modeled by considering a fixed isentropic efficiency. In the coal slurry preheating furnace (MFNC), a small amount of coal is decomposed. Because of small tube diameters in the furnace, it is modeled as plug flow reactor with enthalpy balance and kinetics available in the open literature for the pre-heating stage. (Shan et al., 2015) On the other hand, the EBRs (R1, R2) are modeled as axial dispersed flow (ADF) with recycle stream, because of the large column diameters. (Robinson, 2009) The recycle oil stream is treated as the tear stream for easier convergence of the model. The one-dimensional non-isothermal steady-state mathematical model of EBRs was built with the following features and assumptions: 1) the EBR is operated in a homogeneous bubble flow regime (Ishibashi et al., 2001; Leonard et al., 2015; Ruiz et al., 2005); 2) both slurry and gas flow upward; 3) pseudo-homogeneous condition is assumed for the coal slurry because of the high superficial liquid velocity and small particle size (Wu et al., 2015; Martubez et al., 2010); 4) superficial velocity of the slurry phase is assumed to be constant (Sehabiague et al., 2008); 5) main reactions take place at the slurry phase (Ferrance, 1996); 6) The mass transfer resistance is negligible because of the high operating temperature and pressure (Lenoard et al., 2015); 7) temperature of the gas and slurry phases is the same; 8)

axial dispersion coefficients of the gas and slurry phases are assumed to be the same in a homogeneous bubble flow regime (de Swart, 1996; Sehabiague et al., 2008). Reaction kinetics of both pre-heating and reaction sections are provided in Section 5.2.2. For the EBRs, the ADF model with recycle streams is detailed in Section 5.2.1. Hydrodynamics of the main reactors and the properties models for the whole system are discussed in Section 5.2.3.

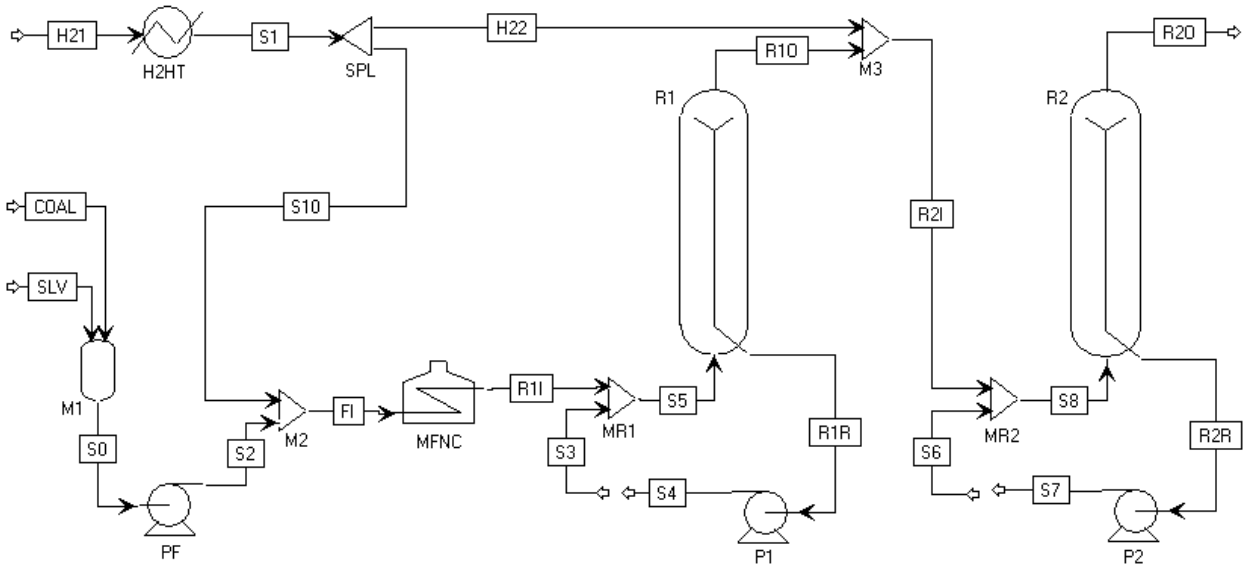

Figure 5.2 Process flowsheet in Aspen Custom Modeler

5.2.1 Reaction Kinetics and Component Specification

The first order irreversible kinetic models with eight-lump components, as shown in Eq. (5.1) to (5.7) proposed by Shan et al. and Jiang et al. are applied for both coal slurry pre-heater and main reactors. (Shan et al., 2015; Jiang et al., 2015) In this model, the dry ash-free (daf) coal is divided into three types: the easy reactive component (C_1), the difficult reactive component (C_2) and the nonreactive component (C_3). The liquefied product is divided into pre-asphaltene and asphaltene (PAA), oil (Oil), water (H_2O) and gas (Gas). C_1 can be converted to PAA, Oil, H_2O and Gas; C_2 can only be converted to PAA; C_3 does not participate in any reaction. PAA can react with H_2 and produce Oil, H_2O and Gas.

$$\frac{dM_{C1}}{dt} = -(k_1 + k_2 + k_3 + k_4)M_{C1} \tag{5.1}$$

$$\frac{dM_{C2}}{dt} = -k_5 M_{C2} \tag{5.2}$$

$$\frac{dM_{PAA}}{dt} = -(k_6 + k_7 + k_8)M_{PAA} + k_1 M_{C1} + k_5 M_{C2} + k_9 M_{PAA} \quad (5.3)$$

$$\frac{dM_{Oil}}{dt} = k_2 M_{C1} + k_6 M_{PAA} \quad (5.4)$$

$$\frac{dM_{Gas}}{dt} = k_3 M_{C1} + k_7 M_{PAA} \quad (5.5)$$

$$\frac{dM_{H_2O}}{dt} = k_4 M_{C1} + k_8 M_{PAA} \quad (5.6)$$

$$\frac{dM_{H_2}}{dt} = -k_9 M_{PAA} \quad (5.7)$$

In the reactions provided above, M_i is the mass fraction of component i using the daf basis of feed coal as benchmark; t is the reaction time and k_i is the reaction rate constant in s^{-1} defined as $k_i = k_{i,0}\exp(-\frac{E_i}{RT})$. The kinetic parameters reported by Shan et al. for the heating stage can be applied for the coal slurry pre-heater by specifying resident time (Shan et al., 2015), while the kinetic parameters reported by Jiang et al. can be applied to the main reactors (Jiang et al., 2015). In ACM, Coal, C_1, C_2, C_3 are specified as solids; Ash, H_2 and H_2O are specified as conventional components; Gas, Oil, PAA and Solvent are specified as pseudo-components. The mass fractions of C_1, C_2 and C_3 based on dry ash free coal are sensitive to the coal type and set to be 0.6278, 0.2914, and 0.0808, respectively, in this study. (Shan et al., 2015; Jiang et al., 2015) Table 5.1 gives the molecular weight (MW) and average normal boiling point (NBP) of the pseudo-components, which is required for calculating physical and thermal properties and converting the kinetic models to molar basis. (Anbar and John, 1978; Yan, 2014; Marzec, 2002; Jiang and Bhattacharyya, 2016; Comolli et al., 1995; Ferrance et al., 1996)

Table 5.1 Component specification in ACM

Component	Average NBP (^{o}C)	Molecular weight
Coal	N/A	1500
Gas	-98	28.2
Oil	232	169
PAA	593	450
Solvent	393	317

As shown in Figure 5.3, the kinetic parameters reported by Shan et al. (Shan et al., 2015) for the heating stage can represent the behavior of the feed furnace very well by comparing with the experimental data. However, the reaction kinetic parameters reported by Jiang et al. (Jiang et al., 2015) for the isothermal stage can give a good estimation of coal conversion and oil yield but not the hydrogen consumption, which is also critical for the direct coal liquefaction process for satisfactory estimate of energy consumption and heat balance. Hence the related kinetic parameters of the main reactor section are re-regressed based on the a 0.01 t/d continuous experimental tubular facility data reported by Jiang et al. (Jiang et al., 2015) in ACM considering the constraints shown in Eq. (5.8). Only the pre-exponential factors $k_{0,1}$, $k_{0,2}$, $k_{0,5}$, $k_{0,9}$ are regressed in this case due to the limited experimental data sets. Table 5.2 shows the updated kinetic parameters of the isothermal stage, while Figure 5.4 shows that the updated kinetic parameters can reasonably represent the experimental data.

$$3 \leq log k_{0,i} \leq 17 \tag{5.8}$$

Table 5.2 Update kinetic parameters for the reactor section

	$E_{a,i}\ (kJ/mol)$	$k_{0,i}\ (min^{-1})$
k_1	-91.47	7.64×10^5
k_2	-91.51	2.01×10^5
k_3	-91.51	4.47×10^4
k_4	-90.53	7.14×10^4
k_5	-92.89	3.63×10^4
k_6	-81.01	1.35×10^5
k_7	-82.19	3.99×10^4
k_8	-84.16	9.00×10^2
k_9	-100.61	2.19×10^5

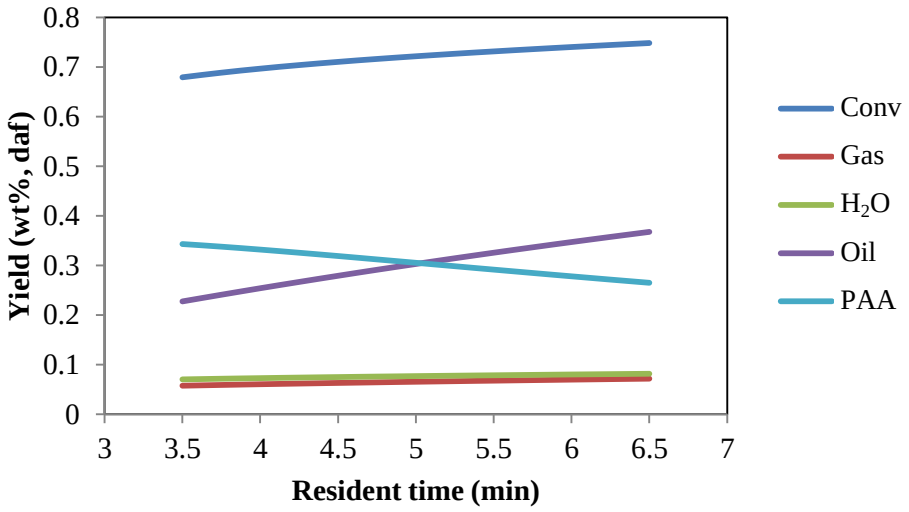

Figure 5.3 Simulation results of the pre-heating stage with original parameters

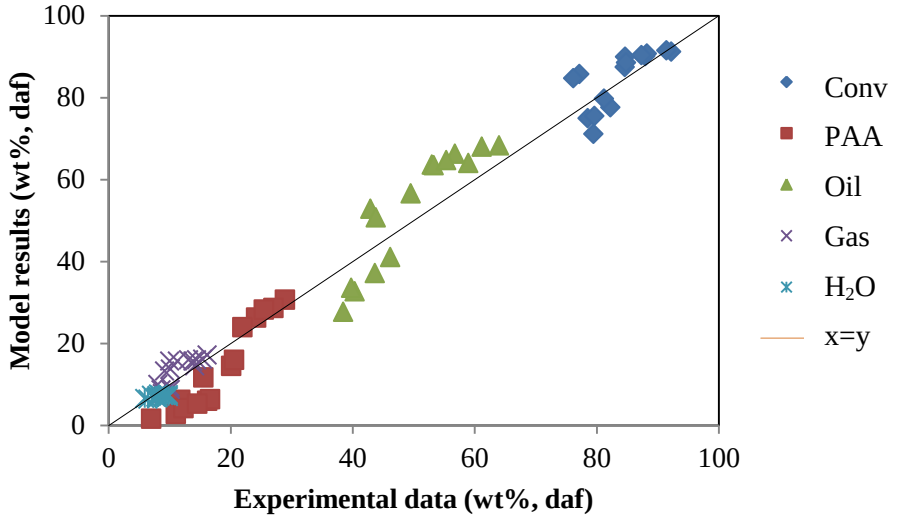

Figure 5.4 Simulation results of the isothermal stage with updated parameters

5.2.2 Mass and Heat Balances

In this study, the commercial-scale EBRs in the CTSL unit are simulated as ADF with recycle stream (Martinez et al., 2010; Robinson, 2009; Chen et al., 2014; Schweitzer and Kressmann, 2004) as shown in Figure 5.5, where $F_{i,g}^{F}$ and $F_{i,sl}^{F}$ are the molar flowrate of component i in the gas and slurry phases in the fresh feed in $kmol/s$; $F_{i,g}^{in}$ and $F_{i,sl}^{in}$ are the molar flowrate of component i of gas and slurry in the reactor inlet in $kmol/s$; $F_{i,g}^{out}$ and $F_{i,sl}^{out}$ are the molar

flowrate of component i of gas and slurry in the reactor outlet in $kmol/s$; $F_{i,sl}^{R}$ is the molar flowrate of component i in the recycle oil in $kmol/s$; $F_{i,sl}^{N}$and $F_{i,sl}^{N}$ are the molar flowrate of component i in the gas and slurry phases in the reactor net product in $kmol/s$; T^{F}, T^{in}, T^{out}, T^{R} and T^{N} are the temperature of the fresh feed, reactor inlet stream, reactor outlet stream, recycle stream and reactor net product, respectively, in K; x is the fraction of slurry in the reactor outlet that is recycled back to the inlet. (Robinson, 2009)

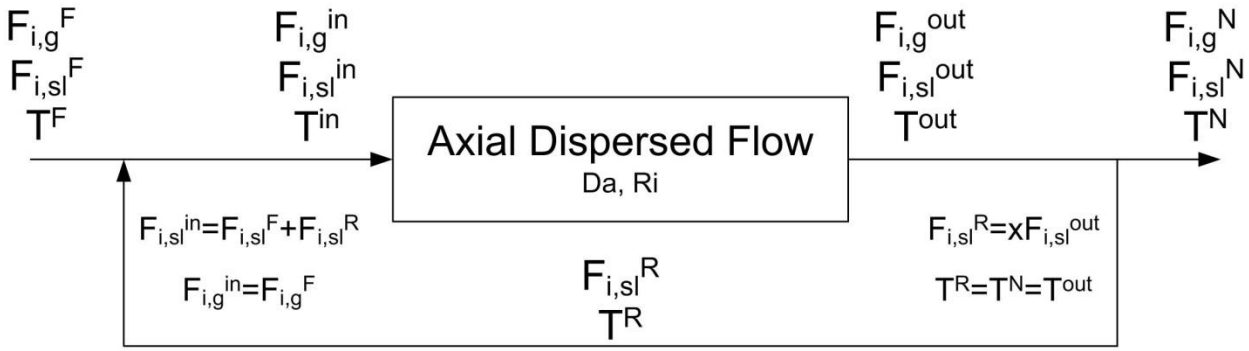

Figure 5.5 Modeling approach of the ebullated bed reactors

With the above assumptions, the mass and energy balance equations are written as shown in Eq. (5.9) to (5.15) for each component, where values of kinetic constants k_i are reported by Jiang et al. as a function of temperature in s^{-1} (Jiang et al., 2015); $C_{i,sl}$ and $C_{i,g}$ are the molar concentration of component i in the slurry and gas phase in $kmol/m^3$; ε_{sl} and ε_g are the slurry and gas holdup; D_a is the axial dispersion coefficient in m^2/s; U_{sl} and U_g are the superficial velocity of the slurry and gas phases in m/s; MW_i is the molecular weight of component i. It should be noted that the reaction kinetics Eq. (5.1) to (5.7) are in mass basis and can be converted to molar concentration basis by using the molecular weight. (Ferrance, 1996)

For the slurry phase:

$$\frac{d}{dz}\left(\varepsilon_{sl}D_a\frac{dC_{C1,sl}}{dz}\right)-\frac{d}{dz}\left(U_{sl}C_{C1,sl}\right)-\varepsilon_{sl}(k_1+k_2+k_3+k_4)C_{C1,sl}=0 \quad (5.9)$$

$$\frac{d}{dz}\left(\varepsilon_{sl}D_a\frac{dC_{C2,sl}}{dz}\right)-\frac{d}{dz}\left(U_{sl}C_{C2,sl}\right)-\varepsilon_{sl}k_5C_{C2,sl}=0 \quad (5.10)$$

$$\frac{d}{dz}\left(\varepsilon_{sl}D_a\frac{dC_{Oil,sl}}{dz}\right)-\frac{d}{dz}\left(U_{sl}C_{Oil,sl}\right)+\varepsilon_{sl}\left(k_2C_{C1,sl}\frac{MW_{C1}}{MW_{Oil}}+k_6C_{PAA,sl}\frac{MW_{PAA}}{MW_{Oil}}\right)=0 \quad (5.11)$$

$$\frac{d}{dz}\left(\varepsilon_{sl}D_a\frac{dC_{PAA,sl}}{dz}\right)-\frac{d}{dz}\left(U_{sl}C_{PAA,sl}\right)$$
$$+\varepsilon_{sl}\left((k_9-k_6-k_7-k_8)C_{PAA,sl}+k_1C_{C1,sl}\frac{MW_{C1}}{MW_{PAA}}+k_5C_{C2,sl}\frac{MW_{C2}}{MW_{PAA}}\right)=0 \quad (5.12)$$

For the gas phase:

$$\frac{d}{dz}\left(\varepsilon_gD_a\frac{dC_{H_2,g}}{dz}\right)-\frac{d}{dz}\left(U_gC_{H_2,g}\right)-\varepsilon_{sl}k_9C_{PAA,sl}\frac{MW_{PAA}}{MW_{H_2}}=0 \quad (5.13)$$

$$\frac{d}{dz}\left(\varepsilon_gD_a\frac{dC_{Gas,g}}{dz}\right)-\frac{d}{dz}\left(U_gC_{Gas,g}\right)-\varepsilon_{sl}\left(k_3C_{C1,sl}\frac{MW_{C1}}{MW_{Gas}}+k_7C_{PAA,sl}\frac{MW_{PAA}}{MW_{Gas}}\right)=0 \quad (5.14)$$

$$\frac{d}{dz}\left(\varepsilon_gD_a\frac{dC_{H_2O,g}}{dz}\right)-\frac{d}{dz}\left(U_gC_{H_2O,g}\right)-\varepsilon_{sl}\left(k_4C_{C1,sl}\frac{MW_{C1}}{MW_{H_2O}}+k_8C_{PAA,sl}\frac{MW_{PAA}}{MW_{H_2O}}\right)=0 \quad (5.15)$$

The energy conservation equation (Onazaki et al., 2000) and the equation for calculating the pressure profile (Deckwer, 1992; Sehabiague et al., 2008) are shown by Eq. (5.16) and (5.17), respectively, where ΔH_r is the heat of reaction based on the hydrogen conversion in $kJ/kmol\ H_2$ given by Wu et al. (Wu et al., 1993; Onazaki et al., 2000); H_{mix} is the volumetric heat capacity of the gas-slurry mixture in $J/(m^3 slurry\ K)$ defined by Eq. (5.18) (Onazaki et al., 2000); ρ_{sl} and ρ_g are the slurry phase and gas phase densities in kg/m^3; $C_{p,sl}$ and $C_{p,g}$ are the heat capacities of the slurry and gas phases in $kJ/(kg\ K)$; g is the acceleration of gravity in m^2/s; T and P are the local reactor temperature in K and pressure in Pa, respectively.

$$\frac{d}{dz}\left(\varepsilon_{sl}D_aH_{mix}\frac{dT}{dz}\right)-\frac{d}{dz}\left(U_{sl}H_{mix}T\right)+\Delta H_r\varepsilon_{sl}k_9C_{PAA,sl}\frac{MW_{PAA}}{MW_{H_2}}=0 \quad (5.16)$$

$$\frac{dP}{dz}+\left(\varepsilon_g\rho_g+\varepsilon_{sl}\rho_{sl}\right)g=0 \quad (5.17)$$

$$H_{mix}=\rho_gC_{p,g}U_g/U_{sl}+\rho_{sl}C_{p,sl} \quad (5.18)$$

The boundary conditions for the gas and slurry at the inlet (bottom, $z=0$) of the reactor are Danckwerts' type as listed in Eq. (5.19) to (5.22), in which the inlet condition $C_{i.g}^{in}$ and $C_{i.sl}^{in}$ is evaluated by Eq. (5.23) and (5.24) after mixing the fresh feed and the recycle oil; T^{in} is the reactor inlet temperature. In Eq. (5.23) and (5.24), D_T is the reactor diameter in m.

$$U_{sl}C_{i,sl} - \varepsilon_{sl}D_a\frac{dC_{i,sl}}{dz} = U_{sl}C_{i.sl}^{in} \quad (5.19)$$

$$U_gC_{i,g} - \varepsilon_gD_a\frac{dC_{i,g}}{dz} = U_gC_{i.g}^{in} \quad (5.20)$$

$$U_{sl}T - \varepsilon_{sl}D_a\frac{dT}{dz} = U_{sl}T^{in} \quad (5.21)$$

$$P = P^{in} \quad (5.22)$$

$$C_{i.sl}^{in} = (F_{i,sl}^F + F_{i,sl}^R)/(0.25\pi D_T^2U_{sl}) \quad (5.23)$$

$$C_{i.g}^{in} = F_{i,g}^F/\left(0.25\pi D_T^2U_g\right) \quad (5.24)$$

The boundary conditions at the outlet (top, $z = L$) of the reactor are listed in Eq. (5.25) to (5.27).

$$\frac{dC_{i,sl}}{dz} = 0 \quad (5.25)$$

$$\frac{dC_{i,g}}{dz} = 0 \quad (5.26)$$

$$\frac{dT}{dz} = 0 \quad (5.27)$$

5.2.3 Hydrodynamics and Property Models

The axial dispersion coefficient (D_a) in m^2/s and gas holdup (ε_g) of the EBRs are modeled by Eq. (5.28) and (5.29), respectively, which were developed based on the data collected or tested for a gas-coal slurry system at the coal liquefaction operating conditions. (Leonard et al., 2015; Baird and Rice, 1975; Kara et al., 1982; Ishibashi et al., 2001) In these equations, the specific enthalpy, heat capacity and density of the gas mixture and the liquid mixture are estimated using Peng-Robison EOS available in ACM by property call. The specific enthalpy of coal is calculated using unconventional property models in ACM with given proximate and ultimate analysis data, while the density and coal is set to be 1346 kg/m^3, and the heat capacity of coal is given by Eq. (5.30), where T is in ^oC. (Tomeczek and Palugniok, 1996; Richardson, 1993)

$$D_a = 0.35g^{1/3}{D_T}^{4/3}{U_g}^{1/3} \quad (5.28)$$

$$U_g/\varepsilon_g = \left(U_g + U_{sl}\right) + 0.114\left(1 - \varepsilon_g\right)^{1.02} \quad (5.29)$$

$$C_{p,s} = 1.13 + 3.58 \times 10^{-3}T + 2.28 \times 10^{-6}T^2 - 9.81 \times 10^{-9}T^3 + 4.63 \times 10^{-12}T^4 \quad (5.30)$$

5.3 Results and Discussion

For the base case study, the key operating conditions and reactor dimensions are set to be same as the commercial scale Shenhua DCL plant, as shown in Table 5.3. (Wu et al., 2015)

Table 5.3 key operating conditions and reactor dimensions (base case)

Variables	Value
Operating conditions	
Coal flowrate (kg/s)	69.44
Solvent flowrate (kg/s)	78.42
Pre-heater outlet temperature (^{o}C)	382
First reactor inlet pressure (bar)	200
Reactor specification	
Reactor diameter (m)	4.8
Reactor length (m)	62.5
Recycle ratio (m^3/m^3)	3

5.3.1 Base Case and Model Validation

With the model input shown in Table 5.3, the stream summary of the base case study is provided in Table 5.4, while the utility consumptions are reported in Table 5.5. In Table 5.4, streams are named corresponds to Figure 5.2. In Table 5.5, utility prices are assumed to be \$16.8 and \$11.1 for electricity and fuels, respectively, where the heating value of the syncrude is assumed to be 46 MJ/kg. (Turton et al., 2012; Jiang and Bhattacharyya, 2016) As reported in Table 5, the total utility cost of the CTSL unit is \$2.2/MJ syncrude, mainly due to the coal slurry preheating furnace. The profiles of both reactors are shown in Figure 5.6 to Figure 5.8. The smaller temperature gradient of the second reactor indicates that most of the conversion is achieved in the first reactor. Table 5.6 shows that with the same feed flowrate and reactor geometry (Wu et al., 2015), the superficial velocity and holdups are close to the industrial data, which indicates that the density model and hydrodynamic correlations are satisfactory. Table 5.6 also shows that the coal conversion and oil yield are close to the industrial data, which indicates that the ADF model with recycle stream is satisfactory for the commercial scale EBRs used for direct coal liquefaction.

Table 5.4 Stream summary of the CTSL unit (base case)

Stream	S0	H21	R1I	R1O	R1R	R2I	R2O	R2R
Pressure (bar)	1.1	202	200	197	197	197	195	195
Temp (K)	409	393	655	732	732	719	731	731
Coal (kg/hr)	69.44							
C_1 (kg/hr)			4.80	0.10	0.13	0.10		
C_2 (kg/hr)			15.88	11.00	14.52	11.00	7.74	10.10
C_3 (kg/hr)			5.10	5.10	6.74	5.10	5.10	6.65
Ash (kg/hr)			3.55	3.55	4.68	3.55	3.55	4.62
Gas (kg/hr)		9.50	11.39	17.43		18.57	19.46	
H_2 (kg/hr)		6.80	5.33	3.81		4.62	4.39	
H_2O (kg/hr)			6.65	7.05		7.05	7.07	
Oil (kg/hr)			9.56	34.50	45.56	34.50	38.42	49.72
PAA (kg/hr)			22.26	1.26	1.66	1.26	0.29	0.38
Solvent (kg/hr)	78.42		78.42	78.42	103.6	78.42	78.42	102.2

Table 5.5 Utility consumptions of the CTSL unit (base case)

Equipment		Heat duty (GJ/hr)	Electricity (kW)	Cost ($/MJ Oil)
H2HT	Hydrogen preheater	200		0.740
MFNC	Coal slurry preheater	379		1.404
PF	Slurry feed pump		2870	0.058
P1	Ebullated pump		85	0.002
P2	Ebullated pump		77	0.002
Total		578	3031	2.205

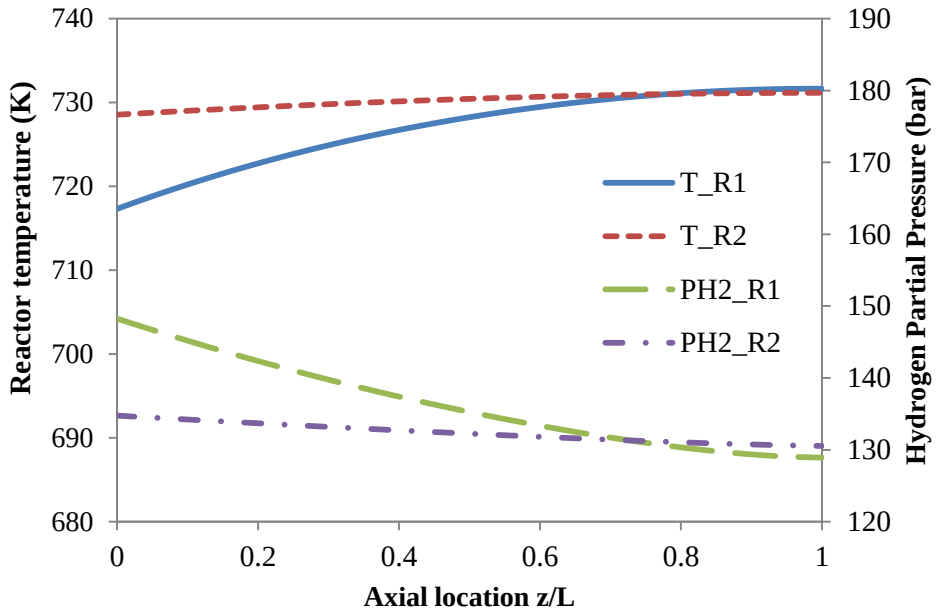

Figure 5.6 Profiles of reactor temperature and hydrogen partial pressure (T-temperature; PH2-hydrogen partial pressure)

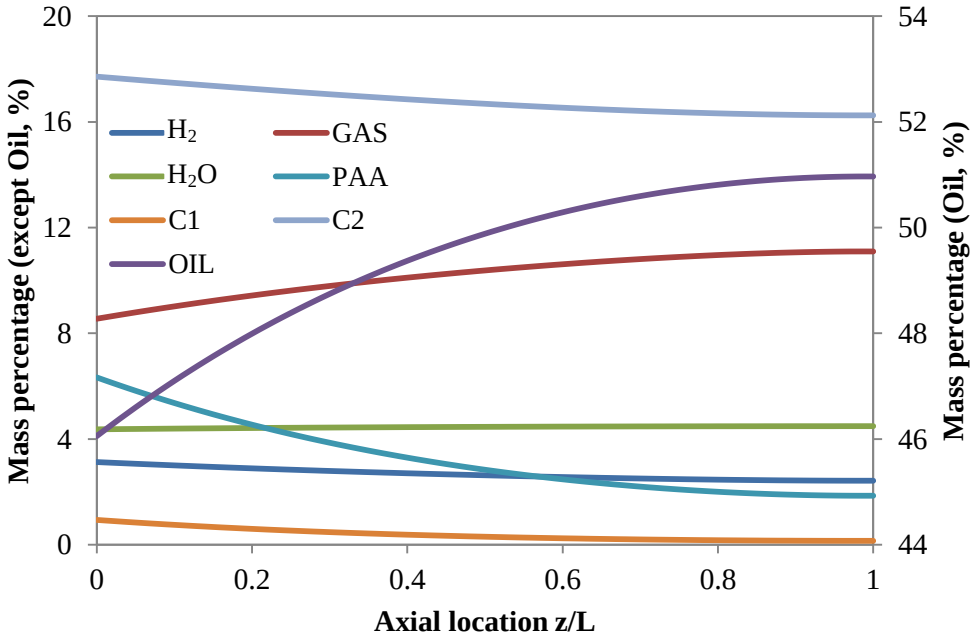

Figure 5.7 Component mass percentage profile (solvent free) of the first reactor

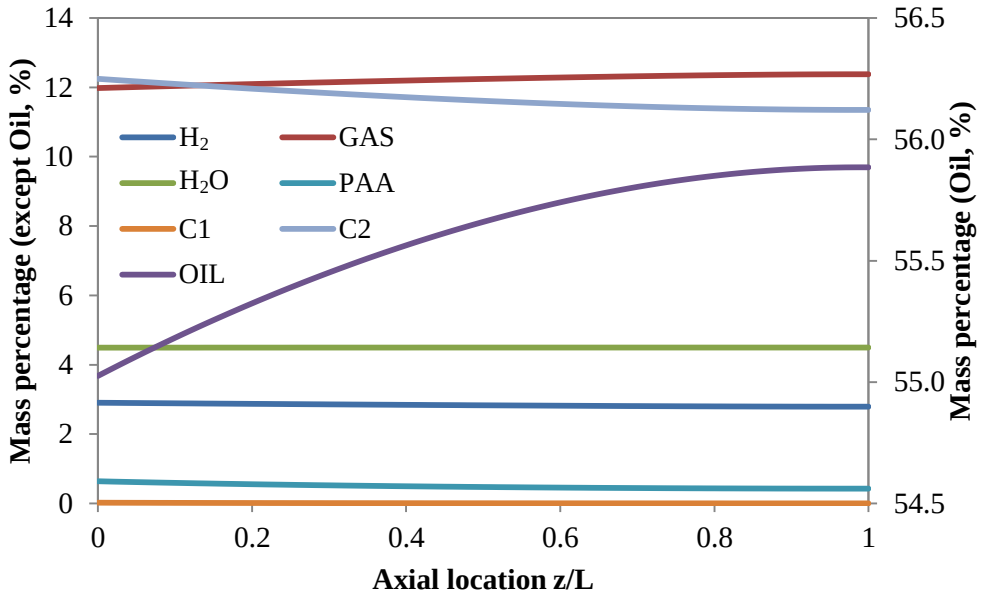

Figure 5.8 Component mass percentage profile (solvent free) of the second reactor

Table 5.6 Model validation for commercial scale EBRs in DCL process

Variables	Model	Industrial
1st Reactor output		
Superficial gas velocity (cm/s)	5.75	5.0
Superficial slurry velocity (cm/s)	2.66	2.5
Hydrogen partial pressure (bar)	129	125
Gas holdup	0.37	0.35
Coal conversion (%, active coal)	80.9	N/A
Oil yield (%, daf)	54.7	N/A
Temperature increase (^{o}C)	76.4	72.8
2nd Reactor output		
Superficial gas velocity (cm/s)	5.99	5.0
Superficial slurry velocity (cm/s)	2.96	2.5
Hydrogen partial pressure (bar)	130	123
Gas holdup	0.37	0.35
Coal conversion (%, daf)	86.6	90.4
Oil yield (%, daf)	60.4	58.0
Temperature increase (^{o}C)	12.0	39.5

5.3.2 Sensitivity Studies

Sensitivity studies are conducted considering different residence time and pre-heating temperature with the same reactor dimension as shown in Table 5.3. As shown in Table 5.7, the coal conversion and oil yield increases with the operating temperature of the ebullated bed reactor which is achieved by increasing preheating temperature, because of the higher operating temperature and lower gas holdup in the EBRs. It is observed that the superficial gas velocity decreases with the temperature, because as the furnace pre-heating temperature increases, more hydrogen is consumed in the pre-heating furnace even though the density of gas phase mixture increases due to coal decomposition. Table 5.8 shows that as the reactor residence time increases, the oil yield and coal conversion increase. However, because of the existence of sulfur and other contaminates, relatively low residence time and high operating temperature and hydrogen partial pressure, the EBRs in the DCL process are usually large and constructed by costly 21/4 Cr-1 Mo-1/4 V steel cladding with SS347. Therefore, optimization of this reactor can be undertaken by considering both the operating and capital costs, as well as product yield.

Table 5.7 Effect of pre-heating furnace outlet temperature

Preheating T (K)	645.2	650.2	655.2	660.2	665.2	670.2
MFNC duty (GJ/hr)	363.2	371.1	378.9	386.7	394.5	402.4
R1 T_{out} (K)	714.0	723.2	731.6	739.2	745.9	751.7
R2 T_{out} (K)	714.1	723.0	731.2	738.4	744.7	749.9
R1 U_g (cm/s)	5.76	5.76	5.75	5.72	5.67	5.60
R2 U_g (cm/s)	6.13	6.07	6.00	5.91	5.81	5.70
R1 U_{sl} (cm/s)	2.66	2.66	2.66	2.65	2.62	2.56
R2 U_{sl} (cm/s)	2.87	2.92	2.96	3.01	3.05	3.09
R1 ε_g	0.371	0.371	0.371	0.369	0.367	0.365
R2 ε_g	0.384	0.380	0.374	0.368	0.362	0.355
Coal conversion (%)	83.2	85.0	86.6	88.2	89.6	90.8
Oil yield (%)	57.3	58.9	60.4	61.8	63.2	64.4

Table 5.8 Effect of reactor resident time

Coal flowrate (kg/s)	41.7	48.6	55.6	62.5	69.4	76.4	83.3	90.3	97.2
R1 T_{out} (K)	739.6	737.7	735.7	733.7	731.6	729.6	727.6	725.6	723.6
R2 T_{out} (K)	739.0	737.3	735.4	733.3	731.2	729.0	727.0	725.0	723.1

R1 U_g (cm/s)	3.45	4.03	4.60	5.18	5.75	6.33	6.90	7.47	8.03
R2 U_g (cm/s)	3.52	4.14	4.75	5.37	6.00	6.62	7.25	7.88	8.51
R1 U_{sl} (cm/s)	1.62	1.88	2.14	2.40	2.66	2.92	3.19	3.45	3.71
R2 U_{sl} (cm/s)	1.83	2.12	2.40	2.68	2.96	3.24	3.51	3.78	4.05
R1 ε_g	0.255	0.288	0.318	0.346	0.371	0.393	0.413	0.431	0.447
R2 ε_g	0.255	0.289	0.320	0.348	0.374	0.398	0.419	0.438	0.455
Coal conversion (%)	93.2	91.5	89.8	88.2	86.6	85.2	84.0	82.8	81.8
Oil yield (%)	65.8	64.4	63.0	61.7	60.4	59.3	58.2	57.2	56.3

5.4 Conclusions

In this section, a mathematical model was developed in Aspen Custom Modeler (ACM) for ebullated-bed DCL reactors based on rigorous reaction kinetics, hydrodynamics and mass and heat balances, which can reasonably predict the gas holdup, coal conversion, oil yield and temperature increase of commercial scale EBRs. The base case study shows that the oil yield and coal conversion are about 60.4% and 86.6%, respectively with a gas holdup of about 0.37. Sensitivity studies indicate that the oil yield and coal conversion increase with an increase in the pre-heater temperature and a decrease in the residence time. However, the utility and capital costs also increase when the pre-heater temperature is increased or the residence time is decreased. To determine the optimal operating condition, a techno-economic study can be conducted by using the detailed process model discussed in this section and capital cost correlations obtained from APEA.

Chapter 6 Modeling of an Direct Coal-Biomass to Liquids Plant

6.0 Overview

DCL technologies have been commercially demonstrated for producing transportation fuels from non-petroleum sources. However, significant amount of hydrogen is required in the DCL process due to the low H/C ratio in coal. As a result, DCL processes are usually associated with a high level CO_2 emission from hydrogen production units. Hence, D-CBTL processes with CCS and shale gas utilization are proposed in this work as an option for reducing CO_2 emission. In this study, the focus is on process simulation and calculation of material and energy balances of novel D-CBTL plants, which can be used as a basis for further studies, such as optimization, techno-economic analysis and life-cycle analysis. In this process, coal with moderate amount of biomass is converted into syncrude through reaction with the hydrogen-donor solvent and gaseous hydrogen in a CTSL unit. Hydrogen required for the liquefaction and product upgrading unit is produced from the liquefaction residue partial oxidation unit and the shale gas steam reforming unit or from the coal/biomass/residue co-gasification unit. Different CCS technologies are evaluated to achieve 90% overall carbon capture if high extent of CO_2 capture is considered. Results of individual plant sections are validated with the existing data, if available.

Our focus in this section is on process synthesis, technology selection and performance analysis, which provides the basis for further studies, such as optimization, life cycle analysis, and techno-economic analysis. In particular, contributions of this work can be summarized as follows: (1) proposed four novel configurations for D-CBTL processes and developed high-fidelity plant-wide models for each of them, (2) utilized shale gas as a novel sources for H_2 in the direct coal biomass gas to liquids (D-CBGTL) process, (3) designed the CCS units for all configurations, (4) investigated the plant performance in terms of productivity, efficiency and CO_2 emission for different hydrogen sources, CCS solvent, extent of CCS and biomass to coal ratio, and (5) compared the D-CBTL and D-CBGTL plant with indirect CBTL plant for various process configurations.

6.1 Conceptual Design and Modeling

BFD of D-CBGTL and D-CBTL plants are shown in Figure 6.1 and Figure 6.2. Liquefaction technology is the core technology for all different configurations. Coal and biomass with a low biomass/coal ratio (8/92 weight basis, base case) are mixed with the recycled oil in the slurry tank, and then pressurized and preheated before being fed to CTSL reactors along with make-up and recycled H_2. The product from the second liquefaction reactor is sent to a hot HP separator. The vapor product from the hot HP separator is then sent to the inline hydrotreater for stabilization. Hydrotreated liquids from the inline hydrotreater and the liquid product from the hot separator are sent to the hydrocarbon recovery and solid/liquid separation unit to be separated into H_2-rich gases, light gases (C_1- C_4), light naphtha (C_5, C_6), heavy naphtha (C_7-177^oC), distillate/gas oil (177-376^oC), solvent oil (376-524^oC) and liquefaction residues (more than 524^oC). H_2-rich gases and solvent oil are recycled back to the CTSL unit. A portion of the light gases is used in the process furnaces, while the remaining is sent to the power island for electricity generation. Naphtha and gas oil are sent to the product upgrading unit for generating on-spec gasoline and diesel as main products. The liquefaction residue is sent to the POX unit for H_2 production.

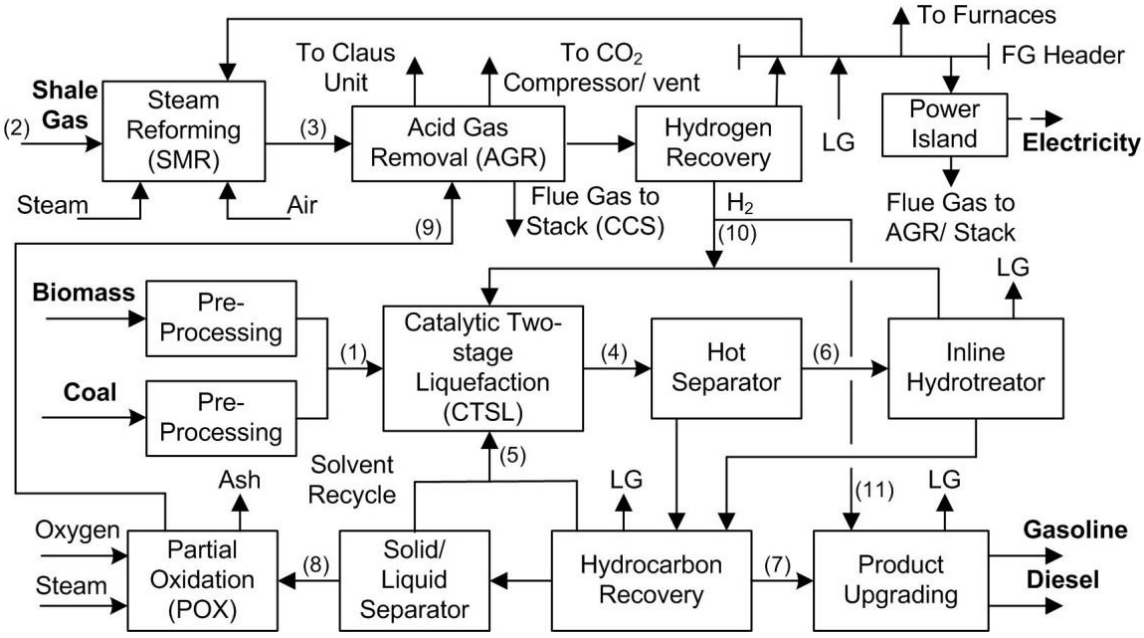

Figure 6.1 BFD of the D-CBGTL plants

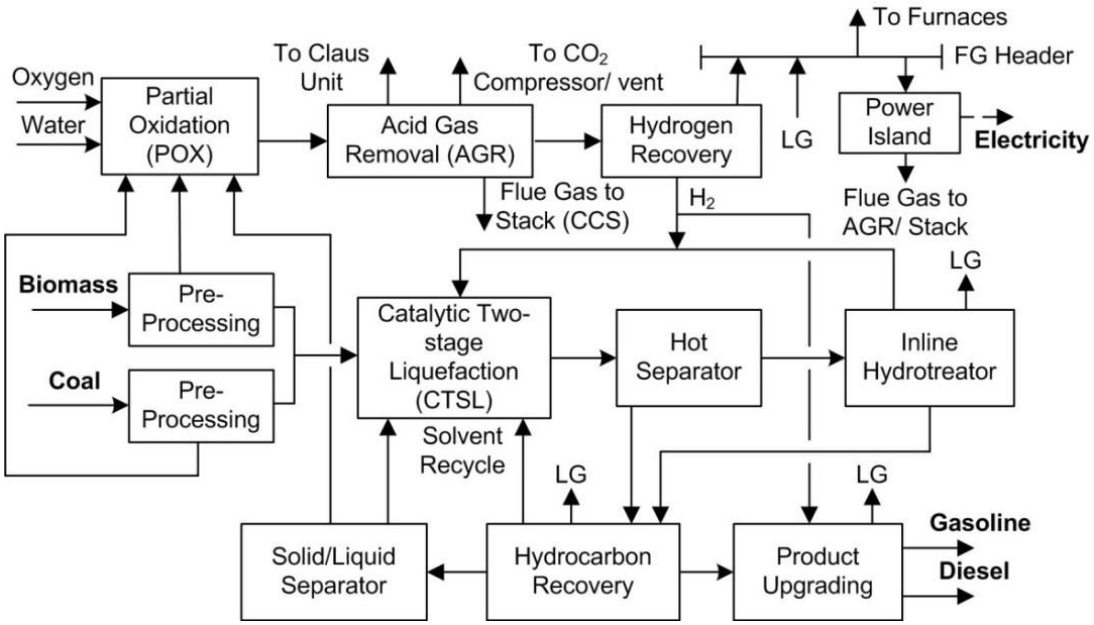

Figure 6.2 BFD of the D-CBTL plants

Because considerable amount of H_2 is consumed in the CTSL unit, hydrogen production is also critical for D-CBTL and D-CBGTL plants. Considering different H_2 sources and CO_2 control targets, four different configurations are considered in our study. In the D-CBGTL-CCS (base case) and D-CBGTL-VT processes as shown in Figure 6.1, a portion of the required H_2 is generated from partial oxidation of the liquefaction residue, while the remaining is generated by shale gas steam reforming. Alternatively, the required H_2 is supplied from coal/biomass/liquefaction residue co-gasification. In the D-CBTL-CCS and D-CBTL-VT processes as shown in Figure 6.2, pre-processed coal and biomass are fed to the liquefaction unit and the POX unit along with liquefaction residues, while other blocks remain the same as the D-CBGTL-CCS and D-CBGTL-VT processes. In all configurations, the syngas from the POX/CG unit and/or the SMR unit is sent to the AGR unit for CO_2 and H_2S removal, and then to PSA unit for H_2 purification. Three different CO_2 capture technologies are considered for the AGR unit-Selexol, MEA, MDEA/PZ. H_2S produced in the POX/CG unit via gasification is removed in the H_2S absorber of the dual-stage Selexol unit, while H_2S produced in the liquefaction and hydrotreating units is removed by chemical absorption using MDEA as solvent. The removed H_2S is then sent to the Claus unit to be recovered as elemental sulfur. In the D-CBGTL-VT and D-CBTL-VT processes, CO_2 captured from the syngas is directly vented to the atmosphere. In the D-CBGTL-CCS and D-CBTL-CCS processes considering high extent of CCS, a portion of

the flue gas produced from the gas turbine or process furnaces also needs to be sent to the AGR unit for post-combustion CO_2 removal, and all CO_2 streams from the AGR unit are sent to the CO_2 compression section for sequestration.

In this section, the steady-state modeling approach of the D-CBTL and D-CBGTL plants is discussed. The plant is divided into five well-defined sections - the liquefaction and product recovery section, the product upgrading section, the syngas production section, the acid gas removal and hydrogen recovery section, and the combined cycle power island. Most of the unit operations are modeled as standard equipment items in Aspen Plus, while yield models are developed in Excel for liquefaction reactors and upgrading units based on the experimental or operational data available in the open literature. Aspen User2 blocks are used to connect Excel with Aspen Plus. In the process model, coal and biomass are specified as unconventional component, while syncrude are specified as either pseudo-components or petroleum assays defined by boiling point ranges. The compositions of Illinois No.6 coal, wood chip and Marcellus shale gas are given in Table 6.1 and Table 6.2. (Bhattacharyya et al., 2011; Bain et al., 1992; Bullin and Krouskop, 2009)

For all case studies, hydrogen, carbon and utility balances have to be satisfied and constrained by Eq. (6.1) to (6.3). In the liquefaction plant, H_2 is consumed due to liquefaction and hydrotreating while it is produced from gasification, steam reforming and catalytic reforming. The make-up H_2 requirement and purge rate of H_2-rich recycle stream from the liquefaction and hydrotreating units are determined by the required H_2 partial pressure (P_{H_2}) and H_2/solid or H_2/oil ratio. Feed flowrates of shale gas and coal/biomass mixture to the syngas production section are determined by the hydrogen balance, as shown in Eq. (6.1). The entire gas oil column bottom produced in the product upgrading unit and a portion of the fuel gas (FG) produced in the entire plant are utilized as heating utilities in the furnaces. Eq. (6.2) is used to determine the percentage of the remaining fuel sent to the power island based on the utility balance. Eq. (6.3) is used to determine the amount of CO_2 to be captured.

$$H_{2,produced\ from\ SMR,POX,catalytic\ reforming} = H_{2,consumed\ in\ liquefaction,hydrotreating} \quad (6.1)$$

$$\frac{F_{FG} \times LHV_{FG} + F_{GO} \times LHV_{GO} - Q_{PF}}{LHV_{FG}} = F_{FG}\ to\ gas\ turbine \quad (6.2)$$

$$\frac{Carbon\ in\ products + Carbon\ in\ captured\ CO_2}{Total\ Carbon\ in\ the\ feedstock} = Extent\ of\ CCS\ (90\%\ , base\ case) \quad (6.3)$$

Table 6.1 Proximate and ultimate analysis of coal and biomass feedstock

	Proximate analysis (dry basis)				Ultimate analysis (dry basis)					
	M	FC	VM	A	A	C	H	N	S	O
Coal	3.08	50.65	37.85	11.50	11.50	71.00	4.80	1.40	3.20	8.00
Biomass	9.58	16.55	82.51	0.94	0.94	48.51	6.17	0.12	0.04	44.22

Table 6.2 Composition of Marcellus shale gas (well 3)

Component	C_1	C_2	C_3	CO_2	N_2
vol%	83.8	12.0	3.0	0.9	0.2

6.2 Liquefaction and Product Upgrading

The liquefaction and product upgrading section is the common section of all different direct liquefaction configurations discussed in this section. It includes the CTSL unit, the inline hydrotreating unit, the hydrocarbon recovery unit, the solid/liquids separation unit and product upgrading units.

6.2.1 Catalytic Two-Stage Liquefaction Unit

In the CTSL unit, coal and biomass are mixed with hot recycle solvents in the slurry tank, preheated and then sent to two ebullated bed reactors in a close-coupled mode with recycled and make-up H_2 stream. (Bechtel and Amoco, 1990; Cheng et al., 2014; Robinson, 2005) Because the heavy oil produced from the 2nd stage is recycled to form feed slurry and is fed back to the 1st stage, two stages are interrelated and treated as a single unit in this study. (Valente and Cronauer, 2005) A yield model is developed for the CTSL unit fed with coal and small amount of biomass. As mentioned in Section 2.3, biomass can promote DCL process under mild condition, while the synergistic effect gets reduced with the increasing temperature being comparatively negligible under the normal operating temperature of the DCL reactors. (Tchapda and Pisupati, 2014; Shui et al., 2011; Coughlin et al., 1986; Anderson and Tuntawiro, 1993; Ai, 2007) Hence, in this study the interaction between coal and biomass is ignored because of the low percentage of biomass in

the feedstock and high operating temperature and pressure, and therefore the yield of the coal biomass co-liquefaction reaction is considered to be a linear combination of the yields from the coal and biomass liquefaction reactions. The yield of liquids and their hydrocarbon distribution from the coal liquefaction reactors are estimated based on the operating data from the DCL proof-of-concept (POC) facility reported by HTI in 1995. (Comolli et al., 1995) Operating conditions in POC-01 Period 26, shown in Table 6.3, were recommended by HTI's study because of its higher efficiency and better operability, and therefore, are considered in our baseline study. (Comolli et al., 1995; Bechtel and Amoco, 1990) There is limited information in the open literature on direct biomass liquefaction using oil as the slurry medium and H_2 as the reduction gas. In this work, data from the Pittsburgh Energy Research Center (PERC) are used as baseline. In the process reported by the PERC, wood chips were fed to the reactor with the recycle oil serving as the solvent. The oil yield was about 45-55% of the dry wood with about 100% conversion of the wood. (Steven, 1987; Behrendt et al., 2008) It is also assumed that the elimination of oxygen from wood can occur by producing H_2O, CO and CO_2. (Sofer and Zaborsky, 2012) Therefore, the yield of bio-oil and gases can be estimated by atom balance with the elemental analysis of bio-oil to be 81 wt% carbon, 10.2 wt% hydrogen and 8.8 wt% of oxygen as reported in the open literature. (Behrend et al., 2008; White et al., 1987) These assumptions result in an estimated oil yield of 47% from the biomass liquefaction, which is consistent with the experimental data. (Behrend et al., 2008) In order to simplify atom balance calculation in the yield model of coal/biomass co-liquefaction, syncrude is specified as pseudo-components in Aspen Plus, with the elemental composition of each crude cut calculated by a linear combination of the corresponding data of coal liquids reported by HTI and biomass liquids reported by PERC. (Comolli et al., 1995; Behrend et al., 2008; White et al., 1987) The yield model of the coal-biomass co-liquefaction process is developed in MS Excel by applying atom balance for calculating H_2 consumption and the yield of gases (i.e. CO, CO_2, NH_3, H_2S, H_2O), since the heteroatoms in the coal and biomass are either converted into gases or contained in the liquids. For the base case with a biomass/coal weight ratio of 8/92, the calculated elemental composition of syncrude and the results from the reactor model are shown in Table 6.4 and Table 6.5.

Table 6.3 Operating conditions of the CTSL unit

Variable	Value	Variable	Value
Reactor inlet pressure (MPa)	22.1	1st stage temperature (°C)	407
Reactor outlet pressure (MPa)	20.7	2nd stage temperature (°C)	432
Hydrogen partial pressure (P_{H_2}, MPa)	13.4	Solvent/feed ratio (wt/wt)	1.82

Table 6.4 Element analysis of raw syncrude (base case)

Crude cut	Average NBP (°C)	Specific gravity	Elemental composition (wt%)				
			C	H	O	N	S
IBP-177 °C	93	0.799	84.75	14.09	0.99	0.16	0.01
177-288 °C	232	0.924	86.92	11.33	1.54	0.20	0.02
288 -344 °C	315	0.975	87.89	10.05	1.84	0.20	0.02
344 -454 °C	399	1.012	88.63	9.93	1.17	0.21	0.04
454-FBP	540	1.097	88.78	8.11	1.10	0.52	1.45

Table 6.5 Outlet stream distribution of the coal/biomass CSTL reactors (base case)

Component	wt%	Component	wt%	Component	wt%
Coal	1.14	C_1	0.57	288 - 344 °C	8.86
H_2O	4.06	C_2	0.45	344 - 454 °C	45.92
H_2S	0.94	C_3	0.47	454 °C - FBP	17.36
CO	0.18	C_4	0.76	Char	0.03
CO_2	0.69	IBP - 177 °C	5.57	Ash	3.45
NH_3	0.43	177 - 288 °C	9.1		

6.2.2 Product Recovery and Inline Hydrotreating

As shown in Figure 6.3, the product from the CTSL reactors is first sent to the hot HP separator. The vapor product from the hot HP separator, consisting of H_2-rich light gases, most of the naphtha (IBP-177°C) and a portion of the gas oil and solvent oil (177-454°C), is then sent to the inline hydrotreater for stabilization. The hydrotreated syncrude is sent to warm and cold HP flash vessels. The vapor product from the cold HP flash separation contains about 80-85% H_2 and therefore most of this H_2-rich stream is recycled back to the liquefaction reactor, while a portion of it is purged to maintain the P_{H_2} in liquefaction reactors. Liquid products from the warm and cold HP flash vessels are sent to the warm and cold LP flash vessels, respectively. The bottom product from the hot HP separator is de-pressurized and sent to the LP reactor liquid flash vessel

where small amount of N_2 is used for stripping. The top product from the LP reactor liquid flash vessel is sent to the warm LP flash vessel while the top product from the warm LP flash vessel is sent to the cold LP flash vessel. Liquid products from the warm and cold LP flash vessels, mainly IBP-454^{o}C syncrude, are sent to the atmospheric distillation column to be separated into light gases, light naphtha, heavy naphtha, gas oil, and liquefaction solvent. The bottom product from the LP reactor liquid flash vessel, a mixture of heavy oil and solid residues, is sent to the vacuum distillation column and the ROSE-SR unit for solid/liquid separation. The bottom product from the atmospheric distillation column, heavy vacuum gas oil (HVGO) from the vacuum distillation column and the deashed oil (DAO) from the ROSE-SR unit are sent to the recycle solvent tank for preparing coal/biomass slurry. Light naphtha, heavy naphtha, and gas oil from the atmospheric distillation column and light vacuum gas oil (LVGO) from the vacuum distillation column are sent to product upgrading units to produce gasoline, diesel and gas oil column bottom.

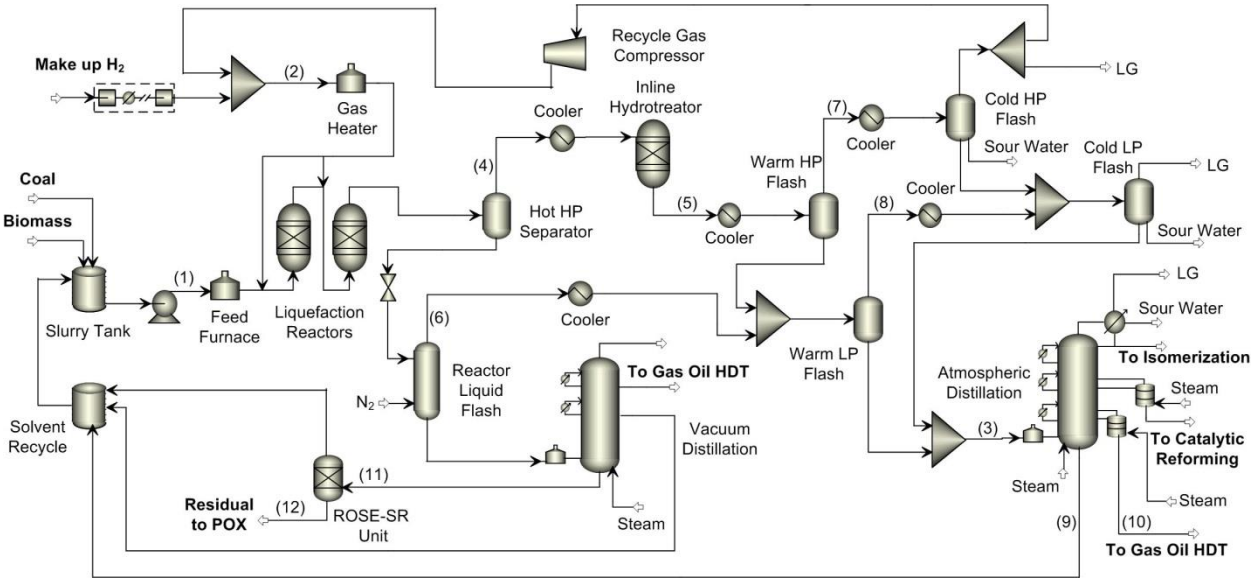

Figure 6.3 Plant configuration of the liquefaction and product recovery section

The plant configuration of the ROSE-SR unit can be found in Figure 6.4. The deashing solvent, which is considered to be mainly toluene in our study, is mixed with the hot stream from vacuum column bottom and then fed into the 1st stage settler with a solvent to vacuum column bottom weight ratio of 3. (Elliott, 1980; Givens and Kang, 1984) The heavy phase from the 1st stage settler, containing 10-20 wt% of the liquefaction liquids along with deashing solvent and

essentially all of the solids, is "let down" to the deashing solvent separator operated at atmospheric pressure. (Givens and Kang, 1984; Gearhart and Nelson, 1983) The light phase from the 1st stage settler, which contains 80-90 wt% of the liquefaction liquids and deashing solvent, is heated and sent to the 2nd stage settler. In the 2nd stage settler, most of the solvent is recovered under supercritical condition as the decrease in density and solubility of the supercritical fluid with the increasing temperature is exploited for solvent separation in the 2nd stage settler. The light phase from the 2nd stage settler, containing mainly supercritical solvent, is cooled in a heat exchanger and then sent to the HP solvent tank for preparing recycle solvent. The heavy phase from the 2nd stage, containing mainly deashed oil and small amount of deasing solvent, is "let down" to another deashing solvent separator. A small portion of the deashing solvent is recovered from the two deashing solvent separators, which is cooled and condensed and sent to the deashing solvent feed tank and then pumped to the HP solvent tank. The DAO is recycled to the liquefaction reactor serving as H-donor solvent and is hydrocracked to improve the performance of liquefaction unit, while the residues is partially oxidized to syngas and shifted to hydrogen in order to reduce the external hydrogen demand of the whole liquefaction system. More information about the POX unit is provided in Section 6.3.2.

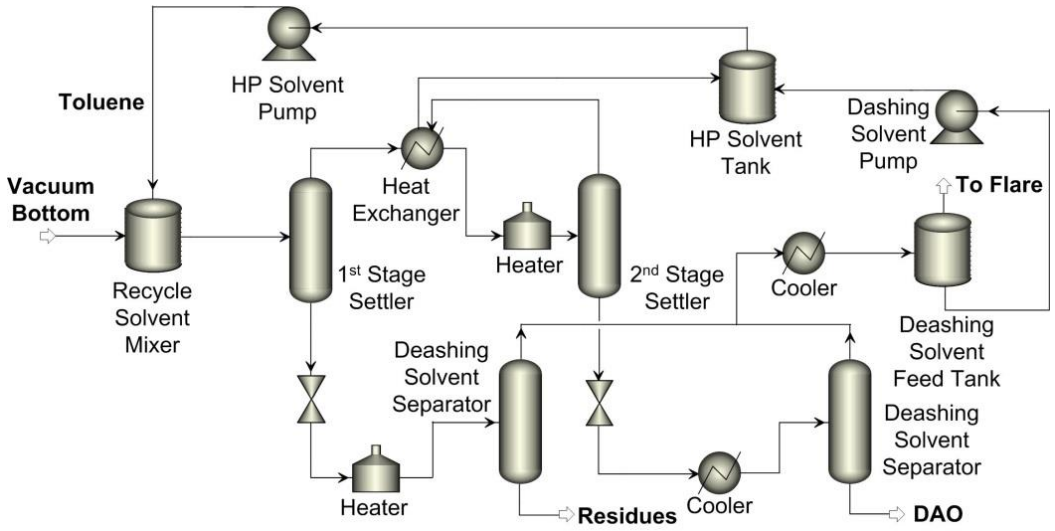

Figure 6.4 Plant configuration of the ROSE-SR unit

The approach to modeling the inline hydrotreater is the same as the liquefaction reactor. (Jiang and Bhattacharyya, 2015) With the elemental analysis of raw syncrude calculated from Section 2.2.1 and known elemental analysis of hydrotreated syncrude reported by HTI (Comolli et al.,

1995; Bechtel and Amoco, 1990), the H_2 consumption of the inline hydrotreater is estimated by atom balance, assuming O, N and S in the syncrude are rejected by producing H_2O, H_2S and NH_3. Table 6.6 lists the elemental analysis of the hydrotreated syncrude obtained from the open literature. (Comolli et al., 1995; Bechtel and Amoco, 1990) For the inline hydrotreater, the syncrude is specified as pseudo-components for the sake of applying atom balance, while syncrude is specified as petroleum assay for other equipment items in the product recovery unit for better estimate of vapor-liquid equilibrium (VLE). For each cut specified in Table 6.4 and Table 6.6, true boiling point distillation curves are available in the open literature. (Comolli et al., 1995; Behrendt et al., 2008) Peng-Robinson EOS is used as the thermodynamic model for the system. (Baldwin and Bills, 1978) Both atmospheric and vacuum distillation columns are modeled using PetroFrac block in Aspen Plus. The 1st stage and 2nd stage settlers in the ROSE-SR unit are modeled as component separators, using solids rejection efficiency and energy balance reported by HTI and assuming 88% and 80% solvent recovery in the light phases from the 1st and 2nd stage settlers, respectively. (Comolli et al., 1995; Fahim et al., 2010) Deashing solvent separators are modeled as flash separators. Table 6.7 and Table 6.8 summarize the operating conditions and design specifications of the key equipment items in the product recovery unit. Detailed specifications of the distillation columns can be found in the Appendix D.

Table 6.6 Elemental analysis of hydrotreated syncrude

wt%	C	H	O	N	S
IBP-177 °C	85.54	14.05	0.01	0.01	0.00
177-288 °C	87.90	12.55	0.01	0.01	0.01
288-344 °C	88.30	11.97	0.01	0.02	0.01
344-454 °C	88.10	11.28	0.01	0.03	0.05

Table 6.7 Operating conditions of the product recovery unit

Equipment	Pressure(1) (bar)	Temperature(2) (°C)	Equipment	Pressure(1) (bar)	Temperature(2) (°C)
Warm HP flash drum	172	232	Cold HP flash drum	170	40
LP reactor liquid flash drum	7.9	405	Warm LP flash drum	7.8	232
Atmospheric distillation tower	2.8	40/320	Cold LP flash drum	7.6	40
Vacuum distillation tower	0.1	65/305	1st stage settler	55	300
Deashing solvent separator	1.0	325/270	2nd stage settler	54.5	370

(1) Top pressure for all towers
(2) Top/bottom temperature for all towers

Table 6.8 Design specifications of the product recovery unit

Equipment	Manipulated variable	Target	Value
Hot HP separator	Operating temperature	ASTM D86 FBP of the vapor product	370 ^{o}C
LP reactor liquid flash drum	Stripping N_2 flowrate	Recovery of the 288-344^{o}C syncrude in vapor	50%
Atmospheric distillation tower	Bottom flow rate of heavy naphtha stripper	ASTM D86 95vol% temperature of light naphtha	107 ^{o}C
	Bottom flow rate of distillate stripper	ASTM D86 95vol% temperature of heavy naphtha	187 ^{o}C
	Bottom flow rate of main column	ASTM D86 95vol% temperature of gas oil	376 ^{o}C
Vacuum distillation tower	Duty of top pump-around	First stage temperature	65 ^{o}C
	Sidestream flow rate of LVGO	ASTM D86 95vol% temperature of LVGO	376 ^{o}C
	Sidestream flow rate of HVGO	Recovery of 890-975^{o}F crude in bottom	77.3%
ROSE-SR unit	Operating temperature of deashing solvent separators	Solvent recovery of deashing solvent separators	98%
	Heat duty of the heat exchanger between settlers	Inlet temperature of the first stage settler	300 ^{o}C

6.2.3 Heat Integration of the Liquefaction and Product Recovery Section

In the D-CBTL and D-CBGTL plants, the coal/biomass slurry and recycled H_2 need to be pre-heated to a high temperature before being fed to the CTSL reactors, which results considerable fuel consumption in the pre-heating furnaces. The product from the liquefaction reactor has to be cooled for separation. In the DCL baseline design reported by Bechtel/Amoco (Bechtel and Amoco, 1990), the recycle H_2 is pre-heated by exchanging heat with the hot stream from the top of the hot and warm HP flash vessels. Even though exchange of heat between cold slurry feed and downstream fluid is not considered by Bechtel/Amoco, it is considered to reduce the duty of the preheat furnaces in the SRC-I, SRC-II and NEDOL processes. (Rhodes. 1980; Morris and Foster, 1983; Thorogood, 1983; Shih, 1995) In this study, a global heat integration analysis is considered for increasing the overall thermal efficiency. Aspen Energy Analyzer is used to design and optimize the heat exchanger network. The minimum temperature approach is set to be 10 ^{o}C. The forbidden matches between streams are specified to avoid operability problem such as that caused by large differential pressure and unexpected leakage during operation.

6.2.4 Product Upgrading Units

One advantage of DCL process is that the products can be processed similar to traditional petroleum products without extensive renewal of current infrastructures. (Vasireddy et al., 2011) Compared with typical petroleum oils, the DCL syncrude obtained from the two-stage liquefaction of bituminous coals is usually low in boiling range, low in hydrogen and high in oxygen, low in heteroatom contents and high in contents of cyclic compounds, and mainly composed of paraffins, naphthenes, and aromatics. (Vasireddy et al., 2011; Mochida et al., 2014; Shinn, 1984) On the other hand, bio-liquids usually contain high amount of oxygenates, such as cyclic ketones, alkyl-phenols, methoxy-phenols, napthols, which can be converted to cyclohexane, alkyl-cyclohexane by hydrotreating. (Bechtel and Amoco, 1990; Behrendt et al., 2008; White et al., 1987) Despite these differences, the syncrude produced in the direct liquefaction plant with low biomass/coal ratio is very similar to petroleum and can be processed through petroleum refining technologies, where hydroprocessing is a major technology. (Zhou and Rao, 1992)

In this study, a significant portion of the aromatics and heteroatom in the low boiling range oil is converted in the inline hydrotreating unit. The hydrotreated naphtha cut from the atmospheric distillation column is low in sulfur and nitrogen and has an octane number of about 70, which is an excellent feed for gasoline production. (Comolli et al., 1995) Isomerization and catalytic reforming technologies are applied to increase the octane number of this naphtha cut. Because the entire gas oil cut from the CTSL reactors is not sent to the inline hydrotreater considering the operating flexibility and product quality (Zhou and Rao, 1992), the gas oil recovered from the atmospheric distillation column needs to be sent to the gas oil hydrotreating unit for further upgrading. In this study, the yields of the upgrading units are obtained from correlations due to the limited information on the detailed feed composition. Utility consumptions in the isomerization and catalytic reforming units are estimated based on the plant throughput using the correlations available from Bechtel Corp. (Bechtel, 1993), while detailed models of the key equipment items are developed to estimate the utility consumption in the gas oil hydrotreating unit, as shown in Figure 6.5.

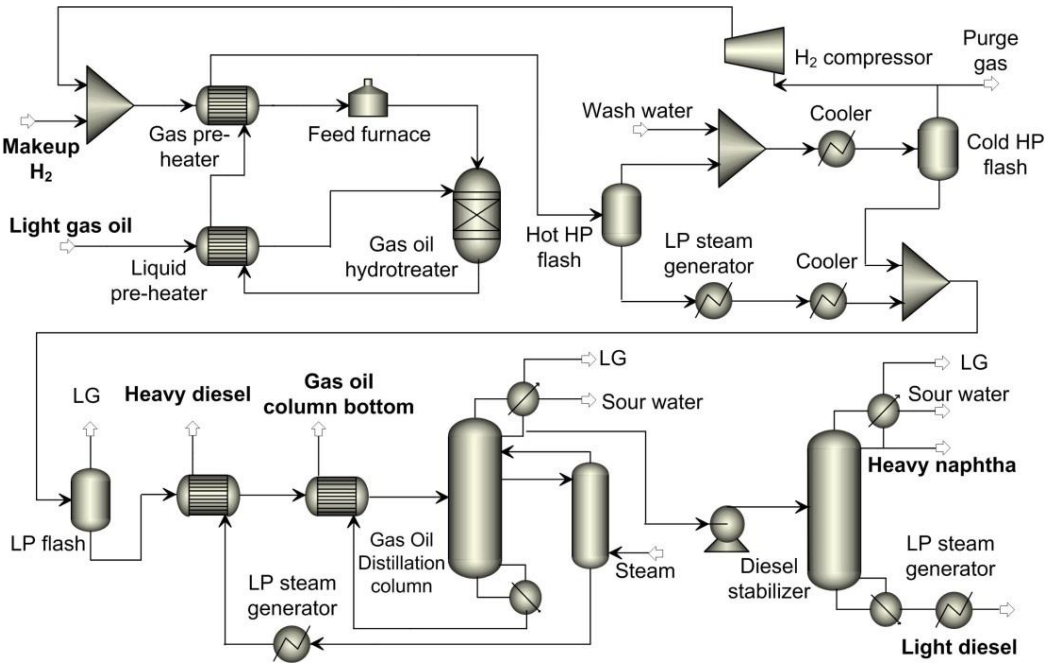

Figure 6.5 Plant configuration of the gas oil hydrotreating unit

In the isomerization unit, n-paraffins in the light straight run naphtha with low octane number are transformed on Pt catalyst into branched chains with the same carbon number but high octane number. The typical yield of isomerization unit used in this study is 0.35 wt% C_3, 2.39 wt% C_4 and 97.26 wt% C_{5+} with a RON of 83. (Fahim et al., 2010) The H_2/oil ratio in the feed is specified to be 0.14 wt% as reported by Bechtel Corp. (Bechtel, 1993) Our study only considers low biomass/coal mix ratio, and most of the oxygenates is hydrotreated and converted to paraffins and naphthenes in the hydrotreater unit. Hence, the distribution of components in the hydrotreated naphtha from biomass/coal co-liquefaction is assumed to be 15 vol% paraffins, 65 vol% naphthenes and 20 vol% aromatics, which are similar to that of DCL naphtha. (Vasireddy et al., 2011; Mochida et al., 2014; Bechtel and Amoco, 1990) A yield model, shown in Eq. (6.4) and (6.5), is used in this study to estimate the yield of H_2 and C_{5+} reformate from the feed composition $(N+2A)_F$ and severity of catalytic reforming (RON_R), where N, A, and RON_R denote naphthenes (vol%), aromatics (vol%) and reformate RON, respectively. (Fahim et al., 2010; Bechtel, 1993; Gary and Handwerk, 2001) Eq. (6.6) gives the relation between RON_R and aromatic vol% in the reformate (A_R vol%). Table 6.9 shows this model can provide a reasonable estimation of DCL liquid catalytic reforming process. (Smith et al., 1982) The MON of

reformate can be estimated by Eq. (6.7). (Gary and Handwerk, 2001; Albahri et al., 2002; Jenkins, 1968)

$$C_{5+}\ (vol\%) = 142.7912 - 0.77033 \times RON_R + 0.219122 \times (N + 2A)_F \quad (6.4)$$

$$H_2\ (wt\%) = -12.1641 + 0.06134 \times C_{5+}\ (vol\%) + 0.099482 \times RON_R \quad (6.5)$$

$$A_R(vol\%) = 1.6857 \times RON_R - 92.994 \quad (6.6)$$

$$MON_R = 22.5 + 0.83RON_R - 20.0SG \quad (6.7)$$

Table 6.9 Validation of the yield model of the catalytic reforming unit

Feed composition		Cases	RON_R = 94.2		RON_R = 97.7	
			Experimental	Model	Experimental	Model
N (vol%)	64.4	C_{5+} (vol%)	92.5	91.4	91.1	88.7
A (vol%)	16.0	H_2 (wt%)	2.50	2.81	3.00	3.00
		A_R (vol%)	65.8	65.8	71.7	71.7

The main purpose of the inline hydrotreater is to stabilize the liquefaction product, while the diesel cut from the inline hydrotreater does not necessarily satisfy the diesel specification. (Wu et al., 2015) Hence, the gas oil hydrotreating unit is required to produce on-spec diesel. In the gas oil hydrotreating unit, the raw gas oil is pre-heated by the hot hydrotreated gas oil and then sent to hydrotreater with heated H_2 stream. H_2-rich stream is recovered from the HP flash drum and recycled back to the reactor. The liquid from the LP flash vessel is sent to a distillation column followed by a diesel stabilizer to separate the hydrotreated product into light gas, heavy naphtha, diesel (177-343^{o}C), and gas oil column bottom (343-454^{o}C). The approach to modeling the gas oil hydrotreating reactor is the same as the inline hydrotreating reactor as described in Section 6.2.2. The gas oil hydrotreater is operated at 180 bar and 350 ^{o}C with a pressure drop of 7 bar, a temperature increase of 83 ^{o}C, P_{H_2} of 124 bar, and a liquid hourly space velocity of 1 h^{-1}. It can be noted that these specifications are similar to that reported by Bechtel/Amoco. (Bechtel and Amoco, 1990) PetroFrac model in Aspen Plus is used to simulate the distillation column and the diesel stabilizer. Peng-Robinson EOS is used as the thermodynamic model. A 'design spec' in Aspen Plus is set up to satisfy the ASTM D86 90 vol% specification of diesel (ASTM D975) by manipulating the bottom flowrate of the gas oil distillation column.

6.3 Hydrogen Production

Significant amount of H_2 is required in the D-CBTL and D-CBGTL plants. The first step to H_2 production is to generate the syngas from fuels, such as natural gas, shale gas, coal, biomass and liquefaction residues. Then the raw syngas is sent to a high temperature shift (HTS) reactor and a low temperature shift (LTS) reactor, where H_2 concentration in the syngas is increased by the water gas shift reaction. In order to reduce H_2 production from external fuels, liquefaction residues from the ROSE-SR unit is used to produce syngas in the POX unit by gasification. Additional H_2 is produced by shale gas steam reforming in the D-CBGTL-CCS and D-CBGTL-VT processes, or by coal/biomass/residue co-gasification (CG) in the D-CBTL-CCS and D-CBTL-VT processes. Throughput of the SMR or CG unit is determined by the overall hydrogen balance, as shown in Eq. (6.1).

6.3.1 Shale Gas Steam Reforming

In the SMR unit, as shown in Figure 6.6, the shale gas is compressed, heated by the steam reformer outlet stream and sent to an adiabatic pre-reformer, where heavier hydrocarbons are converted to methane and syngas through Reactions (6.8) to (6.10). The outlet stream of the pre-reformer is reheated by exchanging heat with the stream reformer outlet stream and then sent to the steam reformer, where most of the methane is converted to syngas by Reactions (6.9) to (6.11). The heat required by the highly endothermic in the steam reformer is produced in the reformer furnace by burning fuel gas taken from the plant fuel gas header. The product from the stream reformer is cooled and sent to HTS and LTS reactors. The syngas from the shift reactors is cooled by generating HP, IP, and LP steams. The syngas from the LP steam generator is sent to a condenser to remove most of the water. The hot flue gas from the reformer furnace is sent to a series of heat exchangers to generate super-heated HP steam used for steam reforming. In this study, the pre-reformer and steam reformer are modeled as equilibrium reactors. (Molburg and Doctor, 2003) The HTS and LTS reactors are modeled as PFRs with kinetics obtained from the open literature. (Bhattacharyya et al., 2011) The reformer furnace is modeled as 'RStoic' reactor in Aspen Plus with specified combustion reactions. The Peng-Robinson EOS is used as the thermodynamic model of the syngas side, while IAPWS-95 is used for the steam side. Operating conditions of all reactors and heat exchangers can be found in Table 6.10.

$$C_nH_m + nH_2O \rightarrow nCO + \left(n + \frac{m}{2}\right)H_2 \ - Q \tag{6.8}$$

$$CO + 3H_2 \leftrightarrow CH_4 + H_2O + Q \tag{6.9}$$

$$CO + H_2O \leftrightarrow CO_2 + H_2 + Q \tag{6.10}$$

$$CH_4 + 2H_2O \leftrightarrow CO_2 + 4H_2 - Q \tag{6.11}$$

Table 6.10 Operating conditions of the shale gas SMR unit

Flowsheet element	Parameter	Value
Shale gas feed	Temperature/pressure	20 °C/20 bar
Compressor	Pressure	30 bar
Steam feed	Temperature/pressure	510 °C/30 bar
Preheaters	Cold stream outlet temperature	510 °C/650 °C
Adiabatic pre-reformer	Pressure drop	1.7 bar
Steam reformer	Temperature/pressure drop	815 °C/1.7 bar
HP/IP/LP steam evaporator	Hot stream outlet temperature	350 °C/215 °C/143 °C
Cooler	Hot stream outlet temperature	40 °C
Feed water heater/economizer	Cold stream outlet temperature	120 °C/227 °C

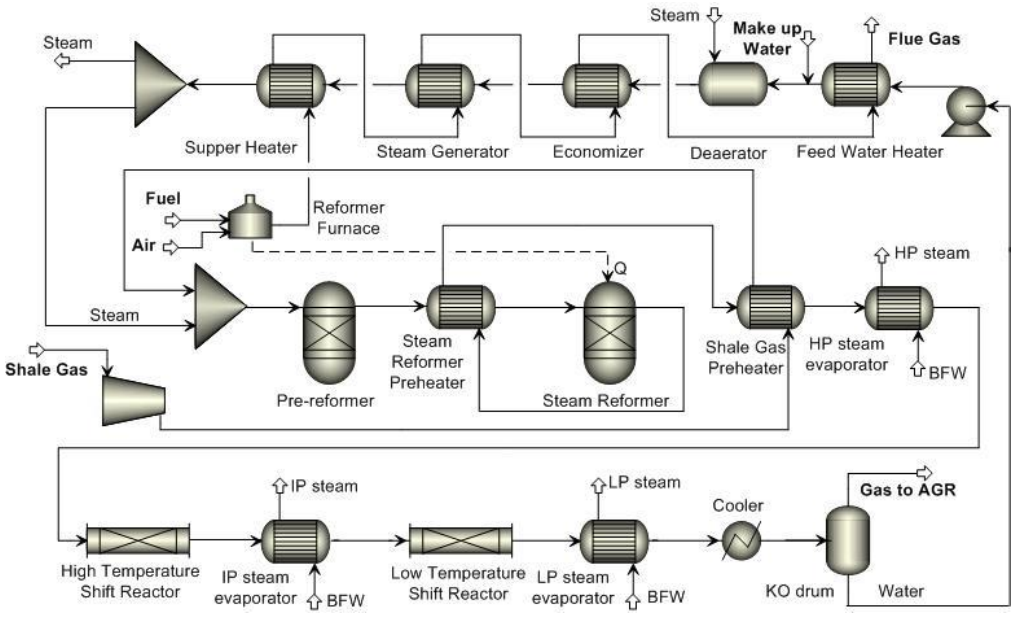

Figure 6.6 Plant configuration of the shale gas SMR unit

6.3.2 Residue Partial Oxidation and Coal/Biomass/Residue Co-Gasification

In the D-CBGTL-CCS and D-CBGTL-VT processes, the hot liquefaction residue from the ROSE-SR unit is gasified in the POX unit as shown in Figure 6.7. The residue containing mainly 510 ^{o}C plus solid, ash and unconverted coal/biomass is sent to an entrained flow gasifier with O_2 obtained from the ASU and steam obtained from the HRSG section. In the D-CBTL-CCS and D-CBTL-VT processes, the liquefaction residue is grinded and mixed with pre-processed coal/biomass and slurry water before being fed to the entrained-flow gasifier. In all cases, the raw syngas from the gasifier is cooled and then sent to the HTS and LTS reactors to convert CO into H_2 similar to the SMR unit. Flow rate of the shift steam to the HTS reactor is manipulated to achieve 95% of overall syngas CO conversion in the two stage water gas shift unit.

Here the gasifier is modeled as an equilibrium reactor, while the HTS and LTS reactors are modeled as PFR reactors. More details about the WGS reactors and co-gasifier can be found in Chapter 3. (Jiang and Bhattacharyya, 2014) The entrained-flow gasifier fed only with the liquefaction residue is operated at 56 bar and 1315 ^{o}C with a steam to residue ratio of 0.4 and a carbon conversion of 99% similar to the data available in the open literature. (Debyshire et al., 1984; Texaco, 1984; Robin, 1976; 1977; Penner, 1980; Gao, 2014) The amount of oxygen fed into the gasifier is manipulated to satisfy the energy balance. Simulation results from the residue gasification show that the H_2 yield of the residue POX unit is about 10.2 wt% of the liquefaction residue. (Comolli et al., 1995; Texaco, 1984)

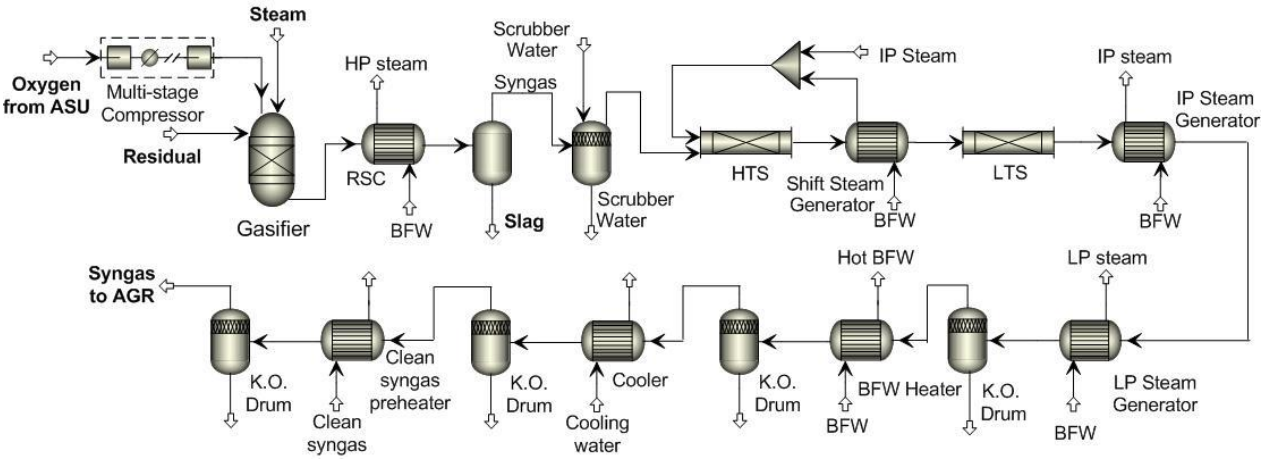

Figure 6.7 Plant configuration of the POX unit

6.4 Acid Gas Removal, H_2 Recovery, and CO_2 Compression Units

The fuel gas released from the liquefaction, product recovery, and upgrading units contains H_2S, which needs to be removed before being utilized in process furnaces or gas turbines. MDEA is considered to be the desired solvent for removing H_2S from fuel gas in presence of CO_2. (Wu et al., 2015) The general configuration of a chemical absorption process is shown in Figure 6.8. The absorber is operated at 38 ^oC and 20 bar. (Wu et al., 2015) The 'RadFrac' model in Aspen Plus with rate-based calculations is used to simulate the absorber and stripper using the kinetics and thermal model available in the open literature. (Austgen et al., 1991; Rinker et al., 1997)

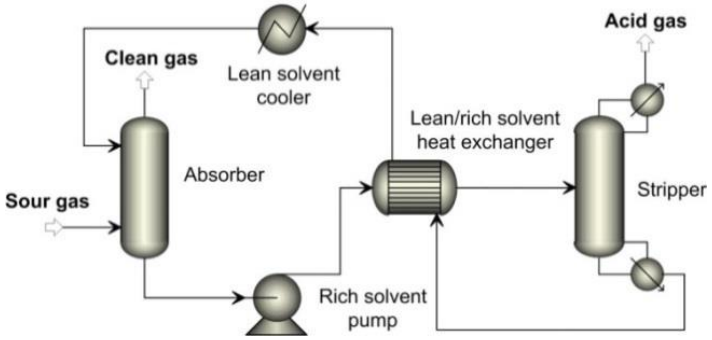

Figure 6.8 Schematic of the amine-based chemical absorption process

For all four process configurations, the gas oil column bottom and fuel gas produced in the process are sent to either process furnaces or a gas turbine, which eventually get converted to CO_2, as discussed in Section 6.1. The major CO_2 emission of the system is from H_2 production units, process furnaces, and the gas turbine. The H_2-rich syngas stream from the POX/CG unit contains not only a significant amount of CO_2, but also a small amount of H_2S. In order to recover pure H_2, those streams are sent to the AGR unit to selectively remove CO_2 and H_2S, no matter if CCS is considered or not. The removed CO_2 is vented or sent to the CO_2 compression unit, depending on whether CCS is considered and the targeted extent of CCS. If high extent of CCS is considered, additional CO_2 needs to be captured from the gas turbine flue gas using post-combustion CO_2 capture technologies, and the amount is determined by carbon balance as shown in Eq. (3). In this study, physical absorption is considered for streams with high P_{CO_2}, while chemical absorption is considered for steams with intermediate or low P_{CO_2}.

For the physical absorption process, the acid gas partial pressure is the main driving force for absorption and has a significant effect on the process efficiency. (Jiang and Bhattacharyya, 2014) For the chemical absorption process, the acid gas partial pressure does not have much effect. For all four configurations, the dual-stage Selexol technology is applied to selectively remove H_2S and the majority of CO_2 from the HP syngas obtained from the POX/CG unit. In the D-CBGTL-CCS and D-CBGTL-VT processes, the extent of CO_2 capture is decided to make the P_{CO_2} of the clean syngas from the HP CO_2 absorber in the Selexol unit to be the same as P_{CO_2} of the IP syngas from the shale gas SMR unit. Then the syngas from the HP CO_2 absorber is mixed with the syngas from the SMR unit, and sent to an IP CO_2 absorber unit using chemical solvent to further remove CO_2. If high extent of CCS is considered, the amount of CO_2 removed in the IP CO_2 absorber unit is determined such that the treated gas P_{CO_2} is the same as the flue gas P_{CO_2}, and this treated gas is mixed with the gas turbine flue gas and sent to a LP CO_2 absorber using chemical solvent to achieve the targeted extent of CCS. In the D-CBTL-CCS and D-CBTL-VT processes, the dual-stage Selexol technology is considered to treat the raw syngas obtained from the POX/CG unit, while an additional chemical absorption unit is required to treat the flue gas obtained from the D-CBTL-CCS process.

The plant configuration of the dual-stage Selexol unit can be found in our previous publication. (Bhattacharyya et al., 2011; Jiang and Bhattacharyya, 2014) The configuration of the chemical absorption unit is similar to Figure 6.8, where multiple absorption columns operating at different pressure is considered, since the syngas and flue gas are available at different pressures and cannot be mixed. Rich solvents from different absorbers are mixed first, and then sent to the lean/rich exchanger and then to the strippers for solvent regeneration. Absorbers in the Selexol unit are modeled by the 'RadFrac' block with equilibrium-stage modeling using the PC-SAFT EOS. MDEA/PZ and MEA are the two chemical solvents considered in this study. All absorbers and strippers in the chemical absorption unit are modeled and sized by the 'RadFrac' block with rate-based modeling using ELECNRTL EOS. Parallel trains are considered if the column diameter exceeds 10 meter. The modeling approach and reaction kinetics of the MDEA/PZ/CO_2 system and the MEA/CO_2 system are described in our previous publications and Chapter 3. (Jiang and Bhattacharyya, 2014)

Removed H_2S stream from the Selexol unit is mixed with the H_2S stream from the MDEA unit and then sent to the Claus unit for conversion to elemental sulfur. The extent of H_2S removal is computed by comparing the gas turbine sulfur tolerance and the SO_2 emission regulation (40 CFR 60.42b) and selecting the lower value. CO_2-rich streams at different pressure levels are vented or sent to different stages in a split-shaft multistage CO_2 compressor, determined by the targeted extent of CCS. The clean syngas from the AGR unit is sent to the PSA unit for producing pure H_2. The number of beds required for PSA units has been approximated by using the study from Bechtel. (Bechtel, 1993) Plant configuration and modeling approach of the Claus and CO_2 compression units can be found in our previous publications and Chapter 3. (Bhattacharyya et al., 2011; Jiang and Bhattacharyya, 2014) The PSA unit is modeled as a component separator in Aspen Plus while designing it using the approach detailed in Chapter 3.

6.5 Combined Cycle Power Island

Most of the flue gas and waste heat produced in the product recovery and upgrading unit, the POX/CG unit and the SMR unit are utilized in the combined cycle power island. The steam generator in the combined cycle power island operates at three pressure levels and not only produces steam to generate electricity but also provides IP and LP steams needed in the POX/CG, product upgrading, and AGR units, as shown in Table 6.11. The modeling approach of the combined cycle plant and its pressure levels is the same as Chapter 3. (Jiang and Bhattacharyya, 2015; Bhattacharyya et al., 2011)

Table 6.11 Configuration of the HRSG section and steam header

Steams	Pressure (bar)	Temperature (ºC)	From	To
HP steam to ST	114	510	POX, GT, SMR	ST HP section
IP steam to ST	25	510	POX, SMR, HCR (through reheater)	ST IP section
LP steam to ST	4	140	GTFG, HCR, SMR POX, HCU	ST LP section
HP steam to header	57		ST HP section	POX, HCU
IP steam to header	9		ST IP section	AGR
LP steam to header	4		ST LP section	AGR, HCU

6.6 Results and Discussion

For the base case conditions, the biomass/coal weight ratio, the plant capacity and the extent of CCS are set to be 8/92 (dry basis), 10000 bbl/day, and 90% (for D-CBGTL-CCS and D-CBTL-CCS). Here, the extent of CCS is defined by Eq. (6.3). The following studies are conducted for analyzing the feasibility of applying CCS and introducing shale gas and biomass into the traditional DCL processes. First, heat integration is applied to reduce the utility consumption, and the AGR unit is designed depending on the carbon balance. Then the material and energy balance of the D-CBTL and D-CBGTL processes is obtained based on the process model of the entire system and compared with the data reported in the open literature for validation. Based on the validated process model, sensitivity studies are conducted by changing the biomass/coal ratio, CCS solvent and the extent of CCS with different hydrogen sources. Finally, the D-CBTL and D-CBGTL processes are compared with the I-CBTL processes.

6.6.1 Heat Integration of the Liquefaction and Product Recovery Section

Temperature changes in key streams in the liquefaction and product recovery section are shown in Figure 6.9, where the cold streams are shown as bars filled with upward diagonals and the hot streams are shown as bars filled with downward diagonals. 25 heat exchangers, steam generators, heaters and coolers are designed by Aspen Energy Analyzer using pinch analysis. Table 6.12 lists the forbidden and matched hot and cold streams in the heat exchanger network design. Stream numbers mentioned in Figure 6.9 and Table 6.12 are shown in Figure 6.3. With the new design, the coal/biomass slurry is heated to about 350 ^{o}C by hot liquefaction product before entering the preheat furnace, while the heat duty of the preheat furnace is reduced by about 52%. These results are similar to the NEDO's DCL experience, where the coal slurry is preheated to 340 ^{o}C in the heat exchangers and the heat duty of the furnace is reduced by about 60%. (NEDO, 2006; IEA, 2009)

Table 6.12 Forbidden and matched hot and cold streams in the heat integration

	4	5	6	7	8	9	10
1	✓	✓	✓	✗	✗	✓	
2			✓	✓	✓	✗	✗
3	✗	✓	✗				✓

✗ - the hot and cold streams are not allowed to exchange heat

✓ - recommended match of hot and cold streams by Aspen Energy Analyzer

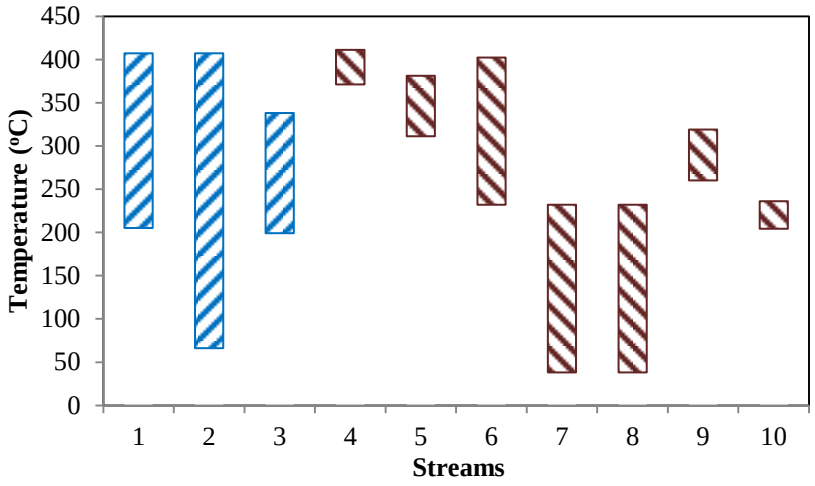

Figure 6.9 Temperature chart of the liquefaction and product recovery section

6.6.2 Carbon Balance and Design of the CO_2 Removal System

Based on the models developed for the liquefaction and product upgrading section and the syngas production section, carbon balances of the D-CBTL and D-CBGTL plants are computed and shown in Table 6.13. In the D-CBGTL processes, 53.9 % of the carbon in the feedstock is converted to gasoline and diesel. In the D-CBTL processes, it is only 43.5 % because the H/C ratio in coal and biomass is less than that in shale gas or natural gas, resulting in less efficiency in the H_2 plant. In order to achieve 90% carbon capture (considered to be high level CCS in this study), another 36.1 % of carbon in the feedstock (78.3 % of CO_2 generated) needs to be captured by the CO_2 capture process in the D-CBGTL-CCS process, and another 46.5 % of carbon in the feedstock (82.3 % of CO_2 generated) needs to be captured in the D-CBTL-CCS process. Based on the design procedure described in Section 6.4, Table 6.14 through Table 6.16 list the main CO_2 sources ordered by P_{CO_2} and flowrate, preliminary selection of absorption technologies, operating conditions and targeted extent of CO_2 removal for each stream.

Table 6.13 Carbon balance of the direct liquefaction plants[(1)]

Carbon in (%)	D-CBGTL	D-CBTL	Carbon out (w/o utility, %)	D-CBGTL	D-CBTL	Carbon out (w/ utility, %)	D-CBGTL	D-CBTL
Coal	77.4	94.6	Gasoline	11.4	9.4	Fuel	53.9	43.5

Biomass	4.6	5.4	Diesel	41.2	34.1	POX/CG	10.7	38.8
Shale gas	18.0		Fuel oil	7.0	5.8	SMR	19.2	
			Fuel gas	10.5	11.9	Gas turbine	9.5	12.1
			H_2 plants	29.9	38.8	Others	6.7	5.6

(1) Fuel gas and fuel oil produced from gas oil column bottom are treated as utility in the case with (w/) utility, but not in the case without (w/o) utility

Table 6.14 CO_2 emission and sources in the D-CBGTL processes

Source	Carbon (%)	CO_2 (mol%)	P_{CO_2} (bar)	CO_2 removal	SO_2 removal	Technology	CO_2 removal (%)
POX (syngas)	11	36	18.5	Yes	Yes	Selexol, Amine	83.6 98.3
SMR (syngas)	12	19	3.9	Yes	No	Amine	98.3
SMR furnace (flue gas)	7	7	0.07	Yes	No	Amine	86.3
Gas turbine (flue gas)	9	3	0.03	Yes(1)	No	Amine	66.5
Others (flue gas)	8			No	No	N/A	

(1) Not considered in the D-CBGTL-VT processes

Table 6.15 CO_2 emission and sources in the D-CBTL processes

Source	Carbon (%)	CO_2 (mol%)	P_{CO_2} (bar)	CO_2 removal	SO_2 removal	Technology	CO_2 removal (%)
CG (syngas)	39	40	21.6	Yes	Yes	Selexol	95.0
Gas turbine (flue gas)	12	3	0.03	Yes(1)	No	Amine	69.8
Others (flue gas)	6			No	No	N/A	

(1) Not considered in the D-CBTL-VT processes

Table 6.16 Configurations and operating conditions of the AGR units

Column	Pressure (bar)	Sour gas from	Clean gas to
HP CO_2 absorber	50.5	POX/CG (syngas)	H_2 recovery
IP absorber(1)	20.7	SMR (syngas) and/or Selexol CO_2 absorber (syngas)	H_2 recovery
LP absorber(2)	1.0	Gas turbine (flue gas) and/or SMR furnace (flue gas)	Stack

(1) Not considered in the D-CBTL processes

(2) Not considered in the D-CBGTL processes

Based on the process model developed in Aspen Plus, the utility consumption and cost of the CO_2 removal and compression units are calculated and shown in Table 6.17 for all four

configurations with a plant capacity of 10000 bbl/day. For the D-CBGTL-CCS (base case) process, two different amine solvent are considered- MEA and MDEA/PZ. Utility consumptions in the Selexol unit, the amine unit and the CO_2 compression unit are similar to the data available in the open literature. (Jiang and Bhattacharyya, 2014; NETL, 2010; Liu et al., 2011; Bhattacharyya et al., 2011) The reboiler duty of the solvent stripper is 3590 kJ/kg if MEA is used as a solvent in the D-CBGTL-CCS process. This duty can be reduced by 14% if using MDEA/PZ as the solvent. (Jiang and Bhattacharyya, 2014) Hence, MDEA/PZ is selected for removing CO_2 from IP and LP CO_2-contianing streams in all case studies and sensitivity studies. Table 6.17 also indicates that utility costs for the D-CBTL-CCS and D-CBGTL-CCS processes are similar. The CCS utility cost for the D-CBTL-VT process is lower than the D-CBGTL-VT process, even though more CO_2 needs to be captured in the D-CBTL-VT process due to the lower carbon efficiency. The reason is that P_{CO_2} of most CO_2-containing streams to be sent to the AGR unit is higher in the D-CBTL processes than that in the D-CBGTL processes, as shown in Table 6.14 and 6.15. As a result, in the D-CBTL processes, most of the CO_2 is captured by the Selexol unit instead of the amine unit resulting in lesser utility penalty for CO_2 capture. The study shows that the CCS technology plays a key role in the overall utility consumption in these plants. While this paper considers only solvent-based technologies due to their maturity, novel technologies for CO_2 capture such as those based on solid sorbents or membranes can be potentially evaluated as alternatives for reducing the penalty for CO_2 capture.

Table 6.17 Utility consumptions and costs for the CCS units

Process	D-CBGTL-CCS	D-CBGTL-CCS	D-CBGTL-VT	D-CBTL-CCS	D-CBTL-VT
CO_2 captured (kmol/hr)	2660	2660	1733	4245	3367
Amine solvent	MEA	MDEA/PZ	MDEA/PZ	MDEA/PZ	N/A
Utility consumptions (electricity (MW)/IP steam (GJ/hr)/LP steam (GJ/hr)/cooling water (GJ/hr))					
Selexol unit	1.98/3/0/57	1.98/3/0/57	1.98/3/0/57	8.32/29/0/255	8.32/29/0/255
Amine unit[(1)]	0.94/0/309/389	0.92/0/297/377	0.34/0/78/77	0.46/0/229/343	0/0/0/0
Compression	9.59/0/0/48	9.59/0/0/48	0/0/0/0	11.58/0/0/61	0/0/0/0
Total	12.5/3/309/494	12.5/3/297/482	2.3/3/78/134	20.4/29/229/659	8.3/29/0/255
Cost[(2)] ($/h)	5077	4913	1265	4919	993

(1) If high extent of CCS is considered, flue gas needs to be cooled before sending it to the amine system. The extra cooler is included in the amine unit.
(2) Costs of electricity, IP steam, LP steam and cooling water are assumed to be $16.8, $14.19, $13.28 and $0.354 per GJ. (Turton et al., 2012)

6.6.3 Material and Energy Balance and Model Validation

Using the steady-state process model developed in Aspen Plus and the design of the AGR unit shown in Section 6.6.2, material and energy balances are computed for all four configurations. For the base case, D-CBGTL-CCS with a capacity of 10000 bbl/day and a biomass/coal weight ratio of 8/92, the flow rate of the key species in the main streams numbered in Figure 6.1 can be found in Table 6.18. Due to the limited information on applications of CCS technologies for DCL processes, simulation results are only validated for the D-CBGTL-VT and D-CBTL-VT processes. The utility consumption in CCS related facilities is validated separately in Section 6.6.2. It is generally accepted that the DCL processes without CCS usually have a thermal efficiency between 60% and 70%. (Wu et al., 2015) As shown in Table 6.19, results from our study are in-between the values reported by HTI (73.4%) and Shenhua (59.8%) and seem reasonable. (Williams and Larson, 2003; Comolli et al., 1995; Bechtel and Amoco, 1990; Bauman and Maa, 2014) The differences are mainly due to different types of coal, sources of hydrogen and process utilities. The carbon and hydrogen content varies with the types of coal, which leads to different hydrogen requirement for liquefaction. Because of the different H/C ratio in coal and shale gas, the hydrogen production efficiency is very different between the coal gasification process and shale gas steam reforming process. Due to the difference in heating value and conversion efficiency of different type of energy sources, types of power and fuel source also affect the overall thermal efficiency of the direct liquefaction processes. Detailed material and energy balances for all four configurations can be found in Table 6.20, which indicates that the thermal efficiency of the direct liquefaction plant can be significantly increased by producing hydrogen from shale gas. Application of CCS will reduce the thermal efficiency by 2.2% if H_2 is produced from steam reforming or 2.1% if H_2 is produced by gasification, which is similar because the penalty of CCS is similar as discussed in Section 6.6.2. It can be concluded from Table 6.20 that utilization of shale gas or natural gas in the DCL process can increase the competitiveness of this technology, if shale gas or natural gas is available at lower price within reasonable transportation distance.

Table 6.18 Stream summary of the small scale D-CBGTL-CCS process

Stream	1	2	3	4	5	6	7	8	9	10	11
Temperature (^oC)	27	21	35	432	267	414	93	302	35	36	36
Pressure (bar)	1	20	22	208	1	208	3	55	55	3	3
Flow rate (kg/s)											
Coal	27.81			1.03				1.03			
Biomass	2.59										
H_2O			0.06	3.18		2.72			0.01		
CO_2		0.14	11.55	1.88		1.77			9.89		
CO			0.12	0.63		0.61			0.30		
H_2			2.04	2.52		2.43			0.74	2.41	0.14
H_2S				2.01		1.85			0.22		
NH_3				0.88		0.81					
CH_4		4.73	1.67	1.89		1.81			0.02		
C_2-C_4		1.09		3.50		3.23					
C_5-177 ^oC				5.15		4.13	3.56				
177-288 ^oC				8.24		4.89	6.65				
288-344 ^oC				8.05	2.59	3.43	6.29				
344-454 ^oC				41.37	40.62	10.81	1.11				
454 ^oC +				15.63	13.57	1.09		2.53			
Ash				3.04	0.03			2.88			

Table 6.19 Comparison between the simulation results and data in the open literature

Process	D-CBGTL-VT	D-CBTL-VT	HTI design(1)	Modified HTI design(2)	Bechtel/ Amoco design(3)	Modified Bechtel/ Amoco design	Shenhua design
Reference			Comolli et al., 1995	Comolli et al., 1995	Williams and Larson, 2003	Williams and Larson, 2003	Bauman and Maa, 2014
Biomass (wt %)	8	8	0	0	0	0	0
Hydrogen source	Shale gas	Coal/ biomass	Natural gas	Coal	Coal	Coal	Coal
Power and fuel source	Fuel gas(4)	Fuel gas(4)	N/A	N/A	Natural gas	Coal	Coal
Efficiency (HHV, %)	66.5	62.1	73.4	70.9	61.6	59.0	59.8

(1) In the original HTI design, utility consumptions are not considered during the efficiency calculation.
(2) It is assumed that the effective thermal efficiency is 57.5% on HHV basis for producing H_2 from coal gasification. (Williams and Larson, 2003)
(3) Estimations are based on the HTI technology for liquefaction, while utility consumptions are considered.
(4) Fuel gas is generated insider plant mainly from the liquefaction unit and product upgrading units.

Table 6.20 Material and energy balances of the direct liquefaction plant (HHV basis[(1)])

Process	D-CBGTL-CCS	D-CBGTL-VT	D-CBTL-CCS	D-CBTL-VT
Energy inputs				
Coal, tonne/hr (GJ/hr)	100.1 (2962)	100.1 (2962)	151.4 (4479)	151.4 (4479)
Biomass, tonne/hr (GJ/hr)	9.3 (163)	9.3 (163)	14.1 (247)	14.1 (247)
Shale gas, tonne/hr (GJ/hr)	21.6 (1105)	21.6 (1105)	N/A	N/A
Energy outputs				
Gasoline, bbl/day (GJ/hr)	2443 (595)	2443 (595)	2443 (595)	2443 (595)
Diesel, bbl/day (GJ/hr)	7557 (1936)	7557 (1936)	7557 (1936)	7557 (1936)
Net power (MW)	52.4	77.8	84.5	111.9
Thermal efficiency (%)	64.3	66.5	60.0	62.1

(1) HHVs of gasoline and diesel are set to be 5.84 and 6.15 GJ/bbl. (Williams and Larson, 2003)

6.6.4 Effect of the Biomass to Coal Mix Ratio

In this study, three biomass/coal weight ratios are investigated. The upper bound of biomass/coal weight ratio is set to be 20/80, because the capacity of BTL or CBTL plants is constrained due to the high transportation cost, low energy density and limited long-term availability of biomass. (Wang and McNeel, 2009; Hartley, 2014) Table 6.21 and Table 6.22 show that the thermal efficiency and carbon efficiency of the direct liquefaction plant keep increasing for both D-CBGTL-CCS and D-CBTL-CCS processes, as more biomass is added to the liquefaction reactor. Even though H_2 consumption in the hydrotreating processes increases with the biomass/coal ratio due to the higher oxygenates contents, overall H_2 consumption in the direct liquefaction plant decreases with the biomass/coal ratio, because the higher H/C ratio in the biomass reduces the H_2 consumption in the main liquefaction reactor more significantly. As a consequence, an increase in the biomass/coal ratio decreases the amount of shale gas or additional coal and biomass required for H_2 production, leading to an increase in the overall carbon efficiency and a decrease in the amount of CO_2 needed to be captured to achieve overall 90% carbon capture. With less CO_2 captured, less steam and electricity are consumed by the CCS facilities. Hence, the overall thermal efficiency of the direct liquefaction plants is increasing with the biomass/coal ratio for both D-CBGTL-CCS and D-CBTL-CCS processes. Even though the simulation results shows that adding biomass to the traditional DCL process can increasing the process efficiency and reduce CO_2 emission, it should be noted that the overall cost of biomass and the capital cost of the pre-processing unit is usually higher than coal due to the lower energy density. (Jiang and

Bhattacharyya, 2016) To decide whether to introduce biomass and what biomass/coal ratio to use, other than efficiency calculation shown here, additional studies such as techno-economic analysis, life-cycle analysis and biomass logistic analysis are required. (Hartley, 2014)

Table 6.21 Effects of the coal biomass mix ratio (D-CBGTL-CCS, 10k bbl/day)

Biomass/coal (wt/wt)	8/92	15/85	20/80
Coal (tonne/hr)	100.1	90.1	84.2
Biomass (tonne/hr)	9.3	17.6	22.7
Shale gas (tonne/hr)	21.6	20.7	20.3
Thermal efficiency (%, HHV)	64.3	66.5	67.6
Total H_2 consumption (% daf feed)	8.61	8.24	8.05
Liquefaction H_2 consumption (% daf feed)	6.70	6.20	6.00
Carbon efficiency (%)	53.9	56.4	57.6
CO_2 captured (kmol/hr)	2660	2366	2240

Table 6.22 Effects of the coal biomass mix ratio (D-CBTL-CCS, 10k bbl/day)

Biomass/coal (wt/wt)	8/92	15/85	20/80
Coal (tonne/hr)	151.4	138.8	132.0
Biomass (tonne/hr)	14.1	26.8	35.4
Thermal efficiency (%, HHV)	60.0	61.5	62.1
Total H_2 consumption (% daf feed)	8.61	8.24	8.05
Liquefaction H_2 consumption (% daf feed)	6.70	6.20	6.00
Carbon efficiency (%)	43.5	45.1	45.6
CO_2 captured (kmol/hr)	4245	3959	3852

6.6.5 Effect of the Extent of CCS

As mentioned earlier, CCS is not considered in the D-CBGTL-VT and D-CBTL-VT processes, where CO_2 is removed from the syngas for hydrogen purification and directly vented to the atmosphere. If the concept of carbon tax or other potential GHG emission related regulation is implemented, the CCS facility will be a necessary part of those alternative fuel production processes. The extent of CCS will be determined by local regulations if applicable. As the penalty of CCS does not increase linearly with the extent of CCS, it is necessary to redesign the process appropriately while evaluating effects of different level of CCS. For the D-CBGTL-CCS and D-CBTL-CCS processes, effects of low and high extent of CCS are studied. If low extent of

CCS is considered, the removed CO_2 from the syngas is sent to the CO_2 compressor for sequestration, and no additional CO_2 needs to be removed from the flue gas. On the other hand, when high extent of CCS is considered in the D-CBGTL-CCS and D-CBTL-CCS processes, additional CO_2 is captured from the flue gas and sent to the CO_2 compressor along with the CO_2 captured from the syngas for being sent to the CO_2 pipeline. Table 6.23 and 6.24 show the effect of the extent of CCS on the thermal efficiency and CO_2 emission with different biomass/coal ratios and hydrogen sources. It is observed that the CO_2 emission of the direct CBTL plant with the hydrogen produced from the shale gas can be reduced by more than half with the thermal efficiency reduced by only 0.5%, if low extent of CCS is considered. On the other hand, high extent of CCS will reduce the thermal efficiency by another 1-1.5% because of the higher penalty of post-combustion CO_2 capture facilities. The difference between low and high extent of CCS is higher in direct liquefaction plants with hydrogen produced from gasification, because most of the CO_2 is generated in the gasification unit with higher partial pressure, and therefore the Selexol technology that has lower penalty than the amine-based technologies can be applied for CO_2 capture. It is also noticed that with the increasing biomass/coal ratio for both cases, the CCS penalty is reduced, because less CO_2 needs to be captured.

Table 6.23 Effects of the extent of CCS (D-CBGTL)

Biomass/coal (wt/wt)		8/92			20/80	
Extent of CCS	High	Low	No	High	Low	No
CO_2 emission (kg CO_2/GJ product)	12.0	26.3	53.2	11.5	21.9	47.2
Thermal efficiency (HHV, %)	64.3	66.0	66.5	67.6	68.7	69.2

Table 6.24 Effects of the extent of CCS (D-CBTL)

Biomass/coal (wt/wt)		8/92			20/80	
Extent of CCS	High	Low	No	High	Low	No
CO_2 emission (kg CO_2/GJ product)	14.3	27.3	77.4	13.8	23.5	72.7[(1)]
Thermal efficiency (HHV, %)	60.0	61.2	62.1	62.1	63.1	63.6

(1)The CO_2 emission from the D-CBTL-VT process with low biomass/coal ratio is 72.7 kg CO_2 per GJ product, about 0.5 tonne/bbl oil, which is similar to the data reported by Shenhua. (Vasireddy et al., 2011)

6.6.6 Direct vs Indirect Liquefaction

ICL and DCL are two commercially proven but very different approaches to produce transportation fuels from coal. The performance of the direct and indirect CBTL plants with a biomass/coal weight ratio of 8/92 is compared in this section, based on the detailed plant-wide models developed in this Chapter and Chapter 3. (Jiang and Bhattacharyya, 2014; 2015) Table 6.25 shows that the CO_2 emission from the I-CBTL plant is much higher than the D-CBTL plant and the D-CBGTL plant, while the thermal efficiency is much lower. That is because more carbon in the feedstock is converted to fuels instead of CO_2 in the direct liquefaction processes. Table 6.25 also indicates that the comparative CCS penalty is less in the I-CBTL plant with high extent of CCS, because most of the CO_2 is produced in either gasification or FT unit and is available at higher partial pressure. In addition, no CO_2 needs to be removed from low pressure flue gas in the indirect approach. Even though the direct liquefaction plant, especially with shale gas utilization, is superior to the indirect liquefaction plant in terms of carbon and thermal efficiency, it should be noted that a detailed techno-economic analysis including assessment of availability of shale gas, in particular, is needed for fair comparison and final decision on commercial application. Those discussions can be found in Chapter 7.

Table 6.25 Performance of the direct and indirect liquefaction plants

Process	Indirect		Direct			
Hydrogen source	N/A		Shale gas		Coal/biomass	
Carbon efficiency (%)	36.4		53.9		43.5	
Extent of CCS	High	No	High	No	High	No
Thermal efficiency (HHV, %)	46.6	48.0	64.3	66.0	60.0	62.1
CO_2 emission (kg CO_2/GJ product)	18.9	118.6	12.0	53.3	14.3	77.4

6.7 Conclusions

Plant-wide models of direct liquefaction plants with four different configurations are developed to analyze the effect of shale gas utilization and CCS on the plant performance. Utility consumption in the liquefaction and product recovery section can be reduced by 52% through heat integration. The AGR unit is designed based on the carbon balance and the CO_2 partial

pressure. Simulation results are validated by comparing with the data available in the open literature. The process model shows that the carbon efficiency of the D-CBTL plant without shale gas utilization is 43.5%, which is 7.1% higher than the I-CBTL plant with a biomass/coal weight ratio of 8/92. The carbon efficiency can be increased to 53.9% if shale gas is utilized for hydrogen production. It is also observed that the D-CBGTL plant with hydrogen produced from the shale gas has the highest thermal efficiency, 66.5% without CCS and 64.3% with high extent of CCS, while the I-CBTL plant has lower thermal efficiency because of its poor carbon efficiency. Carbon and thermal efficiencies of the direct liquefaction plant are found to increase with the biomass/coal ratio regardless of the hydrogen source, because the higher H/C ratio in biomass than in coal reduces hydrogen consumption in the liquefaction unit. Sensitivity studies on the extent of CCS show that the penalty per unit of CO_2 capture increases with the extent of CCS, because it costs more utility to capture CO_2 from low pressure sources. Similarly, utility consumption in the CCS facilities in the direct liquefaction plant is higher than in the indirect liquefaction plant with high extent of CCS, due to CO_2 capture from the low pressure flue gas. In general, the D-CBGTL plant with shale gas utilization has the best performance in terms of carbon and thermal efficiency. In closing, we would like to note this study has mainly focused on process systems analysis, but for selecting the optimal process technology and process configuration, other studies such as optimization, techno-economic analysis, and life-cycle analysis need to be conducted where the process model developed in this work can be leveraged.

Chapter 7 Techno-economic Analysis of Direct Coal-Biomass to Liquids Plants

7.0 Overview

The D-CBTL processes are modified from the traditional technically feasible DCL process to produce alternative fuels with less GHG emission and reasonable capital investment. In Chapter 6, detailed plant-wide models have been developed in Aspen Plus for different direct liquefaction plants with hydrogen derived from different sources and different extent of CCS, which focus on conversion efficiency and CO_2 emission but not economic performance. (Jiang and Bhattacharyya, 2016) To analyze the commercial feasibility of those novel processes, techno-economic studies are required in addition to the material and energy balance analysis. Claimed by multiple researchers, DCL processes may have better economic performance than ICL processes due to their higher thermal efficiency (Vasireddy et al., 2011; Williams and Larson, 2003), while Robinson et al. claims that the economic performance of DCL and ICL process are similar. (Robbinson, 2009) However, there is hardly any techno-economic study of the DCL technology conducted by using rigorous process and economic models especially when considering CO_2 capture, biomass co-processing and different H_2 sources.

In this chapter, the techno-economic analysis is performed using APEA based on high fidelity process models developed in Aspen Plus for four different configurations of direct liquefaction plants, as discussed in Chapter 6. The results of process models and economic models were validated by comparing with open literature. Sensitivity studies are conducted to evaluate the impacts of key investment parameters, design parameters, and potential government-subsidized credits on the main economic measures NPV, IRR, BEOP and equivalent oil price (EOP). The results shows the BEOP of those direct liquefaction processes ranges from $56.9/bbl to $80.5/bbl for large scale (50k bbl/day) operation and from $77.3/bbl to $97.5/bbl for small scale (10k bbl/day) operation with 2015 pricing basis. The economic performance is similar between the indirect and direct liquefaction processes without shale gas utilization. Embedding CCS to the direct liquefaction processes will increase the BEOP by about 10%, while the cheap and

abundant shale gas (especially in the continental US) can make the direct liquefaction processes more competitive.

7.1 Steady-State Modeling and Simulation

In this study, four different plant configurations are considered for direct liquefaction processes, D-CBGTL-CCS, D-CBGTL-VT, D-CBTL-CCS and D-CBTL-VT, with the BFD presented in Figure 7.1. Two sources of hydrogen are evaluated, namely shale gas steam reforming in the D-CBGTL processes or coal-biomass-residue co-gasification in the D-CBTL processes. The CO_2 can be directly vented (VT) or compressed for sequestration (CCS). In Figure 7.1, the solid lines denote the common process sections for all configurations, while the dash lines denoted the process sections varying with different configurations. The liquefaction and hydrocarbon recovery section is designed similar to the CTSL technology from HTI. (Vasireddy et al., 2011; Shui et al., 2010; Mochida et al., 2014; Comolli et al., 1995) Inline hydrotreating approach is introduced to reduce the energy penalty of raw syncrude stabilization step. In addition to vacuum distillation, ROSE-SR technology is used to increase the efficiency of and liquid recovery in the solid/liquid separation process as part of the hydrocarbon recovery unit. (Valente and Cronauer, 2005; Debyshire et al., 1984; Khare et al., 2013) Isomerization, catalytic reforming, and gas oil hydrotreating are applied to upgrade syncrude to on-spec gasoline and diesel. (Zhou and Rao, 1993) Heating duties of the furnaces are provided by utilizing the light gas oil and fuel gas produced inside the DCL plant. Remaining gas from the fuel gas header is sent to the power island for generating electricity and utility steams. Required hydrogen is produced from the syngas via WGS reaction. (Bhattacharyya et al., 2011) In the D-CBTL-CCS and D-CBTL-VT processes, syngas is produced by gasifying a mixture of coal and biomass from the pre-processing units and liquefaction residues from the ROSE-SR unit. In the D-CBGTL-CCS and D-CBGTL-VT processes, syngas is produced by a combination of liquefaction residues POX and shale gas SMR. The syngas from the WGS reactors is sent to the AGR unit and PSA unit to produce high purity hydrogen. In the D-CBGTL-VT and D-CBTL-VT processes, captured CO_2 is vented to the atmosphere. In the D-CBGTL-CCS and D-CBTL-CCS processes considering high extent of CCS, additional CO_2 is captured from the flue gas and all captured CO_2 is sent to the CO_2 compressor for sequestration. The dual-stage Selexol technology is selected to remove CO_2 and H_2S available at high pressure from the POX/CG unit while the MDEA/PZ technology

is selected to remove CO_2 available at intermediate or low pressures from the SMR and combustion units.

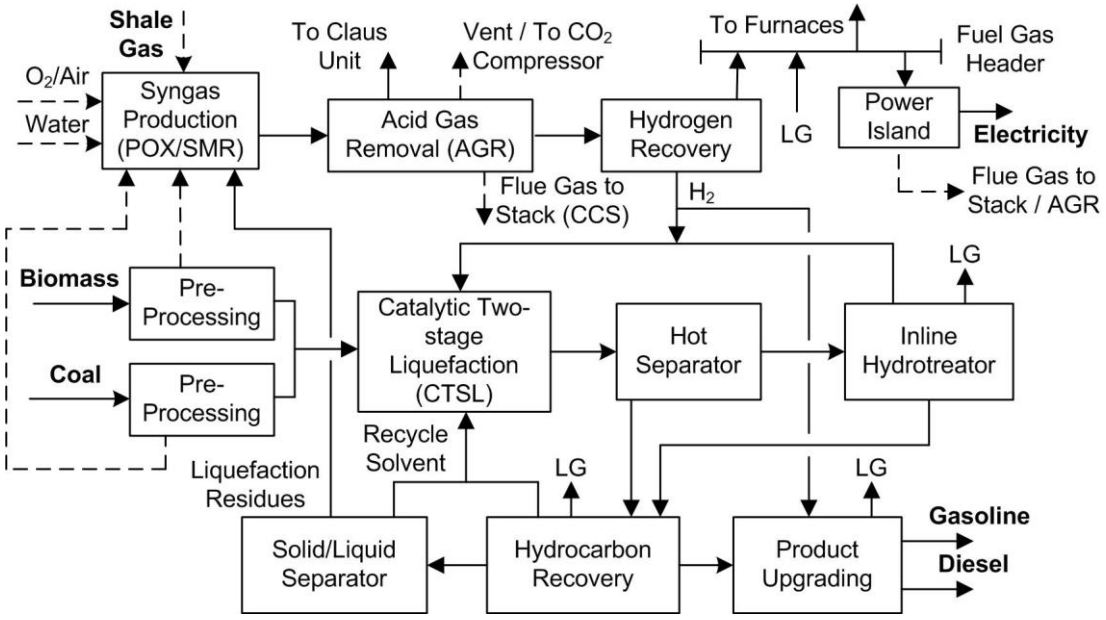

Figure 7.1 General BFD of direct liquefaction processes

In this study, all four direct CBTL processes, D-CBGTL-CCS, D-CBGTL-VT, D-CBTL-CCS and D-CBTL-VT, have been modeled in Aspen Plus. Illinois No.6 coal, wood chip, and Marcellus shale gas are used as feedstocks. (Jiang and Bhattacharyya, 2016) The composition of each feedstock can be found in Chapter 6. Most of the equipment items are simulated using standard library models available in the Aspen Plus library. For the reactors in liquefaction and product upgrading sections, yield models are developed in Excel and validated using the experimental data available in the open literature. These Excel models are integrated into the main flowsheet in Aspen Plus using User2 blocks. Table 7.1 summarized the simulation approach, operating conditions, and property models of the key equipment items. Plant configuration, modeling approach and composition of products and feedstocks can be found in Chapter 6. (Jiang and Bhattacharyya, 2016)

Table 7.1 Summery of the process model of direct liquefaction plants

Section/Block	Simulation Approach	Property Model/Operating Conditions
Liquefaction and hydrocarbon recovery		Peng-Robinson
Liquefaction	Close-coupled yield model for two ebullated-bed reactors in series	1st stage: 407 °C, 22.1 MPa 2nd stage: 432 °C, 20.7 MPa

Inline hydrotreating	Yield model	370 ^{o}C, 17.2 MPa
Distillation columns	PetroFrac	Atmospheric column: 2.8 bar Vacuum column: 0.1 bar
ROSE-SR	Component separator for settlers and flash vessel for deashing solvent separator	Solvent/solid weight ratio: 3 1st stage settler: 300 ^{o}C, 55 bar 2nd stage settler: 370 ^{o}C, 54.5 bar
Product upgrading		Peng-Robinson
Gas oil hydrotreating	Same as inline hydrotreater	350 ^{o}C, 180 bar, LHSV: 1 h^{-1}
Isomerization	Yield model	Hydrogen/oil: 0.14 wt% Targeted RON: 83
Catalytic reforming	Yield model	Targeted RON: 95
Syngas Production		Peng-Robinson/ELECNRTL-RK
Pre-reformer	RGibbs model	Adiabatic; Inlet: 510 ^{o}C, 27 bar
Steam reformer	RGibbs for reformer and Rstoic with combustion reactions for furnace	Reformer: 815 ^{o}C, 25 bar Reformer furnace: 955 ^{o}C
Gasification	RGibbs model	1315 ^{o}C, 56 bar
Water gas shift	Plug flow reactor	CO conversion: 95%
Acid gas removal and hydrogen recovery		ELECNRTL/PC-SAFT
Chemical absorption	RadFrac model with rate-based stages and reaction kinetics	Absorber: 40 ^{o}C Regenerator: 1.7 bar
Physical absorption	RadFrac model with equilibrium stages	Solvent chilling: 2 ^{o}C
Hydrogen recovery	Polybed PSA process modeled as component separator	Adsorption: 26.2 bar Desorption: 6.9 bar
CO_2 compression	Multistage compressor	15.3 MPa for CO_2 pipeline
Power island		Ideal/IAPWS-95
Combined cycle	Stage-by-stage estimation of steam turbine and Aspen Plus standard models for others	Triple-pressure HRSG with reheat: 114/25/4 bar

7.2 Economic Analysis

APEA V8.4 is used to perform economic analysis of the direct liquefaction plants. Figure 7.2 summarizes the procedure that is followed for techno-economic analysis in this study. Stream information, such as temperature, pressure and flowrate, as well as the basic equipment type is automatically specified by directly 'exporting' the plant-wide models developed in Aspen Plus to APEA. In APEA, the capital investment, denoted as the TPC, can be estimated by mapping the equipment items from the Aspen Plus flowsheet to corresponding APEA project component(s), if available. These equipment items are sized using ASTM standards or other correlations available in APEA. Vendor cost obtained from the open literature is used for the equipment items for

which there are no suitable APEA project component and also for those for which yield models were used in Aspen Plus. (Jiang and Bhattacharyya, 2016) Section 7.2.1 provides a more detailed description of project component mapping, sizing and cost estimation. The main source of O&M cost is due to utilities and raw materials. Other O&M costs can be found in Section 7.2.2. In addition, investment parameters are specified. In APEA, economic analysis and sensitivity studies can be conducted by using the Decision Analyzer tool. If plant configuration and/or any key process design parameters listed in Table 7.7 changes, a new process model is developed in Aspen Plus and then 'exported' to APEA for economic analysis. (Jiang and Bhattacharyya, 2016)

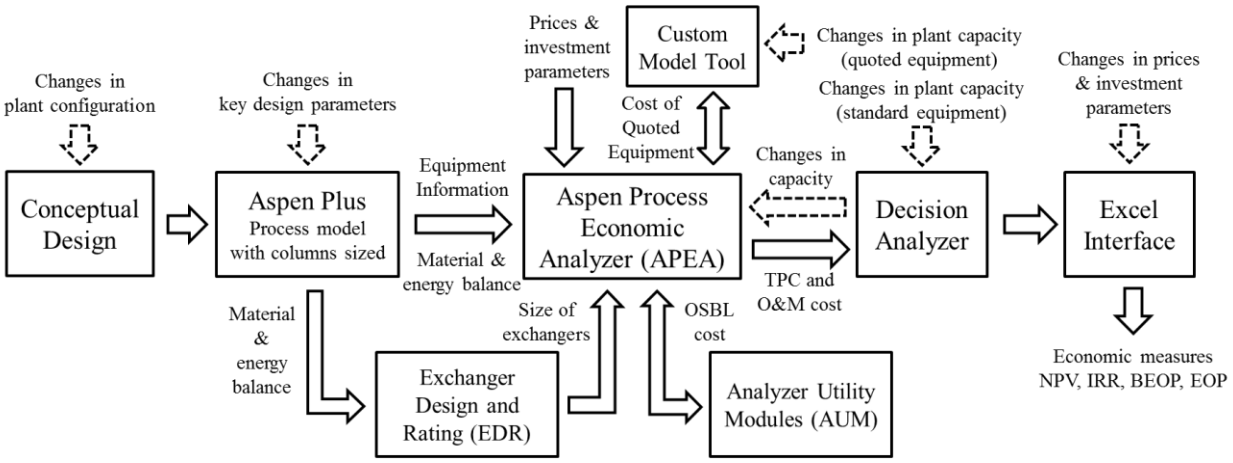

Figure 7.2 Procedure for economic analysis in multi-software environment

Table 7.2 lists the prices of raw materials, labor and products in 2015 basis. The prices of raw material and products are mainly obtained from the US EIA website. The COP is the refiner acquisition cost of crude oil in the PADD1 area (the east coast of US). In this study, NPV and IRR are calculated assuming the wholesale prices of gasoline and diesel are COP plus the refinery margin, \$0.333/gallon for gasoline and \$0.371/gallon for diesel. (Jiang and Bhattacharyya, 2016) BEOP is the COP making the process NPV zero, while EOP is defined as the COP making the process IRR be 12%. The carbon credit is defined as carbon in the additional CO_2 captured by the CCS facilities compared with the petroleum baseline. In the PADD1 area, the CO_2 emission from the petroleum refineries is about 45 kg CO_2/bbl crude oil, which is equivalent to about 8.12 kg CO_2/GJ fuel. (Karras, 2011) It is assumed that if the CBTL facility is located in a place that is subject to carbon tax and if CO_2 emission of the CBTL plant with CCS is lesser than 8.12 kg CO_2/GJ fuel, then the additional CO_2 that is captured and

sequestered can be leveraged to improve the plant economics. In the base case, the price of carbon credit is set to be zero as carbon tax is still fairly uncommon in most locations around the world. Table 7.3 lists the investment parameters for the base case scenario. Here, process contingency is set to be 24% because of the novelty of the direct liquefaction plants. The length of start-up period is set to be 40 days because of the process complicity.

Table 7.2 Prices of raw material, labor, and product (base case)

	Cost ($/unit)		Cost ($/unit)
Coal ($/tonne)	34.0	Supervisor ($/hr)	80
Wood chip ($/dry tonne)	61.5	Crude oil price ($/bbl)	60
Shale gas ($/GJ)	2.25	Electricity ($/MWh)	50
Operator ($/hr)	50	Carbon credit ($/tonne)	0

Table 7.3 Investment parameters (base case)

Parameter	Value	Parameter	Value
Start date of engineering	2015	Utility escalation (%/year)	1
Contingency percent	24%	Working capital percentage (%/FCI)	12
Number of years for analysis	30	Operating charges (% of labor costs)	25
Tax rate	40%	Plant overhead	50%
Interest rate/desired rate of return	10%	General & administrative expenses	8%
Project capital escalation (%/year)	1	Length of start-up period (weeks)	40
Products escalation (%/year)	1	Operating hours per period	8000
Raw material escalation (%/year)	1	Construction time	2.5 yr

7.2.1 Estimation of the Total Project Cost

In this study, all heat exchangers are designed in Aspen EDR; all columns are designed in Aspen Plus using available options for tray/packing sizing; other equipment items such as vessels, pumps and compressors are sized in APEA. The MOC for all project components are selected based on the operating temperature, composition of the service stream (i.e. H_2, H_2S partial pressure), and common industry practice. (Wu et al., 2015; Comolli et al., 1995; Tsai, 2010; Kohl and Nielsen, 1997; Bechtel and Amoco, 1992) For all pumps and reciprocating compressors, spares are considered. The equipment items and sections for which costs cannot be estimated by the Icarus database especially the reactors and product upgrading units, are mapped as ‘quoted’ equipment item in APEA with cost correlations shown in Eqs. (7.1) and (7.2). In

those correlations, *DIP* is the direct permanent investment including ISBL and OSBL cost; C_0 is the base cost; S_0 is the base capacity; S is the actual capacity, *sf* is the scaling factor; and *n* is the number of trains. Eq. (7.1) is used for the 'quoted' equipment with missing information, where the OSBL cost is estimated by considering the BOP. Eq. (7.2) is applied for other 'quoted' equipment items. Parameters in the cost correlations with 2015 pricing basis are obtained from the open literature or derived using the data available in the open literature, as shown in Table 7.4. Various steps for capital cost estimation in multiple-software environment are described here only for the gas oil hydrotreating unit as an example. The configuration of the gas oil hydrotreating unit is shown in Figure 6.5 in Chapter 6, while Table 7.5 lists the corresponding models in APEA, required numbers of items and spares, if any, sizing approach and MOC for each equipment. Complete equipment lists and detailed specifications for all standard equipment items can be found in Appendix E.

$$DIP = (1 + BOP)C_0(S/S_0)^{sf} n^{0.9} \quad (7.1)$$

$$ISBL\ cost = C_0(S/S_0)^{sf} n^{0.9} \quad (7.2)$$

Table 7.4 Parameters for Eqs. (7.1) and (7.2) for quoted equipment items (2015 pricing basis)

Equipment[(1)]	C_0 (MM$)	S_0	S_{max}	S_0 basis	Units	sf	BOP	Reference
Gasifier	137.09	2464	2616	dry feed	tonne/day	0.67	added	Baliban et al., 2011
WGS reactor	3.16	2556	2600	output	tonne/day	0.65	no	Baliban et al., 2011
Isomerization	1.00	13.06	2720	feed	tonne/day	0.62	no	Bechtel, 1998
Catalytic reforming	5.39	36.99	8160	feed	tonne/day	0.6	no	Bechtel, 1998
Air separation unit	57.90	1839	2500	O_2	tonne/day	0.5	added	Baliban et al., 2011
Coal pre-processing	57.50	2464	2616	dry feed	tonne/day	0.67	added	Baliban et al., 2011
Biomass pre-processing	27.98	2000		dry feed	tonne/day	0.67	added	Baliban et al., 2011
CO_2 compressor	31.81	11256		CO_2	tonne/day	0.75	no	NETL, 2010
PSA H_2 recovery	0.84	944		H_2	Nm3/h	0.55	no	Bechtel, 1998
Claus unit	24.23	125		S	tonne/day	0.67	no	Baliban et al., 2011
Steam methane reformer	62.10	26.1	35	feed	kg/s	0.67	no	NETL, 2013
Shale gas pre reformer	12.30	26.10		feed	kg/s	0.67	no	Baliban et al., 2013
ROSE-SR unit	66.70	50800		feed	bbl/day	0.67	no	Bechtel and Amoco, 1992
Liquefaction reactor	94.79	587.79		feed	tonne/hr	0.67	no	Bechtel and Amoco, 1992

(1) The costs of quoted equipment are escalated using the CEPCI.

Table 7.5 Detailed component specifications for the gas oil hydrotreating unit in APEA

Equipment	#Required/Spares	Model in APEA	Sizing	MOC[(1)]

Reactors & vessels				
gas oil hydrotreater	2/0	VT MULTI WALL	APEA	A387F (SS347)
Hot high pressure flash	1/0	VT CYLINDER	APEA	A387D
Cold high pressure flash	1/0	VT CYLINDER	APEA	A516
Low pressure flash	1/0	VT CYLINDER	APEA	A516
Stabilizer condenser drum	1/0	HT HORIZ DRUM	APEA	A516
Main distillation condenser drum	1/0	HT HORIZ DRUM	APEA	A516
Distillation columns				
Main distillation tower	1/0	TW TRAYED	Aspen Plus	A516/A285C
Stabilizer tower	1/0	TW TRAYED	Aspen Plus	A516/A258C
Compressors, pumps & turbines				
Main distillation reflux pump	1/1	CP CENTRIF	APEA	CS casing
Stabilizer reflux pump	1/1	CP CENTRIF	APEA	CS casing
Makeup H_2 compressor	1/1	GC RECIP MOTR	APEA	SS casing
Recycle H_2 compressor	1/0	GC CENTRIF	APEA	SS316 casing
Stabilizer feed pump	1/1	CP CENTRIF	APEA	CS casing
Gas oil feed pump	1/1	CP CENTRIF	APEA	CS casing
Furnaces, boiler & heat exchangers				
Main distillation reboiler	1/0	RB U TUBE	EDR	A213C/A387B
Main distillation condenser	1/0	HE FIXED T S	EDR	A214/A516
Main distillation pumparound	2/0	HE FLOAT HEAD	EDR	A214/A516
Stabilizer reboiler	1/0	RB U TUBE	EDR	A214/A516
Stabilizer condenser	1/0	HE FIXED T S	EDR	A214/A516
Gas pre-heater	1/0	HE FLOAT HEAD	EDR	A214/A516
Liquid pre-heater	1/0	HE FLOAT HEAD	EDR	A213D/A387D
Feed furnace	1/0	FU BOX	APEA	347S
LP steam generator	3/0	HE WASTE HEAT	EDR	CS
Other coolers	6/0	HE FLOAT HEAD	EDR	A214/A516

(1) ( ) denotes cladding material

7.2.2 Estimation of Operating and Maintenance Cost

Other than the raw material costs, costs of utility, operating labor, catalysts and chemicals also have significant contributions on the O&M cost of a chemical plant. In this study, the raw material cost can be easily estimated based on the material and energy balance given steady state simulation. Process fuels, steam and electricity are generated internally from the fuel gas header and the combined cycle power island. As the circulating water system is designed using AUM, process water is the only external utility considered in this economic model. The costs of catalysts and chemicals are listed in Table 6 for all four plant configurations. In APEA, the initial loading of catalysts and chemicals is specified as ‘quoted’ equipment, while costs for replacing catalysts and chemicals are specified under raw materials. For the water gas shift, Claus, isomerization and catalytic reforming units, the initial catalyst cost is included in the equipment

cost. The catalyst in the liquefaction unit is replaced continuously. The catalyst in the catalytic reforming unit is replaced continuously to maintain the desired catalysts activity. (Bechtel, 1998) Other catalysts are replaced every five to ten years, depending on the catalyst life. Replacement costs of those catalysts are amortized when treated as raw materials. The number of operators is calculated based on the economic analysis given by Bechtel and Amoco. (Bechtel and Amoco, 1992)

Table 7.6 Cost of catalyst and chemicals in the direct liquefaction plants (10k bbl/day)

	Unit Cost[(1)]	Initial (k$)/Replacement ($/hr)[(2)]				
	($/unit)	D-CBGTL-CCS	D-CBGTL-VT	D-CBTL-CCS	D-CBTL-VT	Cost source
Catalysts						
Liquefaction	$4.00/kg	661/461	661/461	661/461	661/461	Bechtel and Amoco, 1992
Water gas shift	$16774/m^3	0/75	0/75	0/75	0/75	NETL, 2007; 2010
Claus unit	$4414/m^3	0/15	0/15	0/15	0/15	NETL, 2010
Steam reforming	$22930/m^3	868/33	868/33	0/0	0/0	NETL, 2013
Hydrotreating	$34.17/kg	6754/282	6754/282	6754/282	6754/282	Bechtel, 1998
Isomerization	$4414/m^3	0/4.5	0/4.5	0/4.5	0/4.5	Bechtel, 1998
Chemicals						
Selexol solvent	$3804/m^3	98/2.0	98/2.0	433/9.2	433/9.2	NETL, 2007; 2010
Amine solvent	$2.16/kg	1355/17	301/3.8	350/4.4	0/0	NETL, 2007; 2010
ROSE-SR solvent	$3/gallon	54/1.6	54/1.6	54/1.6	54/1.6	Bechtel and Amoco, 1992
Total		9790/891	8736/878	8252/853	7902/848	

(1) Costs listed are the original value published in different years.
(2) The costs of catalyst and chemicals are escalated with the average Producer Price Index.

7.3 Results and Discussion

The specified key design parameters for the base case scenario and the results obtained from the steady-state process models are provided in Table 7.7 for the four direct liquefaction configurations. While the process model which is the basis for the material and energy balances has been validated in Chapter 6 (Jiang and Bhattacharyya, 2016), estimation of capital cost also needs to be compared with the data available in the open literature if feasible. Section 7.3.1 shows that comparison for capital costs. A number of sensitivity studies are conducted as reported in Sections 7.3.2 to 7.3.4 by considering different hydrogen sources, key design parameters listed in Table 7.7, raw material price listed in Table 7.2, and investment parameters listed in Table 3. In Section 4.5, impacts of potential environmental credits are evaluated.

Finally, the direct liquefaction plant with various configurations is compared with the indirect liquefaction plant in Section 7.3.6.

Table 7.7 Key design parameters and plant performance measures (base case)

			D-CBGTL		D-CBTL	
Key design parameters	Value	Plant performance	CCS	VT	CCS	VT
Plant capacity (bbl/day)	10000	Coal/biomass (tonne/hr)	100/9	100/9	151/14	151/14
Biomass type	Wood chip	Shale gas (tonne/hr)	22	22	0	0
Biomass/coal (wt/wt, dry)	8/92	Gasoline/diesel (bbl/day)	2433/7557	2433/7557	2433/7557	2433/7557
Low pressure CO_2 capture	MDEA/PZ	Net power (MW)	52.4	77.8	84.5	111.9
Extent of CCS if considered	High(1)	Efficiency (%, HHV)	64.3	66.5	60.0	62.1

(1) 90% of carbon in the raw materials is either converted to gasoline and diesel or stored in captured CO_2.

7.3.1 Capital Cost Model Validation

In the limited techno-economic studies conducted for direct liquefaction processes, coal is the only feedstock considered; hydrogen is usually supplied by coal gasification; and no CCS facility is considered. (Robinson, 2009; Bechtel and Amoco, 1992) In this study, the liquefaction reactor feed only contains 8 wt% of biomass in the base case scenario, which is not expected to have significant impact on the TPC estimation. Hence, the capital cost estimation of the D-CBTL-VT process is validated by comparing with the estimates available in the open literature for the DCL plant with different capacities. The estimated costs of the SMR unit and CO_2 compression units are compared with the natural gas to liquids plant and the power plant separately and are found to have good match. (NETL, 2007; 2010; 2013; Baliban et al., 2013) The Decision Analyzer tool in APEA is applied to change the plant capacity from our base case model for fair comparison. For some equipment items, parallel trains have to be considered, because of issues such as hardware constraints, high radial variation, etc. Table 7.8 summarizes the results of the comparison, while Table 7.9 provides detailed comparison of each plant section for the large scale case. Our estimations are found to be similar to the data reported by Shenhua (Robinson, 2009) which is one of the only existing commercial scale DCL plants in the world, but slightly higher than the data reported by Bechtel/Amoco (Bechtel and Amoco, 1992), mainly because the gasification cost estimated by Bechtel/Amoco in 1992 was lower than the data reported by NETL and others (NETL, 2007; 2010; 2013), even after it is escalated by CEPCI.

Table 7.8 Validation of capital cost estimation

Process	D-CBTL-VT[(1)]	D-CBTL-VT[(2)]
Reference	Robinson, 2009	Bechtel and Amoco, 1992
Capacity (bbl/day)	16300	61943
Biomass (wt %)	0	0
Total project cost (MM$, 2015)		
Estimated	2024	6853
Reported	2086	6115

(1) The original capital cost is $1.46 billion for a DCL facility in China in 2008. (Robinson, 2009) This value is adjusted by the reported location factor for China and escalated by CEPCI. (Su, 2010; Larson and Ren, 2003)

(2) The original capital cost is $3.87 billion with 1991 pricing basis. The capital investment of the gasification unit reported by Bechtel/Amoco is lower than most recent estimation reported by NETL. (Bechtel and Amoco, 1992; NETL, 2010; 2007; Baliban et al., 2011)

Table 7.9 Detailed comparison of equipment cost estimation (MM$, 61943 bbl/day)

	Estimated	Reported		Estimated	Reported
Feed drying and handling	103.8	115.2	Hydrogen production[(3)]	250.4	129.3
Liquefaction[(1)]	416.2	455.2	Air separation unit	138.2	165.0
Product upgrading[(2)]	92.6	47.6	Sulfur recovery	46.0	24.1
Hydrogen purification	105.3	96.8	Total equipment cost	1178.1	1053.7
ROSE-SR	25.6	20.6	Total project cost	6711.1	6115.0

(1) Required solvent/feed ratio for liquefaction has been reduced since Bechtel/Amoco did their estimation in 1992.

(2) Naphtha upgrading was not considered in Bechtel/Amoco's design but in our design

(3) The equipment cost for gasification estimated by Bechtel/Amoco is lower than the data published in other resources. (Bechtel and Amoco, 1992; NETL, 2010; 2007; Baliban et al., 2011)

7.3.2 Profitability Analysis of Four Plant Configurations (Base Case)

With the economic parameters listed in Table 7.2 and 7.3 as well as the material and energy balance shown in Table 7.7, the major economic measures of the base case are calculated and reported in Table 7.10. It is noticed that none of the four investigated configurations of the direct liquefaction plants can make profit or have positive NPV due to the current low COP. However, the direct liquefaction plants may start to payback once COP surpasses the reported BEOP, and be competitive with traditional petroleum industries once COP surpasses the reported EOP. The results also shows that the capital investments of the D-CBTL processes are much higher than

those of the D-CBGTL processes, because of the high capital cost and low hydrogen production efficiency of the gasification unit in comparison to the shale gas steam reforming unit. (Jiang and Bhattacharyya, 2016; Williams and Larson, 2003) As a result, the BEOP and EOP of the D-CBGTL processes are higher than those of the D-CBTL processes, which indicate that the direct liquefaction plants will be more profitable if hydrogen is produced from low cost shale gas. Additionally, the relative penalty of CCS based on BEOP is about 10.2% if hydrogen produced from shale gas SMR and residual POX and 8.8% if hydrogen is produced from coal/biomass/residues CG, because CO_2 produced from gasification unit is at higher partial pressure and therefore easier to be captured. (Jiang and Bhattacharyya, 2016)

Table 7.10 Major economic measures (10k bbl/day, base case)

	D-CBGTL		D-CBTL	
Process	CCS	VT	CCS	VT
Total project cost (MM$)	1162	1080	1464	1387
Net present value (MM$)	-408.6	-263.8	-591.7	-453.0
Internal rate of return (%)	6.0	7.3	5.2	6.2
Break-even oil price ($/bbl)	86.1	77.3	97.5	88.9
Equivalent oil price ($/bbl)	101.0	91.5	115.5	107.0

7.3.3 Effect of Economic Parameters and Plant Capacities

Figure 7.3 to Figure 7.6 provide the results due to ±25% changes in the major plant economic inputs for all four configurations of the direct liquefaction plant with a 10,000 bbl/day capacity. The results shows that the BEOP is between $83.4/bbl to $92.2/bbl for the D-CBGTL-CCS process, between $74.5/bbl to $82.9/bbl for the D-CBGTL-VT process, between $93.4/bbl to $104.7/bbl for the D-CBTL-CCS process, and between $84.7/bbl to $96.0/bbl for the D-CBTL-VT process. Figure 7.7 shows the effect of plant capacity in comparison between the small-scale operation (10,000 bbl/day, base case) and the large-scale operation (50,000 bbl/day) for all four configurations. As the plant capacity increases, multiple trains may be required for different process sections. For example, three parallel trains are required by the liquefaction and hydrocarbon recovery section, when the plant capacity reaches 50,000 bbl/day. The results indicate that the BEOP of the D-CBGTL-VT process decreases to $56.9/bbl with high capacity, which is less than the COP of the second quarter of 2015. However, the BEOP of the D-CBTL-

CCS and the D-CBTL-VT processes is still much higher than the COP even with a high plant capacity, because multiple trains are required by the gasification unit, one of the most expensive process sections.

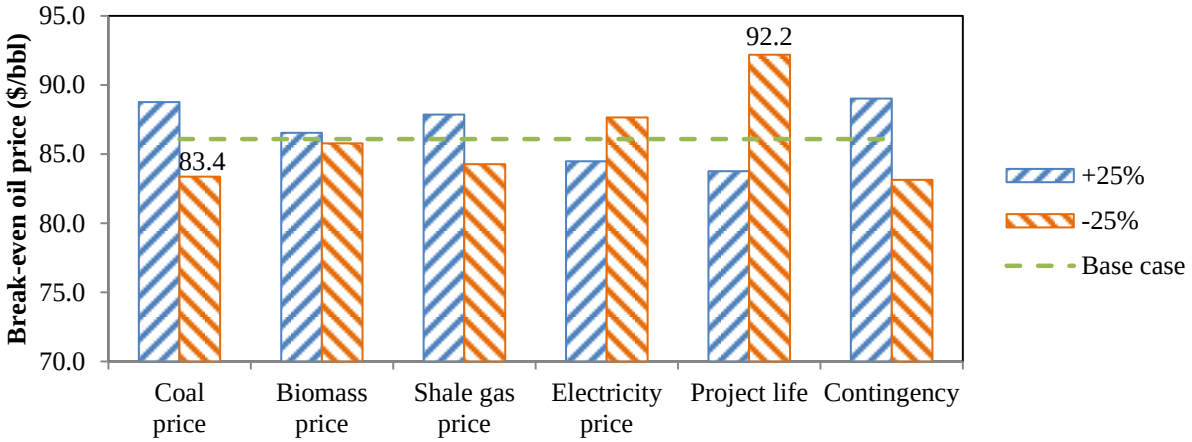

Figure 7.3 Sensitivity studies of the D-CBGTL-CCS process (10k bbl/day)

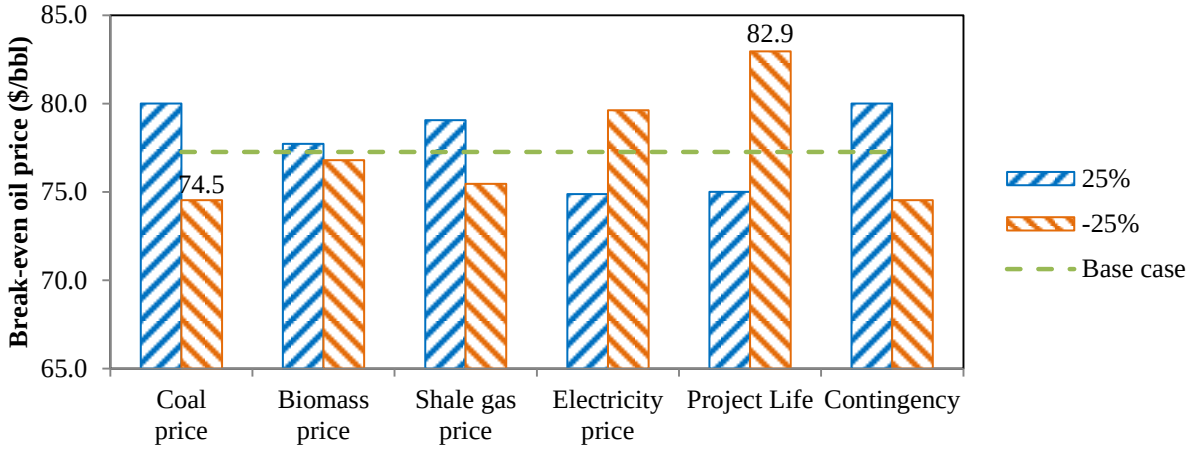

Figure 7.4 Sensitivity studies of the D-CBGTL-VT process (10k bbl/day)

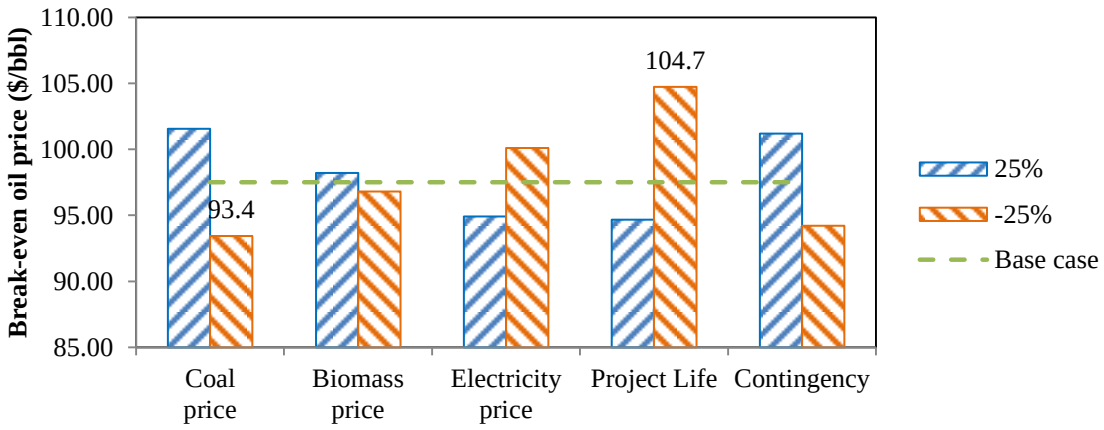

Figure 7.5 Sensitivity studies of the D-CBTL-CCS process (10k bbl/day)

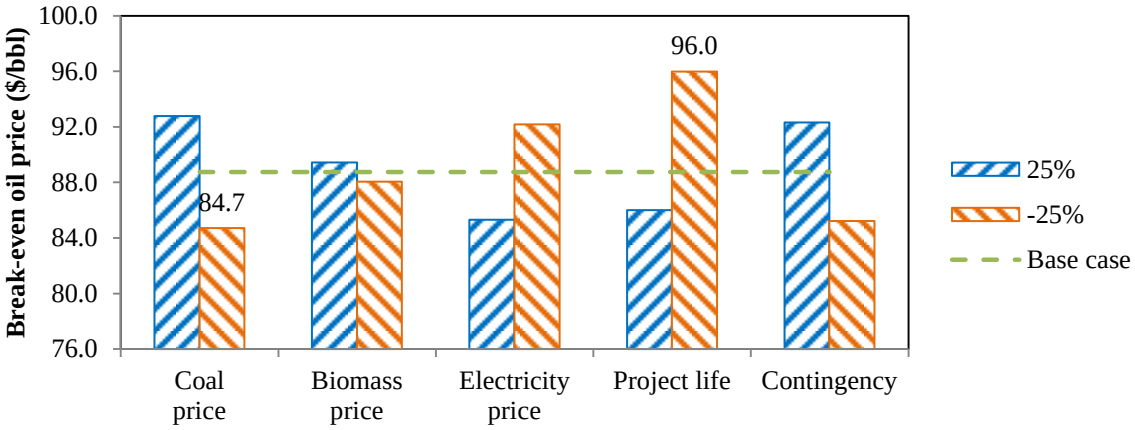

Figure 7.6 Sensitivity studies of the D-CBTL-VT process (10k bbl/day)

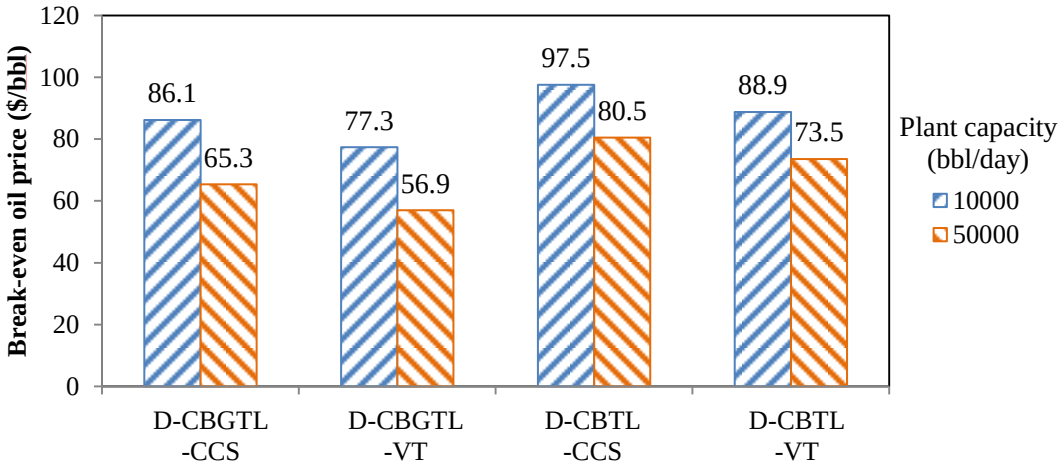

Figure 7.7 Effect of the plant capacity (10k and 50k bbl/day)

7.3.4 Effect of Biomass to Coal Ratio and Extent of CCS

In this study, two levels of biomass to coal weight ratio, 8/92 and 20/80, and two levels of CCS are considered and compared with the direct liquefaction cases without CCS. For the case with low extent of CCS, all CO_2 removed in the hydrogen production and purification unit is sent to the CO_2 compression section preparing for CO_2 pipeline. For the case with high extent of CCS, additional CO_2 is captured from the low pressure sources, such as flue gas, and sent to the CO_2 compression section with the CO_2 captured from the hydrogen plant. The results are shown in Figure 7.8 and Table 7.11. Figure 7.8 indicates that the penalty of CCS increases with the increase in the extent of CCS and decrease in the biomass to coal ratio. Table 7.11 indicates that the CO_2 emission can be significantly reduced even with the low extent of CCS, where no additional CO_2 capture is required. As a result, the BEOP and TPC do not increase considerably if only low extent of CCS is considered. On the other hand, the penalty of CCS per unit of CO_2 capture in the cases with high extent of CCS is higher than that in the cases with low extent of CCS, because not only additional CO_2 needs to be captured but that the additional CO_2 needs to be captured from the low pressure sources significantly increasing the operating cost and capital investment. The results also indicate that the overall cost and the penalty due to CCS decrease with the increase in the biomass content in the feedstock. Due to the higher H/C ratio in the biomass than coal, the hydrogen requirement in the liquefaction reactors gets reduced. As a consequence, the throughput of the hydrogen plant and associated CO_2 emission also gets reduced with the increase in the biomass content. To summarize, addition of more biomass and application of the CCS technology will increase the BEOP of the two processes by about \$8.8/bbl (D-CBGTL) and \$8.6/bbl (D-CBTL).

It is noticed that even with the high extent of CCS and even after taking into account the CO_2 credit due to use of biomass, the D-CBGTL-CCS and D-CBTL-CCS processes with a biomass to coal ratio of 8/92 still have a higher carbon footprint than the petroleum refineries (about 8.12 kg CO_2/GJ product). However, if the biomass to coal ratio increases to 20/80, the CO_2 emission from both D-CBGTL-CCS and D-CBTL-CCS process with high extent of CCS is lower than the petroleum refinery.

Table 7.11 Performance of the direct liquefaction plants with different extent of CCS

Biomass/coal (wt/wt)		8/92			20/80	
Extent of CCS	High	Low	No	High	Low	No
Hydrogen produced from shale gas steam reforming and residues partial oxidation (D-CBGTL)						
Total project cost (MM$)	1162	1112	1080	1123	1044	1024
Internal rate of return (%)	6.0	7.0	7.3	5.9	6.9	7.3
CO_2 emission (kg CO_2/GJ product)	12.0	26.3	53.2	11.5	21.9	47.2
CO_2 emission with biomass credit[(1)] (kg CO_2/GJ product)	9.4	23.7	50.6	5.6	16.0	41.3
Thermal efficiency (HHV, %)	64.3	66.0	66.5	67.6	68.7	69.2
Hydrogen produced from coal/biomass/residues co-gasification (D-CBTL)						
Total project cost (MM$)	1464	1409	1387	1411	1366	1343
Internal rate of return (%)	5.2	5.9	6.2	5.1	5.9	6.1
CO_2 emission (kg CO_2/GJ product)	14.3	27.3	77.4	13.8	23.5	72.7
CO_2 emission with biomass credit[(1)] (kg CO_2/GJ product)	9.9	22.9	73.0	3.2	12.9	62.1
Thermal efficiency (HHC, %)	60.0	61.2	62.1	62.1	63.1	63.6

(1) When biomass credit is accounted, CO_2 produced from biomass is deducted from CO_2 emission, which is the molar flowrate of carbon in the biomass × (1- carbon efficiency of the process) × the molecular weight of CO_2.

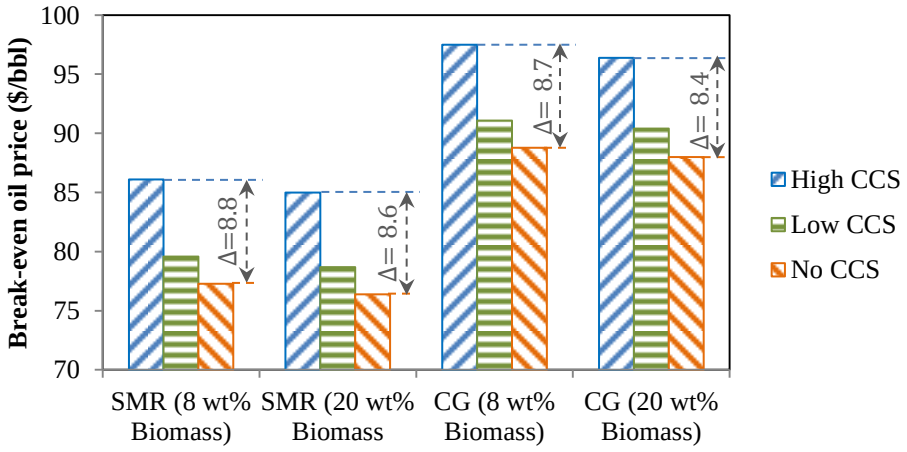

Figure 7.8 Effect of the extent of CCS

7.3.5 Effect of Potential Environmental Credits

In this section, three potential environmental credits are discussed for the D-CBGTL-CCS and D-CBTL-CCS processes with high-level CCS and a biomass to coal ratio of 20/80. For each potential environmental credit, two levels are considered, as shown in Table 7.12. Here, carbon credit is defined as the additional CO_2 captured from the processes with the baseline of

petroleum refineries, which can be traded as a product in a carbon-constrained market. If the renewable/alternative energy certification is considered, the electricity can be sold at a premium. Here, we assume that the electric power generated from biomass qualifies for this credit, which is defined as the total power generated in the combined cycle island multiplied by the biomass HHV percentage in the feedstock. In addition, the federal government may apply lower tax rate to promote the development of renewable or alternative fuel related technologies, denoted as government-subsidized tax credit. The results in Table 7.13 show that the maximum reduction in BEOP is about \$7.1/bbl for the D-CBGTL-CCS process and \$8.8/bbl for the D-CBTL-CCS process if the proposed environmental credits are considered for the cases with a biomass to coal ratio of 20/80 while considering the value of all design and economic parameters the same as the base case. Combined with the sensitivity study shown in Sections 7.3.3 and 7.3.4, the BEOP of the D-CBGTL-CCS and D-CBTL-CCS can be reduced to \$75.5/bbl and \$83.5/bbl at the best case scenario. It is observed that the contribution from the carbon credit and renewable energy certification is not significant because the relatively low biomass percentage in the feed and also due to very high capital and operating costs of the DCL technology. Due to the same reason, the contribution of these two credits is smaller in the D-CBGTL-CCS process than that in the D-CBTL-CCS process.

Table 7.12 Potential environmental credits

Potential environmental credits	Description	High	Low	No
Carbon credit (\$/tonne carbon)	Additional CO_2 captured	30	15	0
Renewable energy certification (\$/MWh)	Electricity from biomass	60	55	50
Government-subsidized tax credit (%)	Incentive tax rate for alternative fuel	30	35	40

Table 7.13 Potential environmental credits for the direct liquefaction plants (10k bbl/day)

Difference in BEOP (\$/bbl)	SMR_CCS		CG_CCS	
Level of the credits	High	Low	High	Low
Carbon credit	-0.2	-0.1	-0.3	-0.2
Renewable energy certification	-0.2	-0.1	-0.5	-0.3
Government-subsidized tax credit	-6.7	-3.1	-8.0	-3.7

7.3.6 Direct vs Indirect Liquefaction Plants

A detailed process and economic model of the I-CBTL plant based on the FT technology was developed in our previous studies using 2014 pricing basis, as shown in Chapter 3 and 4. (Jiang and Bhattacharyya, 2014; 2015; 2016) For fair comparison, previous economic model developed for indirect liquefaction plant with CCS (I-CBTL-CCS) and without CCS (I-CBTL-VT) is updated to the 2015 pricing basis and the same economic parameter listed in Table 7.2 and Table 7.3 of this section except plant contingency. It is noted that 8% of biomass and 10,000 bbl/day capacity are considered for all cases. Because of the difference in sources of CO_2 and their partial pressure, the extent of CO_2 capture is different between the indirect and direct technologies for the cases with the low extent of CCS. (Jiang and Bhattacharyya, 2016) Hence, only the cases with the high extent of CCS and the cases without CCS are considered in this section for fair comparison. For the I-CBTL plants, the plant contingency is set to be 18%, because the technology is more proven and there are more industrial operating experiences than the D-CBTL and D-CBGTL plants. Additionally, the TPC estimation of I-CBTL plants matches well with the industrial data, once 18% plant contingency is applied.

The results are shown in Figure 7.9. The BEOP and EOP of the D-CBTL-CCS and D-CBTL-VT processes are slightly higher than those of the I-CBTL-CCS and I-CBTL-VT processes, while those of the D-CBGTL-CCS and D-CBGTL-VT processes are much lower than the I-CBTL-CCS and I-CBTL-VT processes. It indicates that the direct liquefaction plants are comparatively less competitive than the indirect liquefaction plants even with a higher thermal efficiency, if required hydrogen in the direct liquefaction plants is all produced from gasification. If hydrogen is produced from more efficient and less expensive process, for example shale gas steam reforming, the direct liquefaction plants are more competitive than the indirect liquefaction plants. It is noticed that if the shale gas price is higher, the economic performance of the D-CBGTL-CCS and D-CBGTL-VT processes may be worse than that of the D-CBTL-CCS and D-CBTL-VT processes. Table 7.14 shows that the BEOP for the I-CBGTL-CCS and I-CBGTL-VT processes becomes the same as the I-CBTL-CCS and I-CBTL-VT processes when the price of shale gas increases to $3.70/GJ or $5.38/GJ, respectively.

The results also show that the CCS penalty of indirect liquefaction plants is lower than that of direct liquefaction plants, because additional CO_2 needs to be captured in the direct liquefaction plant to achieve high level of CCS as discussed in Chapter 6 (Jiang and Bhattacharyya, 2016), while the difference between the I-CBTL-CCS and I-CBTL-VT processes is only in the CO_2 compression unit. (Jiang and Bhattacharyya, 2014; 2015; 2016) As mentioned before, the plant contingency is specified to be 24% because the limited commercial experience of the direct liquefaction plants. If the plant contingency is set to be 18%, the same as the indirect liquefaction plant, the BEOP of the D-CBTL-VT processes reduced to \$85.2/bbl lower than that of the I-CBTL-VT process as shown in Figure 7.9, because of reduced capital investment. However, the BEOP of the D-CBTL-CCS is still higher than that of the I-CBTL-CCS process, because of the higher CCS penalty.

Table 7.14 SMR processes versus FT processes (10k bbl/day)

	D-CBGTL-CCS		I-CBTL-CCS	D-CBGTL-VT		I-CBTL-VT
Shale gas price (\$/GJ)	2.25	3.70		2.25	5.38	
Break-even oil price (\$/bbl)	86.1	90.7	90.7	77.3	86.4	86.4

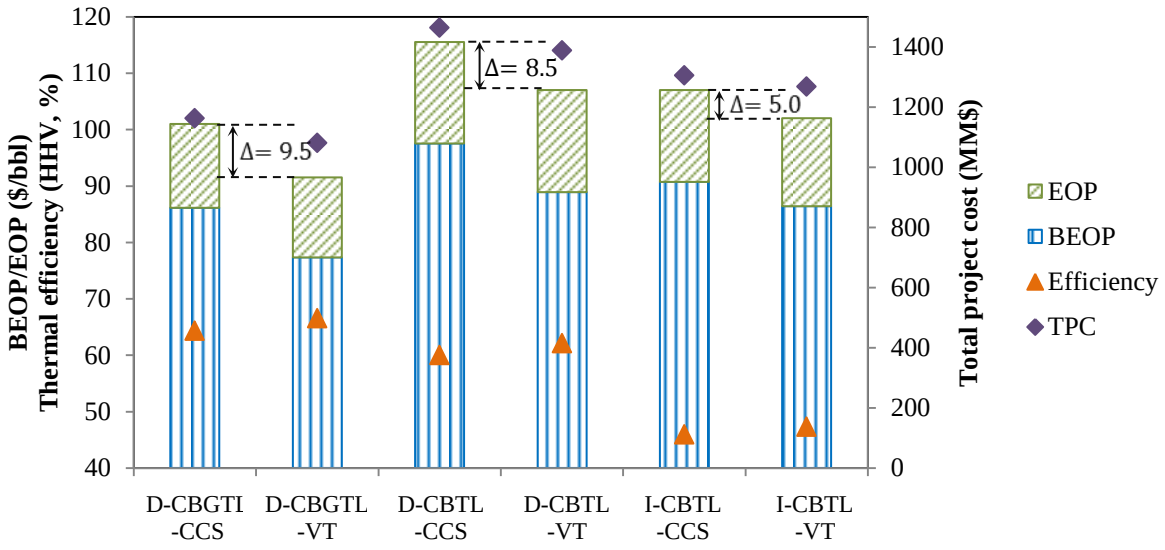

Figure 7.9 Indirect and direct CBTL plants (10k bbl/day)

7.4 Conclusions

In this work, a techno-economic study is conducted for direct liquefaction plants with and without shale gas utilization and CCS. BEOP is evaluated in all sensitivity studies related to technology selection, economic inputs and design parameters, while other key economic measures, including NPV, IRR and EOP, are reported for the base case studies for four different plant configurations. The estimated capital cost is validated by comparing with the data available in the open literature. The results shows that only the large-scale D-CBGTL-VT process, where shale gas is used for hydrogen production and the CO_2 is vented can be profitable due to the extremely low crude oil price. The BEOP of small scale direct CBTL plants without CCS is about $77.3/bbl if hydrogen is produced from shale gas (D-CBGTL-VT) and $88.9/bbl if hydrogen is produced from coal and biomass (D-CBTL-VT). Addition of more biomass and application of the CCS technology will increase the BEOP of the two processes by about $8.8/bbl (D-CBGTL-CCS) and $8.6/bbl (D-CBTL-CCS) if any potential government-subsidized environmental credit is not considered. By comparing with the indirect liquefaction plant with CCS, it is observed that the direct liquefaction plants with CCS is economically better for producing alternative fuels if hydrogen required for liquefaction is produced from a cheap, H_2-rich source that is shale gas. The economic performance of the D-CBGTL-CCS and D-CBGTL-VT processes highly depends on the shale gas price. If CCS is considered, the BEOP from the indirect and direct technologies become the same when the shale gas price increases by about 60% compared to the base case while for the cases without CCS, the shale gas price has to increase by about 140% compared to the base case for the BEOP from both technologies to be the same.

Chapter 8 Techno-economic Analysis of Hybrid Coal-Biomass to Liquids Plants

8.0 Overview

As discussed in Chapters 3 and 6, direct and indirect CBTL plants share a large number of common unit operations, such as coal and biomass pre-processing, gasification for producing syngas, AGR for CO_2 and/or H_2S removal, and the Claus unit for sulfur recovery. The raw syncrude from direct liquefaction plants using CTSL predominantly contains aromatics and naphthenes, with high level of heteroatoms. The raw syncrude from indirect liquefaction plants using slurry FT reactors predominantly contains olefins and paraffins with negligible level of heteroatoms. Thus, in the hybrid indirect-direct CBTL plants, the raw syncrude from direct and indirect liquefaction plants have the potential to produce on-spec fuels with reduced severity and amount of upgrading through proper blending.

8.1 Conceptual Design and Modeling

The BFDs of the hybrid liquefaction plants with CCS are shown in Figure 8.1 and 8.2. In the process without shale gas utilization (H-CBTL-CCS), a portion of the pre-processed coal and biomass is fed to the gasification unit to produce syngas while the remaining is fed to the CTSL unit to produce syncrude directly. After the H_2/CO ratio is adjusted by the WGS reactors, syngas is either sent to the hydrogen recovery unit or to the FT synthesis reactors. The split ratio of syngas is determined by the hydrogen balance, while the split ratio of coal and biomass is determined by the specified direct and indirect syncrude blending ratio. Hydrogen can be produced by shale gas steam reforming instead of co-gasification (H-CBTL-CCS) with less cost and higher efficiency in the hybrid processes (H-CBGTL-CCS), as shown in Figure 8.2. If shale gas utilization is considered, all syngas produced in the gasification unit is sent to the FT synthesis unit, while all syngas produced in the shale gas steam reforming unit is sent to the hydrogen recovery unit.

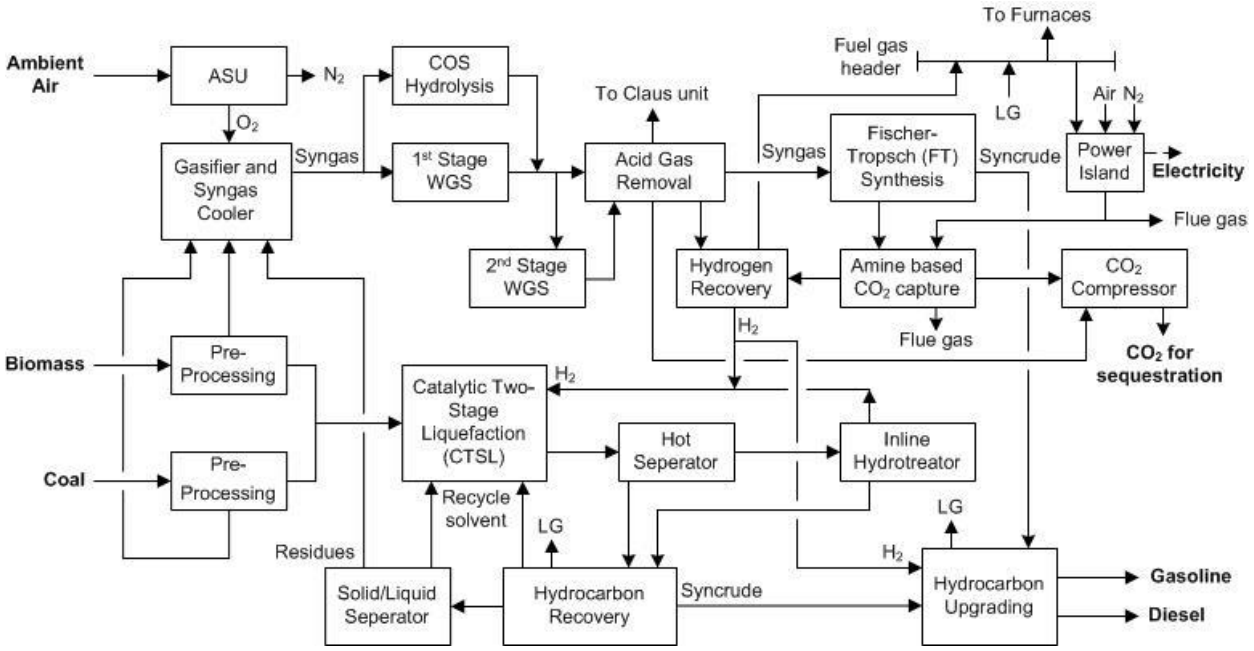

Figure 8.1 BFD of the H-CBTL-CCS plant

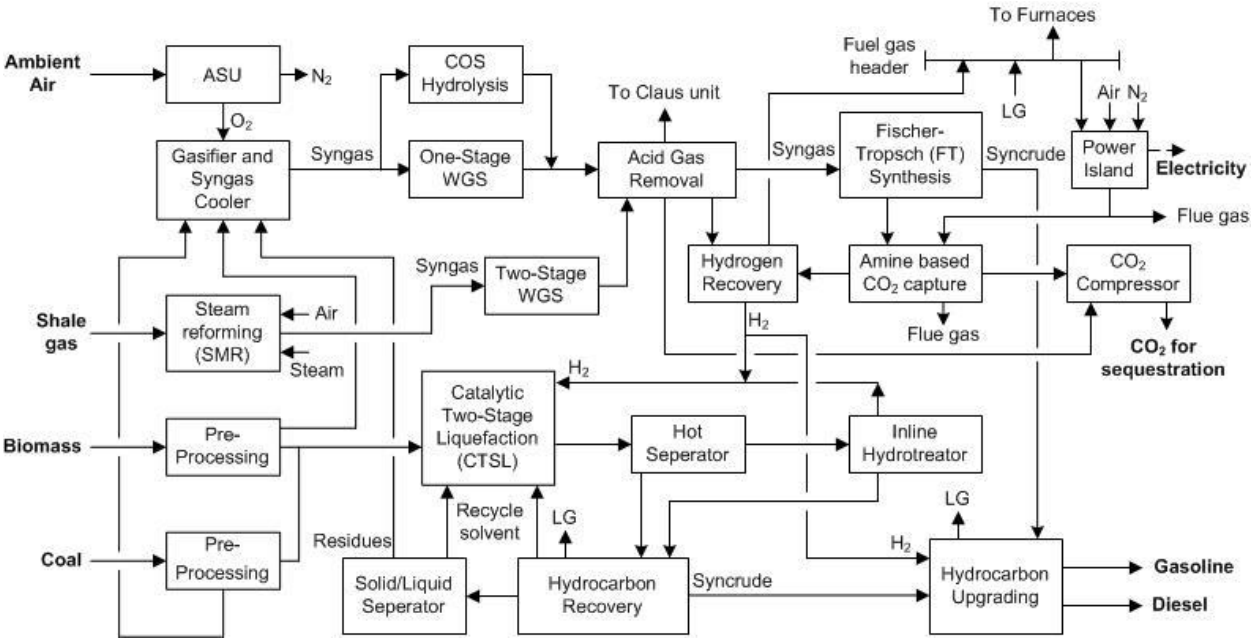

Figure 8.2 BFD of the H-CBGTL-CCS plant

In this study, the hybrid liquefaction plants with CCS have been modeled in Aspen Plus V7.3.2. Table 8.1 summarized the modeling approach of the key equipment in the hybrid liquefaction processes. The detailed modeling approach has been discussed in Chapters 3 and 6 and our

previous publications. (Jiang and Bhattacharyya, 2014; 2015; 2016) Most of the models are developed using Aspen Plus blocks and validated by comparing with the experimental data available in the open literature. Yield models based on the experimental data are developed for the biomass gasification, FT reactor and some of the hydrocarbon upgrading reactors in Excel. Aspen User2 blocks are used to integrate the Excel models with other blocks in Aspen Plus. A stage-by-stage model is developed in Matlab to estimate the performance of the steam turbine.

Table 8.1 Summery of the process model of hybrid liquefaction plants

Section/Block	Simulation Approach	Property Model/Operating Conditions
Liquefaction and hydrocarbon recovery		Peng-Robinson
Liquefaction	Close-coupled yield model for two ebullated-bed reactors in series	1st stage: 407 °C, 22.1 MPa 2nd stage: 432 °C, 20.7 MPa
Inline hydrotreating	Yield model	370 °C, 17.2 MPa
Distillation columns	PetroFrac	Atmospheric column: 2.8 bar Vacuum column: 0.1 bar
ROSE-SR	Component separator for settlers and flash vessel for deashing solvent separator	Solvent/solid weight ratio: 3 1st stage settler: 300 °C, 55 bar 2nd stage settler: 370 °C, 54.5 bar
Fischer-Tropsch synthesis loop		Peng-Robinson/ ELECNRTL-RK
Fischer-Tropsh	Yield model using modified correlation from open literatures and ASF theory for conversion and product distribution	Fe-catalyzed slurry bed reactor at 2000 kPa, 257 °C
Post-FT CO_2 removal	RadFrac with equilibrium stage for physical absorption and rate-based stage for chemical absorption	Absorber at 1965 kPa, 38 °C (MEA or MDEA/PZ) or 2 °C (Selexol)
Autothermal reformer	PFR model in Aspen Plus with power law kinetics	1965 kPa, adiabatic with outlet temperature of 982 °C
Product upgrading		Peng-Robinson
Hydroprocessing	Same as inline hydrotreater	
Isomerization	Yield model	Hydrogen/oil: 0.14 wt% Targeted RON: 83
Catalytic reforming	Yield model	Targeted RON: 95
Syngas Production		Peng-Robinson/ELECNRTL-RK
Pre-reformer	RGibbs model	Adiabatic; Inlet: 510 °C, 27 bar
Steam reformer	RGibbs for reformer and Rstoic with combustion reactions for furnace	Reformer: 815 °C, 25 bar Reformer furnace: 955 °C
Gasification	RGibbs model	1315 °C, 56 bar
Water gas shift	Plug flow reactor	CO conversion: 95%
Acid gas removal and hydrogen recovery		ELECNRTL/PC-SAFT

Chemical absorption	RadFrac model with rate-based stages and reaction kinetics	Absorber: 40 ^{o}C Regenerator: 1.7 bar
Physical absorption	RadFrac model with equilibrium stages	Solvent chilling: 2 ^{o}C
Hydrogen recovery	Polybed PSA process modeled as component separator	Adsorption: 26.2 bar Desorption: 6.9 bar
CO_2 compression	Multistage compressor	15.3 MPa for CO_2 pipeline
Power island		Ideal/IAPWS-95
Combined cycle	Stage-by-stage estimation of steam turbine and Aspen Plus standard models for others	Triple-pressure HRSG with reheat: 114/25/4 bar

8.2 Optimal Fuel Blending

Technologies considered for refining different syncrude are listed in Table 8.2 (Jiang and Bhattacharyya, 2015; 2016), while properties and compositions of raw syncrude and refined syncrude are listed in Table 8.3 and Table 8.4. (de Klerk and Furimsky, 2010; Wu et al.,2015; Comolli et al, 1995) Because the hydrotreated naphtha from the indirect liquefaction route mainly consists of n-paraffins, it is low in octane number and is a poor feed to the catalytic reforming unit with low reformate yield of about 87%. (de Klerk and Furimsky, 2010; Jiang and Bhattacharyya, 2015) On the other hand, straight run naphtha from the direct liquefaction route is rich in naphthenes and aromatics, and therefore high in octane number and is an excellent feed to the catalytic reforming unit with high reformate yield of about 93%. (Comolli et al, 1995; Fahim et al., 2010; Gary and Handwerk, 2001; Jiang and Bhattacharyya, 2016) For the diesel pool, the straight run diesel from the indirect liquefaction route is extremely low in sulfur and high in cetant number/index, because most of the sulfur in the coal and biomass is removed before being sent to the Fisher-Tropsch synthesis unit. In addition, aromatics yield of the Fisher-Tropsch synthesis unit is negligible, while the straight run diesel from the direct liquefaction route has relatively poor properties and requires further upgrading.

Table 8.2 Syncrude refinery technologies

	Indirect CBTL	Direct CBTL
whole syncrude	integrated hydrotreating	inline hydrotreating
wax	wax hydrocracking	
light naphtha	isomerization (GTC's Isomalk2)	isomerization (GTC's Isomalk2)

heavy naphtha	catalytic reforming (UOP's CCR)	catalytic reforming (UOP's CCR)
diesel		diesel hydrotreating

Table 8.3 Properties and compositions of raw and refined syncrudes (gasoline pool)

	Density (kg/m^3)	RON	MON	[R+M]/2	Sulfur (ppm, wt)	Aromatics (vol%)	Olefin (vol%)
Indirect liquefaction							
straight run naphtha*	680	55	50	52.5	trace	trace	
refined light naphtha	625	90	87	88.5	0	0	0
refined heavy naphtha	745	95	87	91	0	61	1.0
straight run heavy naphtha	720	45	40	42.5	0	0	1.0
heavy naphtha from wax hydrocracking unit	725	84	76	80	0	2	40
Direct liquefaction							
straight run naphtha	765	70	64	67	20	19	
refined light naphtha	660	90	87	88.5	20	0	0
refined heavy naphtha	790	95	87	91	20	66	0.2
US standards (ASTM D4814; CA RFG; 40 CFR 80)							
maximum					20	35	
minimum				87			

*After integrated hydrotreating

Table 8.4 Properties of raw and refined syncrudes (diesel pool)

	Density (kg/m^3)	Cetane index	Sulfur (ppm, wt)	Aromatics (vol%)
Indirect liquefaction				
straight run diesel	775	73.3	0	0
diesel from wax hydrocracking	789	73	0	2
Direct liquefaction				
straight diesel	850	33.8	77.5	23.2
refined diesel	880	38.1	10	8.4
US standards (ASTM D975)				
maximum	876		15	35
minimum		40		

Because of the difference in the properties between syncrude from indirect and direct liquefaction routes, it is possible to reduce the penalty of hydrocarbon upgrading units by optimal blending. By blending, less amount of heavy naphtha from indirect liquefaction is

required to be sent to the catalytic reforming unit to achieve the gasoline standard, where less amount of diesel from direct liquefaction is required to be sent to the hydrotreating unit to achieve the diesel standard. It is observed from Table 8.3 and Table 8.4 that the octane number ([R+M]/2) of gasoline and Sulfur content in diesel are the two hardest standards to achieve. Hence, in this study, the percentage of heavy naphtha from indirect liquefaction to the catalytic reforming unit (CCR %) is manipulated to satisfy the octane number standard of gasoline, while the percentage of straight run diesel from the direct liquefaction unit to the diesel hydrotreating unit (HDT %) is manipulated to satisfy the sulfur content limitation of diesel. Table 8.5 provides the results of smart blending with different indirect to direct syncrude weight ratio. Table 8.5 shows that the upgrading cost saved in the cases with any blending ratio in between 0/100 and 100/0 is larger than of the pure indirect liquefaction process (100/0) and the pure direct liquefaction process (100/0), which indicates that the hybrid liquefaction process does reduce the cost of the downstream syncrude upgrading process.

Table 8.5 Smart blending of indirect and direct syncrude

Indirect/Direct	0/100	10/90	20/80	30/70	40/60	50/50
CCR%	0	22.3	58.0	69.9	75.9	79.5
HDT%	92.8	90.6	88.5	85.4	81.3	75.5
Cost saved* (MM$/yr)	0.23	0.64	0.70	0.76	0.83	0.91
Gasoline pool						
Density (kg/m^3)	725	719	714	710	707	704
[R+M]/2	89.5	87	87	87	87	87
Sulfur (ppm, wt)	20	16.8	14.1	11.8	9.6	7.6
Aromatics (vol%)	33.2	28.9	29.0	29.1	29.2	29.3
Diesel pool						
Density (kg/m^3)	852	846	839	833	826	819
Cetane index	37.8	40.8	44	47.2	50.5	53.9
Sulfur (ppm, wt)	15	15	15	15	15	15
Aromatics (vol%)	9.5	8.9	8.4	7.9	7.3	6.7
Indirect/Direct	60/40	70/30	80/20	90/10	100/0	Standards
CCR%	81.8	83.6	84.8	85.8	86.6	
HDT%	66.9	52.6	23.9	0	0	
Cost saved* (MM$/yr)	0.99	1.10	1.29	1.31	0.56	
Gasoline pool						
Density (kg/m^3)	701	698	696	694	692	
[R+M]/2	87	87	87	87	87	>87

Sulfur (ppm, wt)	5.8	4.2	2.7	1.3	0	<20
Aromatics (vol%)	29.4	29.5	29.5	29.6	29.6	<35
Diesel pool						
Density (kg/m^3)	812	804	797	787	775	<876
Cetane index	57.4	61	64.8	68.9	73.3	>40
Sulfur (ppm, wt)	15	15	15	9.7	0	<15
Aromatics (vol%)	6.1	5.3	4.9	3.2	0.7	<35

*In the base case, all heavy naphtha is sent to the catalytic reforming unit, and entire diesel cut is sent to the diesel hydrotreating unit. Equipment life is assumed to be 10 years to annualize the capital cost. The capital and utility cost of upgrading units are available in the open literature. (Jiang and Bhattacharyya, 2016; Bechtel, 1998)

8.3 Economic Analysis

The economic analysis is performed using APEA V8.4 with default pricing basis of 2013 dollars for estimating capital cost of equipment. The steady state model in Aspen Plus is directly 'exported' to APEA with information of streams and equipment items as well as the energy and material balance. Every equipment item is mapped to the appropriate project component in APEA. Table 8.6 lists the price of raw materials and products, labor and product for base case scenario in 2015 pricing basis. The prices of coal and crude oil are obtained from the US EIA website. The type of coal used in this study is Illinois No.6 coal, while the crude oil prices used for comparison is the refiner acquisition cost of crude oil in the PADD1 area (the east coast of US). Table 8.7 lists the values of investment parameters in APEA for profitability analysis. Detailed techno-economic analysis approach can be found in Chapters 4 and 7.

Table 8.6 Cost of raw material, labor and product (base case)

	Cost		Cost
Coal ($/ton)	34.0	Supervisor ($/hr)	80
Wood chip ($/dry ton)	61.5	Crude oil price ($/bbl)	60
Shale gas ($/GJ)	2.25	Electricity ($/MWh)	50
Operator ($/hr)	50		

Table 8.7 Investment parameters (base case)

Parameter	Value	Parameter	Value
Start date of engineering	2015	Utility escalation (%/year)	1
Contingency percent	21%	Working capital percentage (%/FCI)	12
Number of years for analysis	30	Operating charges (% of labor costs)	25

Tax rate	40%	Plant overhead	50%
Interest rate/desired rate of return	10%	General & administrative expenses	8%
Project capital escalation (%/year)	1	Length of start-up period (weeks)	40
Products escalation (%/year)	1	Operating hours per period	8000
Raw material escalation (%/year)	1	Construction time	2.5 yr

8.4 Results and Discussion

In this study, the material and energy balance of the hybrid liquefaction processes is discussed in Section 8.4.1, while the corresponding economic performance is reported in Section 8.4.2. Finally, the hybrid liquefaction processes are compared with the indirect and direct liquefaction processes in Section 8.4.3. In the following case studies, half of the coal and biomass feedstocks is sent to the direct liquefaction route for producing syncrude, while the remaining is sent to the gasification unit and then the FT synthesis unit. It should be noted that the amount of coal and biomass required in the gasification unit for hydrogen production is not accounted for while calculating the direct/indirect split ratio in the hybrid process in this study.

8.4.1 Material and Energy Balance of the Hybrid Liquefaction Processes

Based on the steady state simulation results generated in Aspen Plus, material and energy balances in the hybrid liquefaction processes with shale gas utilization (H-CBGTL-CCS) and without shale gas utilization (H-CBTL-CCS) are shown in Table 8.8 and Table 8.9, respectively. As shown in Table 8.8 and Table 8.9, production of hydrogen from shale gas can increase the carbon and thermal efficiency and decrease the CO_2 emission of the hybrid liquefaction processes, which is similar to the direct liquefaction processes. The thermal and carbon efficiency of the H-CBGTL-CCS process is 56.5% and 43.2%, respectively, which are in between the I-CBTL-CCS and the D-CBGTL-CCS processes. The efficiency of the H-CBTL-CCS process is 55.7% and 38.2%, respectively, which are in between the I-CBTL-CCS and the D-CBTL-CCS processes, as expected.

Table 8.8 Material and energy balance of H-CBGTL-CCS plant (10k bbl/day)

	Flowrate	HHV (%)	Carbon (%)
Feedstock			
Coal	136.3 tonne/hr	80.5	85.1

Biomass	12.7 tonne/hr	4.4	5.0
Shale gas	14.8 tonne/hr	15.1	9.9
Product			
Fuel	10000 bbl/day	50.4	43.2
Power	84.9 MW	6.1	
Efficiency		56.5	43.2
CO_2 Emission	14.3 kg CO_2/GJ		

Table 8.9 Material and energy balance of H-CBTL-CCS plant (10k bbl/day)

	Flowrate	HHV (%)	Carbon (%)
Feedstock			
Coal	166.0 tonne/hr	94.8	94.5
Biomass	15.5 tonne/hr	5.2	5.5
Shale gas	N/A	N/A	N/A
Product			
Fuel	10000 bbl/day	49.3	38.2
Power	91.5 MW	6.4	
Efficiency		55.7	38.2
CO_2 Emission	15.6 kg CO_2/GJ		

8.4.2 Economic Performance of Hybrid Liquefaction Processes

The results obtained from APEA are shown in Table 8.10 for the small scale hybrid liquefaction processes (10k bbl/day) with a biomass to coal weight ratio of 8/92 and a high extent of CCS. A sensitivity study is conducted by considering $\pm$25% changes in the key economic parameters for both hybrid liquefaction processes as shown in Figure 8.3 and Figure 8.4. The results indicate that the BEOP of the H-CBGTL-CCS process is in between \$91.01/bbl and \$101.73/bbl, while that of the H-CBTL-CCS process is in between \$96.17/bbl and \$108.65/bbl for small scale operation. As shown in Table 8.10, even though the thermal and carbon efficiency of the hybrid liquefaction processes is in between the indirect and direct liquefaction processes, the BEOP of the hybrid liquefaction processes is higher than that of the indirect and direct liquefaction processes, because the complexity of the hybrid liquefaction process results in higher capital investment.

Table 8.10 Economic performance of hybrid liquefaction processes (10k bbl/day)

Process	H-CBGTL-CCS	H-CBTL-CCS

Thermal Efficiency (HHV, %)	56.5	55.7
Carbon Efficiency (%)	43.2	38.2
CO_2 Emission (kg CO_2/GJ product)	14.2	15.6
Capital investment (MM$)	1473	1593
Internal rate of return (%)	5.6	5.2
Break-even oil price ($/bbl)	94.5	100.6

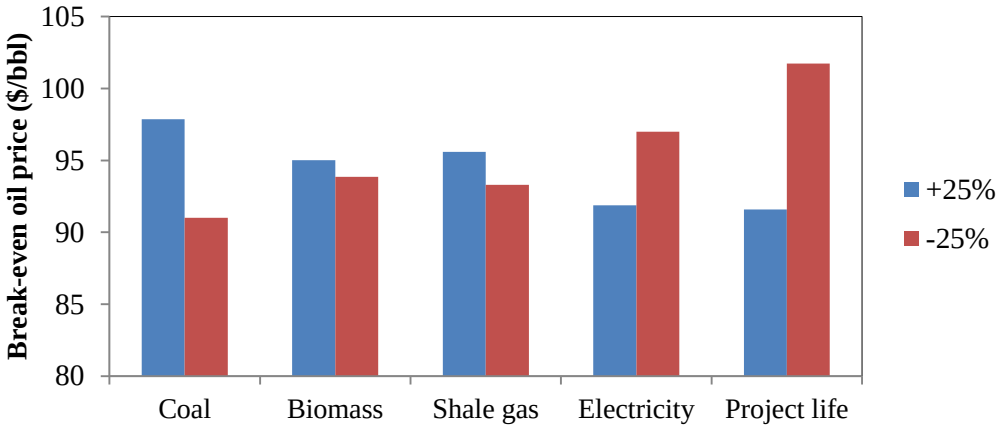

Figure 8.3 Sensitivity studies of the H-CBGTL-CCS process (10k bbl/day)

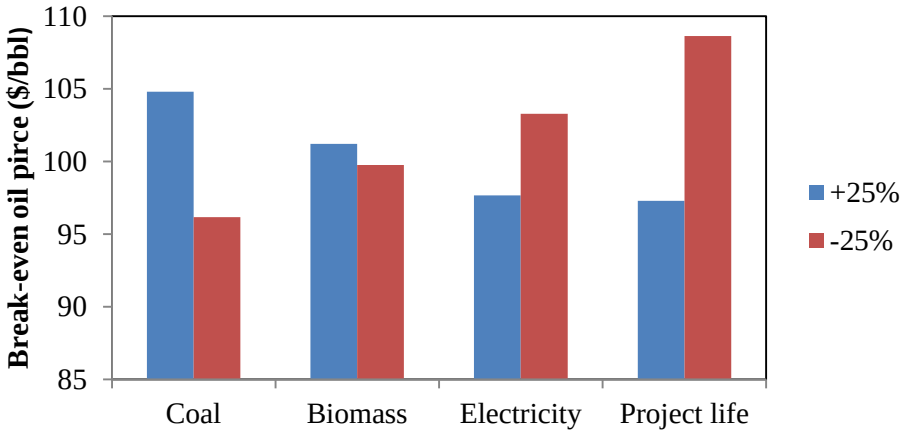

Figure 8.4 Sensitivity studies of the H-CBTL-CCS process (10k bbl/day)

8.4.3 Indirect, Direct vs Hybrid Liquefaction Plants

A detailed process and economic model of the I-CBTL-CCS plant based on the FT technology is developed in our previous studies using 2014 pricing basis, as shown in Chapters 3 and 4. (Jiang and Bhattacharyya, 2014; 2015; 2016) Detailed process and economic models of the D-CBTL-CCS and D-CBGTL-CCS plants are developed in our previous studies using 2015 pricing basis,

as shown in Chapters 6 and 7. (Jiang and Bhattacharyya, 2016) For fair comparison, previous economic model developed for I-CBTL plants is updated to the 2015 pricing basis. It is noted that 8% of biomass and 10,000 bbl/day capacity are considered for all cases.

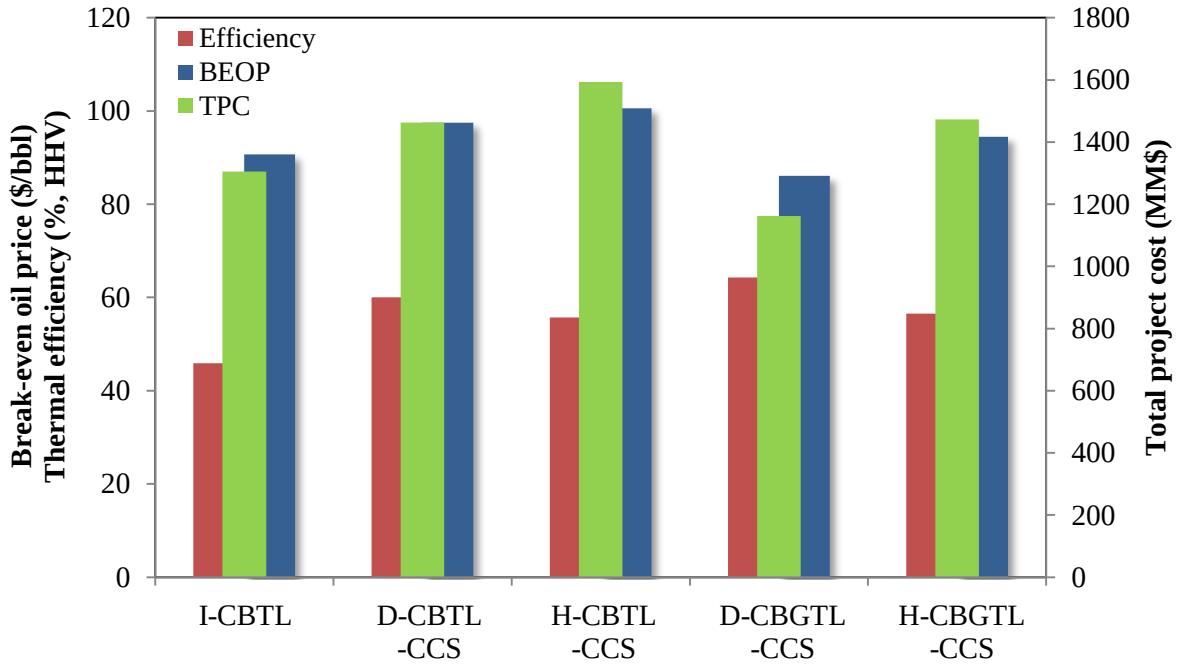

Figure 8.5 Comparison of different liquefaction approach

The results are shown in Figure 8.5. The D-CBGTL-CCS process has the lowest BEOP, because of its high thermal efficiency and low capital investment. The H-CBTL-CCS process has the highest BEOP because of its higher capital investment, even though its thermal efficiency is higher than the I-CBTL-CCS processes. As discussed in Section 8.2, one advantage of hybrid liquefaction process is that it can significantly reduce the penalty of syncrude upgrading section. However, the syncrude upgrading section only contributes about 10% of the overall capital and operating costs in the indirect liquefaction processes (as shown in Section 4.3.2 and Table 4.12), and about 8% of the overall capital and operating costs in the direct liquefaction processes (as shown in Section 7.3.1 and Table 7.9). However, the hybrid liquefaction approach has a more complicated front part, the syncrude production section, which includes gasification, Fischer-Trospch synthesis, and direct liquefaction. None of those technologies is cheap. As a consequence, the total project cost of the hybrid approach is higher than both indirect and direct approach.

8.5 Conclusions

In this work, a techno-economic study was conducted for hybrid liquefaction plants with and without shale gas utilization. Optimal blending of syncrude produced from direct and indirect liquefaction processes was studied. The results show that the capital and operating cost of the hydrocarbon upgrading section can be significantly reduced in the hybrid indirect-direct liquefaction process. However, the complicity of the syncrude production section results in a higher overall capital investment. Therefore, the BEOP of the H-CBGTL-CCS process is higher than both the I-CBTL-CCS process and the D-CBGTL-CCS process, while the BEOP of the H-CBTL-CCS process is higher than both the I-CBTL-CCS process and the D-CBTL-CCS process. The overall thermal efficiency of all liquefaction approach is ranked as following: D-CBGTL-CCS > D-CBTL-CCS > H-CBGTL-CCS > H-CBTL-CCS > I-CBTL-CCS. The TPC of all liquefaction approach is ranked as following: H-CBTL-CCS > H-CBGTL-CCS > D-CBTL-CCS > I-CBTL-CCS > D-CBGTL-CCS. The BEOP of all liquefaction approach is ranked as following: H-CBTL-CCS > D-CBTL-CCS > H-CBGTL-CCS > I-CBTL-CCS >D-CBGTL-CCS.

Chapter 9 Conclusions

In this work, a techno-economic study conducted in Aspen Process Economic Analyzer environment for indirect, direct, and hybrid CBTL plants with CCS using high fidelity system-level and equipment-level models developed in Aspen Plus, Aspen Custom Modeler, Exchanger Design and Rating, Matlab and Excel. The objective is to utilize the computational modeling tools to analyze the effects of biomass, shale gas utilization and CCS application on the overall thermal efficiency and economic performance of different liquefaction technologies. All case studies have been conducted for indirect, direct and hybrid CBTL plants were summarized in Table 9.1 including sensitivity studies of different biomass type, coal/biomass ratio and other key design parameters. More details can also been found in previous chapters and our peer-reviewed publications listed in Appendix F.

For the indirect CBTL plant, following conclusions can be made from the process and economic models: (1) the comparison between the three post-FT CO_2 removal technologies shows that the MDEA/PZ CO_2 removal technology has lesser overall penalty than the Selexol and MEA CO_2 removal technologies; (2) low steam/carbon ratio in the ATR inlet is prefered in FT application as a high H_2/CO ratio in the ATR outlet would result in higher penalty for CCS; (3) the integrated hydrotreating approach can reduce the utility and capital investment in the product upgrading section; (4) the thermal efficiency is found to increase with the decrease in the biomass/coal ratio, the increase in the H_2/CO ratio in the FT inlet stream and the decrease in the extent of CCS; (5) with 2014 pricing basis, the BEOP is found to be between \$88/bbl to \$106/bbl of a small scale I-CBTL-CCS plant (10k bbl/day), and between \$72/bbl to \$86/bbl of a large scale I-CBTL-CCS plant (50k bbl/day) considering $\pm$ 25% changes in the major project economic inputs. (6) the BEOP of the I-CBTL-CCS increases with a decreasing H_2/CO ratio in the FT inlet steam, an increasing biomass/coal ratio and a decreasing extent of CCS; (7) utilizing torrefied biomass can increase the thermal efficiency and decrease the BEOP of the indirect liquefaction processes.

For the direct CBTL plant, following conclusions can be made from the process and economic models: (1) a high-fidelity PDE-based model has been developed for the three-phase direct liquefaction reactor in Aspen Custom Modeler, which can successfully predict the performance of liquefaction reactor; (2) utility consumption in the liquefaction and product recovery section can be reduced by 52% through heat integration; (3) the carbon efficiency of the D-CBTL plant without shale gas utilization is 43.5%, which is 7.1% higher than the I-CBTL plant with a biomass/coal weight ratio of 8/92, which can be increased to 53.9% if shale gas is utilized for hydrogen production in the D-CBGTL plant; (4) carbon and thermal efficiencies of the direct liquefaction plant are found to increase with the biomass/coal ratio regardless of the hydrogen source, because the higher H/C ratio in biomass than in coal reduces hydrogen consumption in the liquefaction unit; (5) the D-CBGTL plant with shale gas utilization has the best performance in terms of carbon and thermal efficiency among with the I-CBTL plant and the D-CBTL plant; (6) the BEOP of small scale direct CBTL plants without CCS is about $77.3/bbl if hydrogen is produced from shale gas (D-CBGTL-VT) and $88.9/bbl if hydrogen is produced from coal and biomass (D-CBTL-VT). Addition of more biomass and application of the CCS technology will increase the BEOP of the two processes by about $8.8/bbl (D-CBGTL-CCS) and $8.6/bbl (D-CBTL-CCS).

For the hybrid CBTL plant, following conclusions can be made from the process and economic models: (1) the optimal blending of syncrude produced from direct and indirect liquefaction processes can significantly reduce the capital and operating cost of the hydrocarbon upgrading section of the hybrid liquefaction process; (2) utilization of shale gas can also help to reducing the BEOP of the hybrid liquefaction approach; (3) total project cost of the hybrid approach is higher than both indirect and direct approach because of the complicity and high investment of the syncrude production section, which leads to the highest BEOP among all different liquefaction approaches.

To summarize, adding biomass can reduce the BEOP of the direct liquefaction approach because it and help to reduce the hydrogen demand in liquefaction reactors. However, adding biomass to the indirect liquefaction process would not help in terms of the economic performance because of its lower energy density. Utilization of low cost shale gas can reduce the BEOP price of both

direct and hybrid liquefaction routes. The overall thermal efficiency of all liquefaction approaches is ranked as following: D-CBGTL-CCS > D-CBTL-CCS > H-CBGTL-CCS > H-CBTL-CCS > I-CBTL-CCS. The TPC of all liquefaction approach is ranked as following: H-CBTL-CCS > H-CBGTL-CCS > D-CBTL-CCS > I-CBTL-CCS > D-CBGTL-CCS. The BEOP of all liquefaction approach is ranked as following: H-CBTL-CCS > D-CBTL-CCS > H-CBGTL-CCS > I-CBTL-CCS >D-CBGTL-CCS.

Table 9.1 Summary of case studies

Cases	1	2	3	4	5	6	7
Configuration	indirect	indirect	indirect	indirect	indirect	indirect	indirect
Pricing basis	2014	2014	2014	2014	2014	2014	2014
Capacity (bbl/day)	10000	10000	10000	10000	10000	10000	10000
Biomass type	wood	wood	wood	wood	wood	wood	bagasse
Biomass/coal	8/92	8/92	8/92	8/92	8/92	8/92	8/92
Shale gas utilization	N/A	N/A	N/A	N/A	N/A	N/A	N/A
H_2/CO in FT inlet	2.0	2.0	2.0	2.0	1.5	1.0	2.0
Hydrotreating	integrated	integrated	integrated	separated	integrated	integrated	integrated
Extent of CCS	high	high	high	high	high	high	high
MP/LP solvent	Selexol	MEA	MDEA/PZ	MDEA/PZ	MDEA/PZ	MDEA/PZ	MDEA/PZ
Efficiency (HHV, %)	40.8	45.7	45.9	59.5	43.9	40.8	46.6
BEOP ($/bbl)	103.6	95.7	95.5	96.0	98.1	106.5	95.9
Cases	8	9	10	11	12	13	14
Configuration	indirect	indirect	indirect	indirect	indirect	indirect	indirect
Pricing basis	2014	2014	2014	2014	2014	2014	2014
Capacity (bbl/day)	30000	50000	10000	10000	10000	10000	10000
Biomass type	wood	wood	wood	wood	wood	wood	wood
Biomass/coal	8/92	8/92	8/92	8/92	8/92	15/85	20/80
Shale gas utilization	N/A	N/A	N/A	N/A	N/A	N/A	N/A
H_2/CO in FT inlet	2.0	2.0	2.0	2.0	2.0	2.0	2.0
Hydrotreating	integrated	integrated	integrated	integrated	integrated	integrated	integrated
Extent of CCS	high	high	medium	low	no	high	high
MP/LP solvent	MDEA/PZ	MDEA/PZ	MDEA/PZ	MDEA/PZ	MDEA/PZ	MDEA/PZ	MDEA/PZ
Efficiency (HHV, %)	45.9	45.9	46.3	46.6	47.3	44.5	43.7
BEOP ($/bbl)	89.8	77.8	94.6	93.6	91.3	98.6	99.5
Cases	15	16	17	18	19	20	21
Configuration	indirect	indirect	indirect	direct	direct	direct	direct
Pricing basis	2015	2015	2015	2015	2015	2015	2015
Capacity (bbl/day)	10000	50000	10000	10000	50000	10000	10000
Biomass type	wood	wood	torrefied	wood	wood	wood	wood
Biomass/coal	8/92	8/92	8/92	8/92	8/92	8/92	8/92
Shale gas utilization	N/A	N/A	N/A	yes	yes	no	no

H_2/CO in FT inlet	2.0	2.0	2.0	N/A	N/A	N/A	N/A
Hydrotreating	integrated	integrated	integrated	N/A	N/A	N/A	N/A
Extent of CCS	high	high	high	high	no	high	no
MP/LP solvent	MDEA/PZ	MDEA/PZ	MDEA/PZ	MDEA/PZ	MDEA/PZ	MDEA/PZ	MDEA/PZ
Efficiency (HHV, %)	45.9	45.9	47.5	64.3	66.5	60.0	62.1
BEOP ($/bbl)	90.7	71.1	89.8	86.1	77.3	97.5	88.9
Cases	22	23	24	25	26	27	28
Configuration	direct	direct	direct	direct	direct	direct	direct
Pricing basis	2015	2015	2015	2015	2015	2015	2015
Capacity (bbl/day)	50000	50000	50000	50000	10000	10000	10000
Biomass type	wood	wood	wood	wood	wood	wood	wood
Biomass/coal	8/92	8/92	8/92	8/92	8/92	20/80	20/80
Shale gas utilization	yes	yes	no	no	yes	yes	yes
H_2/CO in FT inlet	N/A	N/A	N/A	N/A	N/A	N/A	N/A
Hydrotreating	N/A	N/A	N/A	N/A	N/A	N/A	N/A
Extent of CCS	high	no	high	no	low	high	low
MP/LP solvent	MDEA/PZ	MDEA/PZ	MDEA/PZ	MDEA/PZ	MDEA/PZ	MDEA/PZ	MDEA/PZ
Efficiency (HHV, %)	64.3	66.5	60.0	62.1	66.0	67.6	68.7
BEOP ($/bbl)	65.3	56.9	80.5	73.5	86.1	85.0	78.7
Cases	29	30	31	32	33	34	35
Configuration	direct	direct	direct	direct	direct	hybrid	hybrid
Pricing basis	2015	2015	2015	2015	2015	2015	2015
Capacity (bbl/day)	10000	10000	10000	10000	10000	10000	10000
Biomass type	wood	wood	wood	wood	wood	wood	wood
Biomass/coal	20/80	8/92	20/80	20/80	20/80	8/92	8/92
Shale gas utilization	yes	no	no	no	no	yes	no
H_2/CO in FT inlet	N/A	N/A	N/A	N/A	N/A	N/A	N/A
Hydrotreating	N/A	N/A	N/A	N/A	N/A	N/A	N/A
Extent of CCS	no	low	high	low	no	high	high
MP/LP solvent	MDEA/PZ	MDEA/PZ	MDEA/PZ	MDEA/PZ	MDEA/PZ	MDEA/PZ	MDEA/PZ
Efficiency (HHV, %)	69.2	61.2	62.1	63.1	63.6	56.5	55.7
BEOP ($/bbl)	76.4	91.1	96.4	90.4	88.0	94.5	100.6

Chapter 10 Future Work

Because of the high delivered cost and low energy density, biomass does not significantly benefit the CBTL process according to the techno-economic analysis presented in this study. Biomass is a carbon neutral energy resource, and therefore can reduce the GHG emissions of energy processes. (Gray et al., 2007) To further analyze the advantage of biomass utilization, a cradle-to-grave life cycle assessment (LCA) will be helpful. The LCA method has been considered to analyze GHG emissions since 1970s. Many studies have been conducted on LCA of alternative fuels produced from biomass or a mixture of biomass and other fossil fuels. (Kumar and Murthy, 2012) However, barely any of those studies were conducted based on a high-fidelity process and economic models as the work presented in this dissertation. A combination of the presented techno-economic studies and LCA method will improve the current work in the area of coal-biomass to liquids.

In this work, only chemical absorptions (MEA and MDEA/PZ) and physical absorptions (Selexol) are considered for carbon capture. Other than the Selexol technology, Rectisol technology can also been considered to selectively capture CO_2 and H_2S from the syngas produced from gasification unit. Methanol used in the Rectisol technology has a better acid gas solubility than the DEPG used in the Selexol solvent. However, the lower chilling temperature required in the Rectisol technology may lead to a higher operating costs in comparison to the Selexol technology. Final selection can be only made based on rigorous process and economic models. (Mohammed et al., 2014) For capturing CO_2 from medium and low pressure sources, several alternative technologies can be considered other than the standard chemical absorption technologies, such as membranes and adsorption process. Back in 1990s, Bechtel Crop. compared a series of technologies for post-FT CO_2 removal from hydrocarbon-rich systems operating at medium pressure and concluded that inhibited amine MDEA is the best option. (Bechtel, 1993) However, significant effort has been made in improving CO_2 capture technologies, especially in membrane and adsoption technologies, for decades. (Simons et al.,

2009; Kim et al., 2016) Therefore comparison and selection of the medium and low pressure CO_2 capture technologies needs to be updated based on the newly developed technologies.

From the current work, it is concluded that the hybrid liquefaction processes are not promising for producing transportation fuels from biomass and coal. However, only one direct-indirect blending ratio was considered in this study, and the proposed hybrid liquefaction processes have not been optimized. Considering a wide range of blending ratio and implementing plant-wide optimization can possibly further reduce the operating and capital costs of the hybrid liquefaction processes, and therefore might improve the process economics. Plant-wide optimization has been conducted by multiple researchers for energy systems. However, most of those studies were conducted based on simplified process models instead of rigorous models. (Niziolek et al., 2014; Baliban et al., 2013) Based on the high fidelity process models developed in this study, it will be worthwhile to conduct system-level economic optimization using equation orientated approach with the optimization tools available in Aspen Plus and simplified capital cost correlations generated from APEA.

In this work, a simplified yield model has been developed in Excel to estimate the performance of the FT reactor described in Chapter 3. For more accurate prediction of the product distribution during sensitivity study, a high-fidelity PDE-based model of the SBCRs for FT synthesis will be helpful. This model can be developed in ACM platform. The hydrodynamics, kinetics, heat transfer and mass transfer can be modeled rigorously considering axial dispersion in the gas-liquid-solid three-phase SBCRs. Appropriate mass transfer and heat transfer coefficient can be evaluated by correlations available in the open literature. (Sehabiague, et al., 2008; Lemoine et al., 2008; Behkish et al., 2006)

In Chapter 5 of this work, a rigorous mathematical model has been developed for the EBRs used in the CTSL unit in the direct coal liquefaction process. The model is simplified by assuming the mass transfer resistance is negligible because of the high operating temperature and pressure (Lenoard et al., 2015). In the future study, the mass transfer between the slurry phase and the gas phase could be considered to improve the accuracy of the current model. Also, another assumption has been made that the coal slurry is pseudo-homogeneous because of the high

superficial liquid velocity and small particle size. In the future, a more rigorous three-phase model will be helpful to improve the simulation accuracy. In addition, different configuration of the CTSL unit can be considered in the future, such as consideration of a flash separator in between the two EBRs, where some of the gas product is vented and therefore the liquid holdup and utilization of the reactor volume of the second EBR can be increased.

Appendix A ATR Model Validation

The model of the ATR unit is validated by comparing with the data reported in the open literature as shown in Table A.1 through Table A.3. (NETL, 2007; Bechtel, 1993)

Table A.1 Results from the ATR model in comparison to the Bechtel data

	Feed			Product	
Flowrate (kmol/hr)	Recycle	Steam	Oxygen	Model	Reported
H_2O		3068		2378	2365
CO_2	38			944	950
H_2	4507			6088	6114
CO	4316			4017	4018
CH_4	465			205	200
O_2			415		
N_2	1128		2	1128	1128
C_2-C_4	169			0.44	

Table A.2 Results from the ATR model in comparison to NETL's commercial scale ICL plant

	Feed			Product	
Flowrate (kmol/hr)	Recycle	Steam	Oxygen	Model	Reported
H_2O		3367		1814	1904
CO_2	38			269	232
H_2	7289			12855	12679
CO	576			2527	2521
CH_4	2344			548	591
O_2			430		
N_2	4673		8	4673	4673
C_2-C_4	185				

Table A.3 Results from the ATR model in comparison to NETL's small scale ICL plant

	Feed			Product	
Flowrate (kmol/hr)	Recycle	Steam	Oxygen	Model	Reported
H_2O		482		452	456
CO_2	8			48	42
H_2	1251			1454	1455
CO	132			207	216
CH_4	75			23	20
O_2			62		
N_2	644		1	642	644
C_2-C_4	30				

Appendix B Equipment List of the I-CBTL Plant with CCS

Table B.1 Detailed equipment list for the syngas production section (I-CBTL)

Equipment	# Req	# Spares	Model in APEA	Cost source	Material
Biomass handling and drying	1	0	C*	Baliban et al.	N/A
Coal handling and drying	1	0	C*	Baliban et al.	N/A
Air separation unit	1	0	C*	Baliban et al.	N/A
Gasifier (with steam generator)	1	0	C*	Baliban et al.	N/A
Slag separator	1	0	VT CYLINDER	Icarus	SS304
Scrubber	1	0	VT CYLINDER	Icarus	CS
Sour water gas shift reactor	1	0	C*	Baliban et al.	N/A
COS hydrolysis	1	0	C*	Baliban et al.	N/A
Medium pressure steam generator	1	0	HE WASTE HEAT	Icarus	CS
Low pressure steam generator	2	0	HE WASTE HEAT	Icarus	CS
Hydrocarbons preheater	1	0	HE FLOAT HEAD	Icarus	A285C, A214
Boiler feed water heater	1	0	HE FLOAT HEAD	Icarus	A285C, A214
K.O. drum	5	0	VT CYLINDER	Icarus	A516
Fuel gas preheater	1	0	HE FLOAT HEAD	Icarus	A285C, A214
Syngas cooler	2	0	HE FLOAT HEAD	Icarus	A285C, A214
Makeup water heater	1	0	HE FLOAT HEAD	Icarus	A285C, A214
Black water treatment	1	0	VT CYLINDER	Icarus	A516
Black water pump	1	1	CP CENTRIF	Icarus	CS casing
Makeup water pump	1	1	CP CENTRIF	Icarus	CS casing
Multi-stage O_2 compressor	1	0	GC CENTRIF	Icarus	CS casing
Slurry tank	1	1	AT MIXER	Icarus	A285C
Slurry water pump	1	1	CP CENTRIF	Icarus	CS casing
SWS - condenser	1	0	HE FIXED T S	Icarus	A285C, A214
SWS - drum	1	0	HT HORIZ DRUM	Icarus	A516
SWS - reboiler	1	0	RB U TUBE	Icarus	A285C, A214
SWS - reflux pump	1	1	CP CENTRIF	Icarus	CS casing
SWS - tower	1	0	TW TRAYED	Icarus	A516, A285C
SWS bottom pump	1	1	CP CENTRIF	Icarus	CS casing
Claus unit	1	0	C*	Baliban et al.	N/A
Scrubber water pump	1	1	CP CENTRIF	Icarus	CS casing

*Quoted equipment
SWS=sour water stripper

Table B.2 Detailed equipment list for the Selexol unit (I-CBTL)

Description	# Req	# Spares	Model in APEA	Cost source	Material
Tail gas compressor	1	1	GC RECIP MOTR	Icarus	CS casing
NH_3 compressor	1	0	GC CENTRIF	Icarus	SS304
CO_2 absorber	1	0	TW TRAYED	Icarus	A516, A285C

Solvent chilling	2	0	HE FLOAT HEAT	Icarus	A285C, A214
Solvent pre-cooler	1	0	HE FLOAT HEAT	Icarus	A285C, A214
Solvent recycle pump	1	1	CP CENTRIF	Icarus	CS casing
H_2 recovery drum	1	0	VT CYLINDER	Icarus	A516
H_2 recovery compressor	1	0	GC CENTRIF	Icarus	SS316 casing
H_2 recovery cooler	1	0	HE FLOAT HEAT	Icarus	A285C, A214
High pressure flash	1	0	VT CYLINDER	Icarus	A516
Medium pressure flash	1	0	VT CYLINDER	Icarus	A516
Low pressure flash	1	0	VT CYLINDER	Icarus	A516
Rich solvent pump	1	1	CP CENTRIF	Icarus	CS casing
H_2S absorber solvent chilling	1	0	HE FLOAT HEAT	Icarus	A285C, A214
H_2S absorber	1	0	TW TRAYED	Icarus	A516, A285C
Lean solvent pre-cooler	1	0	HE FLOAT HEAT	Icarus	A285C, A214
H_2S concentrator	1	0	TW TRAYED	Icarus	A516, A285C
H_2S concentrator cooler	1	0	HE FLOAT HEAT	Icarus	A285C, A214
Acid gas K.O. drum	1	0	VT CYLINDER	Icarus	A516
Strippered gas compressor	1	0	GC CENTRIF	Icarus	CS casing
Selexol stripper - top product pump	1	1	CP CENTRIF	Icarus	CS casing
Selexol stripper - condenser	1	0	HE FIXED T S	Icarus	A285C, A214
Selexol stripper - drum	1	0	HT HORIZ DRUM	Icarus	A516
Selexol stripper - reboiler	1	0	RB U TUBE	Icarus	A516
Selexol stripper - reflux pump	1	1	CP CENTRIF	Icarus	CS casing
Selexol stripper - tower	1	0	TW TRAYED	Icarus	A516, A285C
Lean solvent pump	1	1	CP CENTRIF	Icarus	CS casing
Lean solvent vessel	1	0	VT CYLINDER	Icarus	A516
Makeup solvent pump	1	1	CP CENTRIF	Icarus	CS casing
CO_2 compressor	1	0	C*	NETL	N/A

*Quoted equipment

Table B.3 Detailed equipment list for the synfuel production and upgrading section (I-CBTL)

Description	# Req	# Spares	Model in APEA	Cost source	Material
Fischer-Tropsch synthesis	1	0	C*	Bechtel	N/A
Autothermal reformer	1	0	C*	Baliban et al.	N/A
Syncrude pump	1	1	CP CENTRIF	Icarus	CS casing
Hydrotreating feed furnace	1	0	FU BOX	Icarus	A213F
Feed/product heat exchanger	1	0	HE FLOAT HEAD	Icarus	A285C, A214
Hydrotreating reactor	1	0	VT MULTI WALL	Icarus	SS347
Product cooler	1	0	HE FLOAT HEAD	Icarus	A285C, A214
High pressure flash	1	0	VT CYLINDER	Icarus	A516
H_2 recycle compressor	1	0	GC CENTRIF	Icarus	SS316
Low pressure flash	1	0	VT CYLINDER	Icarus	A516
Heavy naphtha pumparoud	1	0	HE FLOAT HEAD	Icarus	A285C, A214

Diesel pumparoud	1	0	HE FLOAT HEAD	Icarus	A285C, A214
Heavy naphtha heat exchanger	1	0	HE FLOAT HEAD	Icarus	A285C, A214
Diesel heat exchanger	1	0	HE FLOAT HEAD	Icarus	A285C, A214
Wax heat exchanger	1	0	HE FLOAT HEAD	Icarus	A285C, A214
Main column - condenser	1	0	HE FIXED T S	Icarus	A285C, A214
Main column - drum	1	0	HT HORIZ DRUM	Icarus	A516
Main column - reflux pump	1	1	CP CENTRIF	Icarus	CS casing
Main column - tower	1	0	TW TRAYED	Icarus	A516, A285C
Main column - feed furnace	1	0	FU BOX	Icarus	A213C
Side stripper - heavy naphtha	1	0	TW TRAYED	Icarus	A516, A285C
Side stripper - diesel	1	0	TW TRAYED	Icarus	A516, A285C
Pump to the stabilizer	1	1	CP CENTRIF	Icarus	CS casing
Stabilizer - condenser	1	0	HE FIXED T S	Icarus	A285C, A214
Stabilizer - drum	1	0	HT HORIZ DRUM	Icarus	A516
Stabilizer - reboiler	1	0	RB U TUBE	Icarus	A285C, A214
stabilizer - reflux pump	1	1	CP CENTRIF	Icarus	CS casing
Stabilizer - tower	1	0	TW TRAYED	Icarus	A516, A285C
Hydrocracking	1	0	C*	Shah et al.	N/A
Isomerization	1	0	C*	Bechtel	N/A
Catalytic reformer	1	0	C*	Bechtel	N/A
H_2 recovery (PSA)	1	0	C*	Bechtel	N/A
Diesel storage tank (30 days)	1	0	VT STORAGE	Icarus	A285C
Gasoline storage tank (30 days)	1	0	VT STORAGE	Icarus	A285C

*Quoted equipment

Table B.4 Detailed equipment list for the post-FT CO_2 capture unit (I-CBTL)

Description	# Req	# Spares	Model in APEA	Cost source	MOC
Treated gas K.O. drum*	1	0	VT CYLINDER	Icarus	A516
Feed gas K.O. drum*	1	0	VT CYLINDER	Icarus	SS304
Activated carbon drum*	1	0	VT CYLINDER	Icarus	A516
Rich amine flash drum*	1	0	HT HORIZ DRUM	Icarus	A516
Absorber	1	0	TW PACKED	Icarus	A516**, M107YC
Absorber intercooling	1	0	HE FLOAT HEAD	Icarus	A285C, A214
Lean/rich heat exchanger	4	0	HE PLAT FRAM	Icarus	SS316
Solvent regeneration - condenser	2	0	HE FIXED T S	Icarus	T150A, SS316
Solvent regeneration - drum	2	0	HT HORIZ DRUM	Icarus	A516
Solvent regeneration - reboiler	8	0	RB U TUBE	Icarus	316LW, SS316
Solvent regeneration - reflux pump	2	2	CP CENTRIF	Icarus	SS316
Solvent regeneration - tower	2	0	TW PACKED	Icarus	304L, M107YC
Solvent cooling	1	0	HE FLOAT HEAD	Icarus	A285C, A214
Solvent recycle pump	1	1	CP CENTRIF	Icarus	SS316
Amine storage tank *	1	0	VT STORAGE	Icarus	A285C

*sizing information available in Bechtel's report[18]; **With 1/8 inch SS304 cladding

Table B.5 Detailed equipment list for the combined cycle power plant* (ICBTL)

Description	# Req	# Spares	Model in APEA	Cost source	Material
Clean fuel gas heater	1	0	HE FLOAT HEAD	Icarus	A258C, A214
Fuel gas compressor	1	0	GC CENTRIF	Icarus	CS Casing
Gas turbine	1	0	C*	NETL[2,3]	N/A
Boiler feed water pump	1	1	CP CENTRIF	Icarus	CS Casing
Medium pressure steam reheater	1	0	HE AIR COOLER	Icarus	A214
High pressure steam superheater	1	0	HE AIR COOLER	Icarus	A214
High pressure steam generator	1	0	HE WASTE HEAT	Icarus	CS
High pressure BFW economizer	1	0	HE AIR COOLER	Icarus	A214
High pressure steam blowdown	1	0	VT CYLINDER	Icarus	CS
Low pressure steam generator	1	0	HE WASTE HEAT	Icarus	CS
Low pressure BFW economizer	1	0	HE AIR COOLER	Icarus	A214
High pressure BFW pre-economizer	1	0	HE AIR COOLER	Icarus	A214
Pre-deaerator heater	1	0	HE AIR COOLER	Icarus	A214
Deaerator	1	0	TW TRAYED	Icarus	A516, A285C
Steam packing exhauster	1	0	HE FLOAT HEAD	Icarus	A516, A285C
Air ejector	1	0	HE FLOAT HEAD	Icarus	A516, A285C
Condenser pump	1	1	VP MECH BOOST	Icarus	CS Casing
Surface condenser	1	0	C BAROMETRIC	Icarus	N/A
Steam turbine	1	0	EG TURBO GEN	Icarus	CS Casing
High pressure BFW pump	1	1	CP CENTRIF	Icarus	CS Casing
Medium pressure BFW pump	1	1	CP CENTRIF	Icarus	CS Casing
Low pressure BFW pump	1	1	CP CENTRIF	Icarus	CS Casing

*Quoted equipment
BFW= boiler feed water

Appendix C Economic Model Validation of the I-CBTL Plants

Table C.1 Comparison with Bechtel studies

		Bechtel*	Model	Difference	Notes
		(MM$, 2014)		%	
ISBL cost of each unit					(1)
Unit 100	Syngas production and treatment	2056.6	2280.4	-10.88	
	Pre-processing & gasificaiton	1355.7	1266.8	6.56	
	Syngas treating & cooling	60.8	63.4	-4.26	
	Sour water stripper	5.1	4.9	5.33	
	Acid gas removal	29.9	299.6		(2)
	Sulfur recovery	69.5	70.0	-0.77	
	Syngas wet scrubbing	12.1	13.3	-9.75	
	Air separation unit	523.5	422.3	19.34	
	Ash handling		140.1		(3)
Unit 200	Fischer-Tropsch synthesis loop	800.2	437.3	45.35	(4)
	Fischer-Tropsch synthesis	352.8	326.0	7.61	
	Carbon dioxide removal	226.7	60.6	-6.93**	(5)
	Dehydration and hydrocarbon recovery	114.5	3.0		
	Autothermal reformer	35.1	35.0	-0.35	
	Hydrogen recovery	71.1	15.8		(6)
Unit 300	Product upgrading and refining	243.7	190.5	21.83	(7)
	Wax hydrocracking	69.8	65.9	5.63	
	Hydrotreating	33.0	30.6	7.3	
	Catalytic reforming	50.2	46.4	7.66	
	C_5/C_6 isomerization	11.7	13.4	-14.63	
	C_4 isomerization and alkylation	70.2			
	Others	8.9			(8)
Total ISBL cost		3100.5	2883.0	5.91	
Total project cost***		4748.5	4905.6	-3.31	(9)

*Original data reported in 1998 is escalated to 2014 pricing basis using CEPCI.

**Difference in capital investment for same amount of CO_2 capture

******* TPC includes OSBL, engineering cost, contingency cost.

(1) HRSG section with steam turbine is included in OSBL section in Bechtel's analysis.

(2) In Bechtel's baseline design, CCS is not considered; amine solvent is used in the acid gas removal unit for removing H_2S only in Unit 100.

(3) Ash handling system is considered as OSBL facility in Bechtel's baseline design.

(4) Dehydration unit was considered in Bechtel's design but not in this project. More complicated hydrocarbon recovery unit is considered in Bechtel's design

(5) In Bechtel's baseline design, CCS is not considered. Hence, most of the CO_2 is captured by the post FT CO_2 capture unit in Unit 200. However, in the base case of this study, WGS reactor is used to increase the H_2/CO ratio in the FT inlet. As a result, significant amount of CO_2 is captured in the acid gas removal unit instead of the post-FT CO_2 removal unit.

(6) The capital cost estimate is consistent with the recent data released by NETL for hydrogen production plant.[4]

(7) C_4 isomerization & C_3-C_5 alkylation units are considered in Bechtel's design for upgrading light hydrocarbons to gasoline but these units are not considered in this project.

(8) Saturated gas plant considered by Bechtel is not considered in this project because light gases are used in furnace and gas turbine in this project instead of upgraded into gasoline in Bechtel's design.
(9) The OSBL cost is expected to be higher in this project because more electricity produced.

Table C.2 Comparison with NETL's study on large scale ICL plant

		NETL*	Model	Difference	Notes
		(MM$, 2014)		%	
Bare erected cost of each unit					
Unit 100	Syngas production and treatment	1562.7	1543.6	1.22	
	Preprocessing	295.2	316.3	-7.13	
	Gasifier & accessories	936.7	857.8	8.42	
	Air separation unit	330.7	369.5	-11.72	
Unit 200	Gas cleanup	420.1	420.9	-0.19	(1)
Unit 300	Fuel production and upgrading	480.9	561.4	-13.91	
	without naphtha upgrading	480.9	466.9	2.91	(2)
Unit 400	OSBL facilities	383.8	441.4	15.03	
	Gas turbine & accessories	84.1	86.3	-2.56	
	HRSG & steam turbine	117.7	87.5	25.68	(3)
	Cooling water system	42.0	75.2		(4)
	Slag disposal	139.9	192.5		
Total bare erected cost		2847.4	2970.8	-4.33	
Total project cost**		5214.3	5137.6	1.47	(5)

*Original data reported in 2007 is escalated to 2014 pricing basis using CEPCI.
**TPC includes OSBL, engineering cost, contingency cost.
(1) Dual-stage Selexol unit is used for pre-FT CO_2 removal in NETL's design, which is the same as the base case of this project.
(2) Catalytic reforming & C_5/C_6 isomerization units for naphtha upgrading are not considered in NETL's study but these units are considered in this study.
(3) Difference in power output
(4) Cost of the cooling water distribution system is included in APEA model but not in NETL's case study. Relative error is 12.59% if the cooling water distribution is not considered in this case.
(5) Additional 25% of process contingency is considered for FTS in NETL's study.

Table C.3 Comparison with NETL's study on small scale ICL plant

		NETL*	Model	Difference	Notes
		(MM$, 2014)		%	
Bare erected cost of each unit					
Unit 100	Syngas production and treatment	372.5	377.7	-1.38	
	Preprocessing	60.0	52.4	12.7	
	Gasifier & accessories	234.3	221.0	5.68	
	Air separation unit	78.1	104.2		
Unit 200	Gas cleanup	84.9	173.6		(1)
Unit 300	Fuel production and upgrading	89.4	151.1		(2)
Unit 400	OSBL facilities	79.5	82.4	3.73	
	Gas turbine & accessories	16.7	20.4		(3)
	HRSG & steam turbine	25.7	21.9		

Cooling water system	8.4	14.8		(4)
Slag disposal	28.6	25.4	11.38	
Total bare erected cost	658.0	784.7	-24.96	
Total project cost**	1124.1	1185.2	-5.44	(5)

*Original data reported in 2007 is escalated to 2014 pricing basis using CEPCI.

****** TPC includes OSBL, engineering cost, contingency cost.

(1) CCS is not considered in NETL's design; Area 200 is only for H_2S removal in NETL's study on the small-scale plant.

(2) CCS, catalytic reforming and C_5/C_6 isomerization units are not considered in NETL's study but these units are considered in this study.

(3) Difference in power output

(4) Cost of the cooling water distribution system is included in APEA model but not included in NETL's case study.

(5) Additional 25% process contingency is considered for FTS in NETL's study.

Appendix D Design of Distillation Columns in the D-CBTL Plants

Specifications of the atmospheric and vacuum distillation columns in the product recovery section are listed in Table D.1 to Table D.4. (Bagajewicz and Ji, 2001; 2002)

Table D.1 Specifications of the atmospheric distillation column

Specifications	Value
Number of trays	
Main column	29
Heavy naphtha side-stripper	5
Distillate side-stripper	5
Locations	
Feed to main column (Furnace)	26
Stripping steam to main column (Above stage)	30
Heavy naphtha side-stripper draw and return	15, 14
Distillate side-stripper draw and return	24, 23

Table D.2 Operating conditions in the atmospheric distillation column

Operating Condition	Value	
Main Column		
Condenser temperature	37.8	ºC
Overhead pressure	240	kPa
Pressure drop per tray	1.38	kPa
Feed furnace fractional overflash	3.2	%LV
Bottom product/feed	0.62	kg/kg
Stripping steam/bottom product	4.54	kg/bbl
Side-strippers		
Stripping steam/heavy naphtha	2.27	kg/bbl
Stripping steam/diesel	2.27	kg/bbl

Table D.3 Specifications of the vacuum distillation column

Specification	Value
Total number of trays	6
Feed to main column (Furnace)	6
Stripping steam to main column (Above stage)	7
LVGO sidestream product	2
Top pump-around draw and return	2, 1
HVGO sidestream product	4
HVGO pump-around draw and return	4, 3

Table D.4 Operating conditions in the vacuum distillation column

Operating Condition	Value	
Overhead pressure	60	mmHg
Bottom pressure	70	mmHg
Feed furnace fractional overflash	0.6	%LV
Stripping steam/bottom product	2.27	kg/bbl

Appendix E Equipment List of the D-CBGTL Plant with CCS

Table E.1 Equipment list of the liquefaction and hydrocarbon recovery unit (D-CBGTL)

Equipment	#Required/Spares	Model in APEA	Sizing	MOC[(1)]
Reactors & vessels				
Inline hydrotreater	1/0	VT MULTI WALL	APEA	A387D
Slurry tank	2/0	AT MIX	APEA	A516
Slurry surge tank	1/0	VT CYLINDER	APEA	A285C
Slurry surge tank vent scrubber	1/0	VT CYLINDER	APEA	A516
High pressure high temp flash	1/0	VT CYLINDER	APEA	A387F (SS347)
Low pressure oil separator	1/0	TW TRAYED	Aspen Plus	A387D/A387D
High pressure cold flash	1/0	VT CYLINDER	APEA	A387B
Low pressure warm flash	1/0	VT CYLINDER	APEA	A516
Low pressure cold flash	1/0	VT CYLINDER	APEA	CS
High pressure warm flash	1/0	VT CYLINDER	APEA	A387D
Atmosphere still feed separator	1/0	VT CYLINDER	APEA	A387B
Wash water drum	1/0	HT HORIZ DRUM	APEA	CS
Sour water drum	1/0	HT HORIZ DRUM	APEA	CS
Recycle solvent tank	1/0	VT CYLINDER	APEA	A387D
Atmosphere still condenser drum	1/0	HT HORIZ DRUM	APEA	A516
Stabilizer condenser drum	1/0	HT HORIZ DRUM	APEA	A516
Distillation columns				
Atmosphere still tower	1/0	TW TRAYED	Aspen Plus	316L/316L
Atmosphere gas oil stripper	1/0	TW TRAYED	Aspen Plus	316L/316L
Atmosphere naphtha stripper	1/0	TW TRAYED	Aspen Plus	316L/316L
Stabilizer tower	1/0	TW TRAYED	Aspen Plus	A516/A258C
Vacuum still tower	1/0	TW TRAYED	Aspen Plus	SS410/SS410
Compressors, pumps & turbines				
Atmospheric still reflux pump	1/1	CP CENTRIF	APEA	SS casing
Stabilizer reflux pump	1/1	CP CENTRIF	APEA	CS casing
Slurry tank bottom pump	1/1	CP CENTRIF	APEA	SS316 casing
High pressure slurry feed pump	1/1	P RECIP MOTR	APEA	SS316 casing
Make up H_2 compressor	1/1	GC RECIP MOTR	APEA	SS casing
Recycle H_2 compressor	1/0	GC CENTRIF	APEA	SS316 casing
Stabilizer feed pump	1/0	CP CENTRIF	APEA	CS casing
Stabilizer feed compressor	1/1	GC CENTRIF	APEA	CS casing
ROSE-SR unit feed pump	1/1	CP CENTRIF	APEA	SS316 casing
Atmospheric still bottom pump	1/1	CP CENTRIF	APEA	SS316 casing
Atmospheric still feed pump	1/1	CP CENTRIF	APEA	SS316 casing
Gas oil product pump	1/1	CP CENTRIF	APEA	SS casing
Sour water pump	1/1	CP CENTRIF	APEA	SS casing
LVGO pumparound	1/1	CP CENTRIF	APEA	SS casing

HVGO pumparoud	1/1	CP CENTRIF	APEA	SS casing
VGO product pump	1/1	CP CENTRIF	APEA	SS316 casing
Furnaces, boiler & heat exchangers				
Atmosphere still condenser	1/0	HE FIXED T S	EDR	A214/A516
Atmosphere still feed furnace	1/0	FU VERTICAL	APEA	347S
Stabilizer condenser	1/0	HE FIXED T S	EDR	A214/A516
Stabilizer reboiler	1/0	RB U TUBE	EDR	A214/A516
Slurry feed heat exchanger	2/0	HE FLOAT HEAD	EDR	316S/SS316
Slurry feed heat exchanger	4/0	HE FLOAT HEAD	EDR	316S/A387D (SS316)
Slurry feed furnace	1/0	FU BOX	APEA	347S
H_2 pre heating	1/0	HE FLOAT HEAD	EDR	I825/SS304
H_2 pre heating	1/0	HE FLOAT HEAD	EDR	321S/A387D
H_2 feed furnace	1/0	FU BOX	APEA	347S
Recycle H_2 heat exchanger	3/0	HE FLOAT HEAD	EDR	304LS/304L
Product heat exchanger	1/0	HE FLOAT HEAD	EDR	316LS/A387D (SS316)
IP steam generator	1/0	HE WASTE HEAT	EDR	CS
Water cooler	7/0	HE FLOAT HEAD	EDR	A214/A516
Product heat exchanger	1/0	HE FLOAT HEAD	EDR	A213C/A387C
LP steam generator	3/0	HE WASTE HEAT	EDR	CS

(1) ( ) denotes cladding material

Table E.2 Equipment list of the syngas production unit (D-CBGTL)

Equipment	#Required/Spares	Model in APEA	Sizing	MOC
Reactors & vessels				
Slag separator	1/0	VT CYLINDER	APEA	SS304
Scrubber	1/0	VT CYLINDER	APEA	SS304
Syngas KO drum	2/0	HT HORIZ DRUM	APEA	A516
flue gas KO drum	2/0	HT HORIZ DRUM	APEA	A516
Compressors, pumps & turbines				
Boiler feed water pump	1/1	CP CENTRIF	APEA	CS casing
Shale gas compressor	1/0	GC CENTRIF	APEA	CS casing
Furnaces, boiler & heat exchangers				
Boiler feed water heater	2/0	HE AIR COOLER	EDR	A214
Low pressure steam generator	2/0	HE WASTE HEAT	EDR	CS
Shale gas pre heater	1/0	HE FLOAT HEAD	EDR	A214/A516
Steam reformer pre heater	1/0	HE FLOAT HEAD	EDR	316S/SS316
Medium pressure steam generator	3/0	HE WASTE HEAT	EDR	CS
High pressure steam generator	2/0	HE WASTE HEAT	EDR	CS
Low pressure steam economizer	1/0	HE AIR COOLER	EDR	A214
High pressure steam economizer	1/0	HE AIR COOLER	EDR	A214
High pressure steam superheater	1/0	HE AIR COOLER	EDR	A214
Other coolers	3/0	HE FLOAT HEAD	EDR	A214/A516

Table E.3 Equipment list of the Selexol (AGR) unit (D-CBGTL)

Equipment	#Required/Spares	Model in APEA	Sizing	MOC
Reactors & vessels				
High pressure flash	1/0	VT CYLINDER	APEA	A516
Medium pressure flash	1/0	VT CYLINDER	APEA	A516
Low pressure flash	1/0	VT CYLINDER	APEA	A516
H_2 recovery drum	1/0	VT CYLINDER	APEA	A516
H_2S concentrator	1/0	VT CYLINDER	APEA	A516
H_2S stripper condenser drum	1/0	VT CYLINDER	APEA	A516
Selexol stripper condenser drum	1/0	HT HORIZ DRUM	APEA	A516
Lean solvent vessel	1/0	VT CYLINDER	APEA	A516
Distillation columns				
CO_2 absorber	1/0	TW TRSYED	Aspen Plus	A516/A285C
H_2S absorber	1/0	TW TRSYED	Aspen Plus	A516/A285C
Selexol stripper tower	1/0	TW TRSYED	Aspen Plus	A516/A285C
Compressors, pumps & turbines				
NH_3 compressor	1/0	GC CENTRIF	APEA	SS304 casing
H_2 recovery compressor	1/0	GC CENTRIF	APEA	CS casing
Stripped gas compressor	1/0	GC CENTRIF	APEA	CS casing
Lean solvent pump	2/2	CP CENTRIF	APEA	CS casing
Recycle solvent pump	1/1	CP CENTRIF	APEA	CS casing
Selexol stripper reflux pump	1/1	CP CENTRIF	APEA	CS casing
Rich solvent pump	1/1	CP CENTRIF	APEA	CS casing
Furnaces, boiler & heat exchangers				
Selexol stripper condenser	1/0	HE FIXED T S	EDR	A214/A516
Selexol stripper reboiler	1/0	RB U TUBE	EDR	A214/A516
Recycle solvent cooler	1/0	HE FLOAT HEAD	EDR	A214/A516
H_2S absorber solvent cooler	1/0	HE FLOAT HEAD	EDR	A214/A516
Lean solvent cooler	1/0	HE FLOAT HEAD	EDR	A214/A516
Syngas cooler	1/0	HE FLOAT HEAD	EDR	A214/A516
Other coolers	4/0	HE FLOAT HEAD	EDR	A214/A516

Table E.4 Equipment list of the amine unit (D-CBGTL)

Equipment	#Required/Spares	Model in APEA	Sizing	MOC[(1)]
Reactors & vessels				
MDEA/PZ storage tank	1/0	VT CYLINDER	APEA	A516
GT flue gas condenser	1/0	VT CYLINDER	APEA	A516
MDEA storage tank	1/0	VT CYLINDER	APEA	A516
CO_2 Stripper condenser drum	2	HT HORIZ DRUM	APEA	A516
H_2S Stripper condenser drum	1	HT HORIZ DRUM	APEA	A516
Distillation columns				

High pressure absorber	1/0	TW PACKED	Aspen Plus	A516 (SS304)/M107YC
GT flue gas absorber	2/0	TW PACKED	Aspen Plus	A516 (SS304)/M107YC
SMR flue gas absorber	1/0	TW PACKED	Aspen Plus	A516 (SS304)/M107YC
CO_2 Stripper tower	2/0	TW TRSYED	Aspen Plus	304L/M107YC
H_2S Absorber	1/0	TW PACKED	Aspen Plus	A516 (SS304)/1.0PPR
H_2S Stripper tower	1/0	TW TRSYED	Aspen Plus	304L/1.0PPR
Compressors, pumps & turbines				
Flue gas blower	2/0	FN CENTRIF	APEA	CS
CO_2 Stripper reflux pump	2/2	CP CENTRIF	APEA	SS316 casing
H_2S Stripper reflux pump	1/1	CP CENTRIF	APEA	SS316 casing
GT rich solvent pump	2/2	CP CENTRIF	APEA	CS casing
SMR rich solvent pump	1/2	CP CENTRIF	APEA	CS casing
MDEA/PZ lean solvent pump	1/1	CP CENTRIF	APEA	CS casing
MDEA lean solvent pump	1/1	CP CENTRIF	APEA	CS casing
Furnaces, boiler & heat exchangers				
High pressure absorber pumparound	1/0	HE FLOAT HEAD	EDR	A214/A516
GT absorber pumparound	2/0	HE FLOAT HEAD	EDR	A214/A516
SMR absorber pumparound	1/0	HE FLOAT HEAD	EDR	A214/A516
CO_2 Stripper condenser	2/0	HE FIXED T S	EDR	T150A/SS316
CO_2 Stripper reboiler	2/0	RB U TUBE	EDR	316LW/SS316
H_2S Stripper condenser	1/0	HE FIXED T S	EDR	T150A/SS316
H_2S Stripper reboiler	1/0	RB U TUBE	EDR	316LW/SS316
GT flue gas cooler	1/0	HE FLOAT HEAD	EDR	A214/A516
MDEA/PZ lean/rich exchanger	1/0	HE PLAT FRAM	EDR	SS316
Lean solvent cooler	2/0	HE FLOAT HEAD	EDR	A214/A516
MDEA lean/rich exchanger	1/0	HE PLAT FRAM	EDR	SS316

(1) ( ) denotes cladding material

Table E.5 Equipment list of the hydrocarbon upgrading unit (D-CBGTL)

Equipment	#Required/Spares	Model in APEA	Sizing	MOC[(1)]
Reactors & vessels				
Gasoline storage tank	3/0	VT STORAGE	APEA	A516
Diesel storage tank	6/0	VT STORAGE	APEA	A516
Gas oil hydrotreater	2/0	VT MULTI WALL	APEA	A387F (SS347)
Hot high pressure flash	1/0	VT CYLINDER	APEA	A387D
Cold high pressure flash	1/0	VT CYLINDER	APEA	A516
Low pressure flash	1/0	VT CYLINDER	APEA	A516
Stabilizer condenser drum	2/0	HT HORIZ DRUM	APEA	A516
Main distillation condenser drum	1/0	HT HORIZ DRUM	APEA	A516
Distillation columns				
Main distillation tower	1/0	TW TRAYED	Aspen Plus	A516/A285C
Stabilizer tower	1/0	TW TRAYED	Aspen Plus	A516/A258C
Compressors, pumps & turbines				

Main distillation reflux pump	1/1	CP CENTRIF	APEA	CS casing
Stabilizer reflux pump	1/1	CP CENTRIF	APEA	CS casing
Makeup H_2 compressor	1/1	GC RECIP MOTR	APEA	SS casing
Recycle H_2 compressor	1/0	GC CENTRIF	APEA	SS316 casing
Stabilizer feed pump	1/1	CP CENTRIF	APEA	CS casing
Gas oil feed pump	1/1	CP CENTRIF	APEA	CS casing
Furnaces, boiler & heat exchangers				
Diesel pumparound	1/0	HE FLOAT HEAD	EDR	A214/A516
Gas oil pumparound	1/0	HE FLOAT HEAD	EDR	A214/A516
Main distillation condenser	1/0	HE FIXED T S	EDR	A214/A516
Main distillation feed furnace	1/0	FU VERTICAL	APEA	A213C
Stabilizer condenser	1/0	HE FIXED T S	EDA	A214/A516
Stabilizer reboiler	1/0	RB U TUBE	EDA	A214/A516
H_2 pre heater	1/0	HE FLOAT HEAD	APEA	A214/A516
Feed H_2 furnace	1/0	FU BOX	APEA	347S
Gas oil feed pre heater	1/0	HE FLOAT HEAD	EDR	A213D/A387D
Low pressure steam generator	3/0	HE WASTE HEAT	EDA	CS
Heavy diesel cooler	1/0	HE FLOAT HEAD	EDR	A214/A516
Light gas oil cooler	1/0	HE FLOAT HEAD	EDR	A214/A517
Other coolers	4/0	HE FLOAT HEAD	EDR	A214/A516

(1) ( ) denotes cladding material

Table E.6 Equipment list of the combined cycle power island (D-CBGTL)

Equipment	#Required/Spares	Model in APEA	Sizing	MOC
Reactors & vessels				
High pressure steam blowdown	1/0	HT HORIZ DRUM	APEA	A516
Compressors, pumps & turbines				
High pressure BFW pump	1/1	CP CENTRIF	APEA	CS casing
Medium pressure BFW pump	1/1	CP CENTRIF	APEA	CS casing
Low pressure BFW pump	1/1	CP CENTRIF	APEA	CS casing
Condenser pump	1/1	VP MECH BOOST	APEA	CS casing
Steam turbine	1/0	EG TURBO GEN	APEA	CS casing
Fuel gas compressor	1/0	GC CENTRIF	APEA	CS casing
Gas turbine	1/0	EG TURBO GEN	APEA	CS casing
Furnaces, boiler & heat exchangers				
High pressure pre economizer	1/0	HE AIR COOLER	EDA	A214
High pressure BFW economizer	1/0	HE AIR COOLER	EDA	A214
High pressure steam superheater	1/0	HE AIR COOLER	EDA	A214
Medium pressure steam reheater	1/0	HE AIR COOLER	EDA	A214
Boiler feed water heater	1/0	HE AIR COOLER	EDA	A214
Air ejector	1/0	HE FLOAT HEAD	EDR	A214/A516
Steam packing exhauster	1/0	HE FLOAT HEAD	EDR	A214/A516
High pressure steam generator	1/0	HE WASTE HEAT	APEA	CS

Low pressure steam generator	1/0	HE WASTE HEAT	APEA	CS
Surface condenser	1/0	C BAROMETRIC	APEA	CS

Appendix F Publications and Presentations

PUBLICATIONS

1) Jiang, Y.; Bhattacharyya D. Modeling and Optimization of Catalytic Two-Stage Liquefaction Unit Using Ebullated Bed Reactors. Under preparation.
2) Jiang, Y.; Bhattacharyya D. Economic-based Optimization of Hybrid Coal-Biomass to Liquids Plants with CO_2 Capture and Storage. Under preparation.
3) Jiang, Y.; Bhattacharyya D. Techno-Economic Analysis of Direct Coal-Biomass to Liquids (CBTL) Plants with Shale Gas Utilization and CO_2 Capture and Storage (CCS). *Appl. Energy 2017,* 189, 433-448.
4) Jiang, Y.; Bhattacharyya, D. Modeling of Direct Coal-Biomass to Liquids (CBTL) Plants with Shale Gas Utilization and CO_2 Capture and Storage (CCS). *Appl. Energy* 2016, 183, 1616-1632.
5) Jiang, Y.; Bhattacharyya D. Techno-Economic Analysis of a Novel Indirect Coal-Biomass to Liquids Plant Integrated with a Combined Cycle Plant and CO_2 Capture and Storage. *Ind. Eng. Chem. Res.* 2016, 55, 1677-1689.
6) Jiang, Y.; Bhattacharyya D. Modeling and Analysis of an Indirect Coal-Biomass to Liquids (CBTL) Plant Integrated with a Combined Cycle Plant and CO_2 Capture and Storage (CCS). *Energy Fuels* 2015, 29, 5434-5451.
7) Jiang, Y.; Bhattacharyya D. Plant-Wide Modeling of an Indirect Coal-Biomass to Liquids (CBTL) Plant with CO_2 Capture and Storage (CCS), *Int. J. Greenh. Gas Control* 2014, 31, 1-15.

BOOK CHAPTERS

1) Jiang, Y.; Bhattacharyya D. Sustainable Engineering Economic and Profitability Analysis, In: Ruiz-Mercado, G. and Cabezas, H, (Eds.) *Sustainability in the Design, Synthesis and Analysis of Chemical Engineering Processes*. Elsevier 2016.

PRESENTATIONS

1) Jiang, Y.; Bhattacharyya D. Modeling and Economic Analysis of Direct Coal-Biomass to Liquids (CBTL) Plant with Shale Gas Utilization and CO_2 Capture and Storage (CCS), Paper 564e, AICHE Annual Meeting, San Francisco, CA, USA, November 13-18, 2016.
2) Jiang, Y.; Bhattacharyya D. Techno-Economic Analysis of Indirect, Direct and Hybrid Coal-Biomass to Liquids (CBTL) Plant with CO_2 Capture and Storage (CCS), Paper 66c, AICHE Annual Meeting, San Francisco, CA, USA, November 13-18, 2016.
3) Jiang, Y.; Bhattacharyya D. Techno-Economic Study of an Indirect Coal-Biomass to Liquids (CBTL) Plant with CO_2 Capture and Storage (CCS), Paper 625d, AICHE Annual Meeting, Salt Lake City, UT, USA, November 8-13, 2015.
4) Jiang, Y.; Bhattacharyya D. Sustainable Engineering Economic and Profitability Analysis, Paper 668b, AICHE Annual Meeting, Salt Lake City, UT, USA, November 8-13, 2015.
5) Jiang, Y.; Bhattacharyya D. Techno-Economic Analysis of a Direct Coal-Biomass to Liquids (CBTL) Plant with CO_2 Capture and Storage (CCS), Paper 639f, Salt Lake City, UT, USA, November 8-13, 2015.
6) Jiang, Y.; Bhattacharyya D. Modeling of an Indirect Coal-Biomass to Liquids (CBTL) Plant with CO_2 Capture and Storage (CCS), Paper 249b, AIChE Annual Meeting, Atlanta, GA, November 16-21, 2014.
7) Jiang, Y.; Bhattacharyya D. Techno-Economic Analysis of a Novel Indirect Coal-Biomass to Liquids (CBTL) Plant Integrated with a Combined Cycle Plant and CO_2 Capture and Storage (CCS), Paper 366a, AIChE Annual Meeting, Atlanta, GA, November 16-21, 2014.
8) Jiang, Y.; Bhattacharyya D. Plant-Wide Modeling of an Indirect Coal-Biomass to Liquids (CBTL) Plant with CO_2 Capture and Utilization Integrated with a Combined Cycle Plant, Paper 410a, AIChE Annual Meeting, San Francisco, CA, November 3-8, 2013.

References

1) Ai, J. Preliminary study on hydro-liquefaction kinetics of Shenhua coal macerals and coliquefaction of macerals. Master thesis, China Coal Research Institute, 2007.
2) Albahri, T.A.; Riazi, M.R.; Alqattan, A.A. Octane number and aniline point of petroleum fuels. *ACS Div. Fuel Chem. Preprints* 2002, 47(2), 710-711.
3) Anbar, M., St John, G.A. Characterization of coal-liquefaction products by molecular-weight profiles produced by field-ionization mass spectrometry. *Fuel* 1978, 57, 105-110.
4) Anderson, L.L.; Tuntawiron, W. Coliquefaction of Coal and Polymers to Liquid Fuels. *ACS Div. Fuel Chem. Preprints* 1993, 38(4), 810-815.
5) Andre, R.N.; Pinto, F.; Franco, C.; Dias, M.; Gulyurtlu, I.; Matos, M.A.A.; Cabrita, I. Fluidized bed co-gasification of coal and olive oil industry wastes. *Fuel* 2005, 84, 1635-1644.
6) Austgen, D.M.; Rochelle, G.T.; Chen, C.C. Model of vapor-liquid equilibria for aqueous acid gas-alkanolamine systems. 2. Representation of H2S and CO2 solubility in aqueous MDEA and CO2 solubility in aqueous mixtures of MDEA with MEA and DEA. *Ind. Eng. Chem. Res.* 1991, 30, 543-555.
7) Ayabe, S.; Omoto, H.; Utaka, T.; Kikuchi, R.; Sasaki, K.; Teraoka, Y.; Eguchi, K. Catalytic autothermal reforming of methane and propane over supported metal catalysts. *Appl. Catal. A: General* 2003, 241(1-2), 261-269.
8) Bagajewicz, M.; Ji, S. Rigorous procedure for the design of conventional atmospheric crude fractionation units. 1. Targeting. *Ind. Eng. Chem. Res.* 2001, 40, 617-626.
9) Bagajewicz, M.; Ji, S. Rigorous procedure for the design of conventional atmospheric crude fractionation units. 2. Heat exchanger network. *Ind. Eng. Chem. Res.* 2001, 40, 627-634.
10) Bai, L.; Xiang, H.W.; Li, Y.W.; Han, Y.Z.; Zhong, B. Slurry phase Fischer-Tropsch synthesis over manganese-promoted iron ultrafine particle catalyst. *Fuel* 2002, 81, 1577-1581.

11) Baily, F.C.; Cotton, K.C.; Spencer, R.C. Predicting the Performance of Large Steam Turbine-Generators Operating with Saturated and Low Superheat Steam Conditions. Proceeding 28th Annual Meeting of American Power Conference, General Electric Report 2454-A, Schenectady, NY, 1967.
12) Bain, R.L. Material and Energy Balances for Methanol from Biomass Using Biomass Gasifiers. National Renewable Energy Laboratory, DE-AC36-83CH10093, 1992.
13) Baird, M.H.I.; Rice, R.G. Axial dispersion in large unbaffled columns. *Chem. Eng. J.* 1975, 9, 171-174.
14) Baldwin, R.A.; Bills, J.L. Processes for the production of deashed coal. Patent US4119523, 1978.
15) Baliban, R.C.; Elia, J.A.; Floudas, C.A. Toward Novel Hybrid Biomass, Coal, and Natural Gas Processes for Satisfying Current Transportation Fuel Demands, 1: Process Alternatives, Gasification Modeling, Process Simulation, and Economic Analysis. *Ind. Eng. Chem. Res.* 2010, 49, 7343-7370.
16) Baliban, R.C.; Elia, J.A.; Floudas, C.A. Optimization framework for the simultaneous process synthesis, heat and power integration of a thermochemical hybrid biomass, coal and natural gas facility. *Comput. Chem. Eng.* 2011, 35, 1647-1690.
17) Baliban, R.C.; Elia, J.A.; Floudas, C.A. Novel natural gas to liquids processes: process synthesis and global optimization strategies. *AIChE J.* 2013, 59(2), 505-531.
18) Baliban, R.C.; Elia, J.A., Floudas, C.A. Biomass and natural gas to liquid transportation fuels: process synthesis, global optimization, and topology analysis. *Ind. Eng. Chem. Res.* 2013, 52(9), 3381-3406.
19) Bartis, J.T.; Camm, F.; Ortiz, D.S. Producing Liquid Fuels from Coal. RAND Corporation: Santa Monica, 2008.
20) Batidzirai, B.; Mignot, A.P.R.; Schakel, W.B.; Junginger, H.M.; Faaij, A.P.C. Biomass torrefaction technology: Techno-economic status and future prospects. *Energy* 2013. 62, 196-214.
21) Bauman, R.F.; Maa, P.S. Direct coal liquefaction process, Patent CN104937077A, 2014.
22) Bechtel. Baseline Design/Economics for Advanced Fischer-Tropsch Technology. Bechtel Corp., DE-AC22-91PC90027, Final Report, April 1998.

23) Bechtel. Aspen Process Flowsheet Simulation Model for a Battelle Biomass-Based Gasification, Fischer-Tropsch Liquefaction and Combined-Cycle Power Plant. Bechtel Corp., DE-AC22-93PC91029, Topical Report, May 1998.
24) Bechtel. The Slurry Phase Fischer-Tropsch Reactor a Comparison of Slurry versus Fixed-Bed Reactor Designs for Fischer-Tropsch Distillate Production. Bechtel Corp., DE-AC22-89PC89867, Final Report, June 1990.
25) Bechtel. Baseline Design/Economics for Advanced Fischer-Tropsch Technology. Bechtel Corp., DE-AC22-91PC90027, Quarterly Report, January-March 1992.
26) Bechtel. Baseline Design/Economics for Advanced Fischer-Tropsch Technology. Bechtel Corp., DE-AC22-91PC90027, Quarterly Report, April-June 1992.
27) Bechtel. Baseline design/economics for advanced Fischer-Tropsch technology. Bechtel Corp., DE-AC22-91PC90027, Quarterly Report, July-September 1992.
28) Bechtel. Baseline Design/Economics for Advanced Fischer-Tropsch Technology. Bechtel Corp., DE-AC22-91PC90027, Quarterly Report, January-March 1993.
29) Bechtel. Baseline Design/Economics for Advanced Fischer-Tropsch Technology. Bechtel Corp., DE-AC22-91PC90027, Quarterly Report, April-June 1993.
30) Bechtel and Amoco. Direct coal liquefaction baseline design and system analysis. Bechtel Corp., Amoco Corp., DE-AC22-90PC89857, Quarterly Report, September, 1990.
31) Bechtel and Amoco. Direct Coal Liquefaction Baseline Design and System Analysis. Bechtel Corp., Amoco Corp., DE-AC22-90PC89857, Quarterly Report, January, 1991.
32) Bechtel and Amoco. Direct coal liquefaction baseline design and system analysis, Task III topical report: cost estimates and economics of the baseline and options. Bechtel Corp., Amoco Corp., DE-AC22-90PC89857, Pittsburgh, PA, September 1992.
33) Behkish, A.; Lemoine, R.; Oukaci, R.; Morsi, B.I. Novel correlations for gas holdup in large-scale slurry bubble column reactors operating under elevated pressures and temperatures. *Chem. Eng. J.* 2006, 115,157-171.
34) Behrendt, F.; Neubauer, Y.; Oevermann, M.; Wilmes, B.; Zobel, N. Direct Liquefaction of Biomass. *Chem. Eng. Technol.* 2008, 31, 667-677.
35) Bellman et al. Coal to Liquids and Gas. The National Petroleum Council, 2007, http://www.npc.org/study_topic_papers/18-ttg-coals-to-liquids.pdf. (Last accessed on May 21, 2012).

36) Berispek, V. Studies of an alkali impregnated Cobalt-Molybdate catalyst for the water-gas shift and the methanation reactions. M. S. Thesis, Virginia Polytechnic Institute and State University, Blacksburg, VA, 1975.

37) Bhattacharyya, D.; Turton, R.; Zitney, S.E. Steady-state simulation and optimization of an integrated gasification combined cycle power plant with CO_2 capture. *Ind. Eng. Chem. Res.* 2011, 50, 1674-1690.

38) Bishnoi, S.; Rochelle, G. Absorption of carbon dioxide into aqueous piperazine: reaction kinetics, mass transfer and solubility. *Chem. Eng. Sci.* 2000. 55, 5531-5543.

39) Bullin, K.; Krouskop, P. Composition variety complicates processing plans for US shale gas. *Oil and Gas Journal* March 9 2009.

40) Cavallo, E.; Januszweski, D.; Putek, S. Upgrade hydrocracked resid through integrated hydrotreating. *Hydrocarbon Process.* 2008, 87(9), 83-92.

41) Chen, Z.M.; Huang, Z.B.; Yang, T.; Liu, J.K.; Ge, H.L.; Jiang, L.J.; Fang, X.C. Modeling on scale-up of an ebullated-bed reactor for the hydroprocessing of vacuum residuum. *Cataly. Today* 2014, 220-222, 228-236.

42) Cheng, Z.; Huang, Z.; Yang, T.; Liu, J.; Ge, H.; Jiang, L. et al. Modeling on scale-up of an ebullated-bed reactor for the hydroprocessing of vacuum residuum. *Catal. Today* 2014, 220-222, 228-236.

43) Chiesa, P.; Consonni, S. Shift reactors and physical absorption for low-CO_2 emission IGCCs. *J. Eng. Gas Turbines Power-Trans. ASME* 1999, 121, 295-305.

44) Chiesa, P.; Lozza, G. CO_2 emission abatement in IGCC power plants by semiclosed cycle: Part A-with oxygen-blown combustion. *J. Eng. Gas Turbines Power-Trans. ASME* 1999, 121, 635-641.

45) Chiesa, P.; Lozza, G.; Mazzocchi, L. Using hydrogen as gas turbine fuel. *J. Eng. Gas Turbines Power-Trans. ASME* 2005, 127, 73-80.

46) Christensen, T.S. Adiabatic prereforming of hydrocarbons – an important step in syngas production. *Appl. Catal. A Gen.* 1996, 138, 285-309.

47) Comolli, A.G.; Ganguli, P.; Stalzer, R.H.; Lee, T.L.K.; Zhou, P. The direct liquefaction co-processing of coal, oil, plastics, MSW and biomass. ACS Preprints, Hydrocarbon Research Inc.: Trenton, NJ, pp 300-305, 1994.

48) Comolli, A.G.; Lee, L.K.; Pradhan, V.R.; Stalzer, T.H.; Harris, E.C.; Mountainland, D.M.; Karolkiewicz, W.F.; Pablacio, R.M. Direct Liquefaction Proof-of-Concept Facility, Technical Progress Report POC Run 01. AC22-92PC92148, Hydrocarbon Research Inc., 1995.

49) Coughlin, R.W.; Davoudzadeh, F. Coliquefaction of lignin and bituminous coal. *Fuel* 1986, 65, 95-106.

50) Couhert, C.; Salvador, S.; Commandre, J.M. Impact of torrefaction on syngas production from wood. *Fuel* 2009, 88(11), 2286-2290.

51) Deckwer, W.D. Bubble column reactors. John Wiley & Sons, New York, 1992.

52) Debyshire, F.J.; Varghese, P.; Whitehurst, D.D. Integration of short-contact-time liquefaction and critical solvent deashing with gasification through methanol-to gasoline. US Patent 4440622, 1984.

53) de Kerk, A.; Furimsky, E. Catalysis in the refining of Fischer-Tropsch syncrude. Cambridge: Royal Society of Chemistry, 2010.

54) de Swart, J.W.A. Scale-up of a Fischer-Tropsch slurry reactor. PhD thesis. University of Amsterdam: Amsterdam, Netherlands, 1996.

55) Doctor, R.D.; Molburg, J.C.; Thimmapuram, P.R.; Betty, G.F.; Livengood, C.D. Gasification combined cycle: carbon dioxide recovery, transport and disposal. ANL/ESD-24, Energy System Division, Argonne National Laboratory: Argonne, IL, work sponsored by United States Department of Energy, September 1994.

56) Doust, A.M.; Shahraki, F.; Sadeghi, J. Simulation, control and sensitivity analysis of crude oil distillation unit. *J. Petroleum Gas Eng.* 2012, 3(6), 99-113.

57) Dry, M.E. The Fischer-Tropsch process: 1950-2000. *Catal. Today* 2002, 71, 227-241.

58) Dry, M.E. The Fischer-Torpsch Synthesis. In: Anderson, J.R., Boudart, M. (Eds.), Catalysis Science and Technology, vol. 1. Springer: Berlin, pp. 209-233, 1981.

59) Dugas, R.E. Pilot plant study of carbon dioxide capture by aqueous monoethanolamine, M.S. thesis, University of Texas at Austin: Austin, TX, 2006.

60) Edwards, R. Well-to-wheels Analysis of Future Automotive Fuels and Powertrains in the European Context, WELL-to-TANK Report, Version 3c, July 2011.

61) Elliott, D.C. Process development for biomass liquefaction. *ACS Div. Fuel Chem. Preprints* 1980, 25(4), 257-263.

62) Espinoza, R.L.; Steynberg, A.P.; Jager B.; Vosloo, A.C. Low temperature Fischer-Tropsch synthesis from a Sasol perspective. *Appl. Catal. A Gen.* 186, 13-26, 1999.

63) Fahim, M.A.; Al-Sahhaf, T.A.; Elkilani, A. Fundamentals of Petroleum Refining. 1st Edition, Elsevier Science: Oxford, UK, 2010.

64) Ferrance, J.P. Development of a general model for coal liquefaction. University of Pittsburgh: Pittsburgh, PA, 1996.

65) Fox, J.M.; Tam, S.S. Correlation of slurry reactor Fischer-Tropsch yield data. *Topics in Catalysis* 1995, 2, 285-300.

66) Gamba, S.; Pellegrini, L.A.; Calemma, V.; Gambaro, C. Liquid fuels from Fischer–Tropsch wax hydrocracking: Isomer distribution. *Cataly. Today* 2010, 156, 58–64.

67) Gao J. Coal liquefaction residue and coal water slurry combined gasification nozzle and application thereof. Chinese Patent CN102268300 B, 2014.

68) Gary, J.H.; Handwerk, G.E. Petroleum Refining Technology and Economics. 4th Edition, New York: Marcel Dekker Inc.; 2001.

69) Gearhart, J.A.; Nelson, S.R. ROSE process offers energy savings for solvent extraction, In proceedings from the fifth Industrial Energy Technology Conference Volume II, Houston, TX, April 17-20, 1983.

70) GEE, MS7001EA Gas Turbine Proven Performance for 60 Hz Application, http://www.ge-energy.com.

71) Givens, E.N.; Kang, D. Coal liquefaction process with enhanced process solvent. Patent US4461694, 1984.

72) Gonzales, R.; Phillips, R.; Saloni, D.; Jameel, H.; Abt, R.; Pirraglia, A.; Wright, J. Biomass to energy in the southern United States: supply chain and delivered cost. *Bio Resources* 2011, 6(3), 2954-2976.

73) Gray, D.; White, C.; Tomlinson, G. Increasing security and reducing carbon emissions of the US transportation sector: a transformational role for coal with biomass. 2007.

74) Gross, J.; Sadowski, G. Perturbed-chain SAFT: an equation of sate based on a perturbation theory for chain molecules. *Ind. Eng. Chem. Res.* 2001, 40, 1244-1260.

75) Gruyl, D.; Parmentier, F. Reactor modeling for the Shenhua direct coal liquefaction project. Proceeding of the 18th European Symposium on Computer Aided Process Engineering, 2008.

76) Guo, X.; Liu, G.; Larson, E.D. High-octane gasoline production by upgrading low-temperature Fischer-Tropsch syncrude. *Ind. Eng. Chem. Res.* 2011, 50, 9743-9747.

77) Hartley, D. Modeling and optimization of woody biomass harvest and logistics in the Northeastern United States. PhD Dissertation, West Virginia University: Morgantown, WV, 2014.

78) Hikita, H.; Asai, S.; Ishikawa, H.; Honda, M. The kinetics of reactions of carbon dioxide with monoethanolamine, diethanolamine, and triethanolamine by a rapid mixing method. *Chem. Eng. J.* 1977, 13, 7-12.

79) Hilliard, M.D. A predictive thermodynamic model for an aqueous blend of potassium carbonate, piperazine, and monoethanolamine for carbon dioxide capture from flue gas. Ph.D. Dissertation, University of Texas at Austin: Austin, TX, 2008

80) IAPWS (International Association for the Properties of Water and Steam); IAPWS Industrial Formulation 97, 1997; http://www.iapws.org/.

81) Ibrahim, R.; Darvell, L.; Jones, J.; Williams, A. Physicochemical characterization of torrefied biomass. *J. Anal. Appl. Pyrolysis* 2013, 103, 21-30.

82) IEA, Review of worldwide coal to liquids R, D&D activities and the need for further initiatives within Europe, IEA Coal Research Ltd., RFC2-CT-2008-00006, http://www.iea-coal.org.uk; June 2009 (Last accessed on May 01, 2016).

83) IRENA, *Renewable energy technologies: cost analysis series biomass for power generation*; *IRENA*, working paper; the International Renewable Energy Agency, June 2012; http://www.irena.org/publications.

84) Ishibashi, H.; Onozaki, M.; Kobayash, M.; Hayashi, J.; Itoh, H.; Chiba, T. Gas holdup in slurry bubble column reactors of a 150t/d coal liquefaction pilot process. *Fuel* 2001, 80, 655-664.

85) Jager, B.; Espinoza, R. Advances in Low Temperature Fischer-Tropsch synthesis. *Catal. Today* 1995, 23, 17-28.

86) James, O.O.; Chowdhury, B.; Auroux, A.; Maity, S. Low CO_2 selective iron based Fischer–Tropsch catalysts for coal based polygeneration. *Appl. Energy* 2013, 107, 377-383.

87) Jarullah, A.T.; Mujtaba, I.M.; Wood, A.S. Whole Crude Oil Hydrotreating from Small-Scale Laboratory Pilot Plant to Large-Scale trickle-Bed Reactor: Analysis of Operational Issues through Modeling. *Energy Fuels* 2012, 26, 629–641.

88) Jenkins GI. Journal of Institute of Petroleum 1968; 54: 14.

89) Ji, S.; Bagajewicz, M. Design of crude distillation plants with vacuum units I targeting. *Ind. Eng. Chem. Res.* 2002, 41, 6094-6099.

90) Jia, N. Refinery Hydrogen Network Optimization with Improved Hydroprocessor Modelling. PhD Dissertation, University of Manchester: Manchester, UK, 2010.

91) Jiang, Y.; Bhattacharyya, D. Plant-wide modeling of an indirect coal-biomass to liquids (CBTL) plant with CO_2 capture and storage (CCS). *Int. J. Greenh. Gas Control* 2014, 31, 1-15.

92) Jiang, Y.; Bhattacharyya, D. Modeling and analysis of an indirect coal biomass to liquids plant integrated with a combined cycle plant and CO_2 capture and storage. *Energy Fuels* 2015, 29, 5434-5451.

93) Jiang, Y.; Bhattacharyya, D. Techno-economic analysis of a novel indirect coal-biomass to liquids plant integrated with a combined cycle plant and CO_2 capture and storage. *Ind. Eng. Chem. Res.* 2016, 55, 1677-1689.

94) Jiang, Y.; Bhattacharyya, D. Modeling of Direct Coal-Biomass to Liquids (CBTL) Plants with Shale Gas Utilization and CO2 Capture and Storage (CCS). *Appl. Energy* 2016, 183, 1616-1632.

95) Jiang, H.; Wang, X.; Shan, X.; Li, K.; Zhang, X.; Gao, X.; Weng, H. Isothermal stage kinetics of direct coal liquefaction for Shenhua Shendong bituminous coal. *Energy Fuels* 2015, 29, 7526-7531.

96) Jones, D.; Bhattacharyya, D.; Turton, R.; Zitney, S.E. Optimal design and integration of an air separation unit (ASU) for an integrated gasification combined cycle (IGCC) power plant with CO2 capture. *Fuel Process. Technol.* 2011, 92, 1685–1695.

97) Jones, D.; Bhattacharyya, D.; Turton, R.; Zitney, S.E. Rigorous kinetic modeling, and optimization, and operability study of a modified Claus Unit for an integrated gasification combined cycle (IGCC) power plant with CO_2 capture. *Ind. Eng. Chem. Res.* 2012, 51, 2362–2375.

98) Kara, S.; Kelkar, B.G.; Shah, Y.T. Hydrodynamics and axial mixing in a three-phase bubble column. *Ind. Eng. Chem. Process Des. Dev*. 1982, 21, 584-594.

99) Karras, G. Oil Refinery CO_2 Performance Measurement. Communities for a Better Environment: Oakland, CA, September 2011.

100) Kasule, J.S.; Turton, R.; Bhattacharyya, D.; Zitney, S.E. Mathematical modeling of a single-Stage, downward-firing, entrained-flow gasifier. *Ind. Eng. Chem. Res.* 2012, 51, 6429−6440.

101) Khare, S.; Dell'Amico, M. An overview of solid-liquid separation of residues from coal liquefaction processes. *Can. J. Chem. Eng.* 2013, 91 324-31.

102) Kim, H.; Miller, D.C.; Modekurti, S.; Omell, B.; Bhattacharyya, D. Mathematical modeling of a moving bed reactor for post-combustion CO_2 capture. *AIChE J.* 2016, 62(11), 3899-3914.

103) Klerk, A. Fischer-Tropsch fuels refinery design. *Energy Environ. Sci.* 2011, 4, 1177.

104) Klerk, A.; Furimsky, E. Catalysis in the Refining of Fischer-Tropsch Syncrude. 1st Edition, Royal Society of Chemistry: Cambridge, UK, 2010.

105) Kohl, A.; Nielsen, R. Gas Purification. 5th Edition, Gulf Professional Publishing: Houston, TX, 1997.

106) Koseoglu, O.R. Process for the gasification of heavy residual oil with particulate coke from a delayed coking unit, US Patent EP2737031 A1, 2014.

107) Kreutz, T.G.; Larson, E.D.; Liu, G.; Williams, R.H. Fischer-Tropsch fuels from coal and biomass. Proceeding of the 25th International Pittsburg Coal Conference, 2008.

108) Kumar, D.; Murthy, G. S. Life cycle assessment of energy and GHG emissions during ethanol production from grass straws using various pretreatment processes. *Int. J. Life Cycle Assess.* 2012, 17, (4), 388-401.

109) Kunze, C.; Spliethoff, H. Modeling of an IGCC plant with carbon capture for 2020 *Fuel Process. Technol*. 2010, 91, 934-941.

110) Kuo, J.C. Two-Stage Process for Conversion of Synthesis Gas to High Quality Transportation Fuels. Mobil R&D Corp., DE-AC22-83PC 60019, Final Report, October 1985.

111) Kuo, J.C. Slurry Fischer-Tropsch/Mobil Two-Stage Process of Converting Syngas to High Octane Gasoline. Mobil R&D Corp., DE-AC22-80PC30022, Final Report, June 1983.

112) Lamprecht, D. Hydrogenation of Fischer-Tropsch synthetic crude. *Energy Fuels* 2007, 21, 2509-2513.

113) Larson, E.D.; Jin, H. Biomass conversion to Fischer-Tropsch liquids: preliminary energy balance. Proceeding of the 4th Biomass Conference of the Americas, 1999.

114) Larson, E.D.; Fiorese, G.; Liu, G.; Williams, R.H.; Kreutz, T.G.; Consonni, S. Co-production of decarbonized synfuels and electricity from coal and biomass with CO2 capture and storage: an Illinois case study. *Energy Environ. Sci.* 2010, 3, 28-42.

115) Larson, E.D.; Ren, T. Synthetic fuels production by indirect coal liquefaction. *Energy Sustain Dev* 7(4) (2003) 79-102.

116) Leckel, D. Hydrocracking of iron-catalyzed Fischer-Tropsch waxes. *Energy Fuels* 2005, 19, 1795-1803.

117) Leckel, D. Low-pressure hydrocracking of coal-derived Fischer-Tropsch waxes to diesel. *Energy Fuels* 2007, 21, 1425-1431.

118) Lemoine, R. An algorithm for predicting the hydrodynamic and mass transfer parameters in bubble column and slurry bubble column reactors. *Fuel Process. Technol*. 2008, 89, 322-343.

119) Leonard, C.; Ferrasse, J.H.; Boutin, O.; Lefevre, S.; Viand, A. Bubble column reactors for high pressures and high temperatures operation. *Chem. Eng. Res. Des.* 2015, 100, 391-421.

120) Liu, G.; Larson, E.; Williams, R.; Guo, X. Gasoline from coal and/or biomass with CO_2 capture and storage. 1. Process designs and performance analysis. *Energy Fuels* 2015, 29(3), 1830-1844.

121) Liu, G.; Larson, E.; Williams, R.; Guo, X. Gasoline from coal and/or biomass with CO_2 capture and storage. 2. Economic analysis and strategic context. *Energy Fuels* 2015, 29(3), 1845-1859.

122) Liu, G.; Williams, R.H.; Larson, E.; Kreutz, T. Making Fischer-Tropsch fuels and electricity from coal and biomass: performance and cost analysis, *Energy Fuels* 2011, 25, 415-437.

123) Liu, W.; Xie, X.; Wang, J. Economic and environmental analyses of coal biomass to liquids: A case study in West Virginia, *Poster presentation at the Gasification Systems and Coal & Coal-Biomass to Liquids Workshop*, August 10-11, 2015; http://www.netl.doe.gov.

124) Long, H.A.; Wang, T. Case studies for biomass/coal co-gasification in IGCC applications. Proceeding of ASME Turbo Expo 2011, Vancouver, Canada.

125) Lozza, G. Bottoming steam cycles for combined steam gas power plants: A theoretical estimation of steam turbines performances and cycle analysis. In proceedings of the 1990 ASME Cogen-Turbo symposium New Orleans, USA., 1990, 83-92.

126) Marzec, A. Towards an understanding of the coal structure: a review. *Fuel Process. Technol*. 2002, 77-78, 25-32.

127) Martelli, E.; Kreutz, T.G.; Gatti, M.; Chiesa, P.; Consonni, S. Design criteria and optimization of heat recovery steam cycles for high-efficiency, coal-fired, Fischer-Tropsch plants. Proceeding of ASME Turbo Expo 2012, Copenhagen, Denmark, June 11-15, 2012.

128) Martinez, J.; Sanchez, J.J.; Ancheyta, J.; Ruiz, R.S. A review of process aspects and modeling of ebullated bed reactors for hydrocracking of heavy oil. *Catal. Rev.* 2010, 52, 60-105.

129) Meyer, R.A. Handbook of Petroleum Refining Process. 3rd Edition, McGraw-Hill: New York, NY, 2003.

130) Mochida, I.; Okuma, O.; Yoon, S. Chemicals from Direct Coal Liquefaction. *Chem. Rev.* 2014, 1637-1672.

131) Mohammed, I.Y.; Samah, M.; Mohamed, A.; Sabina, G. Comparison of Selexol and Rectisol technologies in an integrated gasification combined cycle (IGCC) plant for clean energy production. *Int. J. Eng. Res.* 2014, 3(12), 742-744.

132) Molburg, J.C.; Doctor, R.D. Hydrogen from steam-methane reforming with CO_2 capture. Proceedings of the 20th Annual International Pittsburgh Coal Conference, Pittsburgh, USA, September 15-19, 2003.

133) Morris, S.M.; Foster, E.P. The SRC-I Coal Refining Demonstration Plant. International Coal Refining Company, http://www.fischer-tropsch.org; 1983 (Last accessed on May 31, 2016).

134) Nagaoka, K.; Sato, K.; Nishiguchi, H.; Takita, Y. Influence of support on catalytic behavior of nickel catalysts in oxidative steam prereforming of n-butane for fuel cell applications. *Appl. Catal. A Gen.* 2007, 327, 139-46.

135) Najjar, M.S.; Gates, W.C. Partial oxidation of ash-containing solid carbonaceous and/or liquid hydrocarbonaceous fuel, US Patent US4971601 A, 1990.

136) NEDO, Clean coal technologies in Japan, New Energy and Industrial Technology Development Organization, Kawasaki, Japan, 2006.

137) NETL, Baseline Technical and Economic Assessment of a Commercial Scale Fischer-Tropsch Liquids Facility, National Energy Technology Laboratory: Pittsburgh, PA, 2007.

138) NETL, Technical and economic assessment of small-scale Fischer-Tropsch liquids facilities, National Energy Technology Laboratory: Pittsburgh, PA, February, 2007.
139) NETL, Affordable, Low Carbon Diesel Fuel from Domestic Coal and Biomass, DOE/NETL -2009/1349, National Energy Technology Laboratory: Pittsburgh, PA, January 2009.
140) NETL, Cost and Performance Baseline for Fossil Energy Plant Volumn 1: Bituminous Coal and Natural Gas to Electricity, DOE/NETL -2010/1397, November 2010.
141) NETL, Analysis of natural gas-to-liquid transportation fuels via Fischer-Tropsch, National Energy Technology Laboratory, DOE/NETL-2013/1597, National Energy Technology Laboratory: Pittsburgh, PA, September 2013.
142) Neveux, T.; Moullec, Y.; Corriou, J.P.; Favre, E. Energy performance of CO_2 capture processes: interaction between process design and solvent. *Chemical Engineering Transactions* 2013, 35, 337-342.
143) Niziolek, A.M.; Onel, O.; Elia, J.A.; Baliban, R.C.; Xiao, X.; Floudas, C.A. Coal and biomass to liquid transportation fuels: process synthesis and global optimization strategies. *Ind. Eng. Chem. Res.* 2014, 53(44), 17002-17025.
144) NREL, Equipment Design and Cost Estimation for Small Modular Biomass Systems, Synthesis Gas Cleanup, and Oxygen Separation Equipment, NREL/SR-510-39945, National Renewable Energy Laboratory, 2006.
145) Onozaki, M.; Namiki, Y.; Ishibashi, H.; Takagi, T.; Kobayashi, M.; Morooka, S. Steady-State thermal behavior of coal liquefaction reactors based on NEDOL process. *Energy Fuels* 2000, 14, 355-363.
146) Otgonbaatar, U. Overview of Slurry Phase Bubble Column Fischer Tropsch Synthesis reactor and relevant design parameters, 2011; http://ocw.mit.edu/terms.
147) Overstreet, A.D. A screening study of a new water-gas shift catalyst. M. S. Thesis, Virginia Polytechnic Institute and State University: Blacksburg, VA, 1974.
148) Penner, S.S. Assessment of long-term research needs for coal-liquefaction technologies, University of California, San Diego, March 1980.
149) Plaza, J.M., Modeling of carbon dioxide absorption using aqueous monoethanolamine, piparazine and promoted potassium carbonate. PhD Dissertation, University of Texas at Austin: Austin, TX, 2012.

150) Prins, M.; Ptasinski, K.; Janssen, F. More efficient biomass gasification via torrefaction, *Energy* 31(15), 3458-3470, 2006.

151) Puxty, G.; Rowland, R. 2011. Modeling CO_2 mass transfer in amine mixture: PZ-AMP and PZ-MDEA. *Environ. Sci. and Technol.* 2011, 45, 2398-2406.

152) Rafiq, M.H.; Jakobsen, H.A; Husatd, J.E. Modeling and simulation of catalytic partial oxidation of methane to synthesis gas by using a plasma-assisted gliding arc reactor. *Fuel Process. Technol.* 2012, 101, 44-57.

153) Rafiqul, I.; Lugang, B.; Yan, Y.; Li, T. Study on co-liquefaction of coal and bagasse by factorial experiment design method. *Fuel Process. Technol.* 2000, 68, 3-12.

154) Ramos, M.J.; Gomez, J.P.; Dorado, F.; Sanchez, P.; Valverde, J.L. Hydroisomerization of a refinery naphtha stream over platinum zeolite-based catalysts. *Chem. Eng. J.* 2007, 126, 13-21.

155) Reed, M.; Bibber, L.V.; Shuster, E.; Haslbeck, J.; Rutkowski, M.; Olson, S.; Kramer, S. Baseline Technical and Economic Assessment of a Commercial Scale Fischer-Tropsch Liquids Facility. National Energy Technology Laboratory, DOE/NETL-2007/1260, Final Report, 2007.

156) Rhodes, D.E. Process for improving soluble coal yield in a coal deashing process. Patent US4225420, 1980.

157) Richardson, M.J. The specific heats of coals, cokes and their ashes. *Fuel* 1993, 72(7), 1047-1053.

158) Rinker, E.B. Ashour, S.S. Sandall, O.C. Experimental absorption rate measurements and reaction kinetics for H_2S and CO_2 in aqueous DEA, MDEA and blends of DEA and MDEA, GPA Research Report, No. 159, 1997.

159) Robin, A.M. Gasification of residual material from coal liquefaction, Quarterly Report, Texaco Inc., Montebello Research Laboratory, October 1977.

160) Robin, A.M. Hydrogen production from coal liquefaction residues, Final Report, Texaco Inc., Montebello Research Laboratory, December 1976.

161) Robinson, K.K. Reaction engineering of direct coal liquefaction. *Energies* 2009, 2, 976-1006.

162) Ruiz, R.S.; Alonso, F.; Ancheyta, J. Pressure and temperature effects on the hydrodynamic characteristics of ebullated-bed systems. *Catal. Today* 2005, 109, 205-213.

163) Salkuyeh, Y.K.; Mofarahi, M. Reduction of CO_2 capture plant energy requirement by selecting a suitable solvent and analyzing the operating parameters. *Int. J. Energy Res.* 2013, 37, 973-981.

164) Seagraves, J.; Weiland, R.H. Treating high CO_2 gases with MDEA. Optimized Gas Treating Inc., 2009, http://www.eptq.com.

165) Schadel, B.T.; Duisberg, M.; Deutschmann, O. Steam reforming of methane, ethane, propane, butane and natural gas over a rhodium-based catalyst. *Catal. Today* 2009, 142, 42-51

166) Schadel, B.T.; Schwiedernoch, R.; Maier, L.; Deutschmann, O. Reforming of methane with nickel and rhodium- catalysts: An experimental and modelling study. Proceeding of 4th International Conference on Environmental Catalysis, Heidelberg, 2005

167) Schweitzer, J.M.; Kressmann, S. Ebullated bed reactor modeling for residue conversion. *Chem. Eng. Sci.* 2004, 59, 5637-5645.

168) Sehabiague, L.; Lemoine, R.; Behkish, A.; Heintz, Y.J.; Sanoja. M.; Oukaci, R.; Morsi, B.I. Modeling and optimization of a large-scale slurry bubble column reactor for producing 10,000 bbl/day of Fischer-Tropsch liquid hydrocarbons. *J. Chin. Inst. Chem. Eng.* 2008, 39, 169-179.

169) Simons, K.; Nijmeijer, K.; Wessling, M. Gas-liquid membrane contactors for CO_2 removal. *J. Membr. Sci.* 2009, 340, 214-220.

170) Shah, P. P; Sturtevant, G. C.; Gregor, J. H.; Humbach, M. J.; Padtra, F. G.; Steigleder, K. Z. Fischer-Tropsch Wax Characterization and Upgrading, Final Report; DE-AC22-85PC80017; UOP Inc., June 1988; http://www.fischer-tropsch.org.

171) Shah, P.P. Upgrading of Light Fischer-Tropsch Products, Final Report; DE-AC22-86PC-90014; UOP Inc., November, 1990; http://www.fischer-tropsch.org.

172) Shan, X.; Li, K.; Zhang, X.; Jiang, H.; Weng, H. Reaction kinetics study on the heating stage of the Shenhua direct coal liquefaction process. *Energy Fuels* 2015, 29, 2244-2249.

173) Shih, C.T. Experimental hydrodynamic study of the slurry distribution in a vertical slurry heat exchanger. PhD dissertation, University of Nevada: Las Vegas; 1995

174) Shinn, J.H. From coal to single-stage and two-stage products: a reactive model of coal structure. *Fuel* 1984, 63, 1187-1195.

175) Shui, H.; Cai, Z.; Xu, C. Recent advances in direct coal liquefaction. *Energies* 2010, 3, 155-170.

176) Shui. H.; Shan. C.; Cai. Z.; Wang. Z.; Lei. Z.; Ren. S.; Pan. C.; Li, H. Co-liquefaction behavior of a sub-bituminous coal and sawdust. *Energy* 2011, 36(11), 6645-6650.

177) Smith, M.R.; Hubbard, D.A.; Yang, C.C. Logic, technology and effect of coal liquefaction condition on final up-graded product slate. In: Proceedings of the 9th Annual International Conference on Coal Gasification, Liquefaction, and Conversion to Electricity, 1982.

178) Sofer, S.S.; Zaborsky, O.R. Biomass conversion processes for energy and fuels. Springer Science & Business Media: New York, 2012.

179) Spencer, R.C.; Cotton, K.C.; Cannon, C.N. A method for prediction the performance of steam turbine-generators…: 16,500 kW and larger. *ASEM J. ENG. Power* 1963, 85, *249-298*.

180) SRI International. Hydrogen Production from Natural Gas. PEP Yearbook International, Vol. 1E, SRI International: Menlo Park, California, 2007.

181) Stevens, D.J. An overview of biomass thermochemical liquefaction research sponsored by the U.S. Department of Energy. ACS preprints 32(2) Production, analysis and upgrading of oils from biomass, pp. 223–228, 1987.

182) Steynberg, A.P.; Dry, M.E. Fischer-Tropsch Technology. 1st Edition, Elsevier Science: San Diego, 2004.

183) Steynberg, A.P.; Nel, H.G. Clean coal conversion options using Fischer-Tropsch technology. *Fuel* 2004, 83, 765-770.

184) Stiller, A.H.; Dadyburjor, D.B.; Wann, J.; Tian, D.; Zondlo, J.W. Co-processing of agricultural and biomass waste with coal. *Fuel Process. Technol.* 1996, 49, 167-175.

185) Su, H. Economics of geological sequestration and carbon management: a case study of Shenhua's direct coal liquefaction plant in China, PhD thesis, West Virginia University: Morgantown, WV, 2010.

186) Svoronos, P.D.N.; Bruno, T. Carbonyl Sulfide: a review of its chemistry and properties. *Ind. Eng. Chem. Res.* 2002, 41, 5321.

187) Syamlal, M.; Bissett, L.A. METC Gasifier Advanced Simulation (MGAS) Model, Technical Note, NITS report, DOE/METC-92/4108 (DE92001111), 1992.

188) Tarighaleslami, A.H.; Omidkhah, M.R.; Ghannadzadeh, A.; Hesas, R.H. Thermodynamic evaluation of distillation columns using exergy loss profiles: a case study on the crude oil atmospheric distillation column. *Clean Techn. Environ. Policy* 2012, 14, 381-387.

189) Tchapda, A.H. Pisupati, S.V. A review of thermal co-conversion of coal and biomass/waste. *Energies* 2014, 7, 1098-1148.

190) Teles, U.M.; Fernandes, F.A.N. Hydrocracking of Fischer-Tropsch products. *Thermal Engineering* 2007, 6(2), 14-18.

191) Texaco, Gasification of residual material from coal liquefaction, Final Report, Texaco Inc., Montebello Research Laboratory, 1984.

192) Thorogood, R.M. Solvent refined coal reactor quench system. Patent US4414094 A, 1983.

193) Tomeczek, J.; Palugniok, H. Specific heat capacity and enthalpy of coal pyrolysis at elevated temperatures. *Fuel* 1996, 75(9), 1089-1093.

194) Tsai, R.E. Mass Transfer Area of Structured Packing, PhD Dissertation. The University of Texas at Austin: Austin, TX, 2010.

195) Turton, R.; Bailie, R.C.; Whiting, W.B.; Shaeiwitz, J.A.; Bhattacharyya, D. Analysis, Synthesis, and Design of Chemical Process. 4th Edition, Pearson Education: Boston, 2012.

196) Vaezi, M.; Passandideh-Fard, M.; Moghiman, M.; Charmchi, M. Gasification of heavy fuel oils: a thermochemical equilibrium approach. *Fuel* 2011, 90, 878-885.

197) Valente, A.M.; Cronauer, D.C. Analyses of Illinois No.6 coal liquefaction results generated in the Wilsonville, Alabama Unit. *Energy Fuels* 2005, 19, 489-498.

198) Vasireddy, S.; Morreale, B.; Cugini, A.; Song, C.; Spivey, J.J. Clean liquid fuels from direct coal liquefaction: chemistry catalysis technological status and challenges. *Energy Environ. Sci.* 2011, 4, 311-345.

199) Wang, J.; Grushecky, S.; McNeel, J. Biomass Resources, Uses, and Opportunities in West Virginia, Final Report, Division of Forestry and Natural Resources: West Virginia University, Morgantown, WV, 2009.

200) Warzel, J. Fischer Tropsch (FT) Workshop Turbine Engine Applications, FT – Overview & History. Syntroleum Corp., May 2006.

201) Watanabe, K.; Chiyoda, N.; Kawakami, T. Development of new isomerization process for petrochemical by-products. Proceeding of 18th Saudi Arabia-Japan Joint Symposium, Dhahran, Saudi Arabia, November 2008.

202) Weller, S.; Friedel, R.A. Isomer distribution in hydrocarbons from the Fischer-Tropsch process. *J. Chem. Phys.* 1949, 17(9), 801-803.

203) Winslow, J.; Schmetz, E. Direct coal liquefaction overview presented to NETL, by Leonardo Technologies, Inc., March 23, 2009.

204) White, D.H. Wolf, D.; Zhao, Y. Biomass liquefaction utilizing extruder-feeder reactor systems. *ACS Div Fuel Chem Prepr* 1987, 32(2), 106-16.

205) Williams, R.H.; Larson, E.D. A comparison of direct and indirect liquefaction technologies for making fluid fuels from coal. *Energy for Sustainable Development* Vol. 7, No. 4, 2003.

206) Williams, B.P.; Young, N.C.; West, J.; Rhodes, C.; HuCoughlinings, G.J. Carbonyl Sulphide hydrolysis using alumina catalysts. *Catal. Today* 1999, 49, 99-104.

207) Wu, C.; Shi, S.; Zhu, X.; Zhou, M. A mathematical model for tubular reactors in direct coal liquefaction. *Energy* 1993, 18(8), 815-825.

208) Wu, X.; Shu, G.; Li, K.; Xie, S. Technology and Engineering of Direct Coal Liquefaction Process. Science Press: Beijing, China, 2015.

209) Wu, J.; Wang, J.; Cheng, Q.; DeVallance, D. Assessment of coal and biomass to liquid fuels in central Appalachia, USA. *Int. J. Energ. Res.* 2012, 36, 856-870.

210) Xu, G.; Zhang, C.; Qin, S.; Gao, W.; Liu, H. Gas-liquid equilibrium in a CO_2-MDEA-H2O system and the effect of piperazine on it. *Ind. Eng. Chem. Res.* 1998, 37, 1473-1477.

211) Yan, W.U. Precision of NEDOL method for coal-derived relative molecular weight calculation. *Clean Coal Technology* 2014, 20(2), 51-54.

212) Yang, J.I.; Ryu, J.H.; Lee, K.Y.; Jung, N.J.; Park, J.C.; Chun, D.H.; Kim, H.J.; Yang, J.H.; Lee, H.T.; Cho, I.; Jung, H. Combined pre-reformer/reformer system utilizing monolith catalysts for hydrogen production. *Int. J. Hydrogen Energy* 2011, 36, 8850–8856.

213) Zhang, Y.; Chen, H.; Chen, C.; Plaza, J.M.; Dugas R.; Rochelle, G.T. 2009. Rate-based process modeling study of CO2 capture with aqueous monoethanolamine solution. *Ind. Eng. Chem. Res.* 2009, 48, 9233-9246.

214) Zhou, P.; Rao, S.N. Assessment of coal liquids as refinery feedstocks, Prepared for DOE Pittsburgh Energy Technology Center, February 1992.